Functional Genomics Characterisation of the Genetic Pathways that Control Kinetochore Function

By

María Elena Ledesma Fernández

University College London (UCL)

and

The Francis Crick Institute, Mill Hill Laboratory
formerly
MRC National Institute for Medical Research (NIMR)

PhD Supervisor: Peter Thorpe

A thesis submitted for the degree of Doctor of Philosophy (PhD)

University College London

September 2015

Declaration

I, María Elena Ledesma Fernández, confirm that the work presented in this thesis is my own. Where information has been derived from other sources, I confirm that this has been indicated in the thesis.

Signature ---------- Date ----------

Abstract

Kinetochores serve both a structural role linking chromosomes to the mitotic spindle and a regulatory role, controlling the timing of mitosis via the spindle assembly checkpoint. Defects in kinetochore function can lead to aneuploidy, a hallmark of cancer cells. To understand how cells regulate the segregation of their chromosomes during cell division it is important to understand which genes regulate kinetochores function.

I have examined the distribution of the outer kinetochore complex DAM1/DASH complex in the budding yeast *Saccharomyces cerevisiae* using fluorescence imaging. I modified the endogenous *DAD4* and *SPC42* alleles to introduce the gene encoding yellow fluorescent protein (YFP) and red fluorescent protein (RFP) respectively. I have used the synthetic genetic array technology to transfer these two alleles into all of the ~6000 non-essential gene deletions and essential temperature sensitive mutants in yeast. Fluorescence microscopy of these mutant strains has allowed me to examine quantitative and qualitative kinetochore phenotypes. First, I assessed the levels of YFP fluorescence intensity at the kinetochore as a surrogate for protein concentration to determine changes in DAM1/DASH complex homeostasis. Then, I annotated abnormal distributions of YFP fluorescence by visualization.

I have identified a number of mutants that alter Dad4 homeostasis. For example, ~3% of the non-essential deletions and ~27% of essential conditional alleles produce either an increase or a decrease in Dad4 intensity. I have also identified mutants that cause a mislocalisation of Dad4, some of which represent mitotic spindle defects. Finally, I have investigated the mechanism underlying the phenotype caused by a kinase from the cell wall integrity pathway, Pkc1, and its connection to the kinetochore via the microtubule and actin cytoskeleton. This study highlights the importance of chromatin remodeling complexes, RNA processing enzymes and a number of protein kinases in maintaining kinetochore homeostasis.

Table of contents

DECLARATION 2

ABSTRACT 3

TABLE OF CONTENTS 4

LIST OF FIGURES 11

LIST OF TABLES 14

ABBREVIATIONS 16

ACKNOWLEDGEMENTS 19

1. CHAPTER I: GENERAL INTRODUCTION 20

1.1 OVERVIEW OF THE BUDDING YEAST CELL CYCLE 20

1.1.1 The budding yeast life cycle 20

1.1.2 Regulation of the budding yeast cell cycle by cyclins 20

1.2 MITOSIS AND THE MITOTIC SPINDLE 23

1.2.1 The budding yeast microtubule-organising center (MTOC) 23

1.2.2 Microtubules 24

1.2.3 Spindle dynamics 24

1.2.4 Microtubule associated proteins and the kinetochore 25

1.3 THE BUDDING YEAST KINETOCHORE ARCHITECTURE 26

1.3.1 The centromere-kinetochore interface: directing its own assembly 29

1.3.2 The central kinetochore: connecting and adjusting 31

1.3.3 The microtubule-kinetochore interface: attaching, pulling and correcting 32

1.3.3.1 The mitotic checkpoint proteins: a surveillance mechanism for attachment errors 35

1.4 REGULATION OF KINETOCHORES BY POSTTRANSLATIONAL MODIFICATIONS 37

1.5 WHEN THE KINETOCHORE FAILS 38

1.5.1 Aneuploidy: a hallmark of cancer cells 38

1.5.2 Aneuploidy as an evolutionary adaptation 39

1.6 APPROACHES TO STUDY THE KINETOCHORE 40
1.6.1 Visualising kinetochores by fluorescence microscopy 41
1.7 HYPOTHESIS AND AIMS OF THE THESIS 42
1.8 SUMMARY OF FINDINGS 42

2. CHAPTER II: MATERIALS AND METHODS 43
2.1 BUFFERS AND SOLUTIONS 43
2.2 BACTERIAL METHODS 43
2.2.1 Bacterial strains 43
2.2.2 *E. coli* growth media and conditions 43
2.2.3 Electroporation in *E. coli* 44
2.2.4 Plasmid purification from *E. coli* 44
2.3 YEAST METHODS 44
2.3.1 Yeast strains 44
2.3.2 Yeast growth media and conditions 48
2.3.3 Determination of cell density 49
2.3.4 Spot testing 49
2.3.5 Transformations 49
2.3.5.1 Transformation for genomic integration 49
2.3.5.2 Transformation for gap repair 50
2.3.5.3 Transformation for plasmid DNA 50
2.3.6 Yeast crosses 50
2.3.7 Tetrad dissections 50
2.3.8 Replica plating 50
2.3.9 Yeast genomic DNA extraction 51
2.3.9.1 Yeast genomic DNA extraction with phenol “Smash n’Grab” ... 51
2.3.9.2 Fast yeast genomic DNA extraction without phenol 51
2.4 MOLECULAR BIOLOGY 51
2.4.1 Polymerase chain reaction (PCR) 51
2.4.2 Purification of PCR fragments 52
2.4.3 Agarose gel electrophoresis 52

2.4.4 Extraction of fragments from agarose gels 52
2.4.5 Construction of plasmids by gap repair 52
2.4.6 Construction of endogenously-tagged fluorescent kinetochore proteins 53
2.4.7 DNA digestions with restriction endonucleases 53
2.4.8 Antartic phosphatase vector treatment 54
2.4.9 Ligation of PCR product and vector 54
2.4.10 Auxin degradation of Pkc1 54
2.5 HIGH THROUGHPUT PROTOCOLS (SCREENS) 55
2.5.1 Selective Ploidy Ablation (SPA) mini-screen with Spc24 55
2.5.2 Genome-wide screen with Dad4 (SGA) 57
2.5.3 Benomyl sensitivity screen 57
2.6 PROTEIN METHODS 58
2.6.1 Protein extraction 58
2.6.2 SDS PAGE 58
2.6.3 Western Blot 58
2.7 FLUORESCENCE MICROSCOPY 59
2.7.1 Agar pads for 48 well imaging 59
2.7.2 Preparing microscopy slides 60
2.8 IMAGE ANALYSIS 60

3. CHAPTER III: RESULTS 1: OPTIMISATION OF PLASMID-BASED SCREENS, IMAGING AND QUANTITATION METHODS 61

3.1 INTRODUCTION 61
3.1.1 Budding yeast and genome-wide studies 61
3.1.2 Genome-wide microscopy screens 62
3.1.3 Quantitation of kinetochore proteins 62
3.1.4 Aims of this work 62
3.2 RESULTS 64
3.2.1 Plasmid-based screens 64
3.2.1.1 Construction of plasmids coding fluorescent kinetochore

proteins 64

3.2.1.2 Plasmids can be classified into three distinct groups according to fluorescent signal 65

3.2.2 Selection and optimisation of methodology for genome-wide screens image analysis 67

3.2.2.1 Building Volocity protocols 67

3.2.2.2 ImageJ protocols 69

3.2.2.3 Comparison of image analysis methods 70

3.2.2.4 SPA mini-screen with Spc24 (NDC80 complex) 75

3.2.2.5 Kinetochores and spindle poles may move independently of the nucleus and differently at different mitotic phases over a time period of a minute 76

3.2.3 Selection of candidates for genome-wide screens 79

3.2.3.1 Dad2, Dad3 and Dad4 have the highest signal to noise ratio of the structural kinetochore proteins and Ndc10 among the inner kinetochore members 79

3.2.4 Assessment of the use of plasmids for genome-wide screens 80

3.2.4.1 Dad2, Dad3, Dad4 and Ndc10 encoding plasmids are lost in 20-35% of cells 80

3.2.4.2 The plasmids coding for Dad2, Dad3 and Dad4 are functional, the plasmid coding for Ndc10 could not be confirmed 82

3.2.4.3 Variation of fluorescent signal is greater for plasmid-encoded Dad4-YFP than for endogenous Dad4-GFP 82

3.3 SUMMARY AND DISCUSSION RESULTS 1 84

3.3.1 Methodology for imaging and analysis 84

3.3.1.1 Microscopy: trouble shooting 84

3.3.1.2 Image analysis methods 85

3.3.1.3 Pilot mini-screen with Spc24 86

3.3.2 Selection of candidates 87

3.3.3 Assessment of the use of plasmids for the screen 88

4. CHAPTER IV: RESULTS 2: GENOME-WIDE ENDOGENOUS FLUORESCENT MICROSCOPY SCREENS 90

4.1 INTRODUCTION 90

4.2 RESULTS 92

4.2.1 Construction of endogenously tagged fluorescent kinetochore proteins 92

4.2.2 Synthetic Genetic Array (SGA) screens with Dad4 (DAM1 complex) 93

4.2.3 Microscopy screens with Dad4 (DAM1 complex) 94

4.2.4 Foci quantitation 95

4.2.5 Normalisations 95

4.2.6 Less than 3% of the non-essential deletions either increase or decrease Dad4-YFP intensity 98

4.2.6.1 Qualitative analysis of non-essential deletions 100

4.2.7 Around 27% of the essential alleles either increase or decrease Dad4-YFP intensity 103

4.2.8 Fluorescent intensity and standard deviation values correlate 105

4.2.9 YFP fluorescent intensity and RFP fluorescent intensity do not correlate 107

4.2.9.1 Mutants that affect the intensity of the SPB protein Spc42 107

4.2.10 Around 80% of the non-essential mutants identified in the screen produce a Dad4 phenotype when they are retested 110

4.2.11 Categorising mutants 113

4.2.11.1 ~16% of the non-essential mutants that alter the intensity of Dad4-YFP are benomyl sensitive 113

4.2.11.2 Foci distribution curves of mutants 115

4.2.11.3 GO ontology 117

4.2.12 Individual validations: work with some mutants 118

4.2.12.1 The threonine biosynthesis pathway 118

4.2.12.2 The nonsense-mediated mRNA decay (NMD) pathway 123

4.2.12.3 The mitotic exit mutants 126

4.2.12.4 The microtubule associated proteins (MAPs) 128

4.2.12.5 Chromatin remodelers: the RSC and SWI/SNF complexes.. 133

4.2.12.6 Individual kinetochore mutants influence the intensity and localisation of Dad4-YFP differently 135

4.3 SUMMARY AND DISCUSSION RESULTS 2 137

5. CHAPTER V: RESULTS 3: *PKC1* ALLELES CAUSE A KINETOCHORE PHENOTYPE 139

5.1 INTRODUCTION 139

5.1.1 *PKC1* is the homolog of the mammalian PKC 139

5.1.2 Pkc1 and the CWI pathway 140

5.1.3 Pkc1 localisation 141

5.1.4 PKC nuclear roles in other organisms 142

5.1.5 Pkc1 nuclear roles in budding yeast 143

5.2 RESULTS 144

5.2.1 Pkc1 temperature sensitive allele mutations causes a phenotype on the outer kinetochore component Dad4 144

5.2.2 A wild-type copy of *PKC1* in the *URA3* locus complements the phenotype 146

5.2.3 The *pkc1-1* allele has an effect on the entire kinetochore 148

5.2.4 Kinetochore declustering may occur previous to the *pkc1-1* phenotype 151

5.2.5 Localisation of Pkc1 153

5.2.6 Do increased or decreased levels of Pkc1 cause an opposed phenotype on Dad4? 154

5.2.6.1 The Pkc1 overexpression phenotype is background dependent 154

5.2.6.2 Auxin degradation of Pkc1 154

5.2.7 Pkc1 phenotype relationship to the CWI pathway 157

5.2.7.1 The Pkc1 phenotype can be rescued by sorbitol 157

5.2.7.2 The effect of other members of the CWI pathway on Dad4 159

5.2.8 Is the phenotype of *pkc1-1* connected to the stress response pathway? 162

5.2.8.1 Many actin and microtubule mutants produce a quantitative or qualitative phenotype in the screens with Dad4 163

5.2.8.2 Actin and actin-related genes cause a phenotype in Dad4 165

5.2.8.3 Microtubules are defective in the *pkc1-1* mutant 167

5.2.8.4 Recapitulating the *pkc1-1* phenotype with microtubule drugs. 169

5.2.8.5 The Hog1 pathway is activated on *pkc1-1* mutants 170

5.3 SUMMARY AND DISCUSSION RESULTS 3 172

5.3.1 Proposed model 174

6. CHAPTER VI: GENERAL CONCLUSIONS AND FUTURE DIRECTIONS 175

REFERENCES 178

APPENDIX 1: Tables 192

APPENDIX 2: Figures 208

APPENDIX 3: Attachment 211

List of Figures

CHAPTER I: GENERAL INTRODUCTION

Figure 1.1 The budding yeast cell cycle 22

Figure 1.2 Architecture of the budding yeast kinetochore 27

Figure 1.3 Visualising kinetochores through the cell cycle 41

CHAPTER II: MATERIALS AND METHODS

Figure 2.1 SPA methodology 55

Figure 2.2 SGA methodology 57

CHAPTER III: RESULTS 1: OPTIMISATION OF PLASMID-BASED SCREENS, IMAGING AND QUANTITATION METHODS

Figure 3.1 Plasmid encoded SPB-RFP and kinetochore-YFP in yeast cells 65

Figure 3.2 Examples of plasmid classification 66

Figure 3.3 Outline of Volocity analysis 68

Figure 3.4 Outline of ImageJ analysis 70

Figure 3.5 Comparison of plasmid images 72

Figure 3.6 Comparison of plasmid data with published data 74

Figure 3.7 Miniscreen: genes that alter the YFP intensity levels of Spc24 76

Figure 3.8 Movement of kinetochore Mtw1 and SPB Spc42 proteins 78

Figure 3.9 Fluorescence intensities of Class I plasmids 80

Figure 3.10 Plasmid loss 81

Figure 3.11 Fluorescent signal in plasmid-encoded and endogenously tagged kinetochores 83

CHAPTER IV: RESULTS 2: GENOME-WIDE ENDOGENOUS FLUORESCENT MICROSCOPY SCREENS

Figure 4.1 Yeast cells doubly tagged endogenously 93

Figure 4.2 Normalisations 97

Figure 4.3 Screen with Dad4-YFP and the deletion library 99

Figure 4.4 Quantitative and qualitative methods are complementary 102

Figure 4.5 Screen with Dad4-YFP and the TS collection 104

Figure 4.6 Comparison of fluorescence intensity and standard deviation 106

Figure 4.7 Mutants that affect the SPB 109

Figure 4.8 Retest of non-essential deletions that produce a phenotype on Dad4-YFP 112

Figure 4.9 Benomyl sensitivity of non-essential deletions retested for Dad4-YFP phenotype 115

Figure 4.10 Distribution curves for low and high intensity mutants 116

Figure 4.11 GO ontology enrichment analysis 118

Figure 4.12 Deletion of members of the threonine biosynthesis pathway cause a phenotype on Dad4-YFP 120

Figure 4.13 The Dad4-YFP phenotype in *hom2*Δ and *hom3*Δ mutants is rescued with addition of serine and threonine to the media 122

Figure 4.14 The nonsense-mediated mRNA decay (NMD) pathway 125

Figure 4.15 Aberrant localisation of Dad4 in mitotic exit mutants 127

Figure 4.16 The phenotype caused by the MAPs *bim1*Δ and *bik1*Δ in the outer kinetochore is not transmitted to the central kinetochore 129

Figure 4.17 Effects of *STU2* alleles on Dad4-YFP 132

Figure 4.18 Effects of chromatin remodelers in the kinetochore 134

Figure 4.19 Phenotype of different members of the kinetochore on Dad4 136

CHAPTER V: RESULTS 3: PKC1 ALLELES CAUSE A KINETOCHORE PHENOTYPE

Figure 5.1 Protein Kinase C (PKC) isoforms and domains 139

Figure 5.2 Budding yeast Cell Wall Integrity (CWI) pathway 141

Figure 5.3 Effect of *pkc1-1* on the kinetochore protein Dad4..... 145

Figure 5.4 *PKC1* at *URA3* locus complements the *pkc1-1* phenotype 147

Figure 5.5 Effect of *pkc1-1* on the kinetochore proteins Dad3, Mtw1 and Ndc10 149

Figure 5.6 *Pkc1-1* timecourse at 37˚C 152

Figure 5.7 Localisation of Pkc1-GFP 153

Figure 5.8 Pkc1 degradation by an auxin system 156

Figure 5.9 Sorbitol rescue of *pkc1-1* Dad4-YFP phenotype 158

Figure 5.10 Disrupting the CWI pathway cause a Dad4-YFP phenotype .. 161

Figure 5.11 Genetic and physical interactions linking actin and microtubule related mutants with the kinetochore and CWI pathway 164

Figure 5.12 Actin and actin-related mutants produce a phenotype on Dad4 166

Figure 5.13 Tubulin may be defective in *pkc1-1* mutants 168

Figure 5.14 Effect of microtubule poisons on Dad4 170

Figure 5.15 Hog1 is active in the *pkc1-1* mutant..... 171

Figure 5.16 Proposed model for the mechanism behind the *pkc1-1* phenotype on Dad4 174

APPENDIX 2

Figure A Frequency curves 208

Figure B Pkc1 overexpression 209

List of Tables

CHAPTER I: GENERAL INTRODUCTION

Table 1.1 Kinetochore proteins homology 28

CHAPTER II: MATERIALS AND METHODS

Table 2.1 Buffers and solutions 43
Table 2.2 Yeast strains 45
Table 2.3 Plasmids 47
Table 2.4 Plasmids constructed by gap repair 47
Table 2.5 Yeast growth media 48
Table 2.6 List of gene deletions used in SPA mini-screen with Spc24 56

CHAPTER III: RESULTS 1: OPTIMISATION OF PLASMID-BASED SCREENS, IMAGING AND QUANTITATION METHODS

Table 3.1 Classification of plasmids 67
Table 3.2 Ten plasmids chosen for image analysis comparison 71

CHAPTER IV: RESULTS 2: GENOME-WIDE ENDOGENOUS FLUORESCENT MICROSCOPY SCREENS

Table 4.1 Overlap of mutants causing a phenotype in Dad4 with published datasets in the literature 117

CHAPTER V: RESULTS 3: PKC1 ALLELES CAUSE A KINETOCHORE PHENOTYPE

APPENDIX 1

Table A Non-essential deletions that decrease Dad4-YFP intensity 192
Table B Non-essential deletions that increase Dad4-YFP intensity 193

Table C Non-essential deletions that produce a visual phenotype on Dad4-YFP 194

Table D Essential mutant alleles that decrease Dad4-YFP intensity ... 195

Table E Essential mutant alleles that increase Dad4-YFP intensity 196

Table F Non-essential deletions that alter Spc42-RFP intensity..... 197

Table G Essential mutant alleles that alter Spc42-RFP intensity 198

Table H Non-essential deletions that decrease Dad4-YFP intensity in the retest plate..... 199

Table I Non-essential deletions that increase Dad4-YFP intensity in the retest plate..... 200

Table J Non-essential deletions that produce a visual phenotype on Dad4-YFP in the retest plate 201

Table K Non-essential deletions that are benomyl sensitive..... 202

Table L Actin and microtubule mutants that affect Dad4-YFP intensity or localisation 203

Table M List of oligos used 204

Abbreviations

Δ	deletion (of an ORF)
5-FOA	5-Fluoroorotic Acid
APC	anaphase promoting complex
˚C	degree Celsius
CCAN	constitutive centromere-associated network
CDE(s)	centromere DNA element(s)
CDK	cyclin-dependent kinase
CEN	centromere
CIN	chromosome instability
CIP pathway	cell integrity pathway
CEN	centromere
CFP	cyan fluorescent protein
CLASP	CLIP-associated protein
coIP	Co-immunoprecipitation
CPC	chromosomal passenger complex
CWI pathway	cell wall integrity pathway
DIC	differential interference contrast
DMSO	dimethyl sulfoxide
DNA	deoxyribonucleic acid
EB1	end binding 1
E. coli	*Escherichia coli*
EDTA	ethylenediaminetetraacetic acid
FEAR	Cdc fourteen early anaphase release
G1	gap 1
G2	gap 2
G418	geneticin
GAL	galactose
GAP	GTPase activating protein
GDP	guanosine diphosphate
GEF	guanine-nucleotide exchange factor
GFP	green fluorescent protein
GO	gene ontology
GTP	guanosine triphosphate
HYG	hygromycin B
INCENP	inner centromere protein
KAN	kanamycin

kanMX	kanamycin resistant cassette
kb	kilobase pair
kDa	kilo Dalton
k-MT	kinetochore-microtubule
LB	Luria-Bertani broth
LED	light-emitting diode
MAP(s)	microtubule-associated protein(s)
MAPK	mitogen activated protein kinase
MAT	mating type locus
*MAT***a**	yeast mating type a
MATα	yeast mating type alpha
Mb	megabyte
MEN	mitotic exit network
mRNA	messenger RNA
MTOC	microtubule-organising center
NAT (cloNAT)	nourseothricin
NMD pathway	nonsense-mediated mRNA decay
O.D.600	optical density at 600 nm
ORF	open reading frame
PCR	polymerase chain reaction
PEG	polyethylene glycol
PKC	protein kinase C
RFP	red fluorescent protein
RNA	ribonucleic acid
ROIs	regions of interest
RSC complex	chromatin structure remodeling complex
r.u.	relative units
SAC	spindle assembly checkpoint
SBF	Swi4/6 cell cycle box
S. cerevisiae	*Saccharomyces cerevisiae*
SC	synthetic complete
SCF complex	Skp, Cullin, F-box containing complex
SGA	synthetic genetic array
SGD	*Saccharomyces* Genome Database
SILAC	stable isotope labeling by amino acids in cell culture
SPA	selective ploidy ablation
SPB(s)	spindle pole bodi(es)
S-phase	synthesis phase

SRP pathway	stress response pathway
STD	standard deviation
SUMO	small ubiquitin-like modifier
SWI/SNF	SWItch/Sucrose Non-Fermentable
TBZ	thiabendazole
TE	Tris-EDTA
+TIP(s)	microtubule plus-end tracking protein(s)
TS	temperature sensitive
Tris	Tris (hydroxymethyl) aminomethane
UDS	universal donor strain
X-Gal	5-bromo-4-chloro-3-indolyl-β-D-galactopyranoside
YFP	yellow fluorescent protein
YPD	yeast extract peptone dextrose
WT	wild type

Acknowledgments

I would like to start by thanking my supervisor Dr. Peter Thorpe for the opportunity of working in his lab and for his limitless enthusiasm for yeast and mitosis. I feel privileged that I have worked on the last days of an institute full of history, the NIMR, and I have also seen the beginnings of the new Francis Crick Institute. I am vey grateful to the MRC for the funding that has allow me to carry on this thesis and to travel to the other side of the word to awesome conferences and a crazy yeast course where I met great people.

I would like to also acknowledge my second supervisor Dr. David Wilkinson and the rest of my thesis committee members Dr. Robin Lovell-Badge and Dr. Steve Smerdon, for their input and advice besides being a topic unrelated to theirs. Also, Peter Parker and Ian Hagan for suggestions on the Pkc1 work.

Thank you to all the lab members past and present (Lisa, Gudjon, Wenjun, Erika, Sonia, Eleanor and Mathilde) and very especially to Eva Herrero for her help with methods, discussions and for her friendship.

Coffee/cake breaks would have not been the same without Radhma, Radhi, Liz, Alex, Luke, Mike, and although briefly, Jesus, Rita, Anna P, Anna G and specially Erika's brownies. I'll specially remember the positivity and laughs from Anna G, Erika, Matilda, Lisa and Radhi, which always had good words and smiles for me, and the summer spirit of Stella in the middle of January. And of course, Lisa and those chats were we put the world right!

I want to thank my family and friends for always believing on what I could achieve more than myself. Also to Sheila and Peter for being like a family to me on the difficult and stressful years of joggling day office jobs with evening undergraduate science classes so I could end writing this thesis today.

Last but not least, I want to dedicate my thesis to my husband Matt for all his patience and love through these years. Thank you for never complaining about weekends in the lab (even if it was sunny outside), for walking me to the lab and waiting outside in the cold because I was only going to take a plate out of the incubator but ended up running PCRs, for reading my assessments and looking at my figures interested even if they said nothing to you, for getting my dinner ready as I leave the lab, and for be willing to move anywhere in the world just so I can work on what I love.

1. Chapter I: General introduction

This thesis describes my work to understand the regulation of the kinetochore, a multi-subunit protein complex responsible for attaching chromosomes to the mitotic spindle and thus, important for segregating chromosomes during cell division. I have used the budding or baker's yeast, *Saccharomyces cerevisiae* as a model system. In this introduction I will provide background information on cell division in *S. cerevisiae*, the kinetochore and its regulation. This introduction focuses on the budding yeast kinetochore, for more general information in other organisms see reviews such as the following (Rieder and Salmon, 1998; Santaguida and Musacchio, 2009; Cheeseman, 2014).

1.1. Overview of the budding yeast cell cycle

1.1.1. The budding yeast life cycle

S. cerevisiae is typically diploid (*MAT***a**/*α*) containing 2 copies of each chromosome (n=32), but lab strains are often haploid with 1 set of DNA (n=16) (*MAT***a** or *MATα*). Haploid cells can either undergo proliferation (mitotic cell cycle) or mate with a cell of the opposite mating type to form a diploid. When nutrients are available, haploid cells divide by budding; a protrusion (bud) arises from the mother cell, which grows into a new cell that receives a copy of the DNA content and pinches off. If another cell of opposite mating type is nearby, haploid cells chose to mate and fuse into a diploid. When nutrients are not available, diploid cells can undergo meiosis and produce an ascus containing 4 spores, which when the conditions became suitable can germinate into 4 haploid cells (Hartwell, 1974; Herskowitz, 1988).

1.1.2. Regulation of the budding yeast cell cycle by cyclins

The cell cycle is a succession of events that results in growth and division of cells and can be divided into four phases (Figure 1.1). During S-phase DNA is replicated and a new SPB/centrosome is formed and during mitosis chromosome segregation and nuclear division occur. These two phases are separated by two gap phases for growth (G1 and G2) and duplication of cell components (G1).

Budding yeast has a closed mitosis (the nuclear envelope remains intact throughout mitosis) and centromeres remain attached to microtubules connected to the SPB throughout the entire cell cycle. For this reason, kinetochores only disassemble briefly to allow centromeres to disengage from microtubules and be replicated during S-phase

(Kitamura et al., 2007). Reassembled kinetochores are quickly recaptured by microtubules from the old SPB and later, from the new SPB. Mitosis can be further divided into four stages (prophase, metaphase, anaphase and telophase). In budding yeast the key steps of chromosome segregation occur during metaphase and anaphase. During metaphase sister chromatids become bioriented, then cells enter anaphase as the cohesin that binds them together is cleaved by separase and the mitotic spindle elongates pulling sister chromatids to opposite poles while kinetochore microtubules shorten and finally the mitotic spindle disassembles (Tanaka et al., 2005).

These mitotic events are tightly regulated both spatially and temporally since abnormal or uncontrolled cell division leads to cell death or chromosome missegregation – a hallmark of cancer cells. Progression through the cell cycle is highly regulated by cyclin-dependent kinases (Cdks) and their activators, cyclins, which are present specifically at different stages of the cell cycle (Figure 1.1). Unlike mammalian cells, budding yeast has a single Cdk (Cdc28/Cdk), which associates to different cyclins sequentially through the cell cycle (reviewed in Bloom and Cross, 2007). Cyclins are regulated by their synthesis, degradation and by specific inhibitors, see (Novak et al., 2002; Bloom and Cross, 2007).

In budding yeast, the cell cycle starts when G1 cells reach a minimum size and environmental cues are appropriate. During G1, Cln3-Cdc28 promotes synthesis of the other two G1 cyclins, Cln1 and Cln2. Their association with Cdc28 promotes synthesis of the B-type cyclins necessary for S-phase and mitosis, as well as bud emergence and SPB duplication. A checkpoint is in place during the G1/S transition (START), which reduces Cln3-Cdc28 activity in the presence of pheromone signalling or lack of nutrients and thus, prevents the transcription of successive cyclins (Novak et al., 2002; Bloom and Cross, 2007). In addition, the presence of DNA damage activates Rad53, which also prevents transcription of Cln1 and Cln2 by inhibiting their transcription factor SBF (Swi4-Swi6) (Sidorova and Breeden, 1997). The cylins Clb5 and Clb6 are activated at the G1/S transition and are involved in initiation of S-phase. Mitotic cyclins Clb1-4 are capable of initiating late DNA replication when Clb5-6 are not present, although their main function is in mitotic processes such as spindle formation and they need to be degraded for cytokinesis and mitotic exit to occur. Clb5 is also thought to have a role in mitotic spindle assembly (Novak et al., 2002; Bloom and Cross, 2007).

Between S-phase and mitosis, the morphogenesis checkpoint (G2 checkpoint), prolongs G2 when bud formation or cytoskeletal function are defective by impeding degradation of Swe1, which binds to and inhibits Clb-Cdc28 complexes (Lew, 2003). At the

metaphase-anaphase transition, the spindle assembly checkpoint (SAC) (see section 1.3.3.1) can delay anaphase progression and degradation of specific cyclins when chromosomes are unattached to the mitotic spindle. When cells reach telophase, exit from mitosis is achieved by eliminating the activity of Clbs-Cdc28 in two ways, though direct inhibition by Sic1 and by degradation via APC^{Cdh1} (Visintin et al., 1998). In brief, the phosphatase Cdc14, which is normally restricted to the nucleolus is released by the mitotic exit network (MEN) and it is responsible for activating APC^{Cdh1} and the transcription factor Swi5 which in turn initiates transcription of Sic1, an inhibitor of Clb-Cdc28. Spindle misalignment activates the spindle-position checkpoint which delays MEN activation and thus the Clb-Cdc28 inactivation by Sic1 (Novak et al., 2002; Bloom and Cross, 2007).

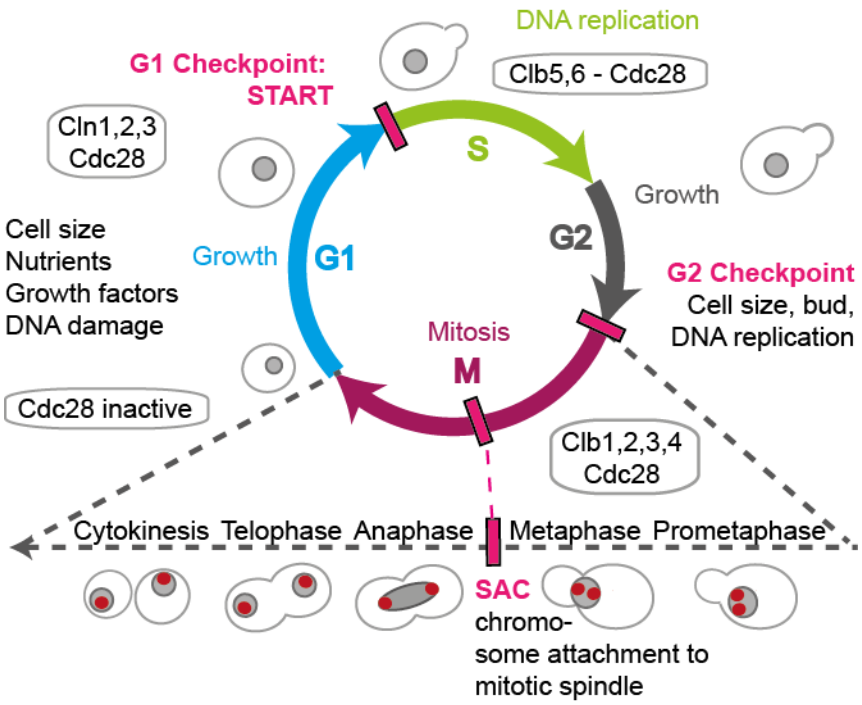

Figure 1.1. The budding yeast cell cycle. Illustration showing the phases of the budding yeast cell cycle. Checkpoints and cyclins present at each state are indicated. The yeast cells show the nucleus (grey) and the SPBs during mitosis (red).

1.2. Mitosis and the mitotic spindle

Mitosis is the cell cycle phase when chromosomes segregate and the nucleus is divided between the mother and the new daughter cell. For chromosomes to be able to segregate, a spindle needs to be formed between SPBs opposing each other. Kinetochores must attach chromosomes to the bipolar spindle that must be able to elongate and pull chromosomes apart towards the poles and finally disassemble to allow cytokinesis to divide the cells.

1.2.1. The budding yeast microtubule-organising center (MTOC).

Spindle pole bodies (SPBs) are the equivalent to mammalian centrosomes. However, since budding yeast has a closed mitosis, they are embedded in the nuclear envelope throughout the cell cycle, unlike centrosomes. SPBs are formed by at least 18 proteins arranged into interconnected layers. This structure enables different layers of the SPB to access both sides of the nuclear envelope, the nucleus and the cytoplasm, and thus nucleate microtubules in both compartments. From these outer layers microtubules are nucleated and organised by the γ-tubulin complex arranged with the minus-ends at the SPB side and the plus-ends at the cytoplasm and nucleoplasm compartments. In addition, a structure called half bridge is associated to a side of the SPB and it is the site for assembly of a new SPB (Adams and Kilmartin, 1999). The height of SPBs is constant (~150 nm), however, their diameter changes from G1 to mitosis and doubles when DNA content doubles in haploid and diploid cells for instance, allowing for an increased capacity to nucleate microtubules (reviewed in Jaspersen and Winey, 2004; Winey and Bloom, 2012).

SPBs must duplicate in order to form a mitotic spindle. In short, duplication is initiated during G1 by elongation of the half bridge and deposition of satellite material (SPB precursor). Following this, the cytoplasmic layers of the new SPB form while remaining connected to the bridge. Next, the bridge retracts and the partially-formed new SPB is inserted in the membrane. Finally, the nuclear layers assemble (Jaspersen and Winey, 2004). In late S phase, when SPBs are duplicated, the connection between the old and new SPBs via the bridge is disengaged in a process dependent on active Cdc28. The two SPBs then move apart, driven by kinesin motors Cin8 and Kip1, to be positioned opposite to each other in the nuclear envelope (Chee and Haase, 2010).

1.2.2. Microtubules

Microtubules are rigid polymers that self-assemble from α and β tubulin heterodimers. In yeast, α-tubulin is encoded mostly by the gene *TUB1* and in less part by *TUB3* and β-tubulin by *TUB2*. Tubulin dimers form long protofilaments and these assemble to form filaments with a hollow core 25 nm in diameter. The protofilaments assemble in the same orientation, creating polarity on microtubules, with exposed β-tubulin at the plus ends and α-tubulin at the minus ends. A crucial property of microtubules is their dynamic instability, which allows them to switch between periods of rapid growth and shrinkage (catastrophe). This dynamic property is a consequence of tubulin proteins being GTPases. Free tubulin dimers in solution are mostly GTP-bound and they assemble into growing plus ends of microtubules. Once bound, they can hydrolyse GTP into GDP and they are retained in the microtubule lattice by the constant addition of new dimers. The tip of the microtubule is formed by tubulin-GTP that hasn't been hydrolysed (GTP cap) and the microtubule grows as long as the rate of addition of tubulin-GTP is greater than the rate of hydrolysis. However, when there is a switch in this rate, the GTP cap is lost and the exposed tubulin-GDP, which has less affinity to microtubules, dissociates. Thus, variations in tubulin concentration and their GTP or GDP-bound state dictates whether microtubules polymerise or depolymerise. Nevertheless, a number of proteins are capable of influencing microtubule dynamics including microtubule associated proteins (MAPs) and molecular motors such as kinesin proteins (Mitchison and Kirschner, 1984; Desai and Mitchison, 1997; Morgan, 2007).

The minus ends of microtubules with exposed α-tubulin are embedded in the SPB and are less dynamic. At the cytoplasmic side, astral microtubules are essential to position the nucleus and orient the SPBs, whereas at the nuclear side they form the mitotic spindle necessary for chromosome segregation (Morgan, 2007).

1.2.3. Spindle dynamics

The mitotic spindle is a dynamic structure that changes throughout mitosis. SPB separation results in the formation of a bipolar spindle composed of 16 kinetochore microtubules and ~4 interpolar microtubules emanating from each pole. Each kinetochore microtubule attaches a single kinetochore (Winey, 1995). In addition, 2-3 microtubules extend from each SPB in the cytoplasmic side (Winey and Bloom, 2012). The length of the mitotic spindle varies throughout mitosis. G1 cells have one SPB and microtubules ~150 nm long. Pre-metaphase spindles are short (130-600 nm) arrays of microtubules. During metaphase, the bipolar spindle is stable and rigid (1.4-2 μm),

however, at the start of anaphase it grows rapidly at a rate of ~1 μm/min. After reaching ~6 μm in length, elongation continues at a lower rate up to a length of 10 μm at anaphase onset. This growth occurs on interphase microtubules at the same time that kinetochore microtubules shorten. Only a few long microtubules remain at the midzone until the spindle finally disassembles to allow cytokinesis at the end of anaphase (Winey and Toole 2001; Winey and Bloom, 2012).

How spindle length is regulated remains unexplained, although in yeast spindle length is thought to be influenced by the balance between the outward force produced by kinesin motors sliding overlapping MTs (elongating the spindle) and the kinetochore inward force toward the poles (shortening the spindle). In support of this, the Murray lab has recently shown that decreasing kinetochore numbers elongates the spindle while adding extra kinetochores shortens the spindle. In addition, they found that microtubule number increased with extra kinetochores (Nannas et al., 2014).

Kinesin motors are essential for spindle assembly and elongation. Although a large number of kinesin motor families are present in mammalian cells, only four nuclear kinesin motors are known in budding yeast. The kinesin-5 motors (Kip1 and Cin8) crosslink and slide microtubules by forming tetramers to assemble bipolar spindles, as does their ortholog Eg5 in higher eukaryotes. The presence of at least one of these kinesin motors is essential for SPB separation and spindle assembly. Kip3 has been described as a kinesin-8 or kinesin-13 with depolymerising activity. Finally, the minus end directed kinesin-14 Kar3 is a depolymerising motor that can change localisation and roles by associating to either the cofactor Cik1 or Vik1 (Tytell and Sorger, 2006).

The four kinesin motors colocalise with kinetochores and have roles in kinetochore-microtubule attachments. For example, Kip1 and Cin8 are important for kinetochore clustering and metaphase configuration, while Kar3 participates in the pulling forces at the metaphase-anaphase transition and binds to SPBs as well as to unattached and incorrectly attached kinetochores (Tytell and Sorger, 2006). Kar3 also participates in kinetochore transport along microtubules during early capture (Tanaka et al., 2005). In addition to the four nuclear motors, two cytoplasmic kinesin motors Kip2 and Kip3 as well as dynein have a role in nuclear and SPB positioning.

1.2.4. Microtubule associated proteins and the kinetochore

A number of microtubule-associated proteins (MAPs), both motor and non-motor, are able to influence microtubule and spindle dynamics. One type of MAPs is the non-motor

microtubule plus-end tracking proteins (+TIPs), which track and bind dynamic microtubule plus ends and can promote both their catastrophe and rescue. In budding yeast, Bim1 (EB1), Bik1 (CLIP-170), Stu1 (CLASP) and Stu2 (XMAP215) (Table 1.1) have a multitude of roles on both astral and nuclear microtubules and can interact by cooperating or competing to increase the number of ways in which they influence microtubules. For example, Bim1 maintains the integrity of the anaphase midzone allowing spindle elongation (Gardner et al., 2008) and later Bim1 phosphorylation by Ipl1 reduces Bim1's affinity for microtubules and this leads to disassembly of the midzone (Zimniak et al., 2009). Moreover, Bik1 was shown to interact with kinetochores and to function in kinetochore separation independent of this role on microtubule dynamics (Lin et al., 2001). Finally, Stu1 localises to unattached kinetochores during prometaphase dependent on Ndc80 and a functional DAM1 complex, and promotes kinetochore-microtubule capture while preventing SPB separation as long as unattached kinetochores persist. Once all kinetochores are attached Stu1 is free to relocate to microtubules where it promotes spindle assembly (Ortiz et al., 2009).

A model was proposed to explain recapture of kinetochores after their disassembly during centromere replication. In this model, Stu2, Bim1 and Bik1 work together to extend microtubules that capture kinetochores laterally. Stu2 localises to unattached kinetochores and upon lateral contact it travels with kinetochores to microtubule ends. From there, possibly together with Bim1 and Bik1, it prevents kinetochores from sliding off shrinking microtubules by promoting microtubule growth. Finally, the DAM1 complex is loaded and end-on attachment is achieved (Tanaka et al., 2005).

The examples discussed here are only few of the many ways in which microtubule associated proteins influence microtubule dynamics and thus, the mitotic spindle and ultimately kinetochore function.

1.3. The budding yeast kinetochore architecture

Kinetochores are formed by over 70 proteins in budding yeast, which are arranged into distinct sub-complexes. Some of these complexes are able to bind DNA (the inner kinetochore) while others bind microtubules (the outer kinetochore), see Figure 1.2. Furthermore, some complexes bridge the inner and outer kinetochore as well as having regulatory functions. However, the role of many kinetochore proteins at the molecular level and their exact position has not been elucidated (McAinsh, Tytell and Sorger, 2003; Westermann, Drubin and Barnes, 2007).

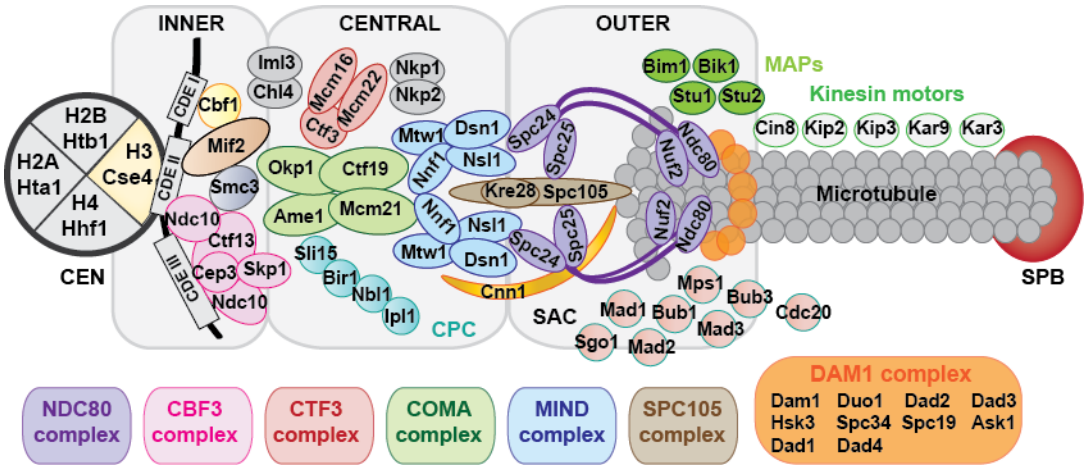

Figure 1.2. Architecture of the budding yeast kinetochore. Illustration of the budding yeast kinetochore. Members of complexes are shown in the same colour. The position of the complexes is not to scale and not necessarily representative.

Budding yeast kinetochores attach to a single spindle microtubule (Winey, 1995) in contrast to mammalian kinetochores, which attach multiple microtubules and are smaller. However, most of yeast kinetochore complexes have higher eukaryotic orthologs (Table 1.1) and a similar general structure. This conservation of structure, sequence and function of eukaryotic kinetochore proteins make yeast a good model to study kinetochores (Yanagida, 2005; Westermann, Drubin and Barnes, 2007).

Kinetochore function is more complex than simply providing a scaffold for microtubules to bind the chromosomes, as reflected by their multiple complexes and associated proteins, such as MAPs and kinesin motors. In addition, many kinases are thought to be involved in kinetochore regulation (Morgan, 2007). Kinetochores are able to direct their own assembly on centromeres and connect chromosomes to the spindle. They are able to establish bipolar attachments and harvest the force from dynamic microtubules converting it into chromosome movement. Additionally, kinetochores provide a platform for the spindle assembly checkpoint (SAC) that detects errors in spindle attachments and prevents cells from entering anaphase with unattached chromosomes, critical to prevent aneuploidy. The multiprotein complexes of the kinetochore thus orchestrate the crucial events of chromosome segregation.

Table 1.1. Kinetochore proteins homology

S. cerevisiae	*S. pombe*	Human	*S. cerevisiae*	*S. pombe*	Human
INNER/CENTRAL KINETOCHORE PROTEINS (Human CCAN)			**OUTER KINETOCHORE PROTEINS (Human KMN)**		
Cse4	Cnp1	CENP-A	**MIND**		**MIS12**
Cbf1	Abp1	CENP-B	Mtw1	Mis12	Mis12
Mif2	Cnp3	CENP-C	Nnf1	Nnf1	Pmf1
Smc3	Sim1	HJURP	Nsl1	Mis14	Nsl1R
COMA		**CENP-O**	Dsn1	Mis13	Dsn1R
Ctf19	Fta2	CENP-P	**SPC105**		**KNL1**
Mcm21	Mal2	CENP-O	Spc105	Spc7	Knl1/Blinkin
Ame1	Mis17	CENP-U	Kre28	Sos7	Zwint-1
Okp1	Fta7	CENP-Q	**NDC80**		**NDC80**
-	-	CENP-R	Ndc80	Ndc80	Hec1
CTF3		**CENP-H**	Nuf2	Nuf2	Nuf2
Ctf3	Mis6	CENP-I	Spc24	Spc24	Spc24
Mcm16	Fta3	CENP-H	Spc25	Spc25	Spc25
Mcm22	Sim4	CENP-K	**DAM1/DASH**		
Nkp1	Fta4	-	Spc34	Spc34	-
Nkp2	Cln2	-	Duo1	Duo1	-
		CENP-TWSX	Dam1	Dam1	-
Cnn1	Cnp20	CENP-T	Dad1	Dad1	-
Wip1	New1	CENP-W	Dad3	Dad3	-
Mhf1	Mhf1	CENP-S	Spc19	Spc19	-
Mhf2	Mhf2	CENP-X	Hsk3	Hsk3	-
		CENP-LMN	Dad2	Dad2	-
Iml3(Mcm19)	Fta1	CENP-L	Dad4	Dad4	-
-	Mis17	CENP-M	Ask1	Ask1	-
Chl4	Mis15	CENP-N			**SKA**
CBF3			-	-	Ska1
Cep3			-	-	Ska2
Ctf13			-	-	Ska3
Skp1					
Ndc10					
AUXILIARY/ASSOCIATED KINETOCHORE PROTEINS					
CPC			**MAPS**		
Ipl1	Ark1	Aurora B	Stu1	Peg1	CLASP 1/2
Sli15	Pic1	INCENP	Stu2	Dis1	XMAP215
Bir1	Bir1/Cut7	Survivin	Bim1	Mal13	EB1
Nbl1	Mug118	Borealin	Bik1	Tip1	CLIP-170
SPINDLE ASSEMBLY CHECKPOINT (SAC)			**SPINDLE/ MOTOR PROTEINS**		
Mps1	Mps1	Mps1/TTK	Kar3	Pkl1, Klp2	HSET
Mad1	Mad1	Mad1L1	Cin8/Kip1	Cut7	Eg5
Mad2	Mad2	Mad2L1	Kip3	Klp5/Klp6	Kif18a
Mad3	Mad3	BubR1	Kip2		
Cdc20	Slp1	Cdc20	Kar9	-	-
Bub1	Bub1	Bub1	Slk19		
Bub3	Bub3	Bub3	She1		
Bub2	Bub2				

1.3.1. The centromere-kinetochore interface: directing its own assembly

For correct chromosome segregation to occur, first, a single kinetochore has to assemble on each chromosome. How is centromeric (CEN) DNA recognised by the kinetochore and how do so many complexes arrange together?

Centromeres are unique chromosome regions where kinetochores assemble to connect the DNA to the mitotic spindle and achieve chromosome segregation. Budding yeast centromeres are excellent tools for the study of centromere function and chromosome segregation since they are both necessary and sufficient for kinetochore assembly. Centromeres in the budding yeast *S. cerevisiae* are short well-defined sequences of only ~120-125 base pairs (called "point centromeres") and are conserved on all chromosomes, unlike in animal cells. They are formed by 3 centromere DNA elements (CDEs): CDEI (~8bp), the AT-rich CDEII (78-86 bp) and CDEIII (~26 bp). In contrast, other eukaryotes have longer centromeres that contain multiple repeated elements (40-100 kb in fission yeast *S. pombe* and >1Mb in vertebrates). The repeat-rich structure of vertebrate centromeres has prevented their precise sequence to be determined and they are neither necessary nor sufficient to direct chromosome segregation (reviewed in Verdaasdonk and Bloom, 2011; Fukagawa and Earnshaw 2014).

Besides differences in *CEN* DNA, both yeast and vertebrates, contain a specialised histone H3 subunit that is specific for centromeric nucleosomes (CENP-A in vertebrates and Cse4 in yeast) (Cheeseman, Drubin and Barnes, 2002). *S. cerevisiae* kinetochores assemble around one or potentially a very few centromere-specific nucleosomes (Keith and Fitzgerald-Hayes, 2000; Furuyama and Biggins, 2007; Coffman et al., 2011; Lawrimore, Bloom and Salmon, 2011). The yeast Cse4 containing nucleosome binds to the central CDEII centromere region while the CBF3 complex and a homodimer of Cbf1 bind to CDEIII and CDEI respectively (McAinsh, Tytell and Sorger, 2003). In addition, a member of the CBF3 complex, Ndc10/Cbf2, has been shown to bind to CDEII region on its own, maybe forming a multimeric structure (Espelin et al., 2003; Perriches and Singleton, 2012).

Kinetochore complexes assemble independently in a hierarchical manner from the H3 variant Cse4 (Collins et al., 2005). The CBF3 complex is necessary for recruitment of all the other kinetochore complexes to the centromere, thus, association of the essential CBF3 complex with a specific centromeric DNA region may well be an initiating event for kinetochore assembly in yeast (Westermann, Drubin and Barnes, 2007). The CBF3 complex is formed by the heterodimer Skp1-Ctf13 and the homodimers Cep3 and

Ndc10 (Cho and Harrison, 2011). The steps for assembly of the CBF3 complex have been described (McAinsh, Tytell and Sorger, 2003). In short, Skp1 binds and phosphorylates Ctf13 assisted by the conserved chaperone Hsp90 and a transient interaction with Sgt1, a co-chaperone, which is also a unit of the SCF ubiquitin ligase complex (Kitagawa et al., 1999). The phosphorylated form of Ctf13 is active and can bind Cep3 forming the Skp1-Ctf13-Cep3 sub-complex, capable of binding Ndc10/Cbf2 and the CDEIII region (McAinsh, Tytell and Sorger, 2003). Ndc10 binds the histone chaperon Scm3 (HJURP in higher eukaryotes) that also binds Cse4 and is necessary for efficient localisation to centromeres of both binding partners. In this way, Ndc10 links the CBF3 complex with the Cse4 containing nucleosome (Cho and Harrison, 2011; Shivaraju et al., 2011). The conserved Skp1 and Sgt1 proteins have been proposed to balance CBF3 formation and stability with turnover (Rodrigo-Brenni et al., 2004).

Although no homologs of the genes that encode members of the CBF3 complex are known in higher eukaryotes, the molecular mechanisms of kinetochore assembly seem to be general (Cho and Harrison, 2011). In vertebrates, the Mis12 kinetochore complex is necessary for assembly of most of the kinetochore and it also interacts with the Hsp90–Sgt1 chaperone complex like CBF3 in yeast. Inhibition of either Hsp90 or Sgt1 causes a reduction in Mis12 subunits and corresponding kinetochore defects. Sgt1 may act to stabilise Mis12 and enhance its association with Hsp90 while Skp1 could oppose the turnover of unassembled Mis12 (Davies and Kaplan, 2010). Thus, the same pathway that is important for the assembly of the CBF3 complex is also important for assembly of kinetochores in higher eukaryotes, which lack CBF3. However, in mammalian cells it seems as though the deposition of CENP-A on chromatin provides the key epigenetic determinant of centromere identity (Fachinetti et al., 2013).

Ndc10 has additional roles to its function linking CBF3 with the nucleosome. Scm3 is an essential protein that localises to the centromeres. It associates with both Ndc10 and Cse4, and it is necessary for establishment and maintenance of a functional kinetochore. A model has been proposed in which Smc3-Ndc10 bind CEN DNA to recruit Cse4 (Camahort et al., 2007). Ncd10 also has a role in spindle stabilisation and cytokinesis. Members of the CBF3 complex localise along the spindle and midzone during anaphase and telophase in addition to their centromeric localisation. Ndc10's localisation to the midzone has been suggested to be mediated by Bir1, part of the chromosomal passenger complex (CPC: Ipl1-Sli15-Bir1-Nbl1 in yeast) and Cdc14, a phosphatase involved in mitotic exit (Bouck and Bloom, 2005).

1.3.2. The central kinetochore: connecting and adjusting

From the *CEN*-bound CBF3, a number of complexes are recruited to form a functional kinetochore in a hierarchical manner (dependent on presence of previous complexes) from innermost to outermost complexes. Several complexes link the inner (DNA binding) and outer (microtubule binding) kinetochore in budding yeast. Mammalian cells don't have an ortholog for the CBF3 complex, however multiple complexes form the CCAN network that fulfil its functions, which includes othologs of inner and central yeast complexes (Table 1.1), such as CENP-C (Mif2) which bind directly to CENP-A/H3 (Westermann et al., 2003; Westhorpe, Fuller and Straight, 2015).

The two main central complexes (COMA and MIND) were the first identified as "bridges" since they link DNA binding and microtubule binding complexes. The COMA/CTF19 complex is formed by two heterodimers, the non-essential Ctf19-Mcm21 and the essential Ame1-Okp1. The essential MIND/MTW1 complex (Mtw1, Nnf1, Dsn1, Nsl1) is part of the outer KMN network (MIS12) in mammalian cells (Table 1.1) (De Wulf, McAinsh and Sorger, 2003). The MIND complex connects multiple complexes together (Maskell, Hu and Singleton, 2010). The Mtw1-Nnf1 heterodimer binds the COMA complex while Dsn1-Nsl1 subunits bind the NDC80 complex's Spc24-Spc25 globular head (Hornung et al., 2011). In addition, the MIND complex also binds the SPC105 complex (De Wulf, McAinsh and Sorger, 2003), which is capable of microtubule binding (Pagliuca et al., 2009). In mammalian cells, the orthologs of the MIND-NDC80-SPC105 (MIS12-KNL1-NDC80) form the outer KMN network. In addition to assisting assembly and strengthening the structure of kinetochores, MIND and COMA complexes have multiple regulatory roles. For instance, Mtw1 functions in biorientation (Pinsky et al., 2003) and the COMA complex in spindle checkpoint (Matson et al., 2012; Pot et al., 2005). Furthermore, the protein Ame1 (COMA) can bind the CPC member Sli15 promoting its function and defective attachment correction (Knockleby and Vogel, 2009).

Many other members of the central kinetochore have been identified that are not so well studied. For instance, the 3 non-essential subunits of the CTF3 complex (Ctf3, Mcm16 and Mcm22) are sometimes considered an extension of the COMA complex as are Nkp1 and Nkp2 (Table 1.1) (Cheeseman et al., 2002), and recruitment of the CTF3 members to the kinetochore is Ctf19 dependent (Measday et al., 2002). Another protein, Chl4, is required for Ctf19-Ctf3 interaction, as well as for Ctf19-Iml3 interaction (Pot et al., 2003). Chl4-Iml3 forms a heterodimer and has a role in sister chromatid cohesion by interacting with Mif2 and Sgo1 (Hinshaw and Harrison, 2013).

The discovery of new kinetochore-associated proteins is proving that the connection between the central and outer kinetochore can be enhanced or inhibited. For instance, Cnn1 is an elongated monomer that is found at low levels through the cell cycle. However, Cnn1 levels increase at the kinetochore during anaphase to equal numbers of NDC80 by combined activity of Ipl1, Mps1 and Cdc28. Cnn1 competitively binds the Spc24-Spc25 base of the NDC80 complex, inhibiting this way the interaction of the NDC80 complex with the MIND and SPC105 complexes (Bock et al., 2012). In a similar way, Ybp2, which is recruited in a CBF3-dependent manner, may act as a negative regulator of the association between outer-central kinetochore complexes (NDC80-COMA-MIND) (Ohkuni et al., 2008). In addition, Ybp2 shares domains and interacts with Slk19 (Ohkuni et al., 2008), a FEAR network component that has been shown to cluster kinetochores (Richmond et al., 2013).

1.3.3. The microtubule-kinetochore interface: attaching, pulling and correcting

The last complexes to be recruited to the kinetochore are those able to bind microtubules. These allow chromosome attachment to the mitotic spindle and thus direct correct chromosome segregation. Important questions remain as to how kinetochore attachments are made and maintained to dynamic microtubule-ends that are constantly polymerising and depolymerising, how incorrect attachments are prevented and corrected, and how do kinetochores couple the force of microtubule depolymerisation with chromosome pulling and movement?

The human outer kinetochore (KMN network) is composed of the MIS12, KNL1 and NDC80 complexes, all which have orthologs in the budding yeast (MIND, SPC105 and NDC80 complexes respectively). In addition, yeast has a non-conserved complex, the DAM1/DASH whose function is performed by the mammalian SKA complex (Table 1.1). The heterotrimeric essential SPC105 complex (one Spc105 protein with two Kre28 proteins) binds NDC80 and MIND complexes and microtubules *in vitro*. The SPC105 complex has been shown to be necessary for recruitment of MAPs (Bim1, Bik1, Slk19) and motors (Cin8, Kar3) to the kinetochore and in turn necessary for bipolar attachment. It is also involved in SAC activity. These functions are conserved in the orthologous human complex KNL1 (Pagliuca et al., 2009).

One of the best studied and conserved kinetochore complexes, the NDC80 complex is formed by four essential proteins: the heterodimers Ndc80-Nuf2 and Spc24-Spc25 connected by their coiled coil region, forming a rod like structure with globular regions at

both ends. The Spc24-25 globular domain is embedded in the kinetochore and the Ndc80-Nuf2 globular domain binds to microtubules (Tanaka and Desai, 2008).

The NDC80 complex binds microtubules directly and mutants in the genes encoding the subunits have profound chromosome segregation defects comparable to mutations in components of the CBF3 complex (Cheeseman et al., 2002; Westermann, Drubin and Barnes, 2007). A loop on the coiled coil region of Ndc80 is necessary for binding to the DAM1/DASH complex member Dam1. Although mutating or deleting this sequence has no effect on lateral microtubule binding of the NDC80 complex, end-on attachment and bi-orientation are defective (Maure et al., 2011).

The NDC80 complex has no intrinsic ability to track microtubule plus-ends and binds microtubules laterally and weakly. In contrast, DAM1 can track microtubule plus-ends and by binding to NDC80 enhances its recruitment and attachment to dynamic microtubule tips by acting like a processivity factor to maintain the kinetochore attached to growing or shrinking microtubules. These findings suggest a mechanism for how the force of depolymerisation could be collected by Dam1 and transmitted to the kinetochore though the Ndc80 complex. Phosphorylation of Dam1 by Ipl1 (the yeast homolog of Aurora B) regulates the affinity of Dam1 for the microtubule lattice as well as the interaction between Dam1 and Ndc80 complexes. In addition, Ipl1 also phosphorylates Ndc80 reducing its affinity for microtubules. Therefore, Ipl1-dependent Dam1 regulation could provide a mechanism to detach incorrect kinetochore-microtubule attachments (Gestaut et al., 2008; Lampert, Hornung and Westermann, 2010; Tien et al., 2010).

The DAM1/DASH complex is a heterodecamer formed by 10 proteins with 1:1 stoichiometry (Table 1.1) (Cheeseman et al., 2001) that forms rings around microtubules *in vitro* (Miranda et al., 2005; Westermann et al., 2005). The assembly of these rings and their interaction with microtubules has been modelled from the mapped subunits of the complex (Ramey et al., 2011). One of its members, Hsk3, keeps the complex together as its absence results in 2 subcomplexes, a larger one that binds microtubules but does not form rings (Dam1-Duo1-Spc34-Spc19-Dad1-Dad3) and a smaller one no capable of microtubule binding (Ask1-Dad2-Dad4) (Miranda, King and Harrison, 2007).

Direct orthologs of the DAM1 complex are not present in higher eukaryotes and, while present, the complex is not essential in fission yeast. While Dam1 is the binding partner of the Ndc80 loop in budding yeast, in human cells, Cdt1 and Ska have been found to bind this loop. Two models have been proposed to describe these interactions. In the “Sleeve model”, Cdt1 mediates a conformational change in Ndc80, which allows Ska to

bind and cluster Ndc80 units together forming a sleeve. In the “Sleeve and clamp model”, Ska and Cdt1 cooperate to form a ring around the microtubules (Matson and Stukenberg, 2012).

In fission yeast, kinetochores bind to 3 microtubules instead of only one and the Ndc80 loop binds the microtubule-associated protein Dis1/TOG that may have an analogous role to Dam1 in budding yeast (Hsu and Toda, 2011). Dam1 in fission yeast is phosphorylated by Plo1 (polo kinase) and this promotes bi-orientation. Differences in Dam1 regulation have been attributed to the different number of kinetochore-microtubule binding sites (Buttrick et al., 2012).

In budding yeast, the DAM1 complex harnesses microtubule dynamics to produce the necessary force for chromosome movement and ensuring chromosome segregation. The DAM1 rings observed *in vitro* are capable of maintaining binding to the tip of growing and shrinking microtubules even when external forces are applied (Asbury et al., 2006). Two models have been described to explain how kinetochores maintain their attachment to dynamic microtubules and couple this to chromosome movement. The “power stroke” or “conformational wave” model describes a DAM1 ring complex that would act to couple the force collected from curling protofilaments of depolymerising microtubules to the kinetochore, causing movement of chromosomes (Asbury, Tien and Davis, 2011). However, smaller oligomers or patches of Dam1 also track depolymerising microtubule ends (Grishchuck et al., 2008). An alternative to this is the “biased diffusion” model, in which binding and unbinding between the kinetochore and the microtubule occur constantly, and attachment’s diffusion is favoured towards the microtubule tip (Hill, 1985; Asbury, Tien and Davis, 2011). In this model, DAM1 would diffuse toward microtubule ends instead of dissociating, biased towards a lower free energy (Gao et al., 2010).

DAM1 rings form around microtubules when 16-25 purified complexes are present, and multiple rings and helices at higher concentrations (Grishchuck et al., 2008). Fluorescent microscopy using GFP-tagged kinetochore proteins initially measured enough copies (16-20) of DAM1 complex (Joglekar et al., 2006) to form a ring around MTs and more recent measurements (~32 copies) (Lawrimore, Bloom and Salmon, 2011) would be enough for multiple rings and helices too. In addition, EM imaging of purified kinetochores bound to stabilised microtubule ends supports a ring model (Gonen et al., 2012). Recently, an oligomerisation-deficient Dam1 complex has been shown to bind kinetochores and microtubules, however, it was not capable to couple to dynamic microtubules under tension *in vitro* to support bipolar attachments (Umbreit et

al., 2014). However, these rings have not been observed *in vivo* and thus, how the DAM1 complex is arranged and how it achieves its function remains elusive.

One final puzzle is that the kinetochore appears to be capable of assembling in reverse. If Ask1 is fused directly to the DNA via an artificial protein tether, functional chromosome segregation is achieved (Lacefield, Lau and Murray, 2009). However, inner kinetochore proteins are still required despite the fact that no-canonical CEN sequence exists. This includes recruitment of Cse4 and the CBF3 complex (Ho et al., 2014) and suggests that the DAM1 complex is important for Cse4 localisation.

1.3.3.1. The mitotic checkpoint proteins: a surveillance mechanism for attachment errors

Chromosome segregation starts with pairs of replicated sister chromatids (chromosomes) closely aligned and bound together by cohesion. Each pair of sister chromatids has two centromeres and two kinetochores and each of these must be attached to opposite spindle poles to achieve biorientation, in what is called amphitelic attachments. The formation of kinetochore-microtubule (k-MT) attachments is a dynamic process of alternating association and dissociation. During the process of kinetochore-microtubule capture, transient incorrect attachments occur such as when only one kinetochore is attached while the other remains unattached (monotelic), or when the lateral attachment has not been converted to end-on attachment. Furthermore, abnormal attachments can occur, for instance, when both kinetochores are attached to the same pole (syntelic). Segregation of non-bioriented chromosomes leads to aneuploidy, thus, the cell must be able to recognise and destabilise incorrect attachments in order to free the kinetochores to form new attachments (increasing detachment frequency), while being able to stabilise correct attachments (Cheeseman, 2014; Godek, Kabeche and Compton, 2015).

Only bipolar attachments are stable and lead to anaphase progression. One mechanism to recognise bioriented k-MT attachments is tension produced at the centromeres by pulling sister kinetochores in opposite directions while the chromatids remain associated by cohesin (McAinsh, Tytell and Sorger, 2003; Tanaka et al., 2005). The major player in tension sensing is the kinase Ipl1 (Aurora B) that is part of the chromosomal passenger complex (CPC) (Table 1.1). In this model, Aurora B at the inner kinetochore between sister chromatids cannot phosphorylate its outer kinetochore substrates when tension is achieved due to the extended kinetochore structure and this stabilises the attachment (Cheeseman, 2014). However, new work has suggested that Aurora B clustering in

either microtubules or centromeric chromatin can discriminate between correct and incorrect attachments to support biorientation (Campbell and Desai, 2013).

Localisation of the CPC complex changes throughout mitosis and reflects its multiple roles in chromosome condensation, bi-orientation, activation of the spindle assembly checkpoint (SAC), spindle anaphase, disassembly and cytokinesis. The CPC kinase Ipl1 is necessary for destabilising and correcting incorrect attachments, for instance, by negatively regulating the budding yeast outer kinetochore DAM1 and NDC80 complexes or the mammalian SKA complex, as well as the microtubule stabiliser Dia3 (Carmena et al., 2012).

By destabilising incorrect k-MT attachments, the CPC activates the SAC to provide extra time for new attachments to form. The SAC is only active at unattached kinetochores and delays anaphase progression by inhibiting the anaphase-promoting complex (APC). In budding yeast, the SAC is activated when Mps1 is recruited to unattached kinetochores and phosphorylates kinetochore proteins such as Spc105, whose phosphorylation recruits Bub1-Bub3. Phosphorylation of Bub1 by Mps1 in turns recruits Mad1, which serves as a scaffold to convert soluble open Mad2 (O-Mad2), which is inactive, into the activated closed Mad2 (C-Mad2) (London and Biggins, 2014). The active C-Mad2 can form a complex with Mad3 and Bub3, the mitotic checkpoint complex (MCC) that can inactivate the APC by binding to its activator Cdc20 (Lau and Murray, 2012), and thus prevents cohesin cleavage.

Once chromosomes are bioriented, Mps1 disassociation from Spc105 allows for SAC silencing and anaphase progression, and it has been suggested that the structural shape of the end-on attachment is what produces a physical separation between Mps1 and the kinetochore proteins, with Dam1 possibly acting as a barrier (Aravamudhan, Goldfarb and Joglekar, 2015). The APC complex is then free to degrade securin, an inhibitor of separase. Free separase cleaves cohesin and sister chromatids are released from each other and segregate towards opposite poles maintaining their end-on microtubule attachments (McAinsh, Tytell and Sorger, 2003; Peters, 2006). In addition, separase activates Cdc14, which mediates mitotic exit (Queralt and Uhlmann, 2008).

A homeostatic system has been described for mammalian cells in which the outer kinetochore acts as a receptor that senses attachment stability and sends a signal to a core control network. This network, composed by the SAC, cyclin-CDK, Aurora and Polo kinases, responds by activating effectors, such as microtubule stabilisers and destabilisers and phosphatases (PP1, PP2A) that regulate the system by providing negative feedback to the core (Godek et al., 2015).

1.4. Regulation of kinetochores by posttranslational modifications

In addition to the interactions between the ~70 proteins forming the kinetochore from CEN DNA to microtubules, a number of kinases, phosphatases and ubiquitin ligases regulate the kinetochore. Thus multiple post-translational modifications are emerging as important regulators of the kinetochore.

Multiple phosphorylation sites have been identified in kinetochore proteins (Cheeseman et al., 2002; Funabiki and Wynne, 2013). The main phospho-regulator of the kinetochore is the conserved kinase Ipl1 (human Aurora B). This serine/threonine kinase is part of the chromosomal passenger complex (CPC), whose localisation is in turn regulated by the cyclin kinase Cdc28 (Cdk1) and the phosphatase Cdc14 (Carmena et al., 2012). Ipl1 regulates the kinetochore-microtubule attachment by phosphorylating Ndc80 and several members of the DAM1 complex (Dam1, Ask1, Spc34, Spc19) (Cheeseman et al., 2002). Furthermore, Ipl1 phosphorylation during anaphase of Bim1 (EB1) unloads this MAP protein from spindle microtubules to promote spindle elongation (Zimniak et al., 2009) and phosphorylation of mitotic spindle protein She1 promotes spindle disassembly (Makrantoni et al., 2014). Moreover, Ipl1 not only has functions on the kinetochore-microtubule interface and its been shown to phosphorylate inner and central components such as Mif2, Cep3 and Dsn1 (Westermann et al., 2003). For instance, Dsn1 (MIND complex) phosphorylation by Ipl1 promotes interactions between inner and outer complexes (Akiyoshi et al., 2013) and Ipl1 phosphorylation of the H3/Cse4 has been suggested to have a role in destabilizing defective kinetochores (Boeckmann et al., 2013). Other kinases include Mps1, which recruit other SAC members to the kinetochore (see section 1.3.3.1).

The activity of kinases is antagonised by phosphatases. One example is the phosphatase Glc7 (PP1) which functions in chromosome segregation by dephosphorylating Ipl1 and Mps1 targets and for instance, it silences the SAC once correct attachments are formed (Pinsky, Nelson and Biggins, 2009; Vanoosthuyse and Hardwick, 2009). For instance, in budding yeast it counteracts Mps1 recruitment of Bub1 to the kinetochore during SAC activation (London et al., 2012). Cdc14 is another phosphatase and dephosphorylates Cdc28 (Cdk1) targets to exit mitosis during anaphase. The finding that Cdc14 dephosphorylates Dsn1 (MIND complex) during metaphase raises the possibility of new kinetochore targets outside anaphase (Akiyoshi and Biggins, 2010).

Cse4 is modified in multiple ways in addition to phosphorylation. For instance, absence of methylation of arginine 37 of Cse4 reduces MIND complex levels without reducing

Cse4, thus being necessary for full kinetochore assembly (Samel et al., 2012). Further, Cse4 levels are controlled by the E3 ubiquitin ligase Psh1, which targets Cse4 for degradation by ubiquitination of excess and ectopically localised protein (Hewawasam et al., 2010; Ranjitkat et al, 2010). Other kinetochore proteins have also been shown to be regulated by ubiquitination, such as Dsn1 by the Mub1/Ubr2 ubiquitin ligase (Akiyoshi et al, 2013). Additionally, several kinetochore proteins from the CBF3 complex (Ndc10 and Cep3) and CPC (Bir1), all which relocalise to the midzone in anaphase, as well as Ndc80 (NDC80) are modified by the ubiquitin-like SUMO (Smt3 in budding yeast) (Montpetit et al., 2006).

1.5. When the kinetochore fails

Checkpoint failure to detect unattached or incorrect kinetochore-microtubule attachments, such as merotelic attachments, likely lead to daughter cells inheriting different number of chromosomes, known as aneuploidy (Holland and Cleveland, 2009). Germline aneuploidy arising during meiosis is thought to account for the majority of miscarriages and some common birth defects such as Down syndrome are caused aneuploidy. In somatic cells, on the other hand, aneuploidy is a hallmark of cancer cells, but it is not clear whether cancer causes aneuploidy or vice versa.

In addition to the regulation of accurate bi-orientation of chromosomes, kinetochore and spindle alignment defects have implications for cancer cell metastasis and stem cell homeostasis. Changes in the orientation of the mitotic spindle in epithelial tumour cells could misplace daughter cells from the basal epithelia, promoting an epithelial-mesenchymal transition that allows cell movement and metastasis (Pease and Tirnauer, 2011). Adult stem cell homeostasis is maintained in some cases by asymmetric division, which generates one stem cell and one progenitor. Misorientation of the mitotic spindle can generate symmetric cell divisions, which alter the balance between self-renewal and differentiation (Cabernard and Doe, 2009).

1.5.1. Aneuploidy: a hallmark of cancer cells

Genomic instability (GIN) refers to a high frequency of mutations, chromosomal rearrangements and aneuploidy and it is characteristic of cancer cells. Many factors lead to these different aberrations, such as defects in DNA replication and repair, telomere maintenance, cell cycle and chromosome segregation. An increase in chromosome segregation errors caused by defects during mitosis leads to chromosomal instability (CIN), which lead to aneuploidy (Giam and Rancati, 2015).

Aneuploidy is present in a large percentage of tumours and it has been shown to be deleterious and promote tumorigenesis (Weaver and Cleveland, 2006; Pellman, 2007; Siegel and Amon, 2012). Many studies have shown that mutant or overexpressed SAC genes induce aneuploidy that results in cancer development (Weaver et al., 2007; Sotillo et al., 2007). Recently, aneuploidy has been linked to aging, in addition to cancer and development (Ricke and Deursen, 2013). Many studies have described how CIN causes aneuploidy and it has been proposed that the way aneuploidy leads to tumorigenesis is by affecting gene expression, altering cell metabolism (Dephoure et al., 2014) and driving cellular transformation throughout changes in levels of oncogenes and tumour suppressors (Giam and Rancati, 2015).

Although it was thought that chromosome segregation errors lead to aneuploidy and chromosome aberrations were caused by DNA damage, Janssen et al (2011) showed that chromosome missegregation can directly cause structural defects in chromosomes during cytokinesis. Furthermore, the Pellman lab has described another mechanism by which chromosome missegregation causes DNA damage and which could also explain chromothripsis, a recently discovered phenomenon in which only one chromosome or chromosome arm contains rearrangements (Stephens et al., 2011). Mitotic segregation errors can result in formation of micronuclei around lagging chromosomes. Inside the micronuclei, DNA replication and repair are defective, possibly as result of defective nuclear import of factors, and this leads to accumulation of DNA damage and fragmentation. Upon nuclear envelope breakdown during the next cell cycle, the aberrant chromosome can be distributed to the new cell (Crasta et al., 2012).

Thus, the relationship between CIN, aneuploidy and cancer seems to be more complex than first thought and not a linear relationship.

1.5.2. Aneuploidy as an evolutionary adaptation

Although aneuploidy had been shown to be deleterious to budding yeast cells under normal circumstances, a study by Rancati et al (2008) suggested that cells use aneuploidy as a rapid adaptive mechanism under conditions of stress. Aneuploidy induces genome-wide variation in gene expression, which can in turn lead to phenotypic variation. Cancer cells may use aneuploidy as a way to rapidly alter their phenotype (Siegel and Amon, 2012).

In large populations of single cell organisms, variation caused by aneuploidy provides an advantage and evolutionary adaptation, and aneuploidy has been found to be present in wild yeast, for instance (Chen, Rubinstein and Li, 2012). In cancer cells

aneuploidy may play a role in drug resistance (Duesberg et al., 2007). On the other hand, aneuploidy is deleterious for the individual cell or organism. Nevertheless, cases of aneuploidy have been found in normal human tissues (Chen, Rubinstein and Li, 2012). It seems that the deleterious or advantageous effect of each specific karyotype produced by aneuploidy would depend on the specific environment (Giam and Rancati, 2015). An example of whole organism aneuploidy, Down's syndrome is associated with increased incidence of child leukemia, however, it is also linked to decreased incidence of solid tumours (Hasle, Clemmensen and Mikkelsen, 2000; Chen, Rubinstein and Li, 2012).

1.6. Approaches to study the kinetochore

In order to determine how correct chromosome segregation is achieved, we need to understand how kinetochores are organised and regulated. The complexity of these structures became obvious with the discovery of many new kinetochore proteins in the last decade. Efforts to understand the function of these proteins examined the interactions between them. A combination of methods including co-immunoprecipitation (coIP), copurification and mass spectrometry studies have identified and grouped numerous kinetochore proteins into complexes (Lechner and Carbon 1991; Janke et al., 2001 and 2002; Cheeseman et al., 2001 and 2002; Westermann et al., 2003), and two-hybrid studies have shed light on how members of these complexes are organised and how the complexes are connected to form the kinetochores (Shang et al., 2003). However, much is still unknown about the structure and organisation of kinetochores and their associated proteins and how they assemble and connect DNA to the spindle microtubules.

Recently, *in vitro* approaches combined with microscopy and computational analyses have been used to study how kinetochore-microtubule attachments and chromosome movements are achieved in different organisms (Driver et al., 2014; Armond et al., 2015). A method for purifying kinetochores has been developed in the Biggins lab which will shed more light into this questions by experimenting *in vitro* (Akiyoshi et al., 2009; Akiyoshi et al., 2010) and it is being used, for example, to reconstruct the kinetochore-microtubule interphase (Akiyoshi and Biggins, 2010). Other labs are joining this effort to reconstruct budding yeast (Gestaut et al., 2010) and human (Altenfeld et al., 2015) kinetochores as well as the minimal mitotic spindle (Hsia et al., 2014) in order to understand how kinetochores assemble and function to ensure correct chromosome segregation.

1.6.1. Visualising kinetochores by fluorescence microscopy

Unlike in animal cells, the 16 centromeres in budding yeast cluster together forming a single focus (Guacci, Hogan and Koshland, 1997). This makes budding yeast a good system to study and quantify kinetochores by fluorescence microscopy. By tagging the kinetochore and the spindle pole body fluorescently we can follow cell division (Figure 1.3). During G1 phase, cells are unbudded and only one focus for the SPB and one for the kinetochore are visible. Chromosomes remain attached to microtubules (Dorn et al., 2005). A small bud emerges at the start of S-phase, while DNA replicates, which will grow to form a daughter cell. Yeast has closed mitosis and thus the nuclear envelope doesn't break unlike in animal cells and chromatin cannot be seen separated until anaphase. Before DNA replication, kinetochores are visualised as a single focus (green) in the nucleus very close to the SPB foci (red). As the SPB duplicates a second SPB focus becomes visible in microscopy images, shortly thereafter the kinetochore clusters also separate. Once the nucleus is positioned at the bud neck and sister SPBs and kinetochores are located in opposite poles (bioriented), the foci can be seen being further apart until finally mitosis is completed and each daughter cell remains with a single focus for each, kinetochore and SPB.

A number of studies have used fluorescence to quantify the levels of specific proteins at the kinetochore and this will be reviewed in more detail in chapter III.

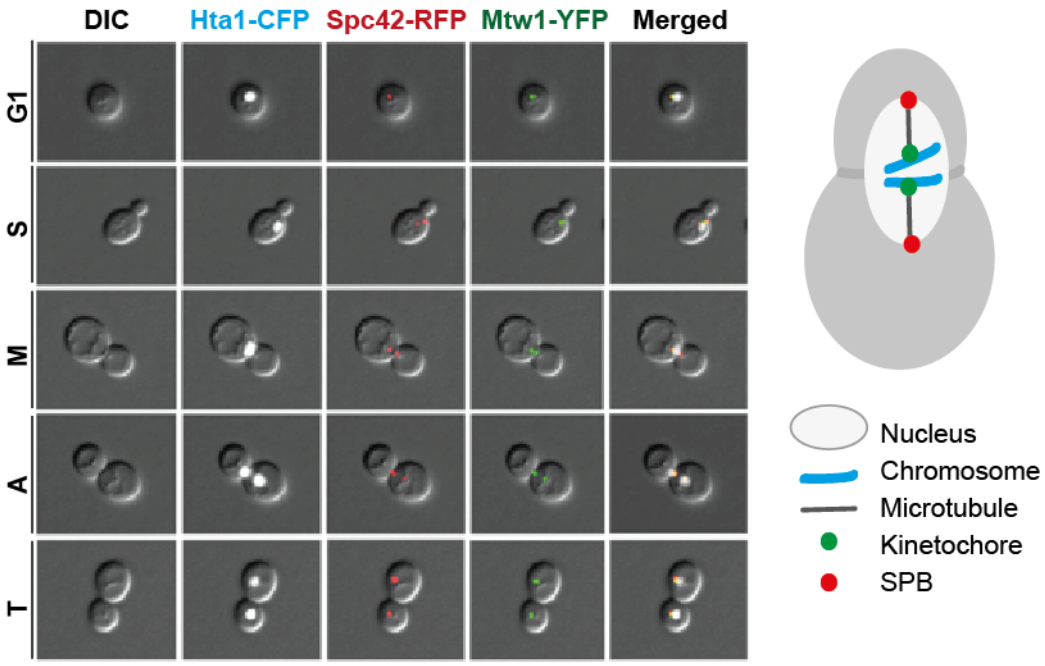

Figure 1.3 Visualising kinetochores through the cell cycle. A budding yeast cell with tagged nucleus (Hta1-CFP) in white, SPB (Spc42-RFP) in red and the kinetochore (Mtw1-YFP) in green, is shown thought the different stages of mitosis: G1, S-phase (S), metaphase (M), anaphase (A) and telophase (T).

1.7. Hypothesis and aims of the thesis

This project is focused upon two main questions. First, I aim to identify genes that affect kinetochore function by a reverse genetics approach. I will transfer fluorescently tagged kinetochore proteins into deletion strains (non-essential knock outs) and temperature sensitive (TS) alleles (essential genes), and then image the resulting fluorescent proteins using fluorescence microscopy. The effect of each mutant on the kinetochore proteins will be assessed by quantitative and qualitative analysis of the resulting fluorescence images. My hypothesis is that genes affecting kinetochore function will produce phenotypic changes, for instance, in concentration or localisation, of the mitotic spindle and that those will be detectable by fluorescence microscopy. I aim to produce a list of mutants that affect the phenotype of a kinetochore protein, e.g. changes in levels and localisation. Second, I aim to identify the molecular mechanism underlying some phenotypic changes identified in part one.

1.8. Summary of findings

Fluorescence analysis of an array of mutants with the SPB protein Spc42 tagged with RFP and the outer kinetochore protein Dad4 (DAM1 complex) with YFP has revealed that less than 3% of the non-essential gene deletions and ~27% of essential temperature sensitive alleles caused a change on Dad4-YFP intensity, or an aberrant Dad4 localisation. Some examples are 5 non-essential chromatin remodelers, which decreased Dad4 intensity while they did not affect Mtw1 fluorescence. A large number of mRNA processing mutants produced phenotypes in Dad4 including all the core members of the nonsense-mediated mRNA decay (NMD) pathway. Moreover, the microtubule plus-end tracking proteins Stu1, Stu2, Bim1, Bik1 all produced phenotypes on Dad4. Finally, a kinase member of the Cell Wall Integrity Pathway (CWI), Pkc1 (mammalian PKC), produced a kinetochore phenotype that was seen across the entire kinetochore. I investigated the mechanism underlying this phenotype and find that it likely arises from defective microtubule function, which may also be linked to actin regulation and the Hog1 stress pathway in budding yeast.

2. Chapter II: Materials and Methods

2.1. Buffers and solutions

Buffers and solutions used are shown in Table 2.1.

Table 2.1. Buffers and solutions

Buffer/Solution	Composition
TE (1x)	10 mM Tris-HCl pH 7.5, 1 mM EDTA
Smash-n-Grab buffer	1% SDS, 2% Triton-X-100, 100 mM NaCl, 10 mM Tris-HCl pH8, 1 mM EDTA
SOC medium	2% tryptone, 0.5% yeast extract, 1 mM NaCl, 0.2 g/L KCl, autoclave and then add 20 mM glucose, 10 mM $MgCl_2$, 10 mM $MgSO_4$
TAE	40 mM Tris (pH 7.6), 20 mM acetic acid, 1 mM EDTA
10x DNA loading dye	25% $Ficoll_{400}$ 10 mM Tris-HCl, 1 mM EDTA, 2.5 mg/ml
Lysis buffer	0.1 M NaOH, 0.05 M EDTA, 2% SDS, 2% b-mercaptoethanol
Loading buffer	0.25 M Tris-HCl pH 6.8, 50% glycerol, 0.05% bromophenolblue
Running buffer (1X)	25 mM Tris, 192 M glycine, 0.1% SDS
Transfer buffer (1X)	25 mM Tris, 192 M glycine, 20% methanol
PBS (for WB)	0.01 M phosphate buffer, 2.7 mM potassium chloride, 0.137 M sodium chloride, pH 7.4

2.2. Bacterial methods

2.2.1. Bacterial strains

Competent *E. coli* cells ElectroMAX DH5α-E with genotype (*F-Φ80lacZΔM15 Δ(lacZYA-argF) U169 recA1 endA1 hsdR17 (rk-, mk+) gal- phoA supE44 λ- thi-1 gyrA96 relA1*) (Invitrogen) and ElectroMAX DH10B with genotype (*F-mcrA Δ(mrr-hsdRMS-mcrBC) Φ80lacZΔM15 ∆ lacX74 recA1 endA1 araD139 Δ(ara,leu) 7697 galU galK –rpsL nupG*) (Invitrogen) were used for bacterial work.

2.2.2. *E. coli* growth media and conditions

E.coli were grown in Luria-Bertani broth (LB) (1% bacto-tryptone, 0.5% yeast extract, 1% NaCl pH 7.5 and 1.5% bacto-agar for solid media). For plasmid selection the media was supplemented with 0.05-0.1 mg/ml ampicillin (LB-Amp, Sigma). Liquid cultures were grown at 37°C in a shaker at 300 rpm. Solid media was incubated at 37°C. Plasmids transformed into bacteria were stored at -80°C by mixing 1:1 volume of

overnight culture in LB-Amp with 50% glycerol. To prepare plates containing X-Gal solution (Thermo Scientific) and IPTG (Thermo Scientific), 40 µl of X-Gal (20 ml/mL stock) and 40µl IPTG (100 mM stock) were added to plates and spread evenly with a sterile spatula.

2.2.3. Electroporation in *E.coli*

Transformation of plasmids into *E.coli* was performed by electroporation into competent cells ElectroMAX DH5α-E or ElectroMAX DH10B. 5 µl of ligation reaction and 20 µl 10% glycerol were added to 20 µL of ElectroMAX DH10B competent cells. For plasmid transformation 5 µl of DNA (≧25 ng) and 25 µl 10% glycerol were added to 10 µl DH5α-E. The mixture was then pipetted into a 2 mm Gene Pulser chilled cuvette (Bio-Rad) and electroporated using a Gene Pulser Xcell system (Bio-Rad) at 2.5 KV, 200Ω and 25µF. SOC medium (1ml) was immediately added and the culture was incubated at 37°C (300 rpm) for a minimum of one hour. Transformations were then plated onto LB-Amp plates and incubated at 37°C.

2.2.4. Plasmid purification from *E. coli*

Bacterial cultures (≧4 ml) were grown overnight at 37°C (300 rpm) and cells were collected by centrifugation (3 min, 13,200 rpm). Purification of plasmid DNA was performed by using a GeneJET Plasmid Miniprep Kit (Thermo scientific) following manufacturer's instructions.

2.3. Yeast methods

Yeast methods are based upon Adams, Gottschling and Kaiser (1997) and Treco and Winston (2008).

2.3.1. Yeast strains

Yeast strains and plasmids used are shown in Tables 2.2 and 2.3 respectively and plasmids constructed by gap repair (see section 2.2.5) in Table 2.4.

Table 2.2. Yeast strains

Strain	Genotype	Source
W8164-2C[1]	*MAT**a** trp1-1 his3-11,15 leu2-3,112 ura3-1 RAD5 MET17 ADE2 LYS2 CEN1-16::GAL-K.l.URA3*	Rodney Rothstein
PT33-7B	*MATalpha ADE2 leu2-3,112 TRP1 lys2- HTA1-CFP MTW1-YFP RAD5 SPC42-RFP::HYG*	Eva Herrero
T6	*[DAD2-YFP SPC42-RFP LEU2 AMP] MAT**a** trp1-1 his3-11,15 leu2-3,112 ura3-1 RAD5 MET17 ADE2 LYS2 CEN1-16::GAL-K.l.URA3 dad2Δ::KAN*	This study
T7	*[DAD4-YFP SPC42-RFP LEU2 AMP] MAT**a** trp1-1 his3-11,15 leu2-3,112 ura3-1 RAD5 MET17 ADE2 LYS2 CEN1-16::GAL-K.l.URA3 dad4Δ::KAN*	This study
T8	*[DAD3-YFP SPC42-RFP LEU2 AMP] MAT**a** trp1-1 his3-11,15 leu2-3,112 ura3-1 RAD5 MET17 ADE2 LYS2 CEN1-16::GAL-K.l.URA3 dad3Δ::KAN*	This study
U2804-1	*MAT**a**/alpha CAN1/can1::STE2pr-Sp_his5 LYP1/lyp1Δ::STE3pr-LEU2 RAD5/RAD5 DYN1/dyn1Δ::KanMX*	Rodney Rothstein
E79-12C	*MAT**a** can1::STE2pr-Sp_his5 lyp1Δ::STE3pr-LEU2 trp1-1 LYS2 leu2-3,112 his3-11,15 MET15 ura3-1 DYN1*	This study
E79-17D	*MATα lyp1Δ::STE3pr-LEU2 can1::STE2pr-Sp_his5 trp1-1 LYS2 leu2-3,112 his3-11,15 MET15 ura3-1 DYN1*	This study
T10	*MATα ADE2 lyp1Δ::STE3pr-LEU2 can1::STE2pr-Sp_his5 trp1-1 LYS2 leu2-3,112 his3-11,15 MET15 ura3-1 DYN1*	This study
T26	*MATα lyp1Δ::STE3pr-LEU2 can1::STE2pr-Sp_his5 trp1-1 LYS2 leu2-3,112 his3-11,15 MET15 ura3-1 DYN1 ADE2+ SPC42-RFP::HYGMx*	This study
T27	*MAT**a** can1::STE2pr-Sp_his5 lyp1Δ::STE3pr-LEU2 trp1-1 LYS2 leu2-3,112 his3-11,15 MET15 ura3-1 DYN1 ADE2+*	This study
T29	*MAT**a** can1::STE2pr-Sp_his5 lyp1Δ::STE3pr-LEU2 trp1-1 LYS2 leu2-3,112 his3-11,15 MET15 ura3-1 DYN1 ADE2+ SPC42-RFP::HYGMx*	This study
T34	*MATα can1::STE2pr_Sp_his5 lyp1Δ::STE3pr-LEU2 SPC42-RFP::HYG, DAD4-YFP::NAT*	This study
T35	*MATα can1::STE2pr_Sp_his5 lyp1Δ::STE3pr-LEU2 SPC42-RFP::HYG, DAD3-YFP::NAT*	This study
T36	*MATα can1::STE2pr_Sp_his5 lyp1Δ::STE3pr-LEU2 SPC42-RFP::HYG, NDC10-YFP::NAT*	This study
T37	*MAT**a** can1::STE2pr_Sp_his5 lyp1Δ::STE3pr-LEU2 SPC42-RFP::HYG, DAD4-YFP::NAT*	This study
T38	*MAT**a** can1::STE2pr_Sp_his5 lyp1Δ::STE3pr-LEU2 SPC42-RFP::HYG, DAD3-YFP::NAT*	This study
T39	*MAT**a** can1::STE2pr_Sp_his5 lyp1Δ::STE3pr-LEU2 SPC42-RFP::HYG, NDC10-YFP::NAT*	This study
PT176	*HTA1-CFP MTW1-YFP SPC42-RFP::HYG snf2Δ::KANMx*	This study
PT177	*HTA1-CFP MTW1-YFP SPC42-RFP::HYG rsc1Δ::KANMx*	This study
PT178	*HTA1-CFP MTW1-YFP SPC42-RFP::HYG rsc2Δ::KANMx*	This study
PT179	*HTA1-CFP MTW1-YFP SPC42-RFP::HYG ylr358cΔ::KANMx*	This study
PT180	*HTA1-CFP MTW1-YFP SPC42-RFP::HYG bim1Δ::KANMx*	This study
PT181	*HTA1-CFP MTW1-YFP SPC42-RFP::HYG bik1Δ::KANMx*	This study
T494	*MATα can1::STE2pr_Sp_his5 lyp1Δ::STE3pr-LEU2 SPC42-RFP::HYG, DAD4-YFP::NAT pkc1pPKC1::URA3*	This study
PT213-11B	*MATα pkc1pPKC1::URA3 pkc1-1::KAN SPC42-RFP::HYGMx DAD4-YFP::NAT*	This study

PT91-18C	*MAT***a** *TRP1 MTW1-YFP RAD5 SPC42-RFP::HYG pkc1-1::KANMx*	This study
PT92	*MAT***a** *DAD3-YFP::NAT SPC42-RFP::HYG pkc1-1::KANMx*	This study
T397	*MAT***a** *his3Δ1 leu2Δ0 met15Δ0 ura3Δ0 TRP LYS NDC10-GFP::HIS3 pkc1-ts::KANMx*	This study
T343	*MATα SPC42-RFP::HYGMx DAD4-YFP::NAT ura3-1::URA3 pGAL-A-PKC1-B-ADH1term_pX48*	This study
T344	*MATα SPC42-RFP::HYGMx DAD4-YFP::NAT ura3-1::URA3 pGAL-A-B-ADH1term_pX48*	This study
T345	*MATα HTA1-CFP MTW1-YFP SPC42-RFP::HYG ura3-1::URA3 pGAL-A-PKC1-B-ADH1Term_pX48*	This study
T346	*MATα HTA1-CFP MTW1-YFP SPC42-RFP::HYG ura3-1::URA3 pGAL-A-B-ADH1Term_pX48*	This study
T350	*MAT***a** *SPC42-RFP::HYGMx DAD4-YFP::NAT ura3-1::URA3 pGAL-A-PKC1-B-ADH1term_pX48*	This study
T351	*MAT***a** *SPC42-RFP::HYGMx DAD4-YFP::NAT ura3-1::URA3 pGAL-A-B-ADH1term_pX48*	This study
T377	*MATα SPC42-RFP::HYGMx DAD3-YFP::NAT ura3-1::URA3 pGAL-A-PKC1-B-ADH1term_pX48*	This study
T378	*MATα SPC42-RFP::HYGMx DAD3-YFP::NAT ura3-1::URA3 pGAL-A-B-ADH1term_pX48*	This study
T379	*MATα SPC42-RFP::HYGMx NDC10-YFP::NAT ura3-1::URA3 pGAL-A-PKC1-B-ADH1term_pX48*	This study
T380	*MATα SPC42-RFP::HYGMx NDC10-YFP::NAT ura3-1::URA3 pGAL-A-B-ADH1term_pX48*	This study
T381	*MAT***a** *SPC42-RFP::HYGMx DAD3-YFP::NAT ura3-1::URA3 pGAL-A-PKC1-B-ADH1term_pX48*	This study
T382	*MAT***a** *SPC42-RFP::HYGMx DAD3-YFP::NAT ura3-1::URA3 pGAL-A-B-ADH1term_pX48*	This study
T383	*MAT***a** *SPC42-RFP::HYGMx NDC10-YFP::NAT ura3-1::URA3 pGAL-A-PKC1-B-ADH1term_pX48*	This study
T384	*MAT***a** *SPC42-RFP::HYGMx NDC10-YFP::NAT ura3-1::URA3 pGAL-A-B-ADH1term_pX48*	This study
T506	*MAT***a** *can1::STE2pr_Sp_his5 lyp1Δ::STE3pr-LEU2 SPC42-RFP::HYG, DAD4-YFP::NAT hom2Δ::KANMx*	This study
T507	*MAT***a** *can1::STE2pr_Sp_his5 lyp1Δ::STE3pr-LEU2 SPC42-RFP::HYG, DAD4-YFP::NAT hom3Δ::KANMx*	This study
T508	*MATα can1::STE2pr_Sp_his5 lyp1Δ::STE3pr-LEU2 SPC42-RFP::HYG, DAD4-YFP::NAT TUB1-CFP::URA3*	This study
T509	*MATα can1::STE2pr_Sp_his5 lyp1Δ::STE3pr-LEU2 SPC42-RFP::HYG, DAD4-YFP::NAT TUB1-CFP::URA3 pkc1-1::KANMx*	This study
PT147-3B	*MATα TRP1 lys2Δ his3-11,15 leu2-3,112 ura3-1 SPC42-RFP::HYGMx DAD4-YFP::NAT*	This study
T393	*MATα TRP1 lys2Δ his3-11::ADH-AFB2::HIS3,15 leu2-3,112 ura3-1 SPC42-RFP::HYGMx DAD4-YFP::NAT*	This study
PT211-9B	*MATα TRP1 lys2Δ his3-11::ADH-AFB2::HIS3,15 leu2-3,112 ura3-1 PKC1-AID-FLAGS::URA3Kc SPC42-RFP::HYGMx DAD4-YFP::NAT*	This study
GFP library[2]	*MAT***a** *his3Δ1 leu2Δ0 met15Δ0 ura3Δ0 TRP LYS XXX-GFP::HIS3*	Grant Brown
Deletion library[3]	*MATα his3Δ1 leu2Δ0 lys2Δ0 ura3Δ0 xxxΔ::KANMX4*	Rodney Rothstein
TS Collection[4]	*MAT***a** *his3Δ1 leu2Δ0 met15Δ0 ura3Δ0 xxx-ts::KANMX*	Brenda Andrews

[1]Reid et al (2011), [2]Huh et al (2003), [3]Winzeler et al (1999) and [4]Li et al (2011).

Table 2.3. Plasmids

Plasmid	Genotype	Source
pHT5	*YFP SPC42-RFP LEU2 β-lactamase*	Erika Aquino
pX48	*Ylplac211 URA3*	Eva Herrero
pHT166	*TUB-CFP β-lactamase LEU2*	Eva Herrero
pHT324	*pPKC1-PKC1 URA3 β-lactamase*	This study
pHT325	*pPKC1-PKC1 URA3 β-lactamase*	This study
pHT389	*pGAL-A-PKC1-B-ADH1Term URA3 β-lactamase*	This study
pHT390	*pGAL-A-B-ADH1Term URA3 β-lactamase*	This study

Table 2.4. Plasmids constructed by gap repair

Plasmid name	Gene	Source	Plasmid name	Gene	Source
pHT8	IPL1	Erika Aquino	pHT62	KIP1	Erika Aquino
pHT12	CEP3	Erika Aquino	pHT63	DAD4	Erika Aquino
pHT13	OKP1	Erika Aquino	pHT64	HSK3	Erika Aquino
pHT14	BIM1	Erika Aquino	pHT65	BUB3	Erika Aquino
pHT15	MTW1	Erika Aquino	pHT66	DYN2	Erika Aquino
pHT17	BIK1	Erika Aquino	pHT67	CNN1	Peter Thorpe
pHT18	SPC24	Erika Aquino	pHT68	TUB1	Peter Thorpe
pHT24	CTF19	This study	pHT69	MHF2	Peter Thorpe
pHT25	DAM1	This study	pHT71	CIN8	This study
pHT26	BUB1	Erika Aquino	pHT72	DAD2	This study
pHT27	CTF3	Erika Aquino	pHT73	DAD3	This study
pHT28	ASK1	Erika Aquino	pHT74	MAD3	This study
pHT29	NUF2	Erika Aquino	pHT75	SPC34	This study
pHT30	DSN1	Erika Aquino	pHT76	KAR3	This study
pHT32	NSL1	This study	pHT77	NKP1	Peter Thorpe
pHT33	SPC19	This study	pHT78	NKP2	Peter Thorpe
pHT34	SPC25	This study	pHT79	IML3	Peter Thorpe
pHT35	NNF1	This study	pHT80	CHL4	Peter Thorpe
pHT40	MAD2	Erika Aquino	pHT81	MCM22	Peter Thorpe
pHT41	SLI15	Erika Aquino	pHT82	MCM16	Peter Thorpe
pHT42	NBL1	Erika Aquino	pHT83	IRC15	Peter Thorpe
pHT43	MCM21	Erika Aquino	pHT84	DYN1	Erika Aquino
pHT44	MOB1	Erika Aquino	pHT85	CDC20	Erika Aquino
pHT47	DAD1	Erika Aquino	pHT86	CBF1	Erika Aquino
pHT48	DUO1	Erika Aquino	pHT87	SKP1	Erika Aquino
pHT49	SGO1	Erika Aquino	pHT88	KIP3	Erika Aquino
pHT50	SPC105	Erika Aquino	pHT89	PAC1	This study
pHT51	NDC80	This study	pHT90	CTF13	This study
pHT52	BIR1	This study	pHT91	NDC10	This study
pHT53	KIP2	Erika Aquino	pHT92	STU1	This study
pHT54	MIF2	Erika Aquino	pHT93	KRE28	This study
pHT55	KIC1	Erika Aquino	pHT94	KAR9	This study
pHT58	AME1	Erika Aquino	pHT100	SCM3	Peter Thorpe
pHT59	WIP1	Peter Thorpe	pHT106	STU2	This study
pHT61	MHF1	Peter Thorpe			

All plasmids code for SPC24-RFP. All plasmids but pHT5 code for “gene”-YFP.

2.3.2. Yeast growth media and conditions

Table 2.5. Yeast growth media

Medium	Composition
YPD rich media	1% yeast extract, 2% bacto-peptone, 2% glucose and 2% bacto-agar for solid media
Synthetic complete (SC) media	109 µM adenine sulphate, 95 µM L-Arginine sulphate, 95 µM L-Histidine HCl, 229 µM L-Isoleucine, 457 µM L-Leucine, 164 µM L-Lysine HCl, 134 µM L-Methionine, 303 µM L-Phenylalanine, 98 µM L-Tryptophan, 166 L-Tyrosine, 178 µM Uracil, 1280 µM L-Valine, 5 g/L ammonium sulphate, 1.7 g/L yeast nitrogen base, 2% glucose and 2.5% difco agar for solid media
Drop out glucose	As SC media without specific supplement(s)
SD media	As SC media without any supplements
SPO	75 mg/l of each: adenine sulphate, L-Histidine HCl, L-leucine, L-Lysine HCl, L-Methionine, L-Tryptophan, Uracil, 0.02 g/ml potassium acetate, 2.5 mg/ml yeast extract, 1 mg/ml glucose and 2% bacto-agar for solid media.
SPO for SGA	12.5 mg/l L-Histidine HCl, 62.5 mg/l L L-leucine, 12.5 mg/l L-Lysine HCl, 12.5 mg/l Uracil, 0.01 g/ml potassium acetate, 1 mg/ml yeast extract, 0.5 mg/ml glucose and 2% bacto-agar for solid media.
5-Fluoroorotic acid (5-FOA)	SC media or the appropriate SD-dropout media containing uracil, 3% bacto-agar, 1 mg/ml 5' FOA

For galactose promoter induction, 2% galactose was added to the media instead of glucose. To prevent soft agar in synthetic media 2 mM NaOH was added to the media to increase the pH before autoclaving. To reduce the amount of phosphoribosylamino-imidazole in cells, an extra 100 mg/litre of adenine was added to our synthetic microscopy media.

To select for drug resistance 300 µg/ml G418 (ChemCruz), 200 µg/ml hygromycin B (Roche), 100 µg/ml nourseothricin (CloNAT) (Werner Bioagents) or 0.05 mg/ml thialysine (Sigma) were added to the media. For addition of G418, hygromycin or NAT to standard drop-out media ammonium sulphate was not used as it reduces the drug efficacy and 1 g/L monosodium glutamate was added. For addition of thialysine to the media lysine drop-out was not used as thialysine is a lysine analog. Microtubule poisons were added to YFP or microscopy media as 15 µg/ml benomyl (Sigma), 15 µg/ml nocodazole (Sigma) or 50-100 µg/ml TBZ (Sigma). Benomyl, nocodazole and TBZ stocks were prepared in DMSO.

Yeast strains were grown at 30°C routinely and at 23°C for microscopy. Temperature sensitive alleles were grown at 23°C as the permissive temperature and 37°C as the restrictive temperature. Strains were stored at -80°C by mixing 1:1 volume of overnight culture in YPD with 50% glycerol.

2.3.3. Determination of cell density

The cell density of yeast cultures was determined by measuring the optical density at 600 nm (OD_{600}) in a CO8000 Cell Density Meter (WPA) using 1cm cuvettes (Fisherbrand).

2.3.4. Spot testing

Cultures were grown overnight at 30°C (23°C for TS alleles) and the $O.D._{600}$ was measured and adjusted. Then 10-fold dilutions were spotted (6 µl spots) onto plates and air dried next to a flame. Plates were incubated at the appropriated temperature for 2-3 days.

2.3.5. Transformations

Transformations were done by a high efficiency lithium acetate method, described here based upon Gietz and Woods (2002).

2.3.5.1. Transformation for genomic integration

Strains were grown in YPD at 30°C overnight (23°C for TS strains). 1 ml of overnight culture was diluted into 50 ml YPD and grown for 3-5 hours until the cell density reaches $O.D._{600}$ 0.5-0.7 (O.D.600 0.6 = ~$2x10^7$ cells/ml). At this point, 40-50 ml of cells were collected by centrifugation (4000 rpm, 5 min) and washed in 10 ml of freshly prepared TE/LiOAc solution, followed by resuspension in 600 µl TE/LiOAc. After mixing 150µg (15µl) of salmon sperm DNA (Sigma-Aldrich), 200-500 ng of transforming DNA and 200 µl of cells, 700 µl TE/LiOAc-40%PEG was added and mixed with pipette. Samples were incubate at 30°C for 30 minutes and then heat shocked at 42°C for 15 minutes (or at 23°C for 30 minutes and heat shock at 30°C for 15minutes for TS strains). Finally, ~ 450µl yeast was plated onto appropriate selection medium. For plating onto drug selection, previous to the plating step, transformations were collected by centrifugation and resuspended in 1ml YPD and grown at 30°C (23°C for TS strains) shaking for 1-4 hours to allow the drug resistance marker gene to be expressed.

2.3.5.2. Transformation for gap repair

Transformations were performed as above (2.3.5.1). In this case 50 ng of cut plasmid was mixed with ~50 ng of PCR insert and ~150 µl was plated out.

2.3.5.3. Transformation for plasmid DNA

Transformations were performed as above (2.3.5.1) but with reduced amounts. Cells were harvested from a 2-5 ml cultures by centrifugation and resuspend in TE/LiOAc as above. Plasmid DNA (50-100 ng) was mixed with 50 µg (5µl) of salmon sperm DNA. Then, 30 µl cells and 140 µl TE/LiOAc-40%PEG were added and mix with pipette. Samples were incubated as above followed by plating into appropriated solid media as required (~100 µl or less).

2.3.6. Yeast crosses

Crosses were done between *MAT***a** and *MATα* strains (which were auxotrophic for different markers) e.g. *MAT***a** *trp1-1 LYS2* with a *MATα TRP1 lys2*∆*.* Mating was done on YPD plates that were grown at 30°C for 1-2 days (or 23°C for 2-3 days for crosses with TS strains). Diploids were selected on appropriate medium e.g. –Trp –Lys plates. Diploids were purified on double selection plates and singles colonies were patched onto SPO media for at least 3 days.

2.3.7. Tetrad dissections

A small amount of tetrads from a SPO plate were mixed into a solution containing 5µl of glusulase enzyme diluted with 95µl dH_2O. After incubation at room temperature for 5 minutes, 10µl of spores were placed on the side of a YPD plate. Dissections were performed by using an MSM300 dissection microscope (Singer Instruments). Plates were incubated at 30°C (23°C for TS strains) for 2-3 days and then tetrads scored by replica plating onto the appropriate selection plates.

2.3.8. Replica plating

Replicas of 600 mm diameter circular yeast plates were made manually using velveteen cloths and replica blocks. Replicas of high-density rectangular plates for high-throughput screens were performed with a Singer RoToR pinning robot (Singer Instruments).

2.3.9. Yeast genomic DNA extraction

2.3.9.1. Yeast genomic DNA extraction with phenol "Smash n'Grab"

3 ml of yeast cultures grown overnight in YPD media at 30°C were collected by centrifugation (5 min, 6000 rpm). The cells were resuspended in 200 µl Smash-n-grab buffer, then 200 µl phenol/chloroform (Invitrogen) and 250 µl glass beads (0.4-0.5mm diameter (Sigma-Aldrich)) were added. The mix was vortexed for 2 minutes and fractionated by centrifugation at 13,000rpm at 4°C for 10 minutes. 100 µl of the aqueous supernatant was transferred to new eppendorf and 200 µl phenol/chloroform was added. After vortexing and a further 10 minutes centrifugation, 50 µl of aqueous supernatant were dialysed in TE for 20 minutes on nitrocellulose membrane filters 0.025 µm (Millipore) and then stored at -20°C.

2.3.9.2. Fast yeast genomic DNA extraction without phenol

100-200 µl of yeast culture grown overnight (or a colony from a plate, resuspended in the 100-200 µl YPD) were fractionated by centrifugation (maximum speed, 1 min). The cell pellets were resuspended in 100 µl of 200 mM LiOAc, 1% SDS solution and incubated for 5 minutes at 70°C. Then, 300 µl of 96-100 % ethanol was added and the mix vortexed. DNA and cell debris were collected by centrifugation at 13000 rpm for 3 minutes and washed with 500 µl of 70% ethanol. The DNA was dissolved in 100 µl of H_2O and fractionated from the cell debris by centrifugation at 13000 rpm for 30 seconds (Looke, Kristjuhan and Kristjuhan, 2011).

2.4. Molecular Biology

Molecular biology techniques that are not described in detail here are based upon those from Sambrook and Russell (2001).

2.4.1. Polymerase chain reaction (PCR)

For high-fidelity PCRs PfuUltra II fusion, HS DNA polymerase (Agilant), Expand High Fidelity PLUS polymerase (Roche) or Q5-High Fidelity polymerase (New England BioLabs) were used in 50 µl reactions following manufacturer's instructions. Typical temperature profiles for the PCR program with Q5-High Fidelity polymerase were: 30 sec for the initial denaturation step at 98°C, followed by 30 cycles of 98°C (10 sec) denaturing, 55°C (30 sec) annealing, 72°C (30 sec/kb) extension and then 72°C for 2 minutes for final elongation. For diagnostic PCR DreamTaq Green (Fermentas) was

used following manufacturer's instructions and the PCR program set at 95°C for 3 minutes for initial denaturation, followed by 30 cycles of 95°C (30 sec), 55°C (30 sec), 72°C (1 min/kb) and final extension step 72°C for 10 minutes. PCR reactions were run either in a T3 Thermocycler (Biometra), a MJ Mini Personal Thermal Cycle (Bio-Rad) or a T100Thermal Cycler (Bio-Rad).

Primers were designed with SeqBuilder (Dnastar) and a list of primers (Sigma-Aldrich) used in this study is shown in Table M appendix 1.

2.4.2. Purification of PCR fragments

PCR products were purified using a GeneJET PCR Purification Kit (Thermo scientific) following manufacturer's instructions. DNA concentration was measured by NanoVue Plus spectrophotometer (GE).

2.4.3. Agarose gel electrophoresis

DNA gel electrophoresis was performed in 0.5-1.5% agarose gels (Invitrogen) according to the size of DNA (1-30 kb 0.5%, 800-12 kb 0.75%, 500-10 kb 1%, 400-7 kb 1.25%, 200-3kb 1.5%) with TAE buffer. Ethidium bromide 500 ng/ml was added to the molten agarose before pouring the gel. DNA was mixed with 10x loading dye and run at 90 V on a mini horizontal submarine Hoefer HE 33 unit (Amersham Biosciences). DNA was visualised using a BioDoc-It imaging system and size of fragments was estimated by comparison to the 1 kb Gene Ruler DNA ladder (Thermo Scientific).

2.4.4. Extraction of fragments from agarose gels

DNA fragments were extracted from agarose gels by using a GeneJET Gel Extraction Kit (Thermo scientific) following manufacturer's instructions.

2.4.5. Constructions of plasmids by gap repair

Oligonucleotide primers were designed on SeqBuilder (DNASTAR) to amplify the genes encoding kinetochore proteins (Table M appendix 1). PCR amplification of those genes was performed with genomic DNA from the strain W8164-2C (Table 2.2). PCRs were carried out in 50 µl as described by manufacturer for Roche, Expand High Fidelity PLUS polymerase or for Agilent, PfuUltra II fusion HS DNA polymerase, using a T3 Thermocycler (Biometra). We performed 30 PCR cycles, with the following temperature

profile: 94°C for 30 sec, 55°C for 30 sec and 72°C for 3-10 minutes. PCR products were verified by agarose gel electrophoresis. PCR products of the correct size were purified. A donor plasmid was cut with appropriate restriction enzyme(s). The cut plasmid and PCR product were combined and transformed into yeast to allow a "gap repair" ligation to proceed *in vivo* (Rothstein, 1983). Resulting yeast colonies containing plasmids were selected on appropriate selection medium. Plasmids were then extracted from yeast cells by the "Smash n' Grab" method described by Hoffman and Winston (Hoffman and Winston, 1987) and transferred into bacteria for purification. The DNA was sequenced by Sanger sequencing (Beckman Coulter Genomics) to verify the correct construct sequence. A plasmid list is shown in Table 2.4.

2.4.6. Constructions of endogenously-tagged fluorescent kinetochore proteins

Firstly, a diploid strain U2804-1 (Table 2.2) that contains the so-called 'magic markers' (prototrophic markers that are only expressed in a specific mating-type (sex) of haploid yeast) was sporulated. Haploid strains containing two magic markers, one specific for *MAT***a** cells and one for *MATα* (E79-12C and E79-17D) (Table 2.2) were obtained by tetrad dissection. Since the strains were *ade2-* which produce high levels of autofluorescence, an *ADE2* PCR product was introduced by transformation and selected on medium lacking adenine, resulting in the strains (*MATα* T10 and *MAT***a** T27) (Table 2.2). T10 and T27 were then transformed with a PCR cassette designed to tag the endogenous *SPC42* gene with RFP and introduce an adjacent hygromycin (HYG) resistance gene [*SPC42-RFP::HYG*]. The resulting strains (*MATα* T26 and *MAT***a** T29) (Table 2.2) were next transformed with the PCR cassette designed to introduce different kinetochore genes tagged with YFP and introduce an adjacent nourseothricin (NAT) resistance gene ["*gene"-YFP::NAT*] resulting in 6 strains. *MAT***a** (T37 (Dad4-YFP), T38 (Dad3-YFP) and T39 (Ndc10-YFP)) and *MATα* (T34 (Dad4-YFP), T35 (Dad3-YFP) and T36 (Ndc10-YFP) (Table 2.2).

2.4.7. DNA digestions with restriction endonucleases

A volume of 30 µl was prepared including 3 µl of restriction buffer, 1 µl of restriction enzyme (New England Biolabs) and 1000-1500 ng of DNA. Reactions were incubated typically at 37°C for at least two hours and purified by using the GeneJET PCR purification Kit (Thermo Scientific) with 20-50 µl of elution buffer.

2.4.8. Antartic phosphatase vector treatment

In order to improve the efficiency of a ligation reaction, phosphate groups from 5' ends can be removed by using Antarctic phosphatase (New England BioLabs). This prevents self-ligation of the vector. A reaction was prepared by adding 1/10 volume of 10X Antarctic Phosphatase Reaction Buffer, 1µl of Antarctic Phosphatase (5 units) and 1-5 µg of the digested plasmid. The reaction was mixed and incubated at 37°C for 1h. Products were purified by using the GeneJET PCR purification Kit (Thermo Scientific) and the final concentration was measured by NanoVue spectrophotometer.

2.4.9. Ligation of PCR product and vector

A 20 µl reaction was prepared on ice by adding 2 µl of 10X T4 DNA Ligase Buffer and 1 µl of T4 DNA Ligase (New England BioLabs) (added last) to a determined amount of vector DNA and insert DNA calculated for the desired molar ratio by using the website http://www.insilico.uni-duesseldorf.de/Lig_Input.html. The molar ratio is selected according to the size of the insert in relation to the vector, e.g. to ligate a 1kb insert and a 4kb vector, a molar ratio of 1:3 (vector:insert) should be used, whereas if both have a similar size, a 1:1 ratio is preferred. Nuclease-free water was used to create a 20 µl total volume the reaction, which was then mixed and incubated at room temperature for 10 minutes (1:3 ratio) or 1 hour (1:1 ratio). The same reaction without including the insert DNA was used as control.

2.4.10. Auxin degradation of Pkc1

A strain tagged for *SPC42-RFP* and *DAD4-YFP* (PT147-3B) was transformed by genomic integration with the *AFB2* gene in the *HIS3* locus (*his3-11::ADH-AFB2::HIS3)*. The resulting strain (T393) was then crossed with a strain previously transformed with the *PKC1* gene followed by an *AID* degron plus 5x*FLAGs* in the *URA3* locus (*PKC1-AID-5xFLAGS::URA3).*

To start degradation of AID-tagged Pkc1, a synthetic auxin, 1-naphthaleneacetic acid (NAA) dissolved in NaOH (Sigma) was used. The strain was grown for microscopy in synthetic media with adenine containing 0.5-1 mM auxin and imaged after 2 hours.

2.5. High Throughput Protocols (screens)

2.5.1. Selective Ploidy Ablation (SPA) mini-screen with Spc24

The plasmid pHT18 (Table 2.4) coding for Spc24-YFP and Spc42-RFP was transformed into the Universal Donor Strain (UD) *MAT***a** W8164-2C (Table 2.2). Selective ploidy ablation (SPA) was performed as described by Reid et al. (2011) to mate the UD containing the plasmid with the 40 strains (Table 2.6) from the deletion library (recipients). Selection steps were performed using a RoToR pinning robot (Singer Instruments) to selectively remove all the chromosomes of the UDS leading to haploid deletion strains containing the Spc24-YFP plasmid.

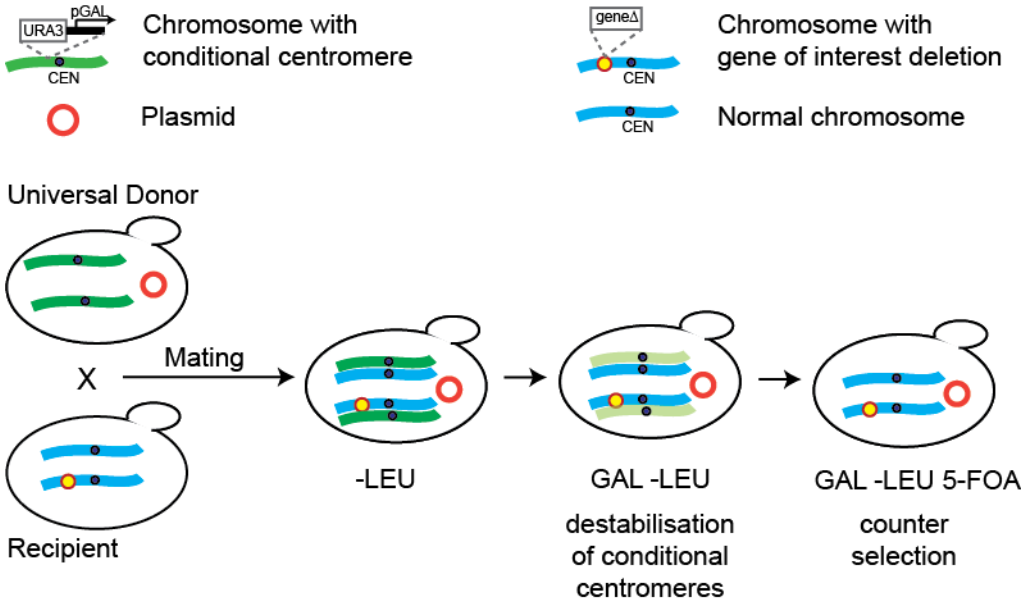

Figure 2.1. SPA methodology. Schematic of the selective ploidy ablation (SPA) method described in Reid et al. (2011).

Table 2.6. List of gene deletions used in SPA mini-screen with Spc24

ORF	*Gene*	Biological Process
YHR064C	*SSZ1*	Protein metabolism
YBL058W	*SHP1*	Protein metabolism
YMR095C	*SNO1*	Metabolism
YLR235C	*YLR235C*	Unknown
YOR144C	*ELG1*	DNA replication
YMR179W	*SPT21*	Transcription
YPL055C	*LGE1*	DNA metabolism, chromosome organization
YPR135W	*CTF4*	DNA repair, DNA damage response, DNA recombination
YBR098W	*MMS4*	DNA repair, DNA damage response, DNA recombination
YNL250W	*RAD50*	DNA repair, DNA damage response, DNA recombination
YLR320W	*MMS22*	DNA repair, DNA damage response, DNA recombination
YPR164W	*MMS1*	DNA repair, DNA damage response, DNA recombination
YML032C	*RAD52*	DNA repair, DNA damage response, DNA recombination
YPL024W	*RMI1*	DNA repair, DNA damage response, DNA recombination
YKL113C	*RAD27*	DNA repair, DNA damage response, DNA recombination
YGL163C	*RAD54*	DNA repair, DNA damage response, DNA recombination
YDR014W	*RAD61*	DNA repair, DNA damage response, DNA recombination
YBR073W	*RDH54*	DNA repair, DNA damage response, DNA recombination
YLR288C	*MEC3*	Cell cycle
YNL273W	*TOF1*	Cell cycle
YCL061C	*MRC1*	Cell cycle
YOR026	*BUB3*	Cell cycle
YPL194W	*DDC1*	Cell cycle
YLR079W	*SIC1*	Cell cycle
YBR107C	*IML3*	Chromosome segregation
YDR254W	*CHL4*	Chromosome segregation
YER016W	*BIM1*	Chromosome segregation
YHR191C	*CTF8*	Chromosome segregation
YPR046W	*MCM16*	Chromosome segregation
YPL008W	*CHL1*	Chromosome segregation
YCL016C	*DCC1*	Chromosome segregation
YDR318	*MCM21*	Chromosome segregation
YMR048	*CSM3*	Chromosome segregation
YJR135C	*MCM22*	Chromosome segregation
YEL061C	*CIN8*	Chromosome segregation
YLR381W	*CTF3*	Chromosome segregation
YPR141C	*KAR3*	Chromosome segregation
YMR078C	*CTF18*	Chromosome segregation
YPL018W	*CTF19*	Chromosome segregation
YOR073W	*SGO1*	Chromosome segregation

2.5.2. Genome-wide screen with Dad4 (SGA)

The *MAT***a** strain T37 (Table 2.2) coding for Dad4-YFP Spc42-RFP was mated with the *MATα* array of deletion strains (Winzeler et al., 1999) by using "Synthetic Genetic Array" (SGA) methodology (Tong et al., 2001). Diploids were selected on media containing the drugs G418, HYG and NAT. Upon sporulation, further selections were made on media lacking leucine and lysine and by addition of thialysine, which collectively selects for haploid MATα. Cells, then further selection steps included sequentially G418, NAT and HYG to select for the deletion allele (*KAN*), the *DAD4-YFP* (*NAT*) and *SPC42-RFP* (*HYG*). All steps were performed using a Singer RoToR pinning robot (Singer Instruments). In the same way the *MATα* strain T34 (Table 2.2) also coding for Dad4-YFP Spc42-RFP was mated with the *MAT***a** TS collection (Li et al., 2011).

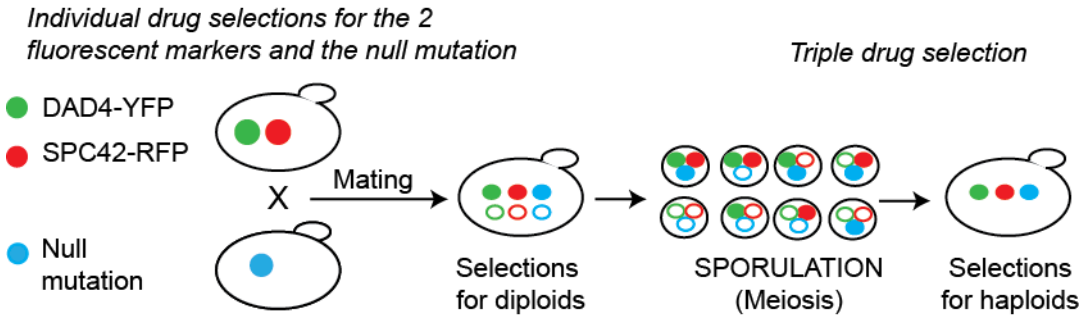

Figure 2.2. SGA methodology. Schematic of the synthetic genetic array (SGA) method described in Tong et al. (2001).

2.5.3. Benomyl sensitivity screen

A 384 colony plate was converted onto a 1536 colony plate (by copying each colony 4 times) and this was then copied onto YPD and YPD containing 15 µg/ml benomyl (Sigma) plates using a Singer RoToR pinning robot (Singer Instruments). After 2 days incubation at 23°C plates were scanned and Screen Mill software (Dittmar et al., 2010) was used to measure colony growth.

2.6. Protein methods

2.6.1. Protein extraction

Protein extractions were performed as described in (Von der Haar, 2007). Briefly, cells were harvested and resuspended in 200 µl lysis buffer. After 10 minutes incubation at 90°C, 5µl of 4 M acetic acid (Sigma) was added and the mix was vortexed for 30 seconds. Following a second 10 minutes incubation at 90°C, 50 µl of loading buffer were added and the mix was centrifuged (1 min 13.000 rpm). Samples were stored at -20°C.

2.6.2. SDS PAGE

Proteins were separated by sodium dodecyl sulfate polyacrylamide gel electrophoresis (SDS PAGE). A volume of 20 µl of protein samples were loaded on Mini-PROTEAN TGX Precast Gels (Bio-Rad) of 8.6 x 6.7 cm and the appropriated %. A molecular ladder was also adder at 10 µl (GE Healthcare). Electrophoresis was performed with a Mini-PROTEAN Tetra system (Bio-Rad) in running buffer at 150 V until the bromophenol blue dye front reached 1 cm from the top and then at 200V until the dye had run out at the bottom of the gel.

2.6.3. Western Blot

Proteins separated by SDS-PAGE were transferred to a 6 x 9 cm polyvinylidene difluoride (PVDF) transfer membrane (GE Healthcare) after equilibration for 15-20 minutes in transfer buffer together with the blotting pads (Bio-Rad) and filter papers (Bio-Rad). The membrane was activated in methanol for 10 seconds and washed in dH_2O for 5 minutes before equilibration. Transfer was made in a Mini-PROTEAN Tetra cell (Bio-Rad) with a stirrer at 4°C for 1 hour at 100V or over night at 30V. The membrane was stained for 3 minutes with ATX Ponceau S red staining solution (Fluka) to confirmed protein transfer. After washing with dH_2O the membrane was blocked in 5-10 ml of 50% PBS (Sigma) / 50% blocking buffer (PBS) (Li-cor Odyssey). The buffer was then replaced with Phospho-p38 MAP Kinase (Thr180/Tyr182) antibody (1:1000) (Cell signalling) in blocking buffer containing 1 µl/ml of 0.1% Tween and incubated at room temperature for one hour or at 4°C over night. After 4 washes of 5 minutes with PBS-0.1% Tween, the membrane was incubated with anti-rabbit IgG, HRP-linked antibody (1:1000) (Cell signalling) in blocking buffer containing 1 µl/ml of 0.1% Tween and 0.01% SDS for one hour at room temperature or at 4°C over night. Next, 5 minutes washes with PBS-0.1% Tween were repeated 4 times. For visualisation, the membrane was incubated for 1 minute in a mix of 2 ECL reagents in a 1:1 ratio (GE Healthcare). After

drying, excess liquid was removed by resting on filter paper, the membrane was placed in a film cassette (ENSTAR) between 2 transparent films. CL-Xposure films (Thermo Scientific) were developed in an Optimax X-ray film processor (Protec). Different times of exposure were taken.

2.7. Fluorescence microscopy

Images were acquired by using a CCD camera (Hamamatsu, Orca ERII) mounted on a Zeiss Axioimager Z2 microscope (Carl Zeiss AG, Germany) with a (Zeiss, Plan-APOCHROMAT) 63 x 1.4NA oil immersion objective lens. Zeiss Immersol 518F immersion oil was used with a refractive index of 1.52. The fluorescence illumination source was a 100W mercury lamp, later changed to a LED light source (Zeiss, Colibri 2). Fluorescence filter cubes were as follows: YFP imaging used Zeiss filter set 46 (excitation BP 500/20; dichroic FT 515, emission BP 535/30), RFP imaging used Zeiss filter set 63HE (excitation BP 572/25; dichroic FT 590, emission BP 629/62), GFP imaging used Zeiss filter set 38HE (excitation BP 470/40; dichroic FT 495, emission BP 525/50) and CFP imaging used Zeiss filter set 47HE (excitation BP 436/25; dichroic FT455, emission BP 480/40). Brightfield contrast was enhanced with differential interference contrast (DIC) prisms. The CCD camera was binned 2 x 2, producing pixels of approximately 205 nm. The dynamic range of the camera is theoretically ~3000 (a full well capacity of 18,000 electrons with a read noise of ~6 electrons). The imaging system has previously been found to deliver a linear response. Images were obtained as 17 vertically separated z-slices at 0.4 µm intervals for the plasmids studies and 21 z-slices at 0.35 µm intervals for the endogenous screen. Exposure times varied between studies and were optimised for the genome-wide screen with Dad4-YFP 40 ms and Spc42-RFP 50 ms. For individual slides often 80 ms was used for both YFP and RFP. Time-lapse experiments were done with CFP, YFP and RFP filters over 1 minute at either one plane or in z-slices as described above.

2.7.1. Agar pads for 48 well imaging

For each 96 well plate, 50 ml of 3% w/v low melting point agarose (Invitrogen) in microscopy media (usually SC+Ade) was made by melting the agarose in the microwave. This can be stored at 60°C for up to a few hours. To prepare each pad, two 48-well steel moulds were positioned on top of a glass coverslip (55 x 75 mm) (Thermo Scientific) leaving holes for 48 wells and ~20 ml of hot agar was poured to fill the holes. An additional glass coverslip was immediately placed on top avoiding bubbles, which formes a 4 layers sandwich. After ~8 minutes the agar is set and the excess agar can be

trimmed off. The sandwich was turned around and the cover slip that was at the bottom (now top) was removed along with the first steel mold. The pad was left to dry next to a Bunsen for ~5 minutes. A volume of 2.5 µl of yeast culture from a 96 well plate was pipetted onto each agar pad and then allowed to dry for ~7 minutes (next to a Bunsen). Finally a new glass coverslip was placed on top avoiding bubbles between the agar pad and the coverslip.

2.7.2. Preparing microscopy slides

Log-phase cells were mixed with low melting point agarose to 0.7% (Invitrogen) and placed on a glass microscope slide (76 x 26 mm) beneath a 22 mm square ~170 µm thick coverslip (Thermo Scientific). The depth of agarose between the slide and coverslip is fixed at 6-8 µm, slightly larger than the diameter of the average yeast cell.

2.8. Image analysis

Two different software packages were used to perform image analysis, Volocity (Perkin Elmer) and Fiji ImageJ (Java). For a schematic of software protocols see Figures 3.3 and 3.4 and Ledesma-Fernández and Thorpe (2015) (attached, appendix 3).

3. Chapter III: Results 1: Optimisation of plasmid-based screens, imaging and quantitation methods

3.1. Introduction

3.1.1. Budding yeast and genome-wide studies

The budding yeast *S. cerevisiae* has proven a very useful organism to study the relationship between genes and their function. This is particularly true for genome-wide studies. The first of these global efforts produced the complete sequence of the budding yeast strain S288C in 1996, the first eukaryote to be sequenced (Goffeau et al., 1996; Clayton et al., 1997). Since then, annotations and corrections to the sequence have been published to form the actualised version we use today (Engel et al., 2014).

In order to understand gene function, another consortium took a wide genome approach and constructed deletions of each open reading frame (ORF), in a long project that started in the 1990's and ended in 2002 (Giaever and Nislow, 2014). They constructed knockouts for 96% of the genes by replacing each target ORF by homologous recombination with a cassette constructed by PCR. This cassette included the *KANMX* marker gene to confer resistance to geneticin (G418) and 20-base long barcodes at each side, which could be used in competition assays to identify each deletion (Winzeler et al., 1999; Giaever et al., 2002).

The genome deletion project found that 19% of genes were essential in rich media (Giaever et al., 2002). This led to other projects in which temperature sensitive strains were constructed for a total of 65% of the over 1100 essential genes. As in the deletion collection, the mutant alleles replaced the endogenous locus and a cassette encoding *KanMX* was also included for selection on G418 (Ben-Aroya et al., 2008; Li et al., 2011).

The use of these libraries has been aided by new methods to combine specific alleles with the libraries (Tong et al., 2001; Reid et al., 2011). Together, they have proven an important tool to identify genes that affect specific phenotypes (Costanzo et al., 2010) and maintain genome structure (Yuen et al., 2007).

3.1.2. Genome-wide microscopy screens

To understand the relationship between genotype and phenotype in yeast, genome-wide fluorescent microscopy methods have also been developed. For example, each ORF has been GFP-tagged to study protein localisation and levels in yeast (Huh et al., 2003). Combining fluorescently tagged collections with the deletion library and the TS collection opens the possibility to observe phenotypes caused by mutations in a genome-wide scale. For example, genome-wide microscopy screens combining the deletion library with plasmid-encoded tagged proteins (Alvaro et al., 2007) or with endogenously tagged proteins (GFP library) (Tkach et al. 2012) have been used to study the DNA damage response. Similarly, mutants that affect spindle morphology were identified in a screen that combined deletion mutants and double mutants with GFP tagged tubulin (Vizeacoumar et al., 2010).

3.1.3. Quantitation of kinetochore proteins

Quantitation of the proteins at the kinetochore is simplified in budding yeast by the fact that the 16 centromeres cluster together. Thus, fluorescent labelling of a kinetochore protein produces a single focus formed by all the molecules contained within the 16 kinetochores. Biochemical techniques can measure total protein levels in the cell but they don't discriminate between proteins specifically located at the centromere and those freely diffusing in the cell. Quantitation of the fluorescent intensity of foci can be used as a surrogate of protein levels loaded at the centromere. Work by Ted Salmon, Kerry Bloom and colleagues used fluorescence quantitation to calculate the stoichiometry of different proteins within complexes at the kinetochore and to determine whether changes in kinetochore levels were found throughout the cell cycle (Joglekar et al., 2006; Joglekar et al., 2008). However, measurements are calculated as a ratio based on the number of Cse4 (CENP-A) molecules associated to the CEN, and different studies report conflicting results, from 1-2 (Shivaraju et al., 2012; Wisniewski et al., 2014) to multiple copies (Lawrimore, Bloom and Salmon, 2011; Coffman et al., 2011).

3.1.4. Aims of this work

This project aims to take advantage of genome-wide microscopy screens using the deletion library and temperature sensitive (TS) collection to identify genes involved in kinetochore regulation. By fluorescently labelling kinetochore proteins, I can study how mutations alter the levels and localisation of these proteins. I aim to create a plasmid-based collection of fluorescently tagged kinetochore proteins and then select one to

combine with the deletion library and TS collection and perform a genome-wide microscopy screen.
This work aims to identify new pathways of kinetochore regulation and contribute to further understanding how kinetochores control chromosome segregation and thus maintain the integrity of the genome.

3.2. Results

3.2.1. Plasmid-based screens

3.2.1.1. Construction of plasmids coding fluorescent kinetochore proteins

To be able to visualise and quantify kinetochore proteins, I created an array of plasmids encoding kinetochore proteins tagged with yellow fluorescent protein (YFP). Additionally, I also tagged Spc42, a spindle pole body (SPB) component, with red fluorescent protein (RFP) to provide a reference marker for the SPB. I had two goals of this work. First, to decide which kinetochore proteins would be ideal for a microscopy screen and second, to optimise methods for cell preparation and imaging analysis. I was helped in the construction of some of these plasmids by an undergraduate student, Erika Aquino.

Each kinetochore gene was amplified using PCR and these products were cloned in a plasmid that creates a YFP fusion and also *SPC42-RFP*. The plasmid and PCR products were not ligated *in vitro*, instead, the PCR products included ~20bp sequences at their ends that match those in the plasmid, allowing *in vivo* recombination to join the two DNAs into a complete vector – a process known as “gap repair” (see methods). The YFP-tagged genes in these plasmids are under the control of a *pCUP1* promoter, which is expressed constitutively but can be gradually upregulated by addition of copper to the growth medium (Butt et al, 1984; Mascorro-Gallardo and Covarrubias, 1996). The resulting plasmids were validated by DNA sequencing and fluorescence microscopy.

Each plasmid thus encodes the SPB protein Spc42 tagged with RFP and a different kinetochore protein tagged with YFP. An example of a fluorescence microscope image of yeast containing one of these plasmids can be seen in Figure 3.1, where both the SPBs (RFP) and kinetochores (YFP) are clearly visible. In G1 cells, one red (SPB) and one green (kinetochore) focus can be seen which are closely aligned. S/G2/M cells often have one or two green (kinetochore) foci between two red (SPB) foci consistent with the expected pattern of the mitotic spindle.

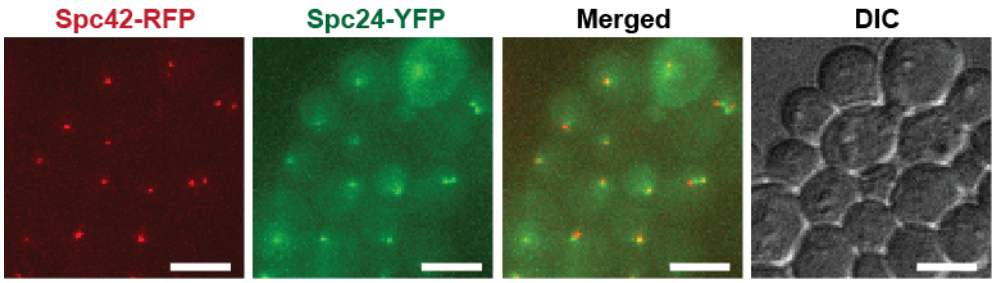

Figure 3.1. Plasmid encoded SPB-RFP and kinetochore-YFP in yeast cells. Yeast cells containing a plasmid that expresses both *SPC42-RFP* and *SPC24-YFP*. Red foci are formed by the Spc42 SPB protein tagged with RFP. Green foci are formed by the YFP tagged Spc24 (member of the NDC80 complex). Scale bars are 5 µm.

In total 68 kinetochore and kinetochore-associated proteins were tagged in this way (Table 2.4).

3.2.1.2. Plasmids can be classified into three distinct groups according to fluorescent signal

I first classified the plasmids into three groups according to foci brightness and background (Figure 3.2, table 3.1). A plate with 68 plasmids was imaged, each containing a different kinetochore gene tagged with YFP. Some plasmids failed to produce a detectable kinetochore focus; instead, they showed a dispersed YFP signal (Class III). A second group of plasmids produced distinguishable kinetochore foci with similar or slightly lower YFP levels in the cell (Class II). Finally, about half of the plasmids had clear red (SPB) and green (kinetochore) foci with lower background levels (Class I). In some of those plasmids, the green signal would form a line or smear rather than a defined focus.

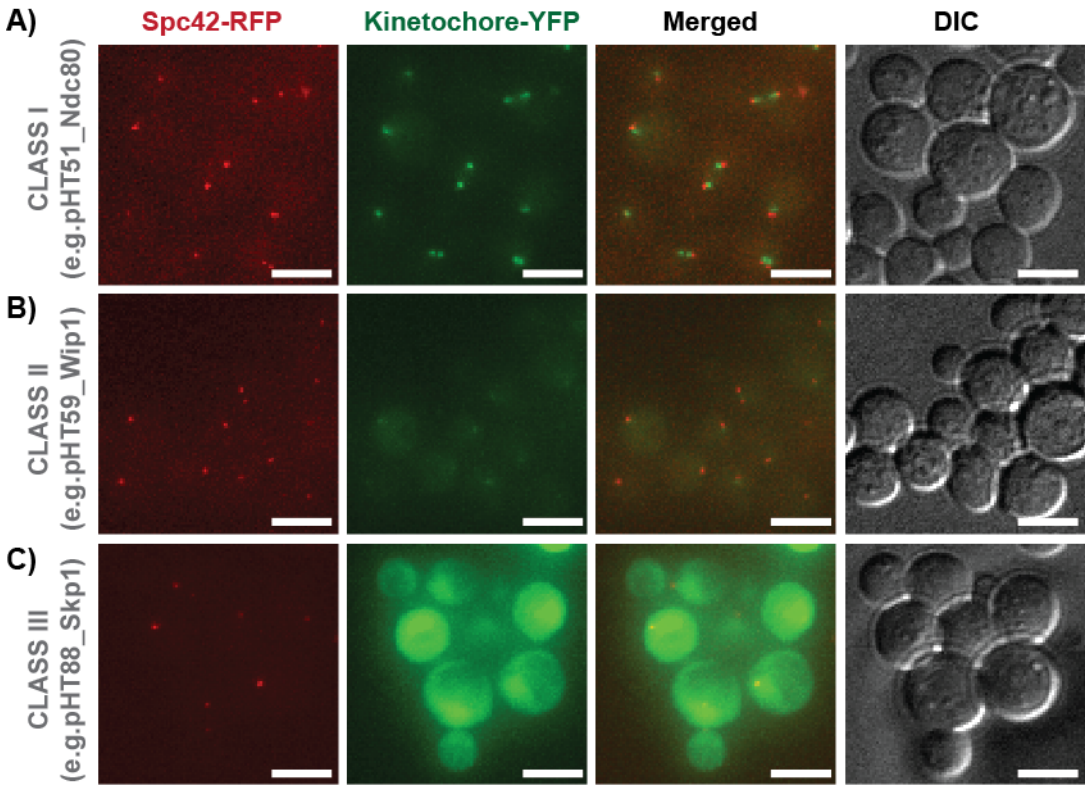

Figure 3.2. Examples of plasmid classification. Manual classification of plasmids into 3 groups: **(A)** (Class I) Bright YFP foci or line with low-medium background, **(B)** (Class II) visible but weak YFP foci with background of similar levels to the foci and **(C)** (Class III) no visible YFP foci with or without high background. Images show yeast cells containing plasmids encoding Spc42-RFP (red) and Ndc80-YFP **(A)**, Wip1-YFP **(B)** or Skp1-YFP **(C)** (green). Scale bars are 5 μm.

Table 3.1. Classification of plasmids

Class	Plasmids (corresponding encoded YFP tagged gene)
Class I (33)	pHT14 (*BIM1*), pHT17 (*BIK1*), pHT18 (*SPC24*), pHT24 (*CTF19*), pHT25 (*DAM1*), pHT28 (*ASK1*), pHT32 (*NSL1*), pHT33 (*SPC19*), pHT34 (*SPC25*), pHT35 (*NNF1*), pHT41 (*SLI15*), pHT47 (*DAD1*), pHT48 (*DUO1*), pHT49 (*SGO1*) pHT50 (*SPC105*), pHT51 (*NDC80*), pHT52 (*BIR1*), pHT53 (*KIP2*), pHT54 (*MIF2*), pHT58 (*AME1*), pHT62 (*KIP1*), pHT63 (*DAD4*), pHT64 (*HSK3*), pHT67 (*CNN1*), pHT68 (*TUB1*), pHT72 (*DAD2*), pHT73 (*DAD3*), pHT75 (*SPC34*), pHT91 (*CBF2*), pHT92 (*STU1*), pHT93 (*KRE28*), pHT94 (*KAR9*), pHT100 (*SCM3*)
Class II (16)	pHT8 (*IPL1*), pHT15 (*MTW1*), pHT26 (*BUB1*), pHT27 (*CTF3*), pHT30 (*DSN1*), pHT42 (*NBL1*), pHT43 (*MCM21*), pHT59 (*WIP1*), pHT61 (*MHF1*), pHT66 (*DYN2*), pHT71 (*CIN8*), pHT76 (*KAR3*), pHT77 (*NKP1*), pHT78 (*NKP2*), pHT85 (*CDC20*), pHT87 (*KIP3*)
Class III (19)	pHT12 (*CEP3*), pHT13 (*OKP1*), pHT29 (*NUF2*), pHT40 (*MAD2*), pHT44 (*MOB1*), pHT55 (*KIC1*), pHT65 (*BUB3*), pHT69 (*MHF2*), pHT74 (*MAD3*), pHT79 (*IML3*), pHT80 (*CHL4*), pHT81 (*MCM22*), pHT82 (*MCM16*), pHT83 (*IRC15*), pHT84 (*DYN1*), pHT86 (*CBF1*), pHT88 (*SKP1*), pHT89 (*PAC1*), pHT90 (*CTF13*)

3.2.2. Selection and optimisation of methodology for genome-wide screens image analysis

In order to quantify the fluorescence intensity of kinetochore and SPB foci, various computational methods were used and compared. This optimisation was done in parallel with work described above.

3.2.2.1. Building Volocity protocols

Automated software protocols were created using “Volocity” image analysis software (Perkin Elmer) to identify cells, differentiate and eliminate dead cells and then, find kinetochores and SPBs inside the remaining cells. A flow chart example of the software protocol is shown in Figure 3.3 A. To quantify the kinetochore, the software first finds bright spots and dilate them 3 times. A second dilation of 5 is then subtracted from a third dilation of 8 to calculate the value for the background (Figure 3.3 B).

An alternative manual approach in Volocity is to use “regions of interest” (ROIs). I manually created a cuboid of 11.4 μm^3 volume around each kinetochore (visible in the YFP channel) and another in a nearby area for the background. To obtain data from

SPBs the manual selection must be repeated for the red RFP channel. Both the automated and manual Volocity measurements return the fluorescence mean, min, max, sum and standard deviation of each selected object (either YFP or RFP) and additionally the x, y and z position. To position the ROIs accurately was difficult and time consuming, prohibitively so for a large screen. Automated protocols are mostly successful when optimised for a specific image or when used on cropped images of individual cells and the quality of the images is good and detailed in Volocity. However, no one protocol was able to identify kinetochores and SPBs in multiple images. The automated protocol needed to be adapted for every image when comparing strains with different intensities such as plasmids of class I and III (Figure 3.2 A-B) and this would present a problem when trying to compare wild-type and mutant images.

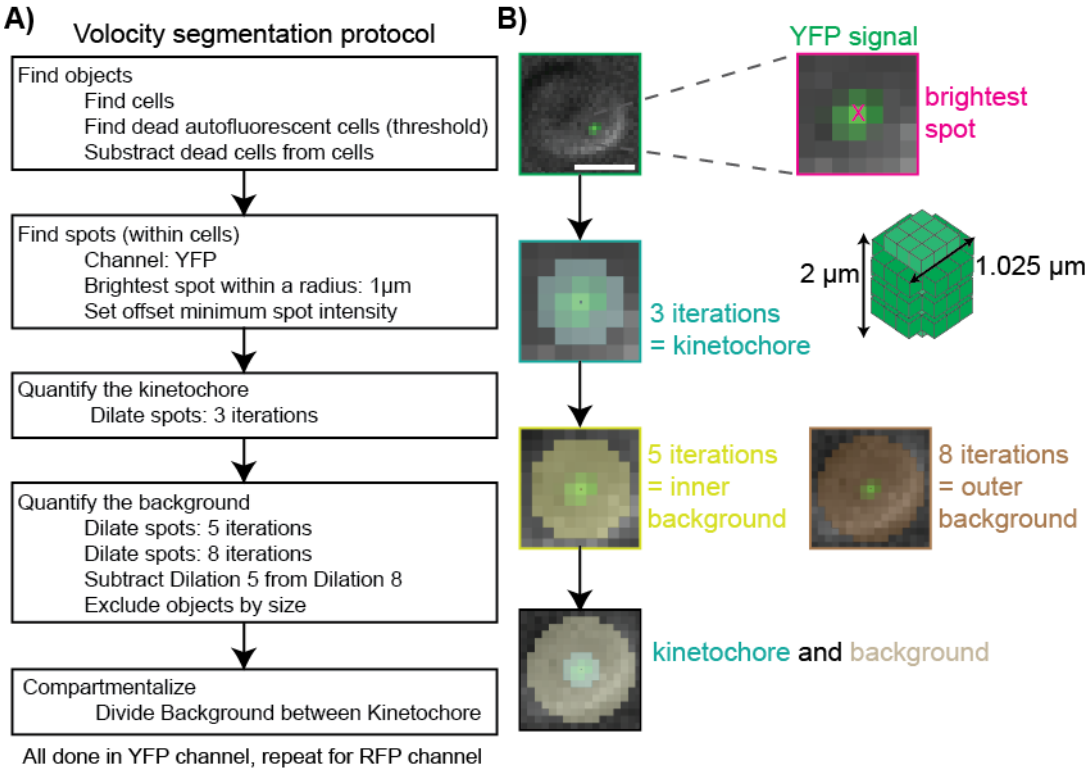

Figure 3.3. Outline of Volocity analysis. A) Flow chart of an automated software protocol for Volocity analysis (Perkin Elmer). **B)** Illustrated example of steps in **(A)** from the "Find spots" step. It shows identification of 1 focus within a yeast cell (top) and dilations to calculate the kinetochore value (insert in green shows the measurements of the box that encapsulates the kinetochore) and the background. Scale bar is 3 µm.

3.2.2.2. ImageJ protocols

A custom software script (FociQuant) was created and tested in the lab to quantify kinetochores and SPBs (Ledesma-Fernández and Thorpe, 2015). This script iterates over every image in a specified folder, a schematic of the software protocol is shown in Figure 3.4 A. Importantly, I can run this script in several different ways, one in which the software attempts to automatically identify spots in the image (fully automated) and another where the position of kinetochore and SPB foci is identified close to ROIs selected manually for each image (manual selection). Third, a semi-automatic script was also tested in which the threshold for detecting foci for each image is manually adjusted.

The manual version is the most accurate (subject to the user's ability to differentiate foci) and can discriminate kinetochores in G2/M cells from those in G1/S phase. However, manually selecting foci is time consuming and not adequate for high-throughput analysis. The fully automated version is considerably faster, since it runs without any user input. This method is able to measure both YFP and RFP foci. Although the automated method is more likely to generate false positives and false negatives, it is the most appropriate method for large-scale analysis of high-throughput screen data.

All methods return an image with boxes around foci identifying kinetochores and corresponding backgrounds as well as identifier numbers for each focus (Figure 3.4 B). The tabulated data includes two-dimensional (2D) and three-dimensional (3D) quantitation for kinetochores (Figure 3.4 C-D). Thus the output allows an individual focus measurement in the tabulated data to be used to identify the specific cell and focus in the microscope image.

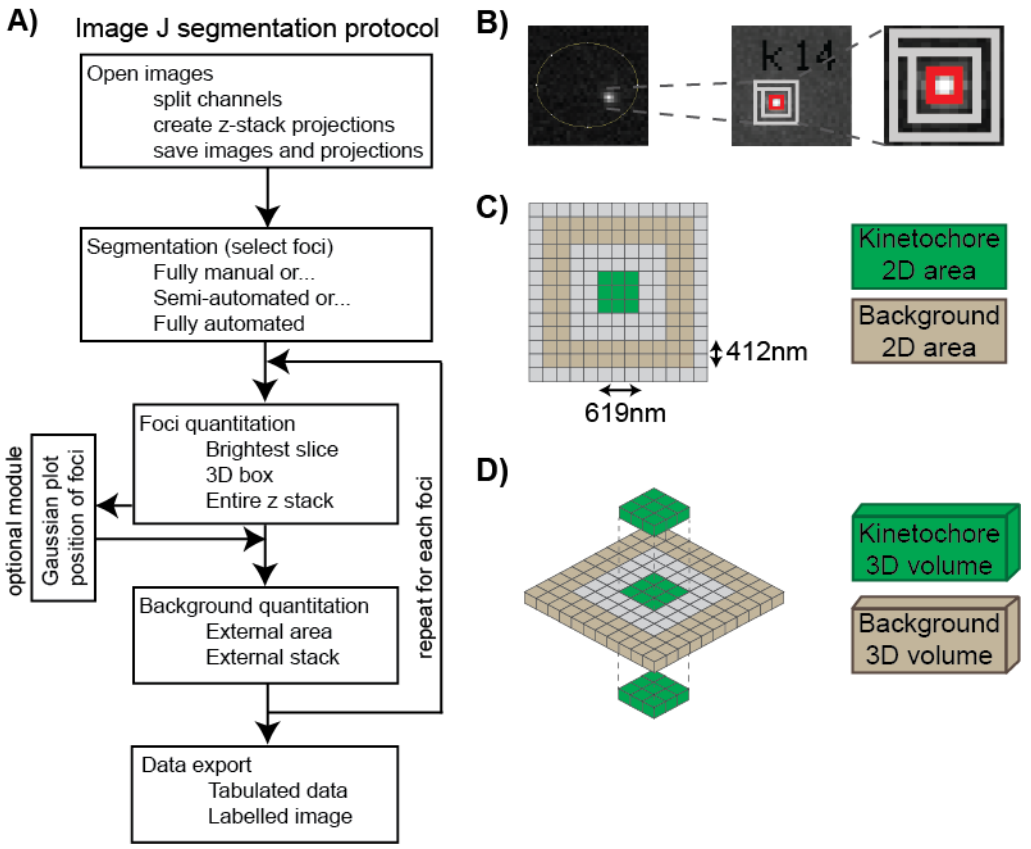

Figure 3.4. Outline of ImageJ analysis. A) Flow chart of the ImageJ script. **B)** YFP focus within a yeast cell and graphical output from the software with identifier number for the focus (in this case K (kinetochore) 14). The fluorescence inside the red box is the kinetochore measurement and the dark area between the grey lines is the background measurement. **C)** Squematic showing the 2D quantitation square which is 3 x 3 pixels for the kinetochore (green). **D)** Squematic showing the 3D quantitation cube which is 3 x 3 x 3 pixels for the kinetochore (green). (Panels A, C and D adapted from Ledesma-Fernández and Thorpe, 2015).

3.2.2.3. Comparison of image analysis methods

To compare image analysis methods I took 10 images from the same plasmid (Spc24-YFP) and another 10 from different plasmids (Table 3.2) and analysed them by different methods. My selection of these particular plasmid-encoded proteins was influenced by previous studies that have characterised them in some detail (Joglekar et al., 2006; Lawrimore, Bloom and Salmon, 2011). Hence, I could compare our data with the published literature. Also I wanted to test our computational methods with images of fluorescently-tagged proteins that covered a range of YFP levels (from weak to strong) (Figure 3.2 A-B) and with different levels of background fluorescence. All 20 images were analysed, the data normalised and the methods compared. Overall, there was good correlation between the different methods, being weakest between the manual

(ROIs) and automatic (protocols) versions of Volocity (R^2=0.7620) and the manual versions of Volocity and ImageJ (R^2=0.7423) (Figure 3.5 A-B). The subtly different automated protocols of Volocity did not show strong differences (data not shown) and had very good correlation with the semi-automated version of imageJ (R^2=0.9799) (Figure 3.5 C). The three ImageJ methods showed very high correlation when comparing the manual and semi-automated versions (R^2=0.9912) as well as semi-automated and automated versions (R^2=0.9289) (Figure 3.5 D-E).

Table 3.2. Ten plasmids chosen for image analysis comparison

Plasmid	Gene	Class	Plasmid	Gene	Class
pHT15	MTW1	II	pHT50	SPC105	I
pHT24	CTF19	I	pHT51	NDC80	I
pHT28	ASK1	I	pHT63	DAD4	I
pHT29	NUF2	III	pHT78	NKP2	II
pHT48	DUO1	I	pHT94	KAR9	I

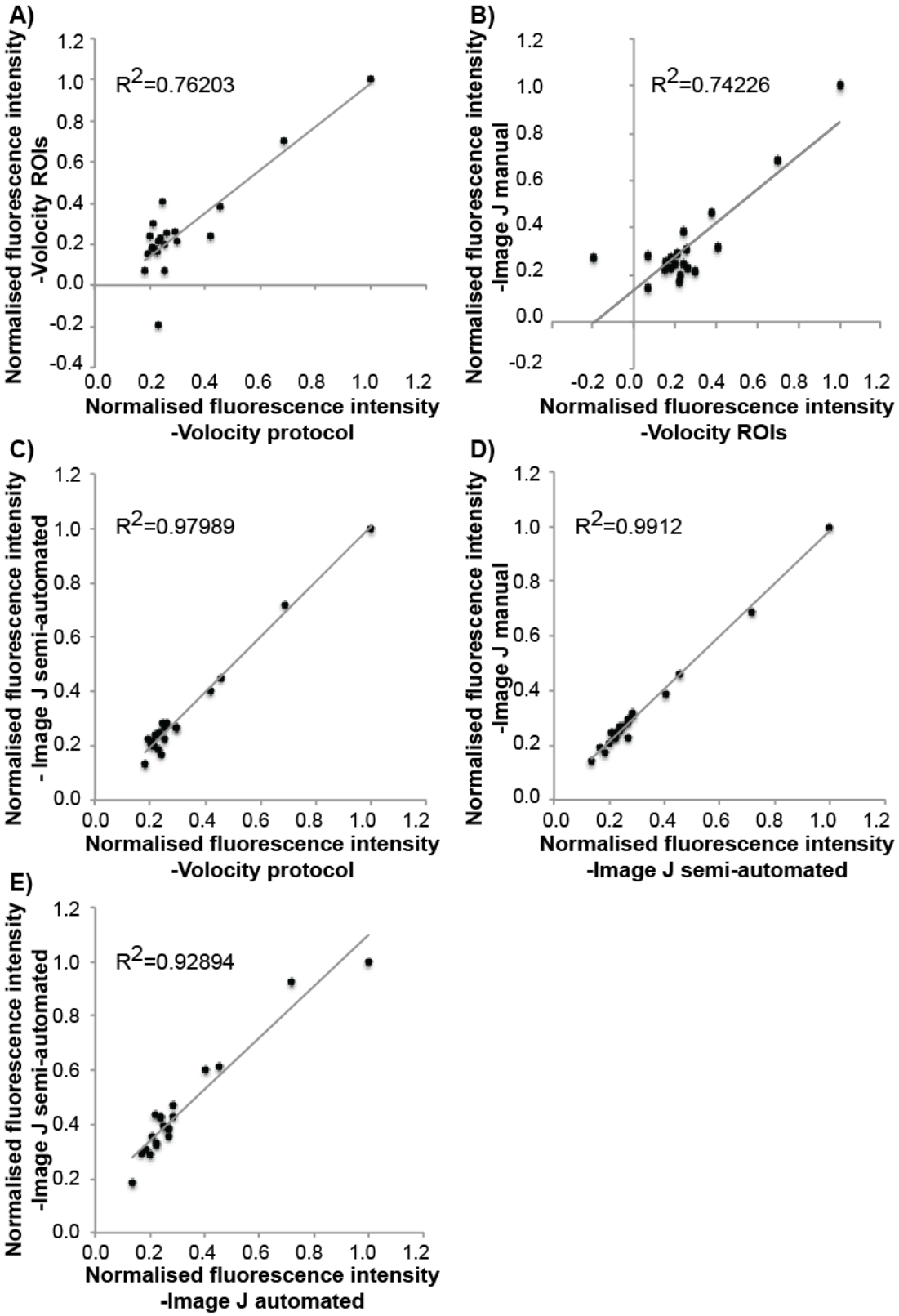

Figure 3.5. Comparison of plasmid images. A) The manual Volocity (ROIs) measurements are compared with the automated Volocity protocol **(A)** and the manual method in ImageJ **(B)**. The semi-automated method in ImageJ is compared with the automated Volocity protocol **(C)**, the manual method in ImageJ **(D)** and the automated method in ImageJ **(E)**. Values used are the mean fluorescence of all the foci in each of the 20 images. The measurements are 3D

mean kinetochore values background subtracted and are normalised by dividing each value by the maximum value.

When comparing data from plasmids with the published data (Joglekar et al., 2006; Lawrimore, Bloom and Salmon, 2011), a correlation of R^2=0.4537 and R^2=0.4422 were the closest match obtained with the semi-automated version of ImageJ and a Volocity protocol respectively (Figure 3.6 A-C). Although, this correlation appears weak, these types of studies typically do not correlate well (Figure 3.6 D). The 7 plasmids encode for the YFP-tagged proteins Mtw1, Ctf19, Ask1, Nuf2, Spc105, Ndc80 and Nkp2. The comparison between the two published sets of data (Figure 3.6 D) includes the same proteins (except Ndc80) with the addition of Cse4, Mif2, Ctf3, Ndc10, Cep3 and Chl4.

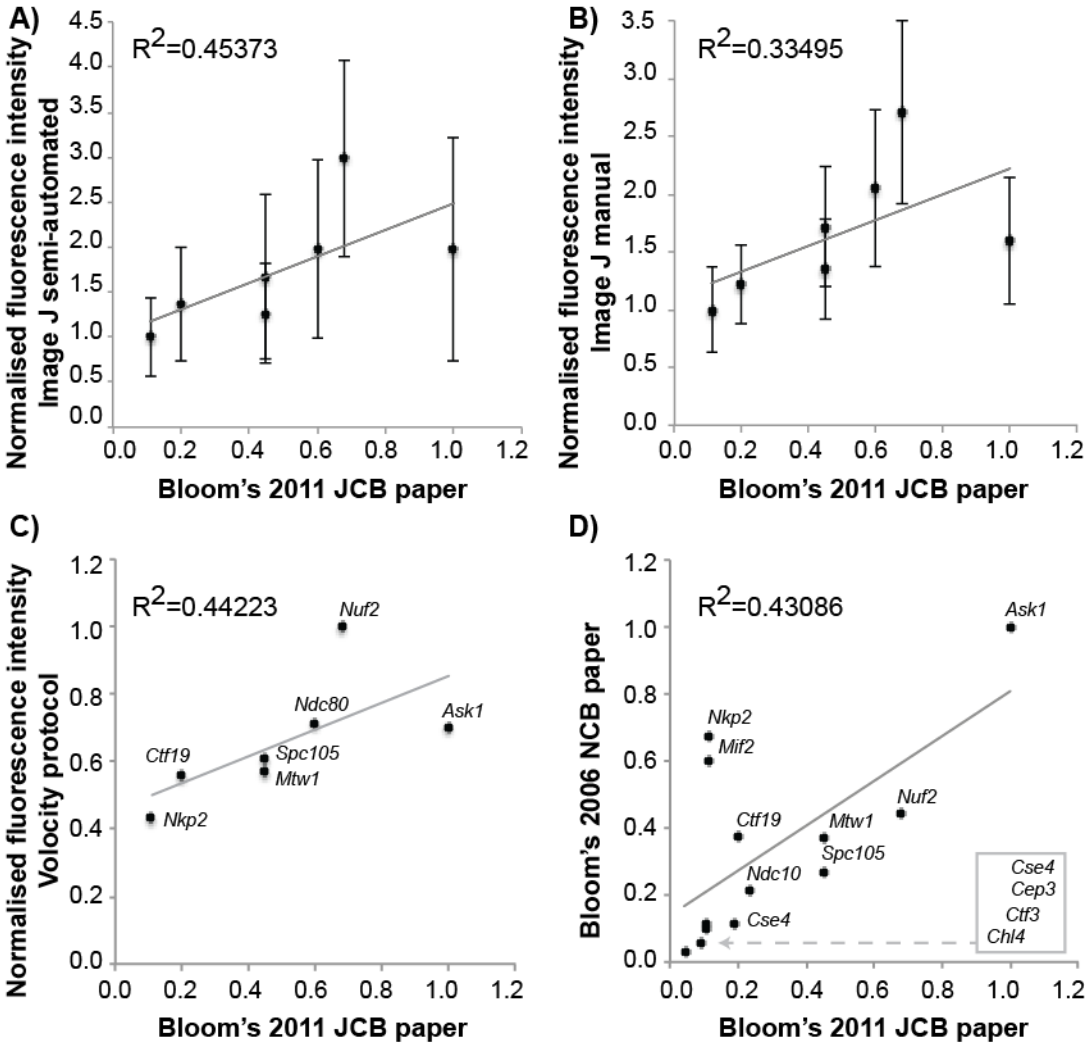

Figure 3.6. Comparison of plasmid data with published data. Published values for 7 plasmids (Lawrimore, Bloom and Salmon, 2011) were compared with the quantitation of those plasmids by ImageJ semi-automated **(A),** manual **(B)** and Volocity protocol **(C)** methods. Values were normalised by dividing each value by the minimum value. **D)** Comparison of the same published values with the values from a previous publication (Joglekar et al., 2006).

No substantial differences were found between most of the methods, thus, the automated version of the ImageJ protocol was chosen as the most appropriate software for a high-throughput screen. This method has the advantage that it uses a quantitation technique that is nearly identical to that previously used by the Bloom lab (Joglekar et al., 2006, Joglekar et al., 2008).

3.2.2.4. SPA mini-screen with Spc24 (NDC80 complex)

To assess our ability to monitor changes in kinetochore phenotype with fluorescence microscopy of tagged kinetochore proteins, I performed a pilot mini-screen. A total of 40 genes known to regulate chromosome segregation were selected from published work by Yuen et al (2007) (Table 2.6). I selected deletions of these genes from the deletion library and used "selective ploidy ablation" (SPA) (see methods) to introduce a plasmid encoding the tagged kinetochore protein Spc24-YFP, part of the NDC80 complex and involved in segregation, spindle checkpoint and kinetochore clustering. The use of the plasmid containing Spc24 was selected based on fluorescence intensity of YFP and RFP signal by comparing the plasmids available at the time. The Selective Ploidy Ablation (SPA) method (Reid et al., 2011) allows me to transfer one or more plasmids from a Universal Donor Strain (UDS) into an array of haploid mutants (see Figure 2.1, methods).

I then imaged the strains by taking advantage of a high-throughput imaging platform that allows me to acquire high-resolution images of the fluorescently-tagged yeast. This method is adapted from that of the Gitai lab (Werner et al., 2009), and involves imaging the yeast on small agar pedestals. I analysed the fluorescence intensity of kinetochore and spindle pole foci within images of Spc24-YFP and Spc42-RFP in the deletion strains as well as in controls by various software protocols outlined above. Some gene deletions were found to alter the intensity levels of Spc24 (Figure 3.7), either increasing (*ssz1*Δ*/pdr13*Δ*)* or decreasing (*lge1*Δ*, bim1*Δ*/eb1*Δ*, mcr1*Δ*, cft8*Δ*, rad27*Δ and *mcm22*Δ) the fluorescent kinetochore signal.

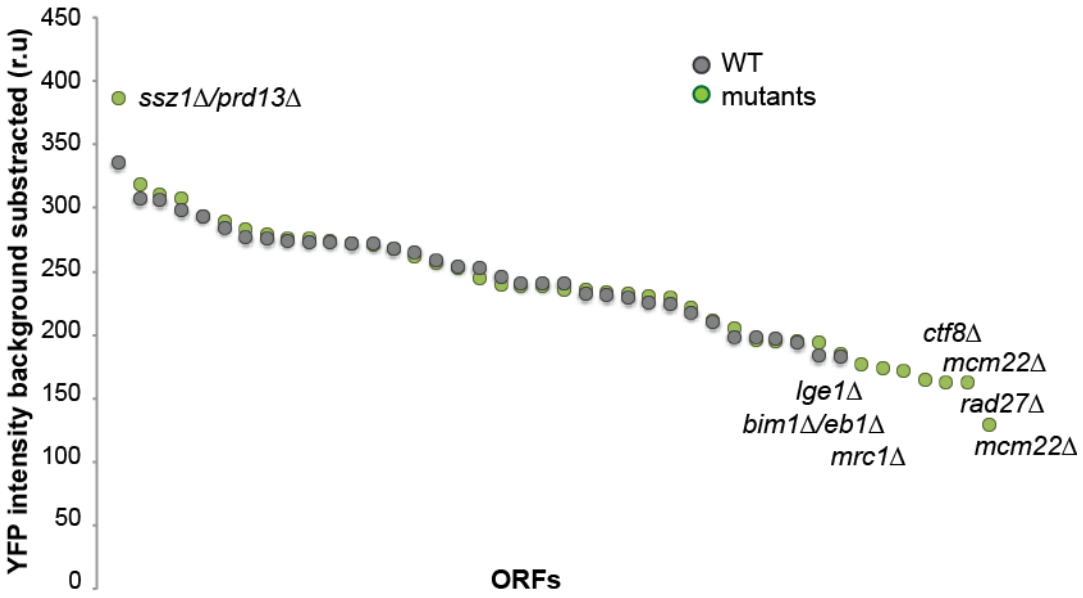

Figure 3.7. Miniscreen: genes that alter the YFP intensity levels of Spc24. Intensities are shown in grey for the wild type (WT) Spc24 used as control. Green indicates Spc24 intensities when crossed to the 40 strains of the deletion library. Those deletions causing intensity levels of YFP to increase or decrease in reference to the WT are named. Images analysed by ImageJ (automatic version). YFP intensity of individual kinetochore signal calculated as kinetochore minus background. Mean intensities per image are shown.

This approach allows me to image and analyse mutants with the tools explained above. However, wild-type controls show as much variation in YFP levels as the mutants.

3.2.2.5. Kinetochores and spindle poles may move independently of the nucleus and differently at different mitotic phases over a time period of a minute

Our image analysis methods all assume that the foci are relatively immobile during the time that the microscope takes to image a multichannel stack. To test if there is any considerable movement of YFP and RFP foci inside the nucleus in the time taken to image a stack, I performed one minute timelapse imaging of cells with a kinetochore protein (Mtw1) tagged with YFP, a SPB protein (Spc42) tagged with RFP and a histone H2A (Hta1) tagged with CFP in order to visualise the nucleus. All of these genes were endogenously encoded. Images were captured approximately every ~5 seconds (the maximum rate of our microscope at that time). I built a protocol in Volocity using the tracking module to record the position of each kinetochore, SPB and nucleus

independently per frame. I then calculated the displacement (μm) and velocity (μm/sec) from the x and y positions in each frame.

When tracking the movement of the foci over time, in most cases the foci did not move significantly during a single minute. However, in a minority of cases quite large displacements could be measured. These larger displacements do not have a uniform speed. Instead, displacements are discontinuous and variable in length (Figure 3.8). I found that the kinetochore foci movement characteristics depended on the cell cycle phase. Cells in G1 phase (Figure 3.8 A-B) have very little movement comparable with the nucleus as whole. However, in other cell cycle phases, the kinetochore and SPB show greater movement (Figure 3.8 C-H). At metaphase no kinetochore remained in focus and so it was not possible to analyse their movement, however, the SPBs show a pattern in which a large displacement is followed by no displacement (Figure 3.8 G-H).

In summary, for most kinetochore foci in our images the movement of the foci during the image acquisition will be minimal. However, I have to accept that for a small subset of foci, significant movement (~50 nm per second) will be observed. To minimise the effects of this movement on our images, I have optimised the acquisition times of our microscope (the time taken to capture an image). This has been helped by using a LED based fluorescent light source which can switch between different colours in ~50 μseconds coupled with multi-pass filters, which prevent the need to switch filters between images. Each kinetochore focus is typically imaged with 3 vertically separated z-slices (3 focal planes) and I can image 3 slices in <3 seconds.

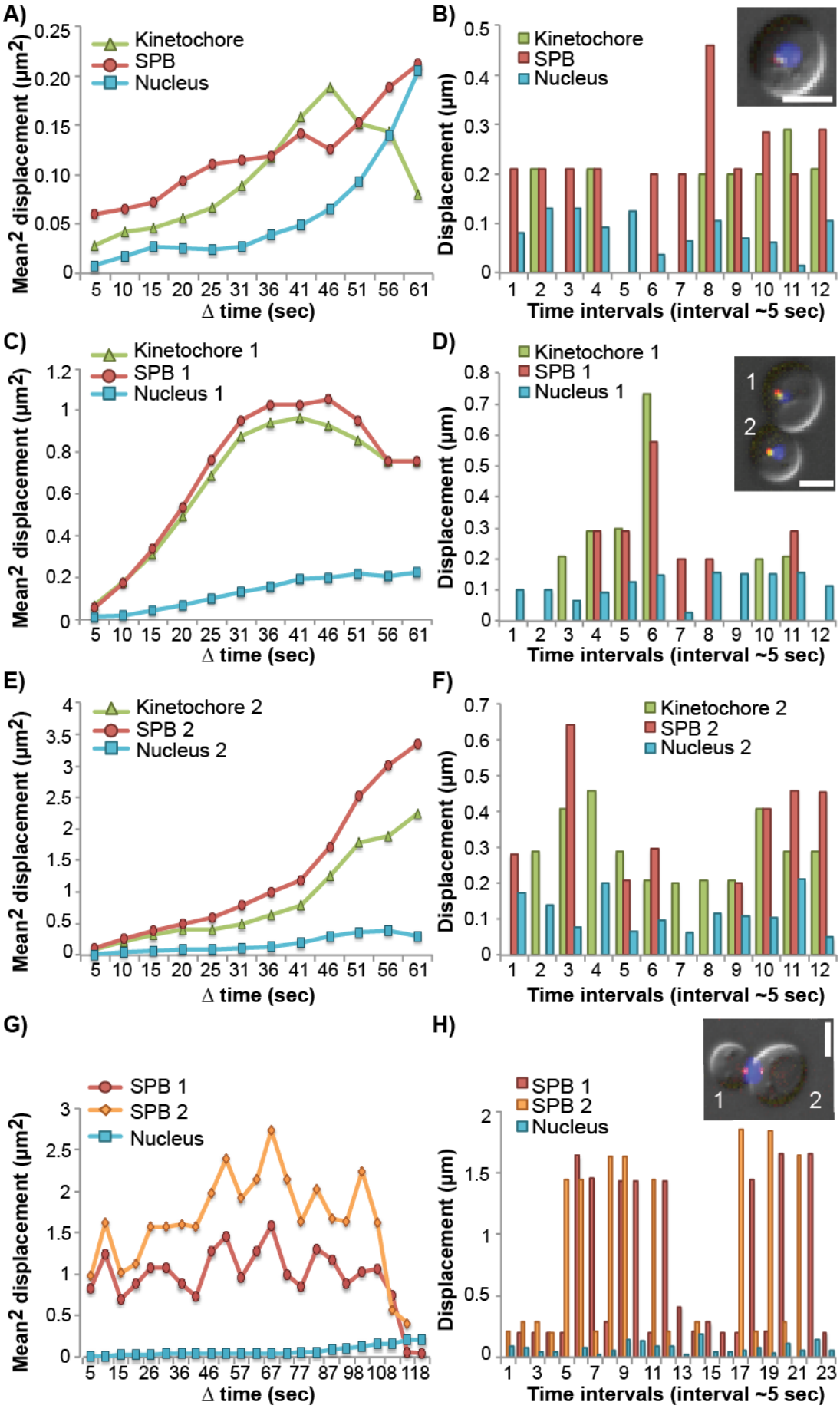
A)
Kinetochore
SPB
Nucleus
Mean2 displacement (µm2)
Δ time (sec)
B)
Kinetochore
SPB
Nucleus
Displacement (µm)
Time intervals (interval ~5 sec)
C)
Kinetochore 1
SPB 1
Nucleus 1
Mean2 displacement (µm2)
Δ time (sec)
D)
Kinetochore 1
SPB 1
Nucleus 1
Displacement (µm)
Time intervals (interval ~5 sec)
E)
Kinetochore 2
SPB 2
Nucleus 2
Mean2 displacement (µm2)
Δ time (sec)
F)
Kinetochore 2
SPB 2
Nucleus 2
Displacement (µm)
Time intervals (interval ~5 sec)
G)
SPB 1
SPB 2
Nucleus
Mean2 displacement (µm2)
Δ time (sec)
H)
SPB 1
SPB 2
Nucleus
Displacement (µm)
Time intervals (interval ~5 sec)

Figure 3.8. Movement of kinetochore Mtw1 and SPB Spc42 proteins
Movement analysed by Volocity software. Graphs on the left panels show average accumulative displacements between the first position at time 0 and each consecutive time in seconds. Bar charts show the displacement in μm measured at each interval of 5 seconds. Time-lapses measurements are shown over a minute for cells in G phase (**A-B**) and post anaphase (**C-F**), and over 2 minutes for cells in metaphase (**G-H**). Scale bars in inserts are 3 μm.

3.2.3. Selection of candidates for genome-wide screens

Four candidates (Dad2, Dad3, Dad4 (outer) and Ndc10 (inner)) were selected based on robustness of the plasmid fluorescence signal.

3.2.3.1. Dad2, Dad3 and Dad4 have the highest signal to noise ratio of the structural kinetochore proteins and Ndc10 among the inner kinetochore members

To further assess the robustness of the fluorescence signal, I selected the group of 33 Class I plasmids with visible bright YFP and RFP foci and low background (Table 3.1). I then compared the signal to noise ratio of the selected plasmids manually and by applying various protocols in Volocity. The plasmids that consistently gave the highest levels of YFP kinetochore intensity were pHT72 (Dad2), pHT94 (Kar9), pHT63 (Dad4) and pHT73 (Dad3) (Figure 3.9). Three of those proteins (Dad2, Dad4 and Dad3) are members of the outer kinetochore DAM1/DASH complex and were then selected as candidates for an outer kinetochore protein screen. Levels of Spc42-RFP produced by these plasmids were very similar (Figure 3.9). None of the plasmids encoding inner kinetochore proteins were among the higher intensity group. Ndc10-YFP had the highest YFP fluorescence signal for any inner kinetochore protein tested (intermediate levels among all plasmids) and also a high RFP signal (Figure 3.9). Ndc10-YFP was then selected as candidate for an inner kinetochore protein screen.

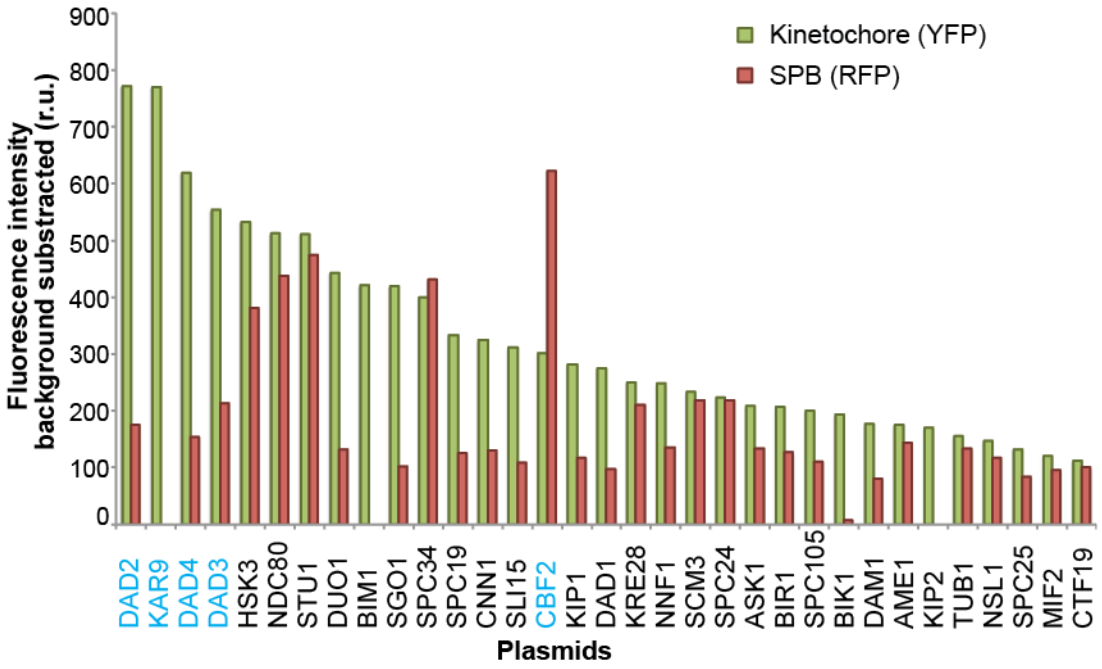

Figure 3.9. Fluorescence intensities of Class I plasmids. Mean intensities of YFP (green) and RFP (red) background subtracted for the 33 plasmids tested. Plasmids selected as candidates are indicated in blue font.

3.2.4. Assessment of the use of plasmids for genome-wide screens

To assess whether the use of these plasmids was suitable for the genome-wide screens, their fluorescence phenotype was compared with endogenously tagged versions of the same genes. The plasmids were tested for stability, functionality and variability of the fluorescent signal.

3.2.4.1. Dad2, Dad3, Dad4 and Ndc10 encoding plasmids are lost in 20-35% of cells

I assessed the stability of the plasmids in yeast cells by measuring the frequency of plasmid loss of the four plasmids (encoding tagged versions of Dad2, Dad3, Dad4 and Ndc10). I grew the plasmids overnight in media lacking leucine to maintain the plasmid (the yeast strain is auxotrophic for leucine synthesis and this is rescued by the plasmid which has a *LEU2* gene). I then plated 500 or 1000 cells on media that either contains leucine (SC) or lacks leucine (-leu). Only cells containing the plasmid will form colonies on –leu plates, whereas all cells will grow on SC media. By comparing the colony counts from both plates I calculated the plasmid loss rates (Figure 3.10 A).

Cells expressing the inner kinetochore candidate, Ndc10, have the greatest plasmid loss rate (35%). Of the outer kinetochore expressing plasmids Dad4 was lost from 30% of cells versus 20% for Dad2 and Dad3. However, there was considerable variation between repeated experiments; Dad4 was the most consistent, with losses between 26 and 33%. Loss of Dad2 plasmid varied from 11 to 31%, Dad3 plasmid from 2 to 32% and Ndc10 from 29 to 44% (data not shown).

To find if these plasmid loss rates correlate with the proportion of cells in an image that do not have visible foci, I calculated the percentage of cells that had no detectable YFP signal in images by manual cell counting (Figure 3.10 B). I found that an average of 23% in Dad4, 41% in Ndc10, 16% in Dad3 and 29% in Dad2 cells had no signal. In summary, there is significant and variable plasmid loss for all of the plasmids tested and consistent with this finding, a proportion of the cells in each image contain no YFP signal (Figure 3.10.C). In contrast, later work shows that 100% of cells expressing endogenously tagged kinetochore genes with YFP have signal (see chapter IV, Figure 4.1).

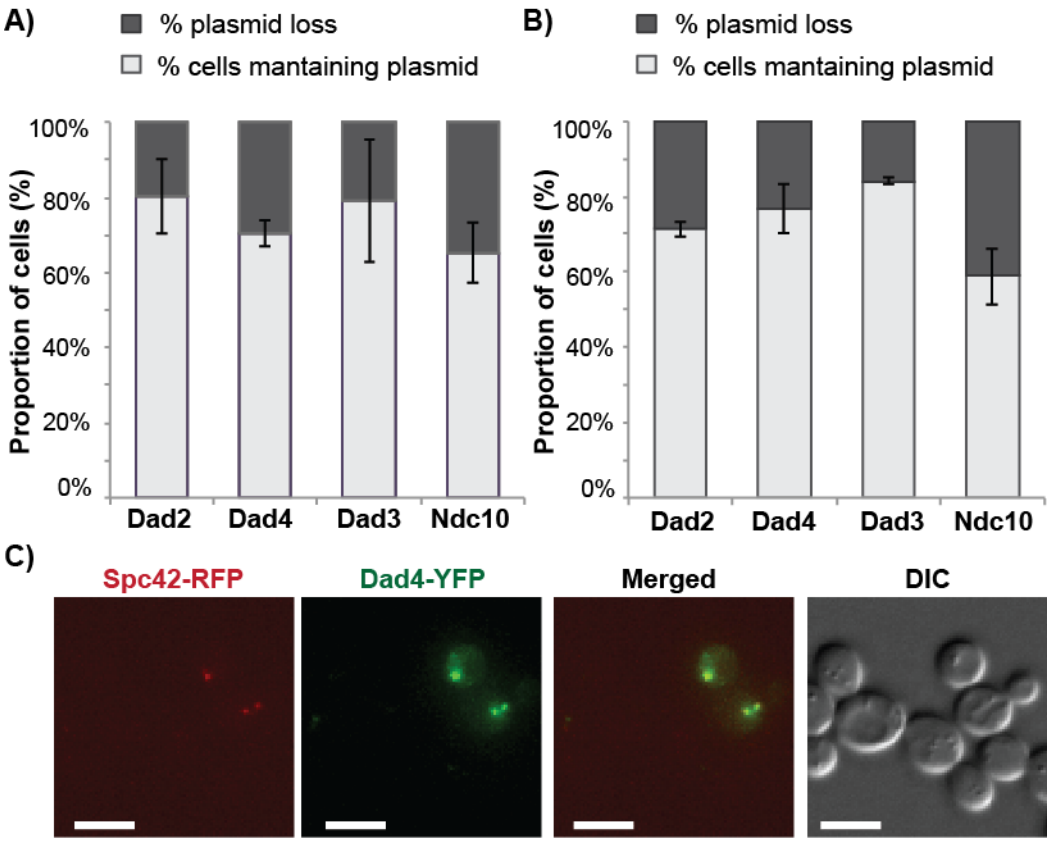

Figure 3.10. Plasmid loss. Calculated plasmid loss from colony plate counts **(A)** and fluorescent foci counts **(B)**. Error bars indicate 95% binomial confidence intervals. **C)** An example image of yeast cells transformed with a plasmid encoding for Spc42-RFP (red) and Dad4-YFP (green). Scale bars are 5 μm.

3.2.4.2. The plasmids coding for Dad2, Dad3 and Dad4 are functional, the plasmid coding for Ndc10 could not be confirmed

To test if the four plasmids (encoding Ndc10, Dad2, Dad3 and Dad4) produced functional protein, I substituted the endogenous copy of the relevant kinetochore genes with a Kanamycin (KAN) coding cassette in cells containing the appropriate plasmid. In these deletion strains, the cells rely upon the plasmid-based copy of the relevant protein for their essential function (each of these genes is essential). The presence of the *LEU2*+ plasmid and endogenous *KANMX* deletion cassette were confirmed by plating on both –leu media and rich media containing the drug G418 respectively. Only cells with the *KAN* insertion are resistant to the drug and can thus grow. The correct position of the *KAN* insertion was confirmed using a diagnostic PCR reaction. The plasmids coding for Dad2, Dad3 and Dad4 were found to be able to complement their corresponding deletions (*dad2*Δ*, dad3*Δ and *dad4*Δ in the strains T6, T8 and T7 respectively (Table 2.2). These cells were viable and contained foci for both YFP and RFP (data not shown). However, numerous attempts to replace the endogenous copy of *NDC10* with a *KANMX* cassette failed, despite the presence of the *NDC10-YFP* plasmid. Therefore I have no evidence that the *NDC10* plasmid is functional and indeed the failure to delete the endogenous gene may suggest that the tagged Ndc10 may not be functional.

3.2.4.3. Variation of fluorescent signal is greater for plasmid-encoded Dad4-YFP than for endogenous Dad4-GFP

I speculated that plasmid loss would cause greater fluctuations in kinetochore fluorescence levels, than when the fluorescent tag is endogenously encoded. This is because some cells may have more than one copy of plasmid while others will have lost it. In addition, the endogenous untagged protein may compete for inclusion into the structural kinetochore and even may be preferentially loaded. To test this hypothesis, I compared images of cells with the *DAD4-YFP* plasmid (pHT63) with images of endogenously-tagged *DAD4-GFP* from the GFP-library (Huh et al., 2003). Although it is not possible to directly compare YFP and GFP fluorescence levels, I compared the variation of signal between a series of images of endogenously- and plasmid-encoded fluorescent kinetochores. An example can be seen in Figure 3.11. The fluorescence levels of kinetochores vary considerably more for plasmid-based expression than for endogenously encoded alleles, as indicated by a larger coefficient of variation (standard deviation/mean, Figure 3.11).

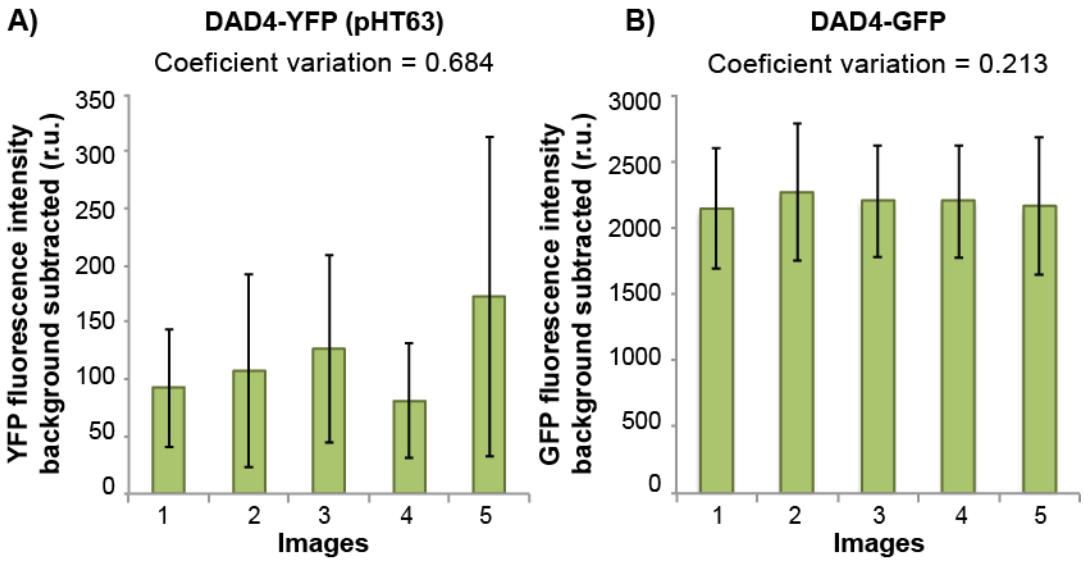

Figure 3.11. Fluorescent signal in plasmid-encoded and endogenously tagged kinetochores. The mean fluorescent intensity values of all the kinetochore foci in 5 images are shown for plasmid-base tagged Dad4-YFP **(A)** and endogenously tagged Dad4-GFP (from the deletion library) **(B)**. Error bars are standard deviation. The calculated coefficient variation is indicated.

When taken together, my data show that a plasmid based approach to insert fluorescently-tagged kinetochore genes into mutants has some key disadvantages compared with using an endogenously encoded version of the gene. These disadvantages would cause problems for quantification. Consequently, I decided to switch my screening strategy and use endogenously-tagged genes for future studies that are described in the next chapter.

3.3. Summary and discussion Results 1

Fluorescent tags can be encoded endogenously by modifying the genomic locus of a gene to include the sequence encoding the fluorophore. Alternatively, the tagged gene sequence can be encoded either ectopically within the genome or on a plasmid. A plasmid approach was first favoured since it allowed us to test many different kinetochore genes and is faster since the SPA method creates the strains for the screen in approximately 5 days (Reid et al., 2011). I constructed plasmids (together with Erika Aquino) coding for 68 kinetochore and kinetochore-associated proteins tagged with yellow fluoresce protein (YFP). In addition, the plasmids also code for the spindle pole body (SPB) protein Spc42 tagged with red fluorescent protein (RFP). In this way, I have been able to visualise both kinetochores and spindle pole bodies in the same cells.

In order to perform a genome-wide fluorescence microscopy screen we needed an imaging and analysis method that was adequate for the nature of this screen.

3.3.1. Methodology for imaging and analysis

3.3.1.1. Microscopy: trouble shooting

The wide-field fluorescent imaging system is established in our lab and modifications were made to improve the quality of the images both by changes in the microscope settings and in the way I prepare the cultures. I acquired high-resolution images of the fluorescently tagged cells by a method adapted from that of the Gitai lab (Werner et al., 2009), which involves imaging the yeast on small agar pedestals.

One important aspect for good imaging is that the object being imaged does not move. A “blurred” image will alter the measured levels of fluorescence. Consequently, I studied the movement of kinetochore foci using time-lapse microscopy. I took images every few seconds for one minute in total, since to capture a 21 layer Z stack of images with multiple colours takes approximately this long. Analysis of the time-lapse imaging of kinetochore foci show that they move with a small diffusion-like motion in most cases but with sudden larger displacements in some cases. To rule out the possibility that this motion was caused by movement of the entire cell or microscope slide, I repeated the time-lapse imaging of a strain with tagged kinetochores, SPBs and nuclei. Since the nuclei are relatively immobile, I can assume that the motion of the kinetochores and SPBs is independent of that of the cell. In my preliminary analysis, it seems that the motion of kinetochores and SPBs differ in different cell cycle phases, with the large

displacements restricted to mitotic phase. This is, of course, consistent with the time when chromosomes and kinetochores are associated to a dynamic spindle.

To minimise the effects of kinetochore motion on my imaging, I made changes in the microscope settings as well as optimizing and reducing the exposures times of YFP and RFP to 40 ms and 50 ms respectively. Also, our lab now has an LED fluorescence illumination system which functions faster than the mercury vapour lamp used previously. These improvements have successfully reduced the imaging time to 20 seconds per stack (21 x 0.35 μm separated focal planes, z-slices). By doing this, the average expected displacement of a kinetochore during the imaging of the entire stack would be 90 nm. Individual kinetochores are typically contained within 3 z-slices reducing the average displacement for an individual kinetochore to an average of 13 nm (with a maximum of up to 420 nm in rare and extreme cases).

3.3.1.2. Image analysis methods

Due to the large number of images that I need to analyse as part of a genome-wide screen, I want to identify kinetochores and spindle poles automatically and obtain measurements such as the fluorescence levels of foci and background as well as their three-dimensional (3D) position. Ideally, the relationship between individual kinetochores and SPBs would be defined i.e. which kinetochores and SPBs are in the same cell. Image analysis methods have been described in the literature (Joglekar et al., 2006; Wu, McCormick and Pollard, 2008; Lawrimore, Bloom and Salmon, 2011). These methods differ in some respects but all are based on integrating pixel values within defined areas (rectangles or circles) on either the plane of highest intensity or the sum of the z-slices. To get a measure of background an area outside the foci area is measured in the same way. For each focus the average pixel value of the background is subtracted from the average pixel value of the foci to derive a corrected foci value.

Manual, semi-manual and automatic image analysis methods were developed and tested for both Volocity and ImageJ (Fiji) software. The Volocity image analysis package is convenient for searching visually for abnormal patterns of fluorescence, however, for automated analysis of multiple images, the best option is the construction of custom software protocols. The Volocity protocols work very well when applied to cropped single cells or for single images with separated cells. However, it is not possible to use the same protocol efficiently between images with very different intensity foci and this makes it unsuitable for large number of images produced in screens. A manual selection procedure was developed in our lab using ImageJ that is accurate and it is able to

differentiate mitotic cells. In addition, it automatically finds the closest SPB to each kinetochore and associates them reducing the time for analysis. However, this manual method is still time consuming and would take a long time to apply to a screen. Thus we developed a fully-automatic ImageJ macro that requires no manual input and is much faster, although is not as accurate as the manual software in some aspects. For instance, it cannot differentiate dead cells. In addition, no cell cycle information is returned. However, some of these issues can be addressed computationally after image analysis. I am able to computationally identify dead cells, based upon the high level of background fluorescence detected using the automatic image analysis software. A possible solution to the problem of relating foci to other foci within cells could be to use the x, y, z positions to calculate distances and associate foci that are very close to each other. Another approach could be to introduce another fluorescent tag, CFP for instance, to mark the nuclear membrane or the cell membrane, in order to make it easier for software to recognise and segment cells. Some other possible software that could be applied in this case to include segmentation would be CellProfiler (Broad Institute), MATLAB (MathWorks) and FindFoci (Herbert, Carr and Hoffmann, 2014). Although, these later approaches are outside the scope of my PhD project, a retrospective analysis of my data may prove informative as the software is improved.

In summary, the automatic ImageJ software can be run on all images in a fast manner and then corrections can be done computationally. In addition, the manual ImageJ software can be applied later to a reduced number of images highlighted by the automatic method for a more detailed analysis.

3.3.1.3. Pilot mini-screen with Spc24

To assess what changes in phenotype could be detected by these imaging methods, and what problems I might encounter when performing the genome-wide screens, I performed a mini-screen. I introduced a plasmid encoding a tagged NDC80 complex member Spc24-YFP into a subset of the deletion library using the SPA method. The resulting images allowed me to test and modify the automated and semi-automated versions of ImageJ image analysis software. Additionally, these data lead me to conduct the “motion” study described above. A set of 9 mutants was found to increase or decrease the intensity of Spc24-YFP (Figure 3.9). This mini-screen validated our imaging approach and significantly helped me refine methodology. However, variability in the images from this screen together with the disadvantages of using plasmids discussed below ultimately led me to abandon the use of plasmids for the genome-wide screens. Thus, I am not confident that the 9 mutants significantly affect kinetochores,

and I do not plan to analyse them further, unless they are validated using endogenously tagged kinetochore proteins.

3.3.2. Selection of candidates

In order to select the best candidates for microscopy screens I imaged the 68 plasmids and compared their fluorescence. The YFP kinetochore signal was variable within the plasmid array and plasmids were assigned into three distinct classes (Figure 3.2, table 3.1). About half of the plasmids had foci clearly distinguishable from the background (Class I), the rest had higher background and either had weak foci (Class II) or no discernable foci (Class III). One reason for these differences could be the stoichiometry of these complexes. In fact, all the DAM1 complex members are in Class I (Table 3.1), and published data indicates that this complex is present in 16-20 (Joglekar et al., 2006) or ~32 copies per kinetochore (Lawrimore, Bloom and Salmon, 2011). In contrast, members of the CTF3 kinetochore complex, which is only present in a single copy (Joglekar et al., 2006) or 2-3 proteins per kinetochore (Lawrimore, Bloom and Salmon, 2011) were Class II/III (Table 3.1). However, not all plasmids match the reported stoichiometry in the literature. For instance, the NDC80 complex is formed by four members in a 1:1:1:1 ratio and it is reported to have 7-8 (Joglekar et al., 2006) ~19 copies per kinetochore (Lawrimore, Bloom and Salmon, 2011). Three members of the NDC80 complex are in Class I as expected, however, the fourth member, Nuf2 has no foci. Despite the correct DNA sequence the tagged version of the gene on the plasmid could have a functional problem preventing its inclusion into a kinetochore. In addition, many of the plasmids that produce fluorescence signals that fall into Class II and III are auxiliary and checkpoint proteins rather than core structural elements of the kinetochore. It should be remembered that plasmid encoded kinetochore proteins generally have to compete for inclusion into the kinetochore with untagged endogenously encoded copies. Unpublished data from our lab suggests that at least for core structural components of the kinetochore, there is a fixed amount of protein that can be included into the kinetochore structure and consequently there is direct competition between plasmid encoded and endogenously encoded protein. Thus for some proteins the fluorescent tag may impede their ability to compete for inclusion.

To find kinetochores for quantification with either Volocity or ImageJ software, fluorescent foci have to be distinguisible from the background. Therefore, Class I proteins were selected for further analysis and three DAM1 complex members (Dad2, Dad3 and Dad4) and one CBF3 complex member (Ndc10) were selected as candidates for screens based on signal to noise ratios produced by these plasmids. However, the

suitable use of plasmids for the screen was put into question by a series of experiments aiming to confirm the equivalence of ectopically-tagged proteins with endogenous.

3.3.3. Assessment of the use of plasmids for the screen

DAD4, *DAD3*, *DAD2* and *NDC10* are all essential genes. This allowed me to test the functionally of the plasmids by deleting the endogenous copy of the corresponding gene. Only if a plasmid encodes a functional protein, will the cells tolerate deletion of their endogenous allele. Although plasmids coding for Dad2, Dad3 and Dad4 were found to be functional, the endogenous *NDC10* gene could not be deleted successfully in cells carrying a *NDC10-YFP* plasmid, suggesting that this plasmid is not functional and perhaps the addition of the YFP sequence at the C-terminal was causing some sort of interference with the protein's function. However, Ndc10 can be endogenously tagged both as haploid (YFP and GFP) and as a heterozygous diploid (with YFP and CFP tags) (Huh et al., 2003; Thorpe et al., 2008). An alternative possibility is that the linker sequence between the gene and the YFP, which is different in the plasmid than in the endogenously tagged strains, caused the lack of functionality. I thus created a new plasmid by substituting the plasmid linker for the E90 strain linker. The resulting strain presented very clear defective phenotypes in two attempts of creating this plasmid but sequencing confirmed mutations in both cases. Another possibility is that this protein does not tolerate moderate overexpression from the *CUP1* promoter (which is active even in the absence of copper in the medium). Ndc10 is a member of CBF3 complex, which orchestrates the assembly of kinetochores, whiles the DAM1 complex is involved in attachment of kinetochores to microtubules. Thus, it is possible that the CBF3 complex homeostasis is under different and stricter regulation than the DAM1 complex.

In addition to these functionality problems with *NDC10*, plasmid loss and variability of kinetochore fluorescence levels between images from plasmid-encoded genes was observed. This variation in fluorescence intensity raised clear problems for any mutant screen. First, I can not be sure whether cells that lack YFP signal have lost the plasmid or have a genuine kinetochore phenotype. Second, I would expect significant variation in intensity of YFP in the population as cells are continuously losing plasmids (for example, cells with recent plasmid loss might have a weak but detectable YFP signal, which could be misinterpreted as a kinetochore phenotype). Also mutants that affect plasmid loss or *CUP1* expression would complicate the interpretation of the data.

Endogenously tagged kinetochore genes from the GFP library were found to have fluorescence foci in every cell and have more stable kinetochore fluorescence levels

across images and colonies of the same strain compared to plasmid based expression. Some variability in fluorescence levels remains even in endogenously encoded kinetochore proteins, which could be due to different stages of the cell cycle. For instance, cells in G1 may have a single kinetochore or they may have already duplicate their kinetochores, however, only one focus would be detected with our microscopy system in both cases. However, it should be noted that there is some considerable degree of variation in kinetochore fluorescence even for endogenously-tagged genes measured at a fixed point in the cell cycle (Joglekar et al., 2006; Ledesma-Fernandez, 2015). This could be caused by variation in folding or maturation of fluorophores or by partial declustering of kinetochores in a subset of cells.

Taking into account all of these data, the use of plasmids for screens was disfavoured, and endogenously-tagged strains for the same candidate genes are discussed in Chapter IV.

Chapter IV: Results 2: Genome-wide endogenous fluorescent microscopy screens

4.1. Introduction

My data shown in Chapter III shows that the plasmid-based fluorescent tagging of kinetochore genes has some disadvantages and I decided to switch strategy to use endogenously-tagged genes for the genome-wide screen. However, this meant that the SPA method to introduce a plasmid into a set of mutants was no longer applicable.

A high-throughput method to construct double mutants was developed in the Boone lab to identify synthetic lethality between yeast genes (Tong et al., 2001). This method, called synthetic genetic array (SGA), has since then been adapted and widely used, for example, to combine tagged strains with mutant arrays such as the GFP collection with the deletion collection (Tkach et al., 2012). The SGA method allows for mating of 2 strains in a high-throughput manner, and a series of copy replicas into selection medias produce an array of strains that are haploid and have any tagged genes and mutations for which we have a selection.

From the work done with plasmids (Chapter III) the highest fluorescence was detected with tagged versions of Dad2, Dad3 and Dad4, all members of the DAM1/DASH complex. Other members of this complex when tagged with fluorophores also had strong fluorescence signals. One reason for this could be the stoichiometry, since this complex is present at the kinetochore in 16-20 (Joglekar et al., 2006) or ~32 copies (Lawrimore, Bloom and Salmon, 2011), higher number than any other kinetochore complex. Although the use of plasmids had been abandoned, and thus the selection process doesn't necessarily apply, high levels of fluorescent signals would be an advantage for a genome-wide microscopy screen. In fact, the fluorescence signal of members of the DAM1 complex is higher than that of Ndc10 (Figure 4.1), Mtw1 or Mif2 (Ledesma-Fernández and Thorpe, 2015) when comparing endogenous strains.

The DAM1/DASH complex is the outermost kinetochore complex and it is essential for correct chromosome segregation. The 10 members of this complex form rings around microtubules *in vitro* (Miranda et al., 2005; Westermann et al., 2005). The DAM1 complex is able to track microtubule plus-ends where it recruits and binds to the NDC80 complex and, in this way, it maintains the attachment of kinetochores to dynamic microtubules (Lampert, Hornung and Westermann, 2010). In addition, it harnesses these dynamics to produce the necessary force for chromosome movement and ensuring chromosome segregation (Asbury et al., 2006).

Some members of the DAM1 complex such as Dam1 have been widely used in studies of the outer kinetochore and information about this protein is available. However, for some members such as Dad3 and Dad4, two of the last three members to be identified, (Cheeseman et al., 2002; Li et al., 2005) not much information is available. A two-hybrid screen on mitotic spindle and kinetochore proteins in *S. cerevisiae* identified novel interactions between the kinetochore, specifically the DAM1 complex, and chromatin associated proteins. These included interactions of poorly-characterised subunits of the DAM1 complex such as Dad4 with the SWI chromatin remodeling complex and the mediator complex (Wong et al., 2007). These data suggested that the DAM1 complex would be an interesting candidate to perform the screen. A screen with an outer kinetochore protein, in addition, may reveal genes that are important for microtubule-kinetochore attachment that may not be detected with an inner kinetochore protein.

For the endogenous microscopy screen I decide to tag also endogenously the SPB protein Spc42 as a reference. Spc42 has been widely used as readout of SPB in the literature tagged with fluorescent proteins, including RFP (Huh et al., 2003).

In this work, I have taken advantage of the SGA methodology to combine a doubly tagged strain for the outer kinetochore protein Dad4 and the SPB protein Spc42 with the entire deletion library and the TS collection. Imaging of the resulting mutant array of tagged strains and analysis of the fluorescent signal has revealed a number of deletions and alleles that alter the intensity or localisation of Dad4.

4.2. Results

4.2.1. Construction of endogenously tagged fluorescent kinetochore proteins

In order to use the SGA approach I had to construct *DAD4-YFP* and *SPC42-RFP* alleles compatible with this technology. Briefly, both fluorescent alleles must be linked to selectable markers and these combined in a strain with a so-called "magic marker". Magic markers are simply markers whose expression is controlled by sex-specific promoters, i.e. expressed only in either *MAT***a** or *MATα* cells. In short, I have constructed strains that contain the *SPC42-RFP* gene linked to a hygromycin resistance gene (*SPC42-RFP::HYG*) and a tagged kinetochore gene, such as *DAD4-YFP* linked to nourseothricin resistance gene (*DAD4-YFP::NAT*). In addition, the strains also contain two "magic markers", *can1::STE2pr-Sp-his5* where *HIS5* is only expressed in *MAT***a** cells and *lyp1Δ::STE3pr-LEU2* where *LEU2* is only expressed in *MATα* cells. These strains are compatible with the SGA methodology (Tong et al., 2001). Three strains *MAT***a** (T37 (Dad4-YFP), T38 (Dad3-YFP) and T39 (Ndc10-YFP)) and three *MATα* (T34 (Dad4-YFP), T35 (Dad3-YFP) and T36 (Ndc10-YFP)) were successfully obtained (Table 2.2) and microscopy confirmed the presence of YFP and RFP signal in all cases (examples in Figure 4.1). Fluorescent signal is present in 100% of the cells for both YFP and RFP. Although the intention was to perform the screen with an outer kinetochore protein, I also constructed the strain with the inner protein Ndc10. In chapter III, the plasmid-encoded Ndc10-YFP was likely not functional. However, I was readily able to tag the endogenous *NDC10* allele and cells appear morphologically normal as do their Ndc10-YFP foci, unlike the high background and aberrant foci observed in the plasmid-encoded Ndc10-YFP.

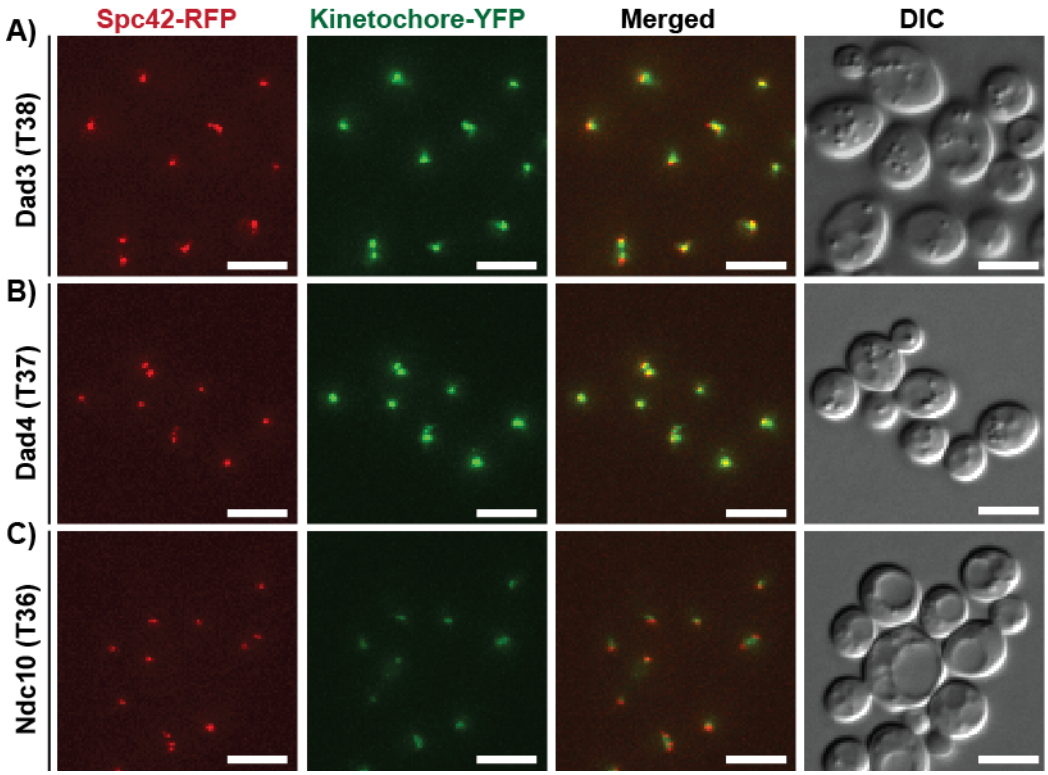

Figure 4.1. Yeast cells doubly tagged endogenously. Red foci represent the Spc42 SPB protein tagged with RFP. Green foci represent the YFP tagged Dad3 (**A**), Dad4 (**B**) and Ndc10 (**C**) kinetochore proteins. Images visualised by Volocity. Scale bars are 5 µm.

4.2.2. Synthetic Genetic Array (SGA) screens with Dad4 (DAM1 complex)

Strains for three tagged kinetochore proteins were successfully constructed. As discussed before, signal for Dad3 and Dad4 (outer DAM1 complex) is stronger than for Ndc10 (inner CBF3 complex), thus, this complex was selected. I used SGA to transfer the two fluorescence alleles (*DAD4-YFP* and *SPC42-RFP*) into the deletion library and the temperature sensitive collection. A schematic of this SGA approach is outlined in the Materials and Methods. In brief, the doubly-tagged strain was mated with an array of deletion strains (each deletion is marked with a Kanamycin resistance gene) to create heterozygous diploid strains. These diploid strains were then put through meiosis to create new haploid strains containing a mix of the parental alleles. Initially, haploid cells were selected using the *lyp1Δ::STE3pr-LEU2* magic marker, a second round of selection introduces Kanamycin to select for the deletion, a third round of selection then introduces nourseothricin to select for the tagged kinetochore gene and finally hygromycin was included to select for the *SPC42-RFP* allele. The resulting cells should

be *MATα* haploids that contain the deletion and the two fluorescent alleles. All the selection steps were performed on solid agar medium using a Singer RoToR pinning robot to transfer the thousands of strains between the different selective media. The same process was repeated to combine the alleles with the temperature sensitive collection.

My version of the *MATα* deletion library contains 6144 strains of which 1302 are wild-type controls that have a *his3Δ::KANMX* deletion (note that all the other deletion strains are *his3Δ1*). This set of strains was re-arrayed from the deletion collection (Winzeler et al., 1999) by Bob Reid in Rodney Rothstein's lab and was used to develop the SPA methodology (Reid et al., 2011). Of the 4842 mutants, 96 are duplicates and 4746 correspond to unique ORF deletions. The temperature sensitive (TS) collection contains 1334 strains with 754 unique alleles, which correspond to 475 unique ORFs (Li et al., 2011). This is because some of the alleles are repeated in the collection and in addition, different alleles for the same ORF are often included. The 6144 *MATα* strains in the deletion collection were combined with the *MAT***a** T37 doubly-tagged strain (*DAD4-YFP SPC42-RFP*) (Table 2.2). The 1334 *MAT***a** strains in the temperature sensitive collection were combined with the *MATα* T34 doubly-tagged strain (*DAD4-YFP SPC42-RFP*) (Table 2.2). Strains were arranged into 384-colony plates and the SGA protocol was performed as outlined in the Materials and Methods; the TS collection manipulations were all performed at 23˚C.

4.2.3. Microscopy screens with Dad4 (DAM1 complex)

Each of the 384-colony plates was copied onto four 96-colony plates. Prior to microscopy, strains were grown in 96-well liquid plates overnight in synthetic complete media containing adenine at 23˚C. Cultures were diluted in the morning and imaged a few hours later in 48-well agar pedestals. Imaging was performed as described in the Materials and Methods; a z-stack of 21 focal planes each separated by 0.35 μm with two-channel image acquisition (YFP and RFP).

Normally, only one image per strain was taken for the deletion mutants and 3 images for the TS alleles. In each case the field of view was selected manually to provide an optimal image in terms of focus and number of cells.

4.2.4. Foci quantitation

The automated version of the ImageJ script (FociQuant) described previously (Chapter III) was used to analyse the intensity of the foci in each image as described in the Materials and Methods and Ledesma-Fernández & Thorpe 2015 (attached in appendix 3).

The fluorescence intensity value for each focus is calculated as the mean YFP value minus the median background. For each strain the mean value of all the foci within an image was used to represent the kinetochore foci fluorescence of that strain.

4.2.5. Normalisations

It is known from other high-throughput studies looking at colony growth that arrays of mutants grown in plates are subjected to differential growth that is not necessarily due to the mutation in question. For instance, colonies at the periphery of the plate grow better than colonies in the centre, as do colonies neighbouring colonies with slow growth. A number of factors can affect growth in these types of screens and these have been described in the literature and methods have been used to correct for these effects (Baryshnikova et al., 2010).

I wanted to determine whether there was also a position effect that would affect the fluorescence intensity values in my imaging screen. When plotting the mean kinetochore fluorescence value per image in the order that the images were taken, groups can be seen clearly (Figure 4.2 B) These groups of images start with low fluorescence values which increase progressively until they drop abruptly at the beginning of a new group. Each of these groups corresponds to a separate pad. I noticed an effect across all of the 120 pads in the screen; the highest values had a tendency to be towards the right of the pad, as seen in the typical kinetochore fluorescence values for a single pad (first panel in Figure 4.2 A). This could be a pad position effect or a temporal effect, as the pads were imaged in the following order: (column 1(row F to A), column 2 (row A to F), column 3 (row F to A) and so on, the last images were column 8 (row A to F).

To correct for this effect I used a script developed in the lab that normalises any array based high-throughput data (Olafsson and Thorpe, 2015; source code available here https://sourceforge.net/projects/zspatialcorrect/). This PERL script corrects the values in each well upon adjustment to the median of each column and each row, all relative to the median value of the plate (second panel in Figure 4.2 A) and then normalises all the

values in the screen relative to the median of the entire screen (third panel in Figure 4.2 A). As shown in Figure 4.2 A, when correcting and normalising the scores, the highest values remain the highest. For instance, the highest value in column 1 before normalisation is still the highest after the corrections. However, the noise is reduced (Figure 4.2 B-C). From this point on, the term ‘intensity’ in the context of fluorescence will be used to reflect the mean kinetochore intensity with the median background subtracted and normalised by position on the plate and the screen.

A)

Original scores

	1	2	3	4	5	6	7	8
A	213.893	224.959	219.029	300.552	279.171	374.190	290.123	313.551
B	273.531	251.190	255.871	353.424	339.831	330.789	305.780	320.963
C	214.292	249.299	261.263	318.970	358.181	230.509	233.229	305.059
D	218.147	238.689	257.111	181.737	450.264	301.309	195.974	316.877
E	230.529	231.369	278.398	278.326	384.352	359.077	230.043	327.061
F	209.129	237.514	232.014	24.778	324.465	325.121	319.210	318.530

Corrected scores

	1	2	3	4	5	6	7	8
A	279.275	268.458	244.140	292.715	211.767	327.836	310.049	277.449
B	327.501	283.276	269.569	334.173	261.014	273.023	314.293	273.448
C	275.012	288.137	281.712	306.471	286.115	179.494	248.493	264.296
D	280.409	279.069	279.101	170.779	379.740	251.836	212.780	277.655
E	280.838	259.796	288.436	255.416	301.875	297.651	234.896	275.886
F	276.234	282.736	258.847	18.663	258.784	280.490	340.858	284.150

Corrected and normalised scores

	1	2	3	4	5	6	7	8
A	260.604	249.788	225.469	274.044	193.096	309.166	291.378	258.778
B	308.830	264.605	250.898	315.502	242.343	254.352	295.622	254.777
C	256.342	269.466	263.041	287.800	267.444	160.823	229.822	245.625
D	261.738	260.398	260.430	152.108	361.069	233.165	194.109	258.984
E	262.167	241.125	269.765	236.745	283.204	278.980	216.225	257.215
F	257.563	264.066	240.176	-0.008	240.113	261.819	322.187	265.480

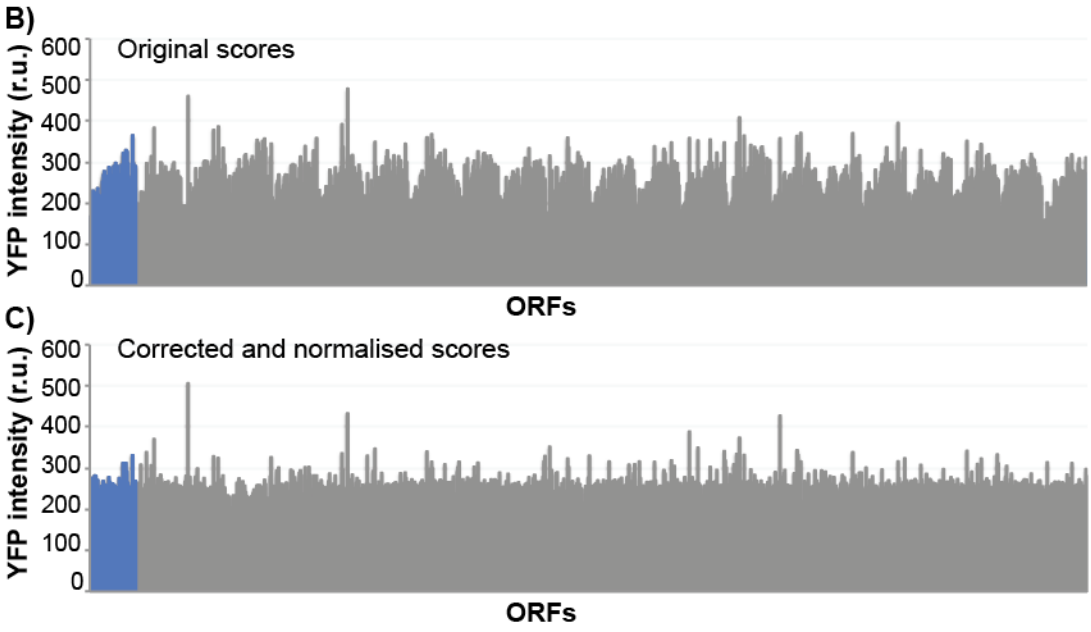

Figure 4.2. Normalisations. A) Example of YFP intensity values (background subtracted (r.u)) in a pad showing the original values as well as corrected and normalised values. Higher values are coloured darker. Each cell represents a strain and its position within the microscopy pad is indicated by row letters and column numbers. **B-C**) Original scores are neither corrected nor normalised (**B**) or corrected and normalised (**C**) per strain in order taken of 22 pads from the screen with the non-essential genes**.** The width of one pad with 48 strains is indicated in blue as reference. YFP intensity values plotted are mean values of all the foci within an image to represent a strain. Foci values were calculated as kinetochore fluorescence background subtracted (r.u). Quantitation was performed by automated FociQuant (**B-C**).

4.2.6. Less than 3% of the non-essential deletions either increase or decrease Dad4-YFP intensity

I plotted the YFP kinetochore intensity values in rank order, from lowest to highest, of each non-essential ORF deletion (in green) as well as over 1300 controls (in blue) (Figure 4.3 A). I found that wild-type YFP intensities are clustered and most mutants are wild type-like although a few have higher or lower intensities. Plotting the variation (Figure 4.3 B-C), mutants have a bigger spread, but the same median (mean). The mean fluorescence intensity of all the strains (mutants and wild types) is 257.15 r.u. The mutant that produces the highest intensity causes an increase of 106% (528.84 r.u.) over the mean value, and the lowest mutant a decrease of 68% (77.74 r.u.).

The range of Dad4-YFP intensities is continuous (Figure 4.3 A), hence there is no obvious cut-off that defines mutants with high-intensity or low-intensity Dad4-YFP. A number of cut-off methods were assessed and for the analysis described here, I have used the position of the second most extreme wild-type measurement as a cut-off. For high intensity Dad4-YFP mutants this represents 3 standard deviations above the mean and for the low intensity mutants 2 standard deviations below the mean.

Using this approach, I found that less than 3% of the non-essential gene deletions affect Dad4 intensity, either increasing or decreasing it. This corresponds to 72 mutants that decreased the intensity of Dad4-YFP and 56 mutants that increased it (Tables A-B appendix 1). Selecting a more conservative cut off of up to the first wild type would correspond to 47 low intensity mutants and 40 high intensity mutants, bringing down the total from 2.7% to 1.9% of ORFs affecting Dad4 intensity.

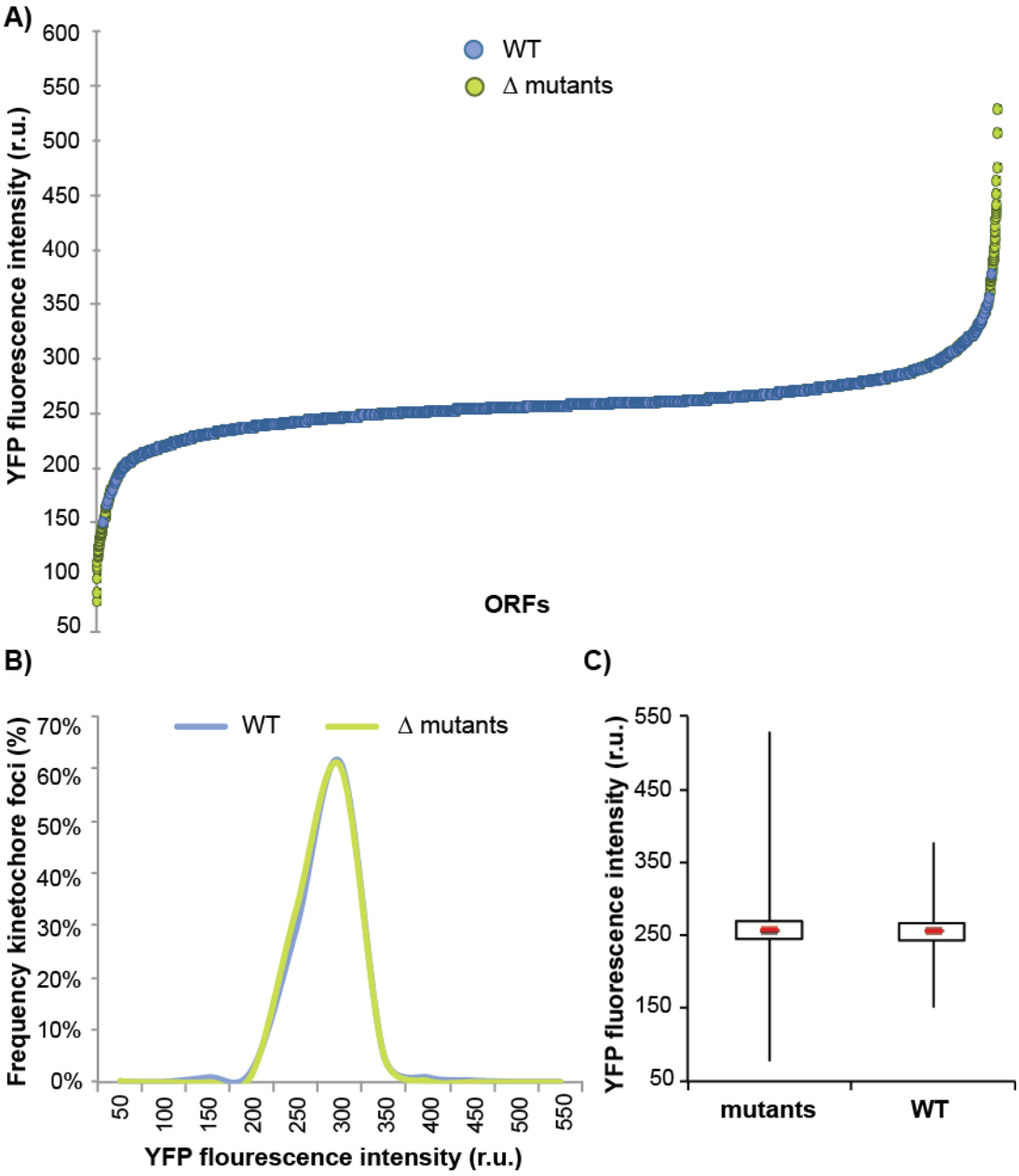

Figure 4.3. Screen with Dad4-YFP and the deletion library. A) Fluorescent YFP intensities (background subtracted) and normalised of each ORF in rank order of intensity. ORF deletions are shown in green and wild types in blue. **B**) Distribution of foci intensities of mutants (green) and wild types (blue). **C**) Box plot showing a similar median and mean for both mutant and wild type populations but a bigger spread in the mutants. **A-B-C**) Mean values of all foci within an image are used to represent each strain.

4.2.6.1. Qualitative analysis of non-essential deletions

The distinction between wild-type strains and deletion mutants causing the most extreme changes in fluorescence intensities could be easily identified by eye. For example, the deletion that results in the lowest fluorescence intensity, *rpl1b*Δ (a ribosomal gene, and one of the deletions that increase the YFP intensity the most, *bud23*Δ (a methyltransferase involved in bud site selection), are clearly different from the wild type both, qualitative (Figure 4.4 A) and quantitative (Figure 4.4 B). However, for many mutants it is difficult to distinguish the changes in fluorescence visually.

Parallel to the quantitative analysis of the non-essential deletions, I performed a qualitative analysis of these mutants. By examining the images by eye, I annotated a list of mutants that caused a 'visual' phenotype that I judged to be different from wild-type cells. This included large and bright foci, very weak foci and abnormal YFP distribution. Some examples with a very striking phenotype are shown in Figure 4.4 C. *Bik1*Δ (mammalian CLIP-170) is a microtubule associated protein important for chromosome segregation and in this mutant Dad4-YFP has an aberrant distribution with 1 or 2 lines extending away from the kinetochore. Since Dad4 is part of the DAM1 complex, which is thought to form a ring around microtubules, I hypothesise that these lines represent a spreading of Dad4 along the microtubules towards the SPB. A similar phenotype can be seen in the kinetochore protein mutant *ctf19*Δ. Aberrant phenotypes in which Dad4-YFP form lines, suggesting spindle defects, are not exclusive to kinetochore and spindle components. The deletion *sst2*Δ, a GTPase activator for Gpa1, a component of the mating pathway shows a similar YFP phenotype (Figure 4.4 C).

I identified 85 non-essential deletions with visual phenotypes (Table C appendix 1). Surprisingly, only 17 out of the 85 qualitatively annotated visual mutants overlapped with low or high intensity mutants in the quantitative method (using the cut off up to second wild type) (Figure 4.4 D). In order to understand this discrepancy I looked at the data from a different perspective, by examining the distribution of foci intensities for each mutant that I had identified as having altered Dad4-YFP intensity. For example, Figure 4.4 E shows the distribution of YFP intensity values for four mutant and one wild-type strains. In the wild type, most foci have intensity values between 200 and 500. *nas6*Δ, was included as a control since it was not found to differ from the wild type either computationally or visually (Figure 4.4 F) and it has a very similar Dad4-YFP distribution and mean/median as wild-type cells (Figure 4.4 E). On the other hand, the mutant that decreased Dad4-YFP intensity the most according to the quantitative method (*rpl1b*Δ), and which has clearly weaker foci compared with the wild type (Figure 4.4 F), has a

single population of foci with lower intensity than wild type. Unexpectedly, a mutant that increased Dad4-YFP intensity (*hom2*Δ) and has brighter foci, which are readily visible in the micrographs (Figure 4.4 F), has a population wild type-like and two more populations with much higher mean, indicating that the population of foci is heterogeneous. Finally, a visual mutant that was missed by the quantitative method (*bik1*Δ*)* (Figure 4.4 F) shows two subpopulations, one with lower and one with higher mean than the wild type. Because the value that we use to represent a strain is the mean of all the foci measurements per image, this could explain how a number of mutants with variability in the intensity of their kinetochore foci may be missed. For example, the odd localisation of Dad4 in specific mutants such as *bik1*Δ*, ctf19*Δ or *sst2*Δ (Figure 4.4 C), is detected by the software as multiple foci with different intensities (Ledesma-Fernández and Thorpe 2015). Thus, the two methods are complementary and the 85 mutants identified by the qualitative assessment were included into the non-essential list of deletions that alter Dad4 fluorescence.

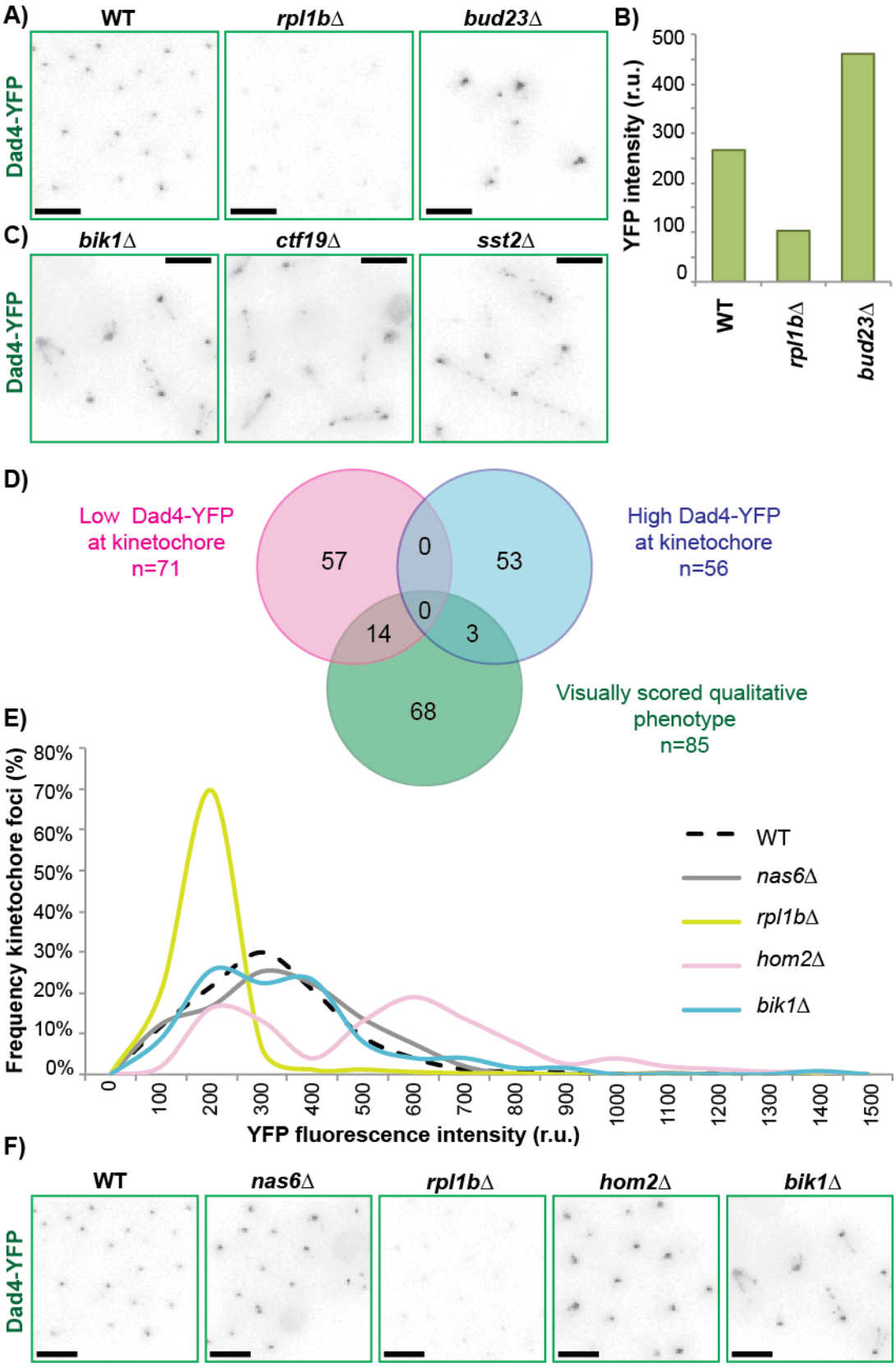

Figure 4.4. Quantitative and qualitative methods are complementary. A) Example of Dad4-YFP foci in wild type cells versus 2 mutants, one that decreases Dad4-YFP intensity (*rpl1b*Δ) and one that increase it (*bud23*Δ). **B**) Quantitation of foci shown in (**A**) analysed by automated FociQuant. **C**) Example of Dad4-YFP

distribution in mutants that alter Dad4 localisation. **D**) Venn diagram showing the poor overlap between the qualitative analysis and the quantitative analysis. **E**) Foci distribution curves of wild type and mutants. **F**) Example of Dad4-YFP foci for the strains analysed in (**E**). All scale bars are 5 μm.

4.2.7. Around 27% of the essential alleles either increase or decrease Dad4-YFP intensity

I did the same analysis as that shown in Figure 4.3 for the essential TS alleles (Figure 4.5). No wild types are included in the TS collection so only the mutant distribution is shown in Figure 4.5. The mean fluorescence intensity of all the alleles in the screen is 312 r.u. higher than the mean in the non-essential deletions screen. The mutant that produces the highest intensity causes an increase of 93% (603 r.u.) over the mean value, and the lowest mutant a decrease of 76% (74 r.u.).

In this case, since no wild types are included to compare, I selected a cut off based on the distribution of the data. The low intensity cut-off of under 200 r.u and the high-intensity cut-off of over 400 r.u. (Tables D-E appendix 1). These cut-offs represent 1.5 standard deviations below the mean and 1.5 standard deviations above the mean respectively. These criteria give 69 mutants, out of the 1193 strains (that had grown and had produced data) decreasing Dad4-YFP and 97 increasing it.

Overall, I found that 27% of essential ORFs affect Dad4 intensity. This corresponds to 142 unique alleles and 126 unique ORFs.

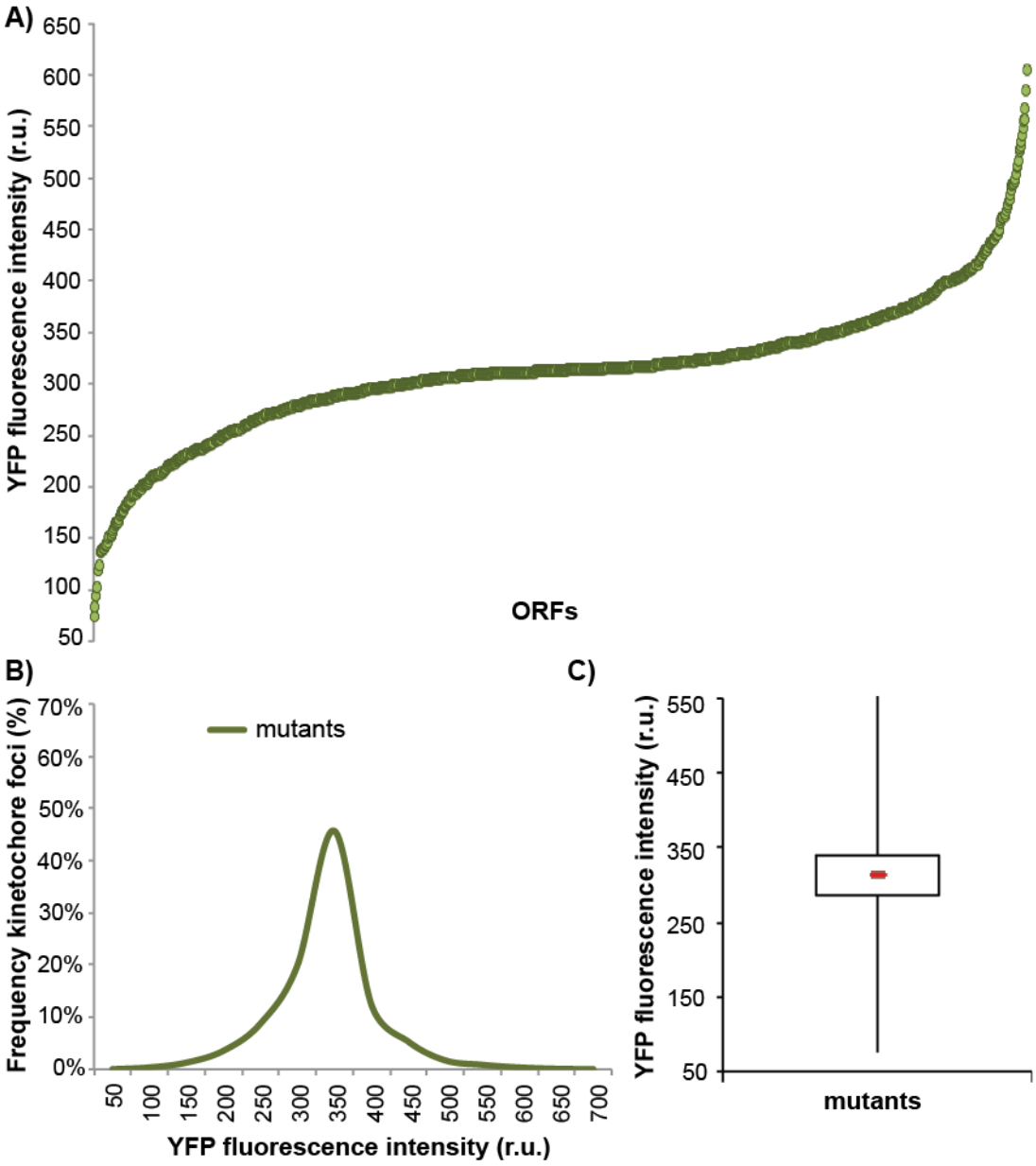

Figure 4.5. Screen with Dad4-YFP and the TS collection. A) Fluorescent YFP intensities, background subtracted and normalised of each TS allele in rank order of intensity. **B**) Distribution of foci intensities. **C**) Box plot showing the distibution of the TS mutants population. **A-B-C**) Mean values of all foci within an image are used to represent each strain.

4.2.8. Fluorescent intensity and standard deviation values correlate

Although I expect the standard deviation to increase with increasing fluorescent intensity, some mutants may be more variable and have higher that expected standard deviation values. In order to find mutants with higher intrinsic variability, I plotted the standard deviations of the YFP kinetochore intensity values in rank order and produced a similar graph to the one shown in Figure 4.3 A (data not shown). Standard deviation values generally correlate with intensity values. Mutants that have higher intensity values have larger standard deviations (Figure 4.6 A). I compared the overlap between non-essential mutants with the lowest and highest intensities (up to the second wild type cut off) (Figure 4.6 B) and those with lowest and highest STD values (also up to the second wild type cut off) (Figure 4.6 C).

Out of the 71 mutants that decrease Dad4-YFP the most, 14 have the lowest standard deviations, which indicates that the foci population is homogeneous and all foci have low intensity values. Genes in this group have very different functions and include two chromatin remodelers and 2 proteins with exodeoxyribonuclease activity (Figure 4.6 B). On the other hand, more than half of the mutants with the top 56 intensities have high standard deviation indicating a heterogeneous population with mixed foci of various intensities. Most of those mutants are somehow involved in metabolic processes and more than half of them are mitochondrial with enrichment for mitochondrial translation. Of those, several are members of the mitochondrial small and large ribosome. In addition, 2 of the 3 members of the conserved core of the nonsense-mediated mRNA decay (NMD) pathway are in this group (Figure 4.6 C).

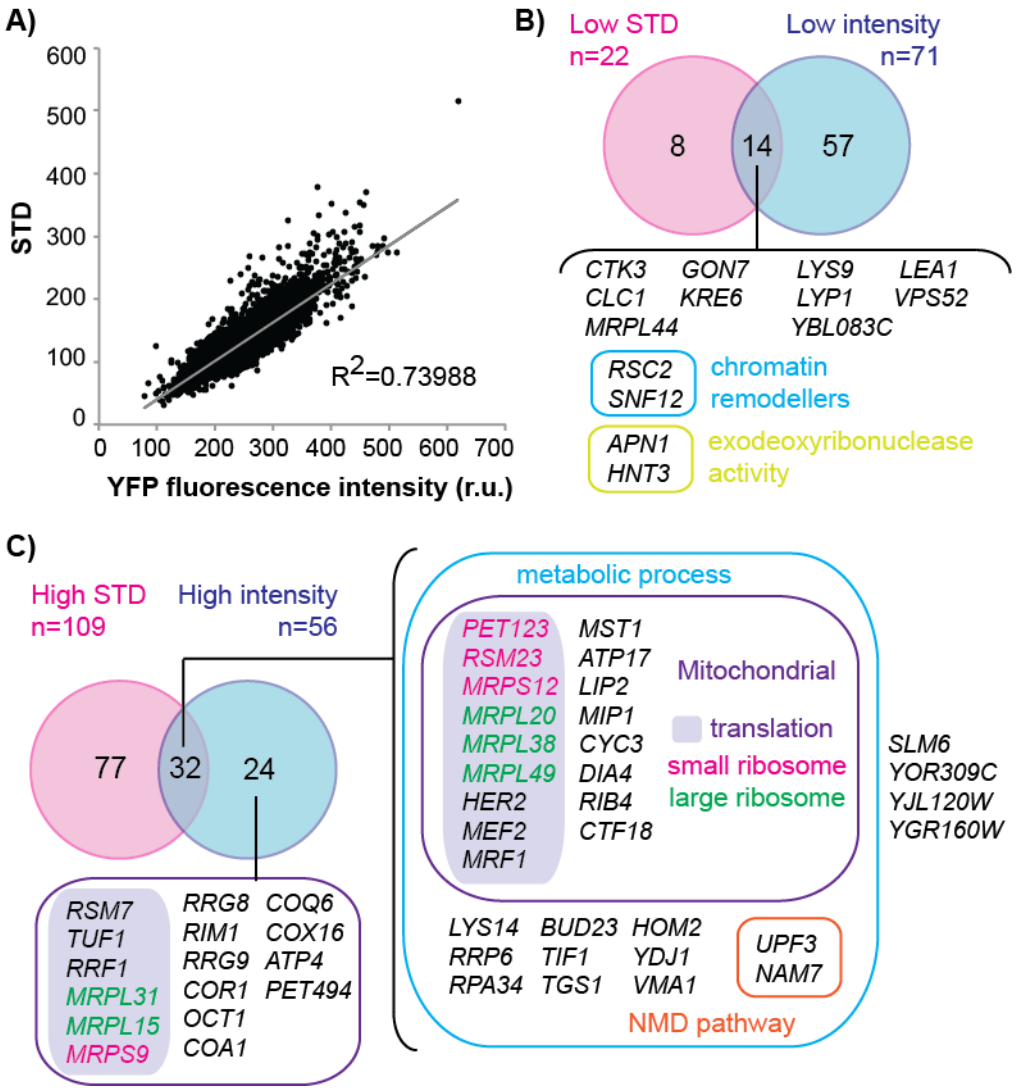

Figure 4.6. Comparison of fluorescence intensity and standard deviation. A) Correlation between mean YFP intensity values and STDs for Dad4-YFP in the non-essential deletions. Overlaps of deletions that cause low Dad4-YFP intensity values and low STDs (**B**) or high intensity values and high STDs (**C**). Gene names of overlaps are indicated as well as enriched GO terms. Cut offs for intensities are up to the second wild type for both intensities and STDs. GO terms analysis performed by GOrilla (Eden et al., 2007, 2009).

4.2.9. YFP fluorescent intensity and RFP fluorescent intensity do not correlate

The fluorescent intensity values of YFP did not correlate with the RFP values (Figure 4.7 A), suggesting that changes in amount of Dad4 at the kinetochore do not correspond with changes in Spc42 at the SPB. Thus, a different set of mutants affecting the SPB could be identified that do not necessarily affect the kinetochore, or in the same way.

4.2.9.1. Mutants that affect the intensity of the SPB protein Spc42

Although a study of the SPBs is outside the scope of this project, the images were quantified in parallel. The standard deviation also correlates with the RFP intensities although it is weaker than for the YFP (Figure 4.7 B). For the non-essential deletions screen the mean is 161 r.u. and 128 r.u. for the screen with the TS alleles. In the non-essential deletions screen, unlike with Dad4 (Figure 4.3), the spread of the mutants is not different from the wild types with those having some of the top low and high values (Figure 4.7 C). For this reason, a cut off based on the wild types as done for Dad4 cannot be used if it is assumed that some deletions will change Spc42-RFP intensity. With a conservative cut off of 3 STDs 8 non-essential deletions decrease Spc42-RPF intensity and 42 increase it (Table F appendix 1). For the TS screen, with the same cut off, 27 strains were found to increase the RFP intensity, corresponding to 22 unique alleles and 19 unique ORFs. No mutants had intensities lower than 3 STDs and only one was in the 2STD range (Table G appendix 1).

One of the ORFs with strongest intensities is the F-box Cdc4, which appears 7 times in the top 27 alleles of the TS screen with several alleles (*cdc4-1* (4 times), *cdc4-2*, *cdc4-3* (2 times)) (Table G appendix 1). Cdc4 is involved in spindle pole separation, as well as Cdc34 (also a high intensity mutant) (Freed et al., 1999). Furthermore, *cdc31-1* appears twice as top high intensity mutant and is involved in spindle pole duplication (Baum, Furlong and Byers, 1986). GO ontology enrichment analysis performed by GOrilla (http://cbl-gorilla.cs.technion.ac.il/) on the ORFs that alter Spc42 fluorescence intensity shows strong enrichment for 4 groups (Figure 4.7 D). A large group contain genes involved in the cell cycle including members of the SPB, kinetochore complexes COMA and CTF19, mitotic checkpoint, septin ring and the budding yeast Cdk1 (Cdc28). In addition the histone acetyltransferase complex, and specifically the SLIK (SAGA-like complex) was enriched. The processes of Arp2/3 complex-mediated actin nucleation and vesicle fusion with Golgi apparatus were also represented. Physical interaction

between genes included in the four groups and other mutants altering Spc42-RFP levels are shown in Figure 4.7 D.

Although no visual analysis was done for the SPB screen, I observed a very interesting phenotype in some *CDC24* alleles (Figure 4.7 E). Cdc24 is the GEF for the Rho-like Cdc42 GTPase necessary for polarity. Multiple SPBs form bipolar (likely misoriented) and multipolar spindles in enlarged cells, with small-medium size buds. This could indicate a polarity defect with bipolar spindles not moving to the bud but going to a next round of duplication and separation.
We have sent the collection of images to Sue Jaspersen's lab at the Stowers Institute, where they will be analysed further to explore the SPB phenotypes.

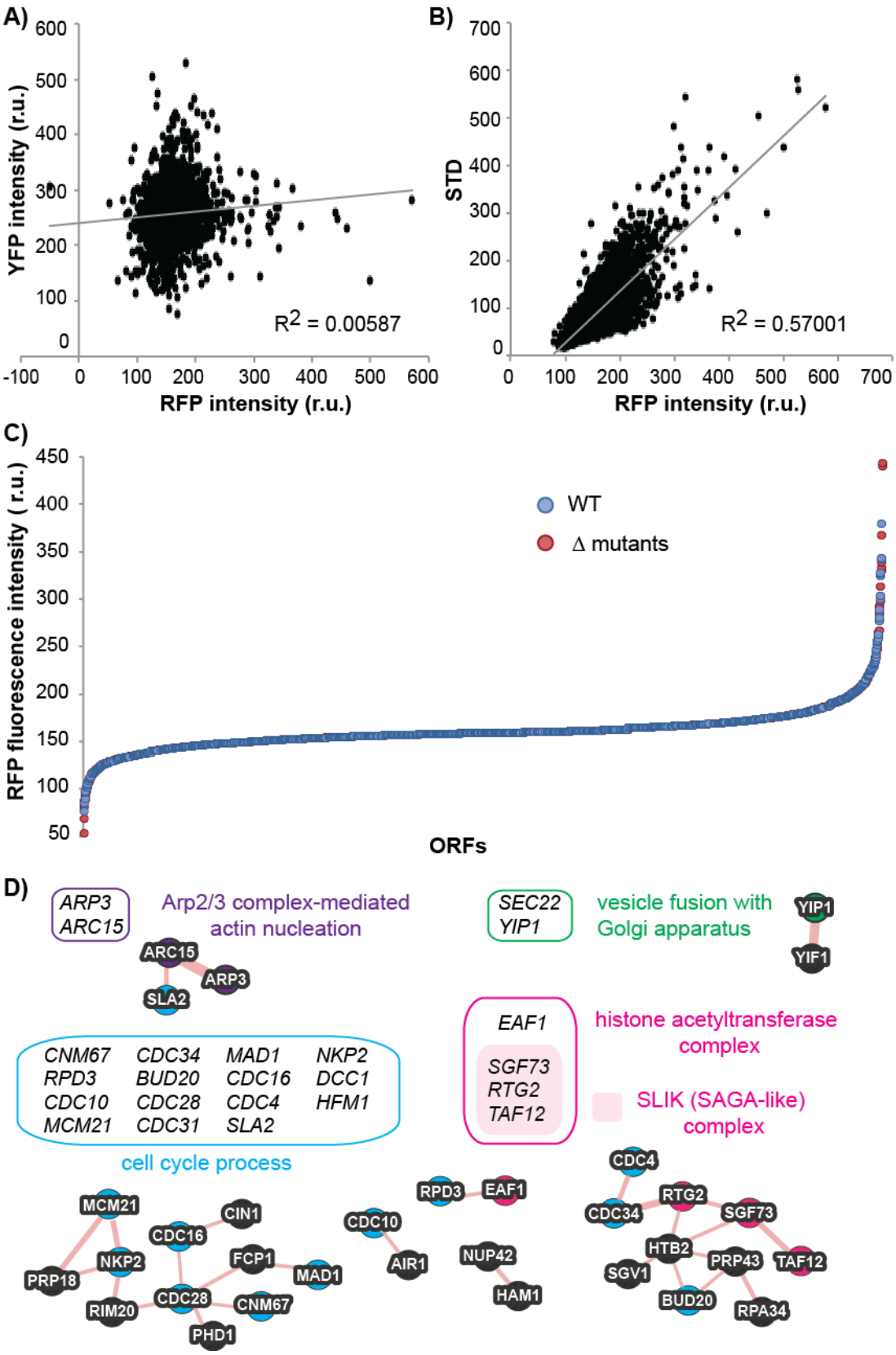
A)
YFP intensity (r.u.)
RFP intensity (r.u.)
R2 = 0.00587
B)
STD
RFP intensity (r.u.)
R2 = 0.57001
C)
RFP fluorescence intensity (r.u.)
ORFs
WT
Δ mutants
D)
ARP3
ARC15
Arp2/3 complex-mediated actin nucleation
ARC15
ARP3
SLA2
SEC22
YIP1
vesicle fusion with Golgi apparatus
YIP1
YIF1
EAF1
SGF73
RTG2
TAF12
histone acetyltransferase complex
SLIK (SAGA-like) complex
CNM67 CDC34 MAD1 NKP2
RPD3 BUD20 CDC16 DCC1
CDC10 CDC28 CDC4 HFM1
MCM21 CDC31 SLA2
cell cycle process
MCM21
CIN1
CDC16
NKP2
FCP1
MAD1
PRP18
RIM20
CDC28
CNM67
PHD1
RPD3
EAF1
CDC10
AIR1
NUP42
HAM1
CDC4
RTG2
CDC34
SGF73
HTB2
PRP43
TAF12
SGV1
BUD20
RPA34

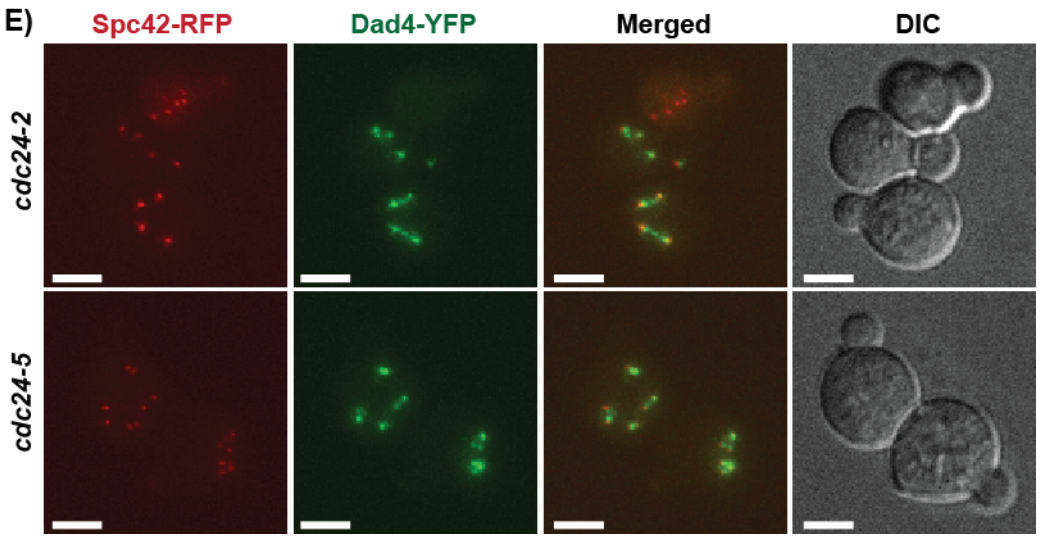

Figure 4.7. Mutants that affect the SPB. Correlation of RFP intensity values with YFP intensities (**A**) and STDs of RFP values (**B**) Values are background corrected and normalised**. C**) Fluorescent RFP intensities (background subtracted) an normalised of each ORF in rank order of intensity. ORF deletions are shown in red and wild types in blue. **D**) GO terms enriched for the list of deletions and alleles that increase/or decrease RFP signal. Physical interactions are shown between genes included in the GO terms and other genes that also altered RFP intensity. Colored circles behind the gene names indicate their inclusion in one of the enriched groups. **E**) Yeast cells of two *CDC24* alleles grown at the restrictive temperature (37˚C). Green foci represents Dad4-YFP and red foci Spc42-RFP. Images visualised by Volocity. Scale bars are 5 μm.

4.2.10. Around 80% of the non-essential mutants identified in the screen produce a Dad4 phenotype when they are retested.

I retested 338 strains for the non-essential screen and also included 45 wild types as controls. The retested strains included 192 unique ORF mutants that decrease, increase or produced a visual phenotype (from the 195 in Figure 4.4 D). The remaining 146 had either produced a smaller effect (outside the selected cut off but close) or they had given no different intensity than the wild type in the screen but were spindle related genes or annotated as regulators of Dad4 in the database Saccharomyces Genome Database (SGD) (http://www.yeastgenome.org).

I plotted the YFP intensity values in rank order, from lowest to highest, of each non-essential deletions (green) and controls (blue). Two clear groups of mutants have foci intensities either larger or smaller than the wild types (Figure 4.8 A). The distribution of fluorescence foci in mutants shows two subpopulations (Figure 4.8 B) and the spread is larger for the mutants (Figure 4.8 C).

The cut off used in this case was up to the first wild type. This produces a list of 68 mutants that decrease the intensity of Dad4 and 108 that increase it (Tables H-I appendix 1). Additionally, 26 deletions were annotated as having a visual phenotype (Table J appendix 1). The low intensity mutants would show between 33% and 52% decrease in intensity over the mean value of wild-type intensities, while the high intensity mutants would produce an increase between 25% and 144%. These retests suggest that the false positive rate using the cut-offs described above is ~20% (Figure 4.8 D). I did not assess false negative rate, but it may be relatively high for mutants whose Dad4-YFP intensity values fall close to the cut-offs.

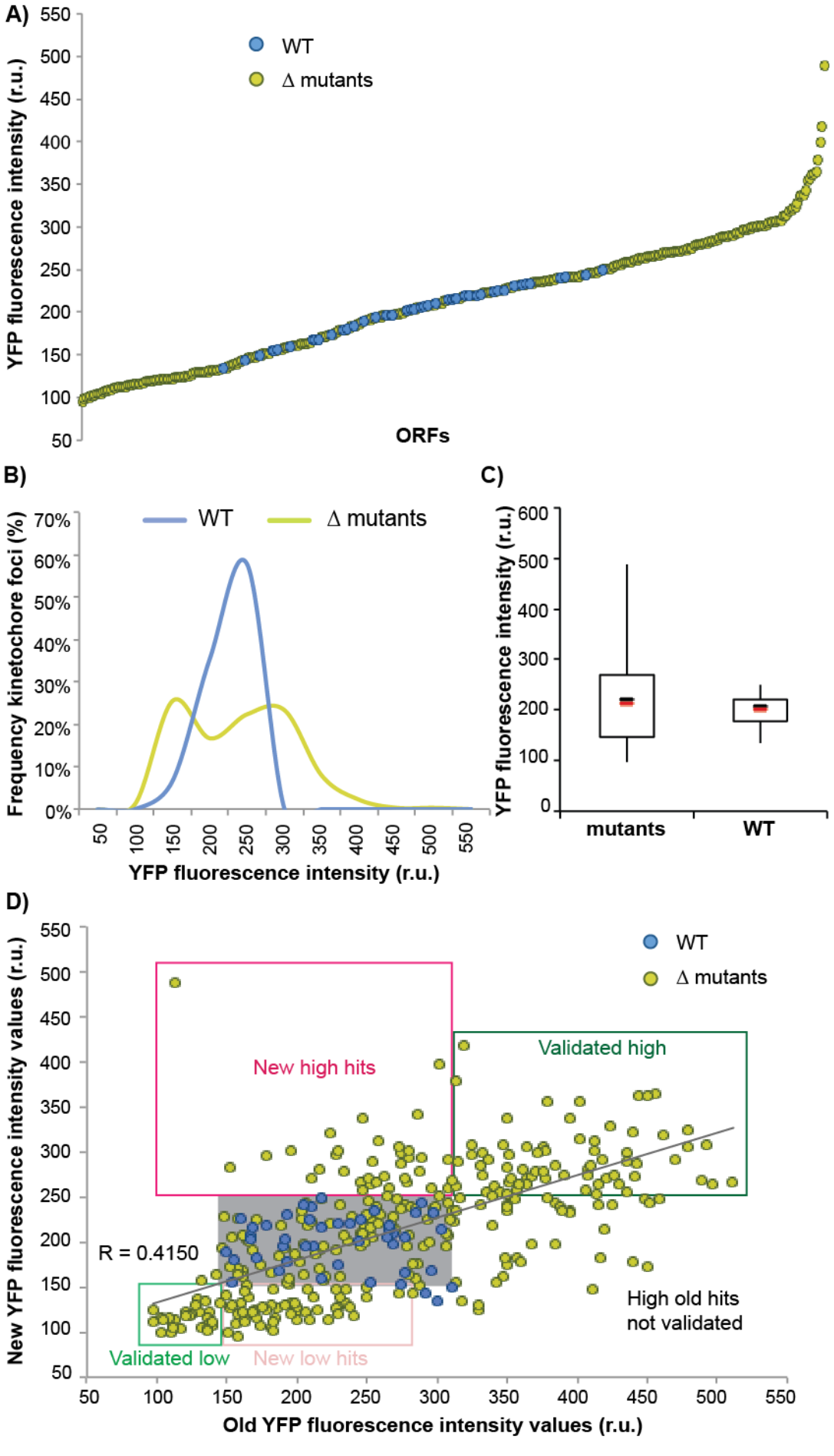
A)
YFP fluorescence intensity (r.u.)
ORFs
WT
Δ mutants
B)
Frequency kinetochore foci (%)
YFP fluorescence intensity (r.u.)
C)
YFP fluorescence intensity (r.u.)
mutants
WT
D)
New YFP fluorescence intensity values (r.u.)
Old YFP fluorescence intensity values (r.u.)
New high hits
Validated high
Validated low
New low hits
High old hits not validated
R = 0.4150

Figure 4.8. Retest of non-essential deletions that produce a phenotype on Dad4-YFP. A) Fluorescent YFP intensities (background subtracted) not normalised of each ORF in rank order of intensity in the validation set. ORF deletions are shown in green and wild types in blue. **B**) Distribution of foci intensities of mutants (green) and wild types (blue) and shown as a box plot (**C**). **D**) Correlation between the old and new YFP values (background subtracted) (all not corrected not normalised).

4.2.11. Categorising mutants

In order to classify the mutants identified in the screens I tested them for benomyl sensitivity, I also looked at foci distributions and performed GO ontology enrichment analysis.

4.2.11.1. ~16% of the non-essential mutants that alter the intensity of Dad4-YFP are benomyl sensitive

I arrayed the non-essential mutants that give a Dad4-YFP phenotype on a 384-colony plate and copied this onto media containing benomyl with the RoToR pinning robot to assess the strains sensitivity to benomyl. I used the colony measurement engine ScreenMill (Dittmar et al., 2010) to compare size colony of the strains copied onto 15% benomyl versus rich media. Benomyl is used as a microtubule poison in budding yeast as it binds to β-tubulin sequestering tubulin dimers and supressing microtubule dynamics (Singh et al., 2008). Mutants that are sensitive to benomyl are likely to perform a function that affects microtubule dynamics or that are dependent of correct spindle and kinetochore-microtubules attachments. The knock out of the mitotic checkpoint protein Bub3 (budding uninhibited by benomyl) was used as a control. Sixteen deletions gave a growth defect with a z-score above 2 (two standard deviations variation from the mean), between the values for the 2 *bub3*Δ controls included. An additional 38 deletions gave a growth defect above 1, which was used as a cut off (Table K appendix 1). The mutant *pac2*Δ was the most sensitive strain, more than the control *bub3*Δ (Figure 4.9). This result serves as a good control as Pac2 is necessary for tubulin heterodimer formation.

This plate included mutants that both did and did not affect Dad4-YFP; out of the 54 benomyl-sensitive strains (z-score above 1), 47 had produced a Dad4 phenotype either in the main screen, the retest or both. The only benomyl sensitive mutant that had been identified as increasing Dad4-YFP intensity in the screen was *hom2*Δ. In addition, *cdc73*Δ (visual phenotype in screen), *elm1*Δ and *gal11*Δ (both not identified in the screen) had given a high intensity phenotype when retested. All other benomyl sensitive

mutants had produced a visual, a low intensity phenotype, or both. These observations suggest that mutants that affect microtubule dynamics are more likely to affect Dad4 by decreasing its levels or delocalising it. In contrast, the high intensity phenotype may be related to processes mostly not related to the spindle function.

The chromatin remodelers *rsc1*Δ, *rsc2*Δ and *dbf2*Δ and *taf14*Δ*,* the latter of which is a subunit of several complexes including the SWI/SNF, were benomyl sensitive in addition to their Dad4-YFP phenotype. This suggests a possible function for these chromatin remodelers in mitosis and spindle function. Furthermore, *hom2*Δ and *hom3*Δ*,* two members of the threonine biosynthesis pathway were also benomyl sensitive and had increased and decreased Dad4 levels respectively. In addition, out of the 16 most benomyl-sensitive strains, 10 of them (YOL001W (*PHO80*), YOR073W (*SGO1*), YKL048C (*ELM1*), YEL027W (*VMA3*), YLR447C (*VMA6*), YJL179W (*PFD1*), YDR080W (*VPS41*), YPL253C (*VIK1*), YDL160C (*DHH1*), YGR056W (*RSC1*)) were common hits with a list of genes sensitive to latrunculin (an inhibitor for actin assembly) (Hillenmeyer et al., 2008).

This screen also revealed some mutants that grow slightly better on benomyl, such as *slk19*Δ, *kre28*Δ and specially *mrpl25*Δ. This may suggest that the deletion of these genes confers microtubule stabilisation and thus the strains grow better with microtubule destabilising drugs.

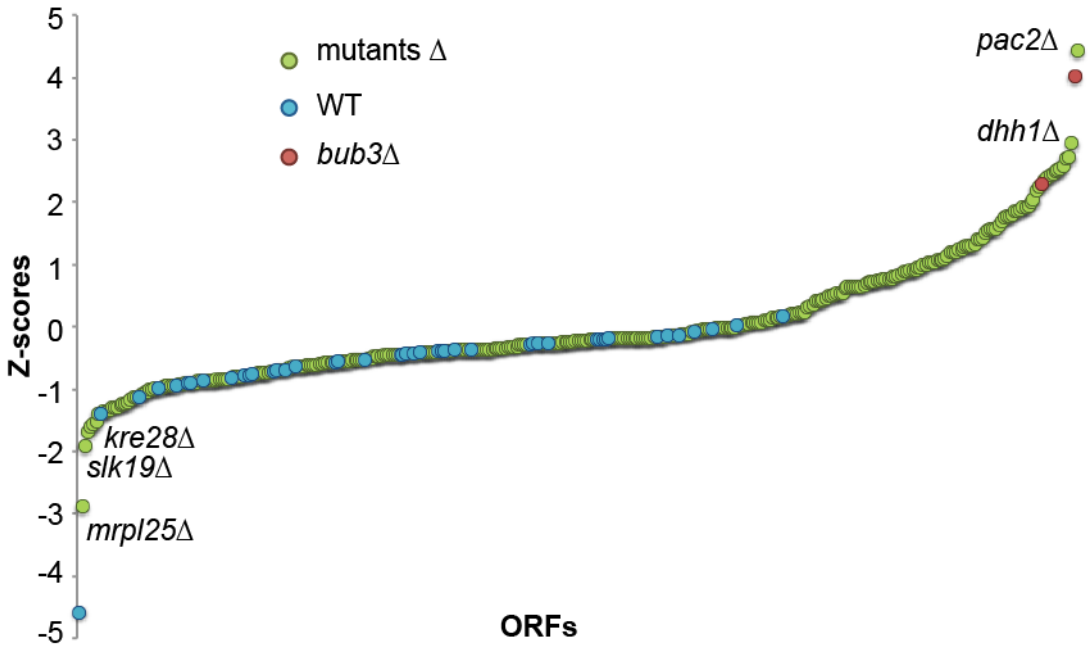

Figure 4.9. Benomyl sensitivity of non-essential deletions retested for Dad4-YFP phenotype. Z-scores in rank order represent the growth defect of each ORF deletion (green) and wild types (blue). *Bub3*Δ was used as control (red).

4.2.11.2. Foci distribution curves of mutants

In Figure 4.4 E I showed the distribution of Dad4-YFP kinetochore intensities in a "low intensity" mutant as a single population, while a high intensity mutant had more than one population of kinetochore intensities. I wanted to see if the double population was specific for this *hom2*Δ mutant or more general for high intensity mutants. I plotted distribution curves for all the high intensity mutants that I had retested and a few low intensity mutants. While a single population was a common for the low intensity mutants, all the high intensity mutants had 2 or more populations (Figure A appendix 2). This suggests that at least for the non-essential mutants, in low intensity mutants foci are homogeneous with decreased fluorescence whereas in high intensity mutants there is more variation within cells with some having much stronger foci than others.

The same population effect was seen for the few low and high intensity mutants tested from the essential TS screen, and four examples are shown in Figure 4.10. These mutants had the following values (r.u.) in the TS screen: *brl1-C371R* (85), *bcp1-ts* (102), *sgv1-23* (529) and *prp6-1* (549).

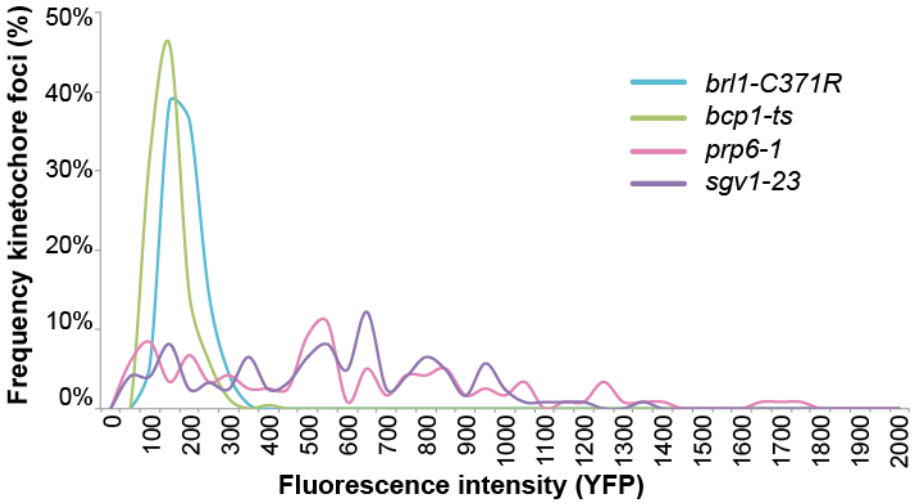

Figure 4.10. Distribution curves for low and high intensity mutants. Foci distribution curves four TS mutants.

4.2.11.3. GO ontology

I compared my list of mutants that affect Dad4-YFP with datasets from the literature. Some examples of enrichment are shown in Table 4.1. Out of the total number of 321 mutants, 107 are CIN genes (59 out of the 126 essential ORFs). Also enriched are mutants that are synthetic lethal/sick with genes required for sumoylation and SUMO dependent degradation such as Upl1, Smt3 and Ubc9; which have roles in regulating chromosome segregation and cohesion.

Table 4.1. Overlap of mutants causing a phenotype in Dad4 with published datasets in the literature.

Screen	ORFs in screen	Common hits	Rank Score	Publication
Yeast Chromosomal INstability (CIN) genes Master list	723	107	$1x10^{-17}$	Stirling et al. (2011).
Yeast Chromosomal INstability (CIN) essential genes	324	59	$2x10^{-13}$	Stirling et al. (2011).
Synthetic lethal/sick with *ulp1-333sgg*	332	50	$1x10^{-08}$	Makhnevych et al. (2009)
Synthetic lethal/sick with *ubc9-2*	313	44	$11x10^{-06}$	Makhnevych et al. (2009)
Synthetic lethal/sick with *smt3-331*	184	30	$3x10^{-06}$	Makhnevych et al. (2009)
Chromosome instability (CIN) genes	130	22	$3x10^{-05}$	Yuen et a. (2007)

Datasets obtained from Screen Troll (Thorpe et al., 2012). Rank score is an approximation of the *p*-value of the likelihood of overlap between the two datasets.

As shown in Figure 4.6 non-essential deletions that increase Dad4-YFP intensity are enriched for mitochondrial genes including mitochondrial translation and for metabolic processes. When combining the mutants from the non-essential and essential screens (Tables A-E appendix 1) and performing GO ontology enrichment analysis, many groups including mitochondria and ribosomal genes are found to be enriched in the Dad4-YFP mutants and a large number are nuclear. Some of these groups are shown as an example in Figure 4.11. As expected many mutants are mitotic cell cycle genes including microtubule, kinetochore and SAC components with enrichment for the DAM1 complex. A large number of mutants are implicated in RNA processes including the spliceosomal complex and the nonsense-mediated mRNA decay pathway. Nuclear pore and transport proteins including RNA transport are also represented, as are DNA replication and DNA repair genes. Genes involved in chromatin organisation are also

enriched in the Dad4-YFP mutants, including members of the RSC complex. Finally, a number of kinases, some of which are known to be important in the cell cycle, such as Cdc28, Cdc5, Mps1, Ilp1, Dbf2 or Cks1 were identified. However, many others haven't been reported to have a mitotic role, such as the aspartate kinase Hom3 or the cell wall remodeling serine/threonine kinase Pkc1. In addition, the threonine biosynthesis pathway was enriched.

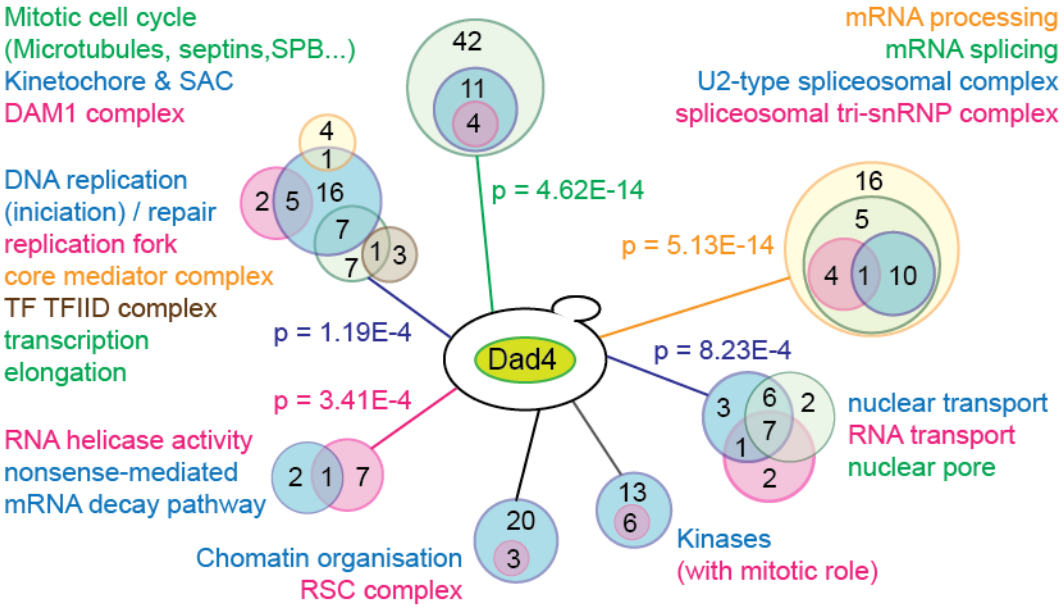

Figure 4.11. GO ontology enrichment analysis. Schematic showing examples of GO ontology terms enriched in the Dad4-YFP mutants. The analysis was performed using Gorilla (http://cbl-gorilla.cs.technion.ac.il/) and SGD Slim Mapper (http://www.yeastgenome.org/cgi-bin/GO/goSlimMapper.pl). The name of group represented in each coloured circle is listed in the matching colour, *p*-values are shown in some cases and are coloured matched to the listed categories.

4.2.12. Individual validations: work with some mutants

4.2.12.1. The threonine biosynthesis pathway

The deletions of four members of the super-pathway of threonine biosynthesis presented a visual phenotype (Table C appendix 1). In addition, *hom2*Δ increased Dad4-YFP signal while *hom3*Δ decreased it (Figure 4.12 A). When these strains were retested, *aat2*Δ fail to grow, however, *hom2*Δ and *hom3*Δ validated as increasing and decreasing Dad4-YFP intensity respectively, and *thr1*Δ, showed an increase in Dad4 fluorescence that was not previously detected.

Hom3 and Hom2 are the enzymes that catalyse sequential steps of the conversion from pyruvate to L-threonine; from L-aspartate to L-aspartyl-4-P (Hom3) and then to L-aspartate semialdehyde (Hom2). Thr1 works downstream by catalysing conversion of homoserine to O-phospho-L-homoserine (Figure 4.12 A).

When I imaged these three mutant strains individually, RFP levels were wild type-like and similar for all the strains. *thr1*Δ had only slightly higher levels of YFP (10% increase). However, *hom2*Δ Dad4-YFP levels were 61% higher than wild type and *hom3*Δ Dad4-YFP levels were decreased by half compared with wild type (Figure 4.12 B). The difference between wild-type and *hom2*Δ and *hom3*Δ foci is ready visible (Figure 4.12 C).

Both *hom3*Δ and *thr1*Δ were benomyl sensitive, especially *hom3*Δ. However *hom2*Δ cells did not have a growth defect on benomyl, and in fact, grew better than wild type cells (Figure 4.12 D). Both *hom2*Δ *and hom3*Δ were benomyl sensitive in the previous high-throughput test for benomyl sensitivity of mutants (Table K supplement).

Surprisingly, when I performed diagnostic PCR to confirm the presence of the correct deletion, two bands, corresponding to the deletion and to the wild-type gene were found in samples from *hom2*Δ *and hom3*Δ cells from my SGA screen and in *hom2*Δ from the deletion collection. This had been reported for some haploid deletion mutants (Giaever and Nislow, 2014).

In order to investigate the *hom2*Δ *and hom3*Δ mutants further making sure they had no wild-type copy of the gene, I introduced the deletions by amplifying the *KANMX* cassette from the strains in the deletion collection and transforming the doubly tagged wild-type strain T37 (T506, T507) (Table 2.2).

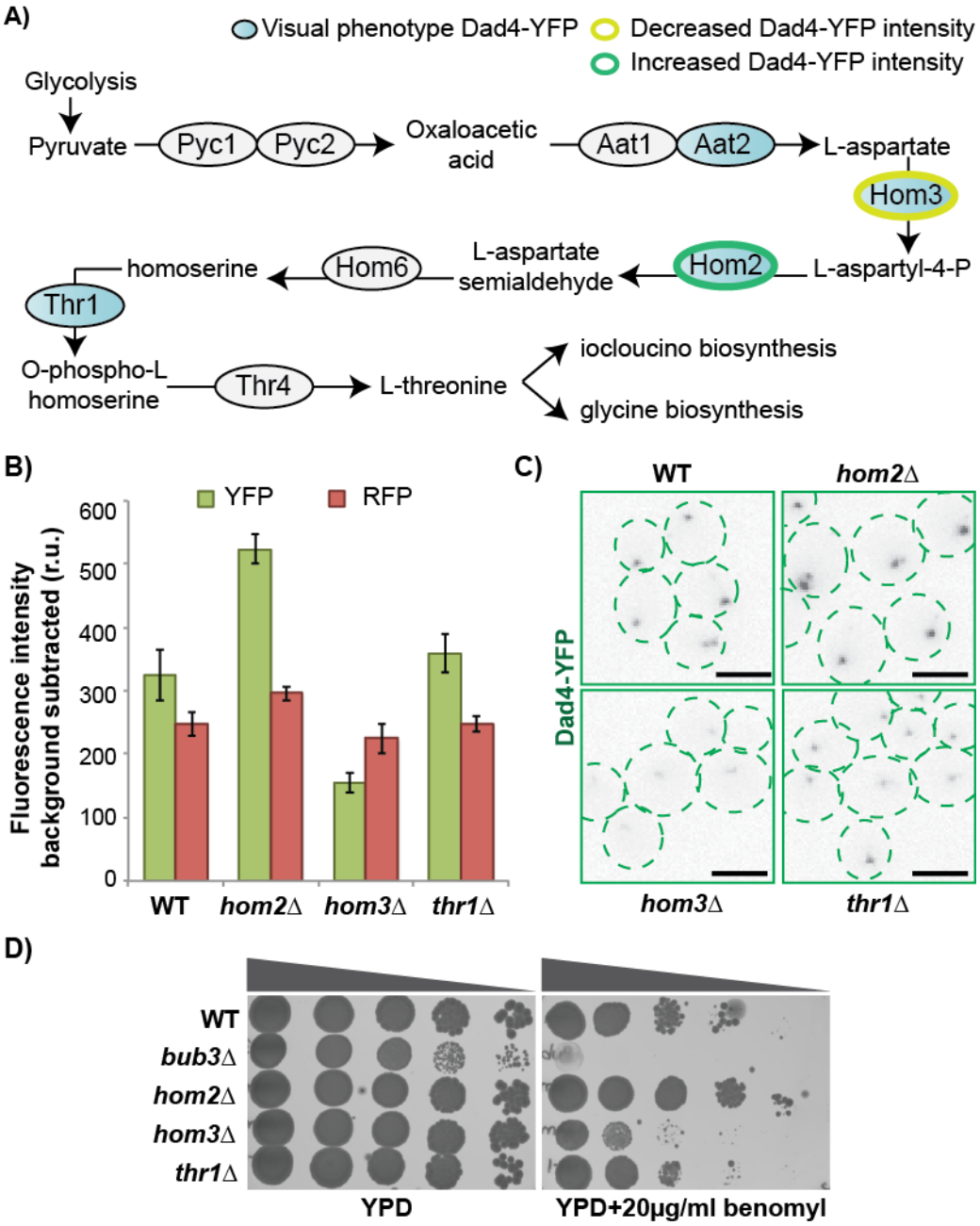

Figure 4.12. Deletion of members of the threonine biosynthesis pathway cause a phenotype on Dad4-YFP. A) Schematic showing the threonine biosynthesis pathway. Deletions of members that caused a visual phenotype in Dad4-YFP are coloured in blue. Dark green border indicates that the deletion increased Dad4-YFP intensity and clear green border that decreased Dad4-YFP. **B**) Fluorescence intensity, background subtracted of Dad4-YFP (green) and Spc42-RFP (red) of foci quantified by automated FociQuant. Error bars are standard deviation of the mean. **C**) Example of Dad4-YFP foci in wild type cells versus 3 mutants. Scale bars are 5 µm **D**) 10-fold serial dilutions spotted onto YPD with or whitout 20 µg/ml benomyl (30˚C). The wild type used is T37 and *bub3*Δ was included as a positive control.

These mutants are part of the super-pathway of threonine biosynthesis and our synthetic growth media lacks serine and threonine, therefore I tested whether the lack of these two amino acids was the cause of this phenotype.

Neither the YFP nor the RFP intensities of the wild type (T37) cells changed when the cultures were grown with added serine and threonine (Figure 4.13 A). In contrast, the YFP intensity in the *hom2*Δ mutant was rescued to wild type levels, when it was grown in media with added serine/threonine. The average RFP signal value didn't change with added serine/threonine although the standard deviation decreases under this condition (Figure 4.13 A). The distributions of intensities of Dad4-YFP intensities (Figure 4.13 B), of wild type and *hom2*Δ mutants are similar with added serine/threonine. However, without these two amino acids, *hom2*Δ presents a very small population of cells with normal YFP intensity values (similar to wild type) and multiple populations with increasingly higher values. YFP foci are visually enlarged (Figure 4.13 C) and additionally YFP foci can be seen that do not localise to close to SPBs. The mutant cells are enlarged and round.

The *hom3*Δ mutants did not grow when grown in media lacking serine/threonine. When the amino acids were added, the low signal phenotype previously observed (Figure 4.12 B) was rescued (Figure 4.13 D). In fact, the signal in this media is slightly higher (22 %) than the wild type, and the RFP signal was unchanged. This suggests that although they are non-essential genes, under the conditions in which they were grown (with media lacking serine/threonine) they became essential. Duplications could have occurred and the SGA methodology could have selected for these mutations.

In summary, the kinetochore phenotype of *HOM2/3* mutants likely results from deficiency in serine and threonine. Since, global translation of proteins is likely to be affected by reduced amino acid concentrations it is difficult to pinpoint the precise reason for the kinetochore phenotype.

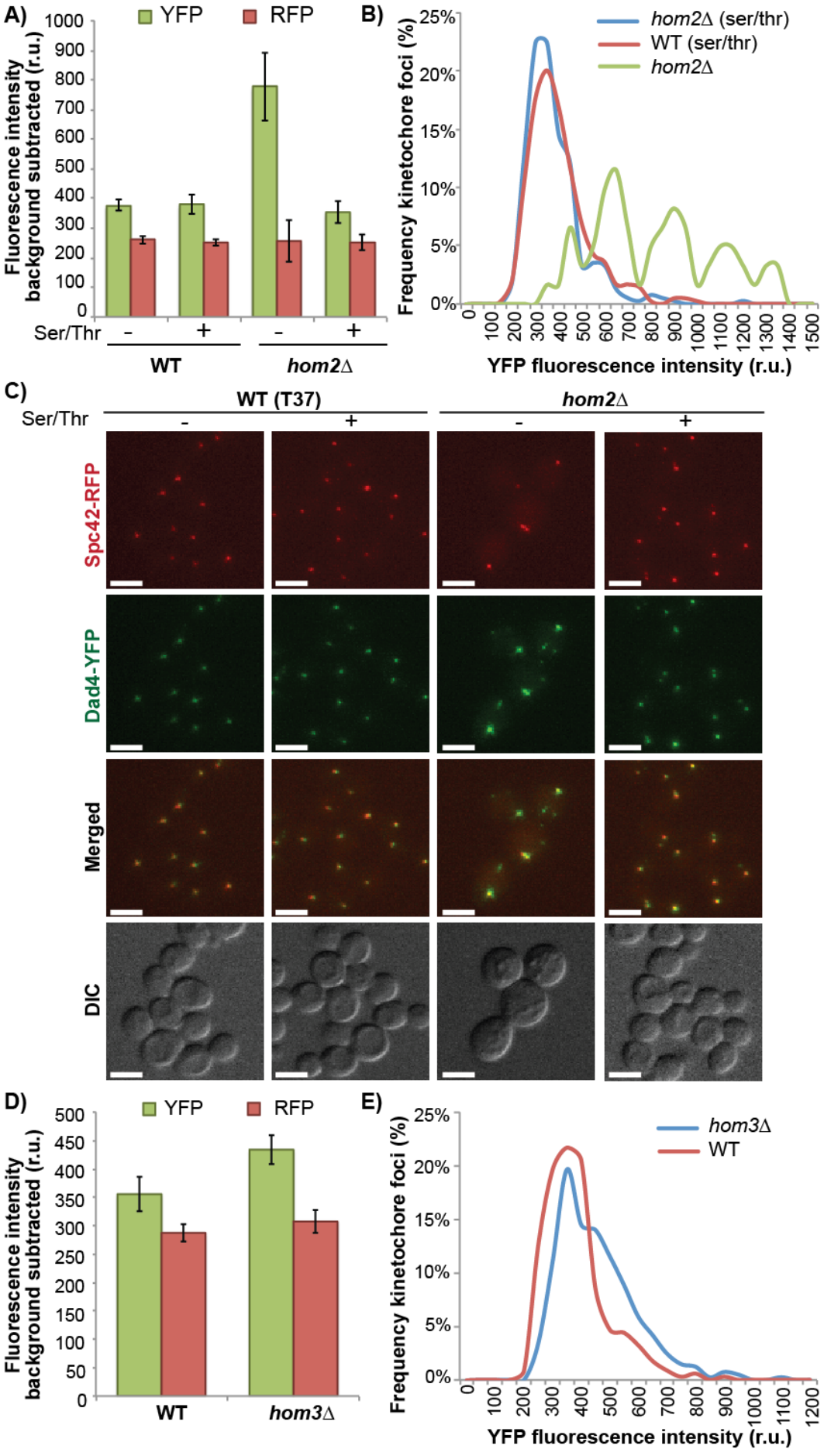
A)
YFP
RFP
Fluorescence intensity background subtracted (r.u.)
1000
900
800
700
600
500
400
300
200
100
0
Ser/Thr
-
+
-
+
WT
hom2Δ
B)
hom2Δ (ser/thr)
WT (ser/thr)
hom2Δ
Frequency kinetochore foci (%)
25%
20%
15%
10%
5%
0%
0
100
200
300
400
500
600
700
800
900
1000
1100
1200
1300
1400
1500
YFP fluorescence intensity (r.u.)
C)
WT (T37)
hom2Δ
Ser/Thr
-
+
-
+
Spc42-RFP
Dad4-YFP
Merged
DIC
D)
YFP
RFP
Fluorescence intensity background subtracted (r.u.)
500
450
400
350
300
250
200
150
100
50
0
WT
hom3Δ
E)
hom3Δ
WT
Frequency kinetochore foci (%)
25%
20%
15%
10%
5%
0%
0
100
200
300
400
500
600
700
800
900
1000
1100
1200
YFP fluorescence intensity (r.u.)

Figure 4.13. The Dad4-YFP phenotype in *hom2*Δ and *hom3*Δ mutants is rescued with addition of serine and threonine to the media. A) Fluorescence intensity (background subtracted) of Dad4-YFP (green) and Spc42-RFP (red) of foci quantified by manual ImageJ FociQuant. Error bars are standard deviation of the mean. **B**) Foci distribution curves of WT and *hom2*Δ in media with and without serine and threonine. **C**) Yeast cells of WT and *hom2*Δ in media with and without serine and threonine. Green foci represents Dad4-YFP and red foci Spc42-RFP. Images visualised by Volocity. Scale bars are 5μm. **D**) Fluorescence intensity (background subtracted) of Dad4-YFP (green) and Spc42-RFP (red) foci quantified by manual ImageJ FociQuant analysis. Error bars are standard deviation of the mean. **E**) Distrubution of foci intensities in WT and *hom3*Δ.

4.2.12.2. The nonsense-mediated mRNA decay (NMD) pathway

Upf1/Nam7, Upf2/Nmd2 and Upf3 are components of the nonsense-mediated mRNA decay (NMD) pathway (He et al., 1997). This pathway has two roles, to detect and degrade mRNAs with premature stop codons, and to regulate gene expression of some wild-type genes (He and Jacobson, 1997). Several kinetochore RNAs have been shown to increase in NMD mutants (Dahlseid et al., 1998; Kebaara and Atkin, 2009).

*upf3*Δ, *nam7*Δ and *nmd2*Δ were in the 8 deletions that increased Dad4-YFP intensity the most (corresponding to ≥3 STDs greater than wild type) of the retest plate (Table I appendix 1). When I imaged these strains individually on slides, the YFP signal increased 23, 33 and 41% in the *upf3*Δ, *nam7*Δ and *nmd2*Δ deletions respectively (Figure 4.14 A). The foci distribution for these mutants is similar, with multiple populations covering a much wider range than the wild-type values. This suggests that there is a heterogeneous population with foci of very variable intensities (Figure 4.14 B). In fact, these mutant cells have an aberrant distribution of Dad4-YFP with higher number of YFP foci than expected and which vary in sizes and intensities (examples in Figure 4.14 C). Since the quantification had been done with the automated ImageJ analysis method, the final values could be misleading as the program counts all the foci. I repeated the analysis by using the ImageJ manual analysis method and selecting only the YFP foci that was next to an SPB RFP foci. This method gave higher increased values with 41%, 72% and 91% increase in Dad4-YFP intensity in *upf3*Δ, *nam7*Δ and *nmd2*Δ respectively, compared with a modest (≤20%) increase in Spc42-RFP signal (Figure 4.14 D). Hence, the population of weak Dad4-YFP foci in these images are generally not adjacent to SPBs and may either not represent true kinetochore foci or could indicate de-clustered kinetochores. Furthermore, although these mutants increase Dad4-YFP kinetochore intensity, there is still a population of kinetochores with wild-type Dad4-YFP levels (Figure 4.14 E). These observations suggest that the Dad4-YFP

fluorescence is highly variable in these mutants. This could be indicative of aneuploidy, however, another possibility in these mutants is that *DAD4* RNA could accumulate, resulting in increased Dad4 protein levels and thus the fluorescence intensity. These levels would be variable within the unsynchronised cell populations, consistent with the variation of signal. Additional foci not colocalised to SPBs could represent an excess of Dad4 protein not loaded to the kinetochore, or binding microtubules. It is likely that there is a problem with the spindle since a proportion of cells, especially in *upf3*Δ and *nam7*Δ had both SPBs and kinetochores duplicated and retained close together in one cell, which was budded with a bud of larger size (Figure 4.14 F-G).

In summary, my data points to the possibility of kinetochore RNAs being directly regulated by the NMD pathway (as previous studies have done), although I cannot rule out that this effect could also be indirect, caused by global changes of other RNA levels (and thus protein levels) that may affect regulators of the kinetochore.

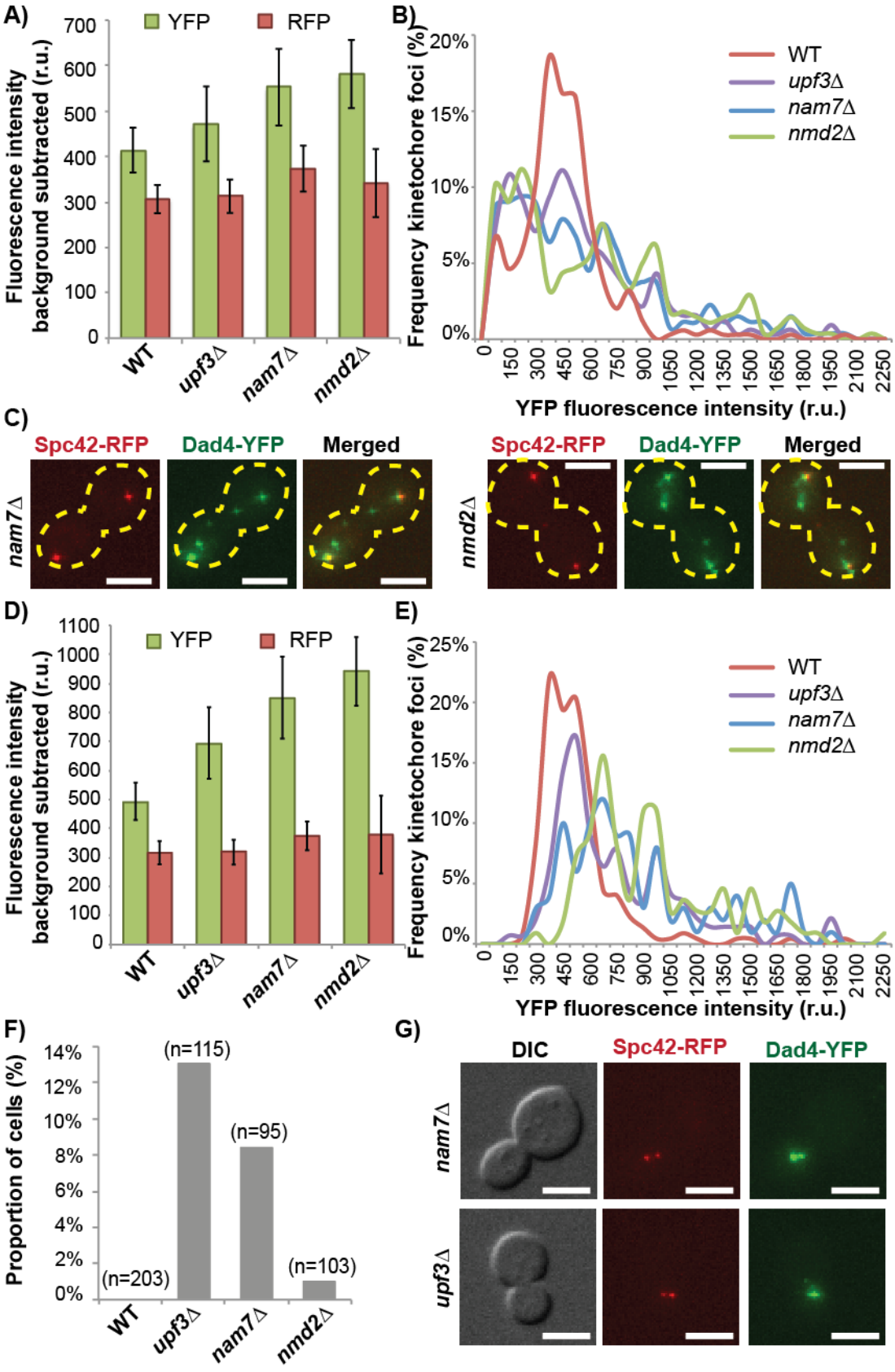

Figure 4.14. The nonsense-mediated mRNA decay (NMD) pathway. A) Mean fluorescent intensity values (background subtracted) for Spc42-RFP (red) and Dad4-YFP (green) (**A**) or Mtw1-YFP (**D**) in WT and mutants. Image analysis performed by the ImageJ automated FociQuant (**A**) or manual FociQuant (**D**). Error bars are standard

deviation of the mean. Foci distribution curves of WT and mutants for Dad4-YFP (**B**) and Mtw1-YFP (**E**). **C**) Example of cell in telophase with 2 SPBs (red) and multiple Dad4-YFP foci (green) in 2 different mutants. **F**) Number of cells with both SPBs and kinetochores in the "mother" cell having a bud larger than the mother. **G**) Examples of these type of cells in 2 mutants. Scale bars are 5 µm.

4.2.12.3. The mitotic exit mutants

Slk19∆ was identified by the qualitative method as causing an abnormal localisation of Dad4-YFP. Many cells were round and enlarged and presented several abnormalities such as extra SPBs and kinetochore foci. In addition, some cells had a Dad4-YFP signal extending in long lines connecting the two dividing cells apparently in telophase (Figure 4.15 A). This could be an indication of a spindle defect as the localisation of Dad4-YFP may localise with the long anaphase spindle of cytokinesis mutants. *SLK19* encodes a member of the FEAR regulatory network. In addition, Slk19 has been involved in stabilisation of mitotic spindles (Zeng et al., 1999) and kinetochore clustering (Richmond et al., 2013). In Figure 4.15 B cells are shown to have more YFP foci than RFP foci, although some Dad4-YFP foci seem to be too far from each other to be both within the nucleus. Since Slk19 has multiple functions in the kinetochore-spindle and cells are unsynchronised, these phenotypes could be reflecting a combination of these roles.

Slk19 has been shown to be involved in Cdc14 release from the nucleolus to the nucleus in early anaphase and from there to the cytoplasm at the end of anaphase (Faust et al., 2013). Other FEAR/MEN members have also been identified in this screen. For instance *cdc14-3*, *cdc5-1* and *tem1-3* decreased Dad4-YFP intensity at the restrictive temperature and were all validated (Table D appendix 1). In contrast, *esp1-1* (separase) increased Dad4-YFP intensity (not validated) (Table E appendix 1). In addition, different alleles of *DBF2* produced variable effects, increasing, decreasing and giving a visual phenotype, an example of which can be seen in Figure 4.15 C. Cdc14 dephosphorylates Dsn1, a central kinetochore component (Akiyoshi and Biggins, 2010) and its constitutive recruitment to the outer kinetochore leads to lethality (Olafsson and Thorpe 2015). These data are therefore consistent with an important role of the FEAR/MEN network in regulating kinetochore and spindle function.

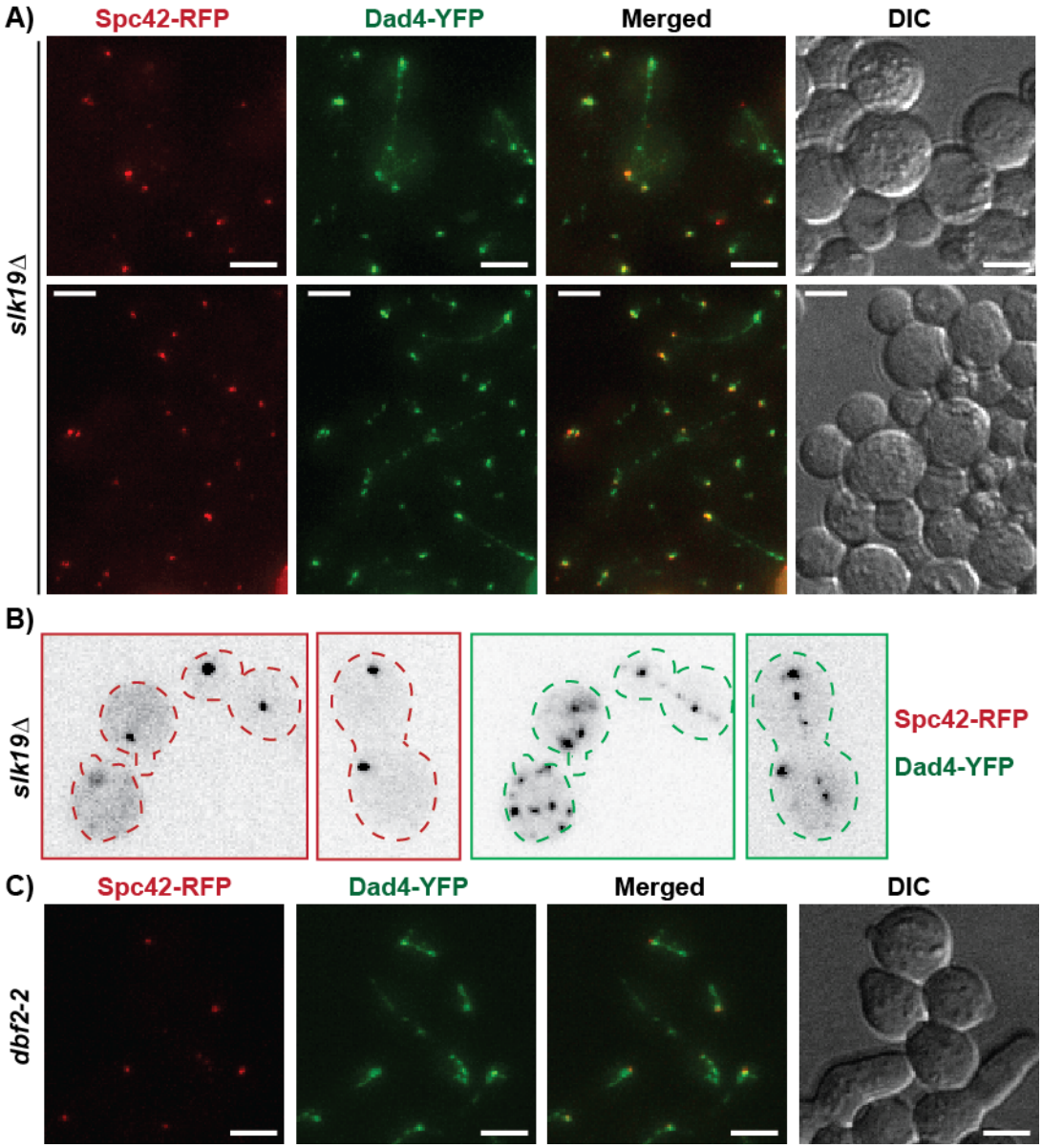

Figure 4.15. Aberrant localisation of Dad4 in mitotic exit mutants. A) Examples of cells with aberrant Dad4 localisation in a *slk19*Δ background. Red foci represent Spc42-RFP and green foci Dad4-YFP. More YFP (green) foci than RFP (red) foci are shown (ImageJ visualisation) (**B**). **C**) Cells with Spc42-RFP (red) and Dad4-YFP (green) in a *dbf2-2* mutant allele. Error bars in all the images are 5 μm.

4.2.12.4. The microtubule associated proteins (MAPs).

Budding yeast has four important microtubule plus-end tracking proteins (+TIPs) with multiple roles in spindle dynamics and kinetochore-microtubule attachment. The deletion of these four genes produced different phenotypes on Dad4 fluorescence. *bik1*Δ cells have a visual phenotype with aberrant Dad4 localisation (Figure 4.4 C). *bim1*Δ cells also have a visual phenotype in the screen with lines extending from the foci (Figure 4.16 F). After re-imaging *bim1*Δ in slides the lines were not observed, however, Dad4 intensity halved (Figure 4.16 A) with a single population of foci (Figure 4.16 B). In addition the Spc42-RFP signal was reduced by ~30-40% in *bim1*Δ cells, indicating a general spindle defect.

In order to see if these phenotypes could be recapitulated in other kinetochore proteins, I crossed the *bim1*Δ and *bik1*Δ strains from the deletion library with a strain tagged for Spc42-RFP and Mtw1-YFP. The fluorescent signal in Mtw1 does not decrease significantly in any of these genetic backgrounds (Figure 4.16 C) and the foci distributions show a wild type-like curve (Figure 4.16 D). Supporting this, the Mtw1 foci in these mutants look similar to the wild type foci by visual examination (Figure 4.16 E). Furthermore, Spc42-RFP signal decreased by 40% in *bim1*Δ and 30% in *bik1*Δ. These data suggest that the MAP mutant phenotype is restricted to the outer kinetochore, perhaps only on the DAM1 complex.

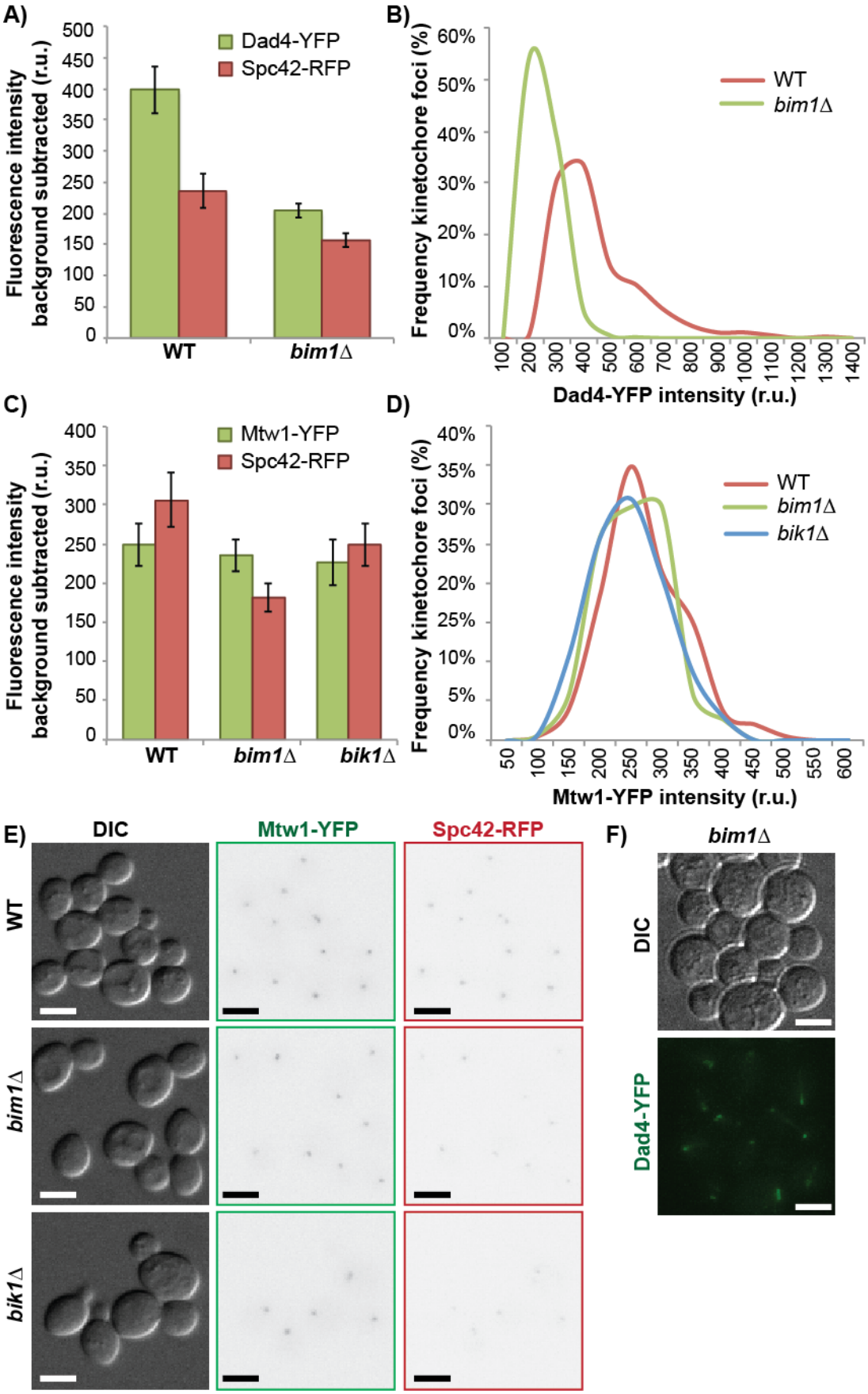
A)
Fluorescence intensity background subtracted (r.u.)
Dad4-YFP
Spc42-RFP
WT
bim1Δ
B)
Frequency kinetochore foci (%)
WT
bim1Δ
Dad4-YFP intensity (r.u.)
C)
Fluorescence intensity background subtracted (r.u.)
Mtw1-YFP
Spc42-RFP
WT
bim1Δ
bik1Δ
D)
Frequency kinetochore foci (%)
WT
bim1Δ
bik1Δ
Mtw1-YFP intensity (r.u.)
E)
DIC
Mtw1-YFP
Spc42-RFP
WT
bim1Δ
bik1Δ
F)
bim1Δ
DIC
Dad4-YFP

Figure 4.16. The phenotype caused by the MAPs *bim1*∆ and *bik1*∆ in the outer kinetochore is not transmitted to the central kinetochore. Dad4-YFP (**A**) or Mtw1-YFP (**C**) (green) and Spc42-RFP (red) background subtracted intensity of foci quantified by manual ImageJ FociQuant. Error bars are standard deviation of the mean. Distribution of Dad4-YFP (**B**) and Mtw1-YFP (**D**) foci intensities of mutants and WT are shown. **E)** Images of cells with Mtw1 (central kinetochore protein) tagged with YFP (green foci) and Spc42 (SPB protein) tagged with RFP (red foci). **F**) Cells with Dad4 (outer kinetochore protein) tagged with YFP (green foci). Scale bars are 5 µm in all images.

stu2-10 and *stu2-13* mutants were identified in the screen as increasing Dad4-YFP intensity with a 2 standard deviations (STD) cut-off and *stu2-11* when extending to a 1 STD cut-off. All three were validated in the retest and here *stu2-12* was in the extended list of mutants with decreased YFP intensity. The SGA screen combining T34 with the TS collection did not include wild-type controls and it was only imaged at the restrictive temperature. To confirm if these mutant alleles altered the YFP fluorescence, I imaged them individually in slides after 5 hours of growth at both, permissive (23˚C) and restrictive (37˚C) temperatures along with the wild-type strain T34.

For all the *STU2* alleles tested, the YFP intensity is higher at the restrictive temperature although the difference in *stu2-11* is minimal and at both temperatures is similar to the wild type. Although the YFP levels of *stu2-12* increase when switched to the restrictive temperature, they remain lower than the wild type at 23˚C and similar at 37˚C. In contrast, the Dad4-YFP intensity of *stu2-13* increases 55% at 37˚C from wild type like levels at 23˚C. *stu2-10* causes an increase of Dad4-YFP intensity of 23% when switching from 23˚C to 37˚C but has a 2-fold increase compared to the wild type even at 23˚C (Figure 4.17 A). There are no significant differences in the RFP levels between temperatures although RFP levels are higher in *stu2-13* than other strains at both temperatures (Figure 4.17 B).

To confirm these changes in Dad4-YFP fluorescence, I examined the images by eye. Figure 4.17 C shows examples of each *STU2* allele at both temperatures. The visual analysis of Dad4-YFP foci corresponds with the results from the automated quantitation. For instance, in *stu2-12* cells the Dad4-YFP foci look weaker than the wild type at both temperatures and in *stu2-11* the foci appear normal at 23˚C and stronger at 37˚C. The alleles *stu2-12* and *stu2-13* both have clearly strong foci at 37˚C.

In addition to the changes in Dad4-YFP intensity, I notice that *stu2-13* and *stu2-11* cells had large buds of the same size as the mothers and their duplicated SPBs and kinetochores remained in one of the two nascent daughter cells (Figure 4.17 D-E). A

phenotype has been described in *STU2* mutants in which the bipolar spindle is achieved but chromatids do not separate (He et al., 2001). Finally, in some *stu2-13* cells the SPBs were appropriately localized but the kinetochores are declustered (Figure 4.17 D). Stu2 has been implicated in kinetochore-microtubule capture (Tanaka et al., 2005). Consequently, my data support a critical role of Stu2 in kinetochore function.

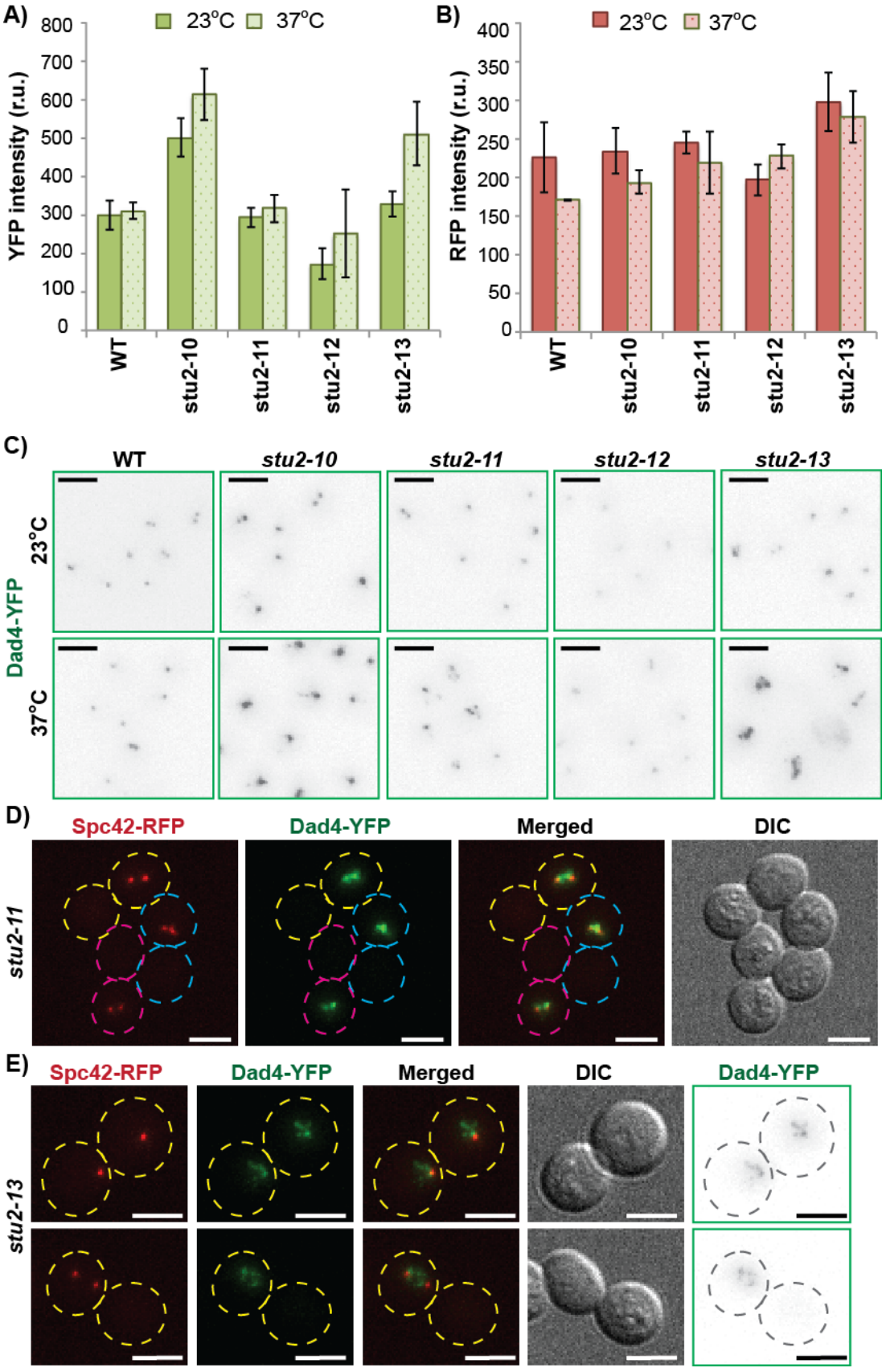

Figure 4.17. Effects of *STU2* alleles on Dad4-YFP. A) Mean fluorescent intensity values (background subtracted) for Dad4-YFP at 23˚C (dark green) and 37˚C (pale green) **B**) Mean fluorescent intensity values (background subtracted) for Spc42-RFP

at 23˚C (red) and 37˚C (pink). Image analysis performed by the ImageJ automated FociQuant (**A-B**). Error bars are standard deviation of the mean (**A-B**). **C)** Images of various *STU2* alleles and a WT (T34) at 23˚C and 37˚C. Foci represents Dad4-YFP. **D**) Yeast cells showing an arrest with big buds and misaligned spindles in the mutant *stu2-11*. **E)** Yeast cells showing a cell in telophase (top panel) and a cell with a big bud (bottom panel) with declustered kinetochores. Foci represent Dad4-YFP (green) and Spc42-RFP (red) (**D-E**). Scale bars are 5 µm in all images.

4.2.12.5. Chromatin remodelers: the RSC and SWI/SNF complexes.

A number of complexes are able to regulate gene expression by remodeling chromatin (RSC complex) or regulating the state of nucleosomes (SWI/SNF complex). Some members of these complexes were identified in my Dad4-YFP screen. For instance, *rsc2*Δ*, dbb7*Δ *and snf12*Δ strains were identified as low intensity mutants. Although *rsc1*Δ and *ylr358c*Δ (a protein of unknown function that partially overlaps with Rsc2) were not identified by the quantitative method, they were annotated by visual analysis as producing very weak foci (Figure 4.18 A). All of these except *dbb7*Δ were validated as low intensity mutants in the retest plate (Table H appendix 1) In addition, *ylr358c*Δ, *rsc1*Δ, *rsc2*Δ and *ldb7*Δ strains were classified as benomyl sensitive (Table K appendix 1).

Dad4-YFP intensity decreased (40-53%) in all of these SWI/SNF mutants except *snf2*Δ (Figure 4.18 B) and the foci distribution curves also showed a similar shape for the mutants, which was different from the wild type and *snf2*Δ (Figure 4.18 C). No significant differences were found for the RFP SPB signal.

I tested whether the levels in fluorescence would also affect other kinetochore protein by crossing these deletions from the deletion collection with a strain tagged for Mtw1-YFP and Spc42-RFP. Here, Mtw1-YFP fluorescence decreased in *rsc2*Δ cells (a modest 19% decrease) and increased 30% for *ylr358c*Δ with no change for the others. All foci distribution curves are like wild type with the exception of *ylr358c*Δ. However, in this case, RFP signal decreased 40-50% (Figure 4.18 D-E).

It has been shown that the F-box protein Dia2 is involved in assembly of the RSC complex (Andress et al., 2011). The null mutant of *DIA2* produced a visual phenotype with multiple Dad4-YFP foci distributed along lines in some cells (Figure 4.18 F).

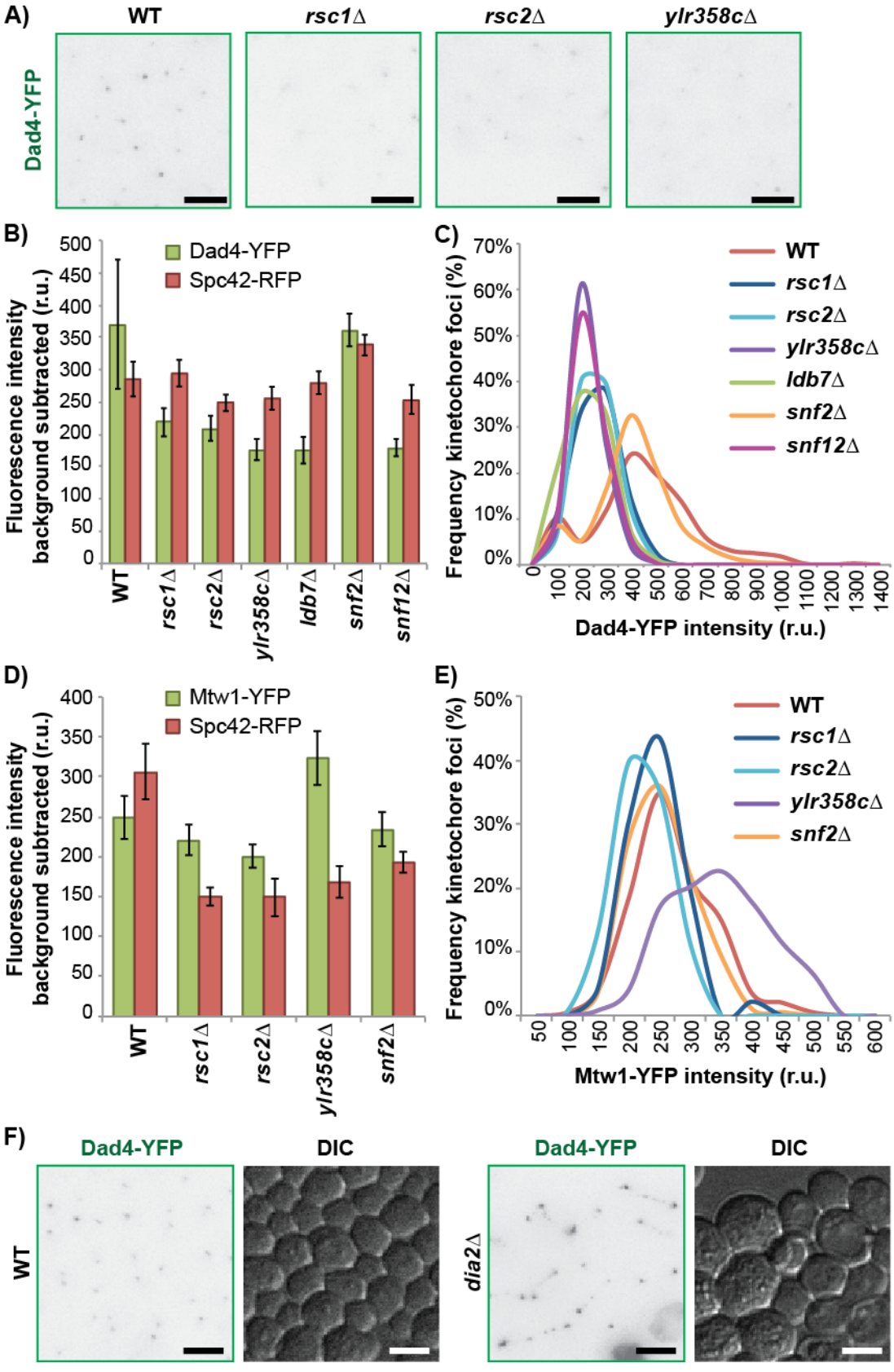

Figure 4.18. Effects of chromatin remodelers in the kinetochore. A) Examples of Dad4-YFP foci in WT and mutants **B**) Dad4-YFP (background subtracted) intensity (green) of foci quantified by automated ImageJ FociQuant and Spc42-RFP background-subtracted intensity (red). Error bars are standard deviation of the mean.

Distribution of Dad4-YFP **(C)** and Mtw1-YFP **(E)** foci intensities of mutants and WT are shown. **D)** Mtw1-YFP (background subtracted) intensity (green) of foci quantified by manual ImageJ FociQuant and Spc42-RFP background-subtracted intensity (red). Error bars are standard deviation of the mean. **F)** Cells with Dad4 (outer kinetochore protein) tagged with YFP (green foci) in WT and *dia2*Δ. Scales bars are 5 µm in all images.

4.2.12.6. Individual kinetochore mutants influence the intensity and localisation of Dad4-YFP differently.

Although outside of the scope of this project, my data could be studied further to investigate the effects of different kinetochore complexes and proteins in Dad4-YFP.

For instance, in *kre28*Δ cells Dad4-YFP is extended in lines, possible along microtubules (Figure 4.19 A), as it is in *ctf19*Δ (Figure 4.4 C). The YFP signal between two SPBs in post-metaphase cells can be seen separated into two foci in wild-type cells but not on *ctf19*Δ, where it remains between the 2 poles forming a short thick line (Figure 4.19 B) and YFP intensity decreases by half while RFP signal remains unchanged (Figure 4.19 C). This “line” distribution of Dad4-YFP in mutants such as *kre28*Δ and *ctf19*Δ, as well as the MAPSs *bim1*Δ and *bik1*Δ and the kinetochore associated *slk19*Δ, suggest that the restricted location of DAM1 complex proteins to the microtubule tips and the kinetochores is specifically regulated.

In contrast, *ask1-2 and spc34-ts* have stronger and defined foci (Figure 4.19 D). Ask1 and Spc34 are part of the DAM1 complex and mutants of genes encoding other members of this complex present a variety of phenotypes. In *dam1-5* cells the Dad4-YFP signal is delocalised with no or very weak foci in most cells. In contrast, *dam1-1* cells often have strong or aberrant Dad4-YFP foci. *duo1-2* cells give a Dad4-YFP signal that is diffused but between the two SPBs in anaphase cells. In addition, some cells have 3 SPBs and 2 lines of Dad4-YFP connecting them (Figure 4.19 D).

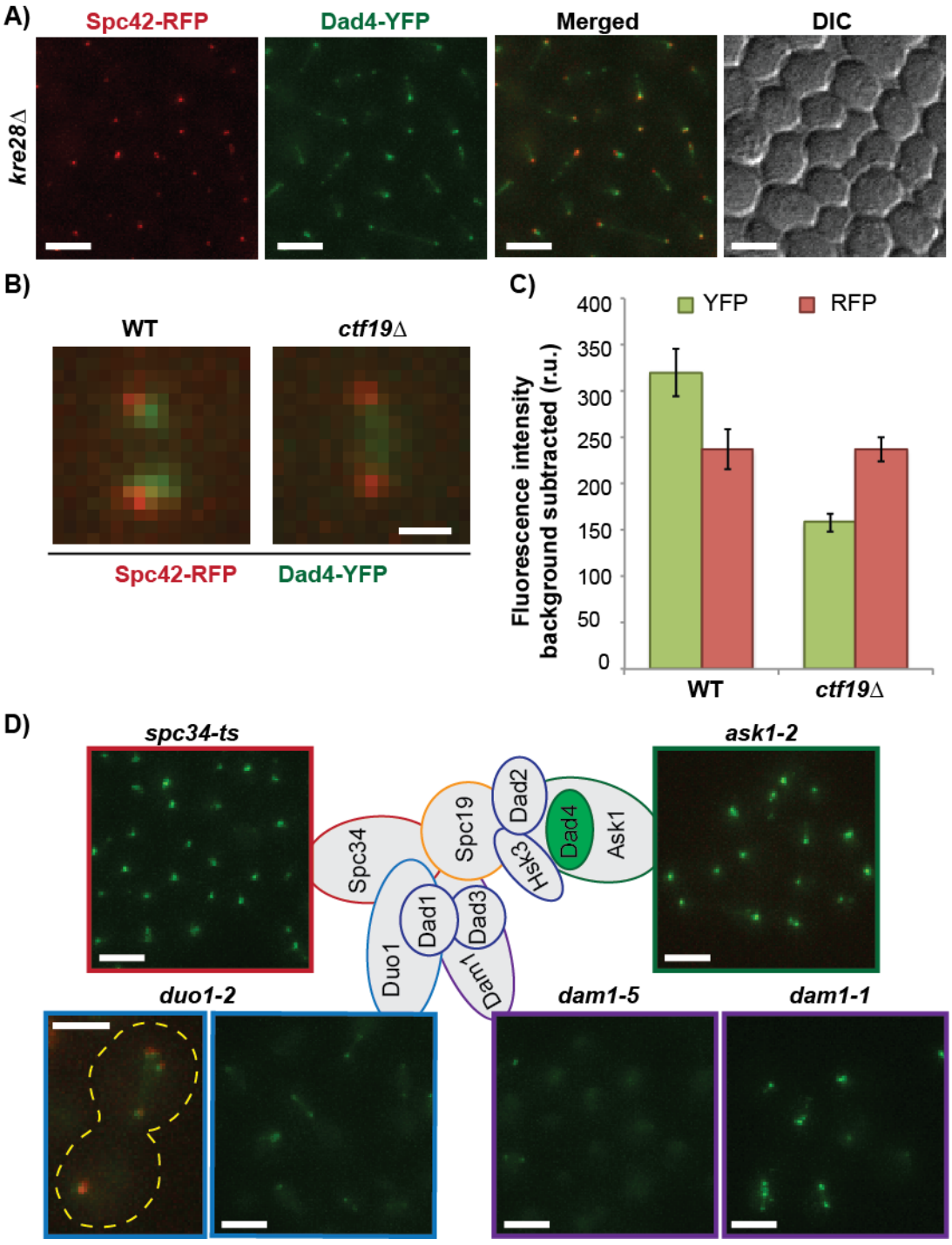

Figure 4.19. Phenotype of different members of the kinetochore on Dad4.
A) Yeast cells tagged for Spc42-RFP (red foci) and Dad4-YFP (green foci) in a *kre28*Δ background. **B**) This magnified image shows the SPB-RFP (red) and Dad4-YFP (green) of a mitotic cell in WT and *ctf19*Δ cells. **C**) Mean fluorescent intensity (background subtracted) for Spc42-RFP (red) and Dad4-YFP (green). Image analysis performed by the ImageJ automated FociQuant. Error bars are standard deviation of the mean. **D**) Examples of the different effects of DAM1 complex alleles on Dad4-YFP. A schematics shows the suggested structure of the DAM1 complex (adapted from Ramey et al., 2011). Scale bars are 5 μm

4.3. Summary and discussion results 2

I have performed a genome-wide fluorescent microscopy screen for the kinetochore protein Dad4 and analysed the data both quantitatively and qualitatively (by visual inspection). I chose a protein from the DAM1 complex given its stoichiometry and thus more robust signal. I identified ~321 mutants that affect Dad4-YFP kinetochore foci and studied a number of classes of these in more detail.

There are a number of limitations to the screening method. The first is the time taken to image each 96-well plate. Each 96-well plate was separately analysed as two 48-pad microscopy plates. It took at least one hour to image each of these 48-pad plates, resulting in variations in Dad4-YFP intensity across plates and between different plates. We addressed this noise in the data by normalising and smoothing the data. A second problem is that not all strains are in log phase. Some mutants grow slowly and consequently I was unable to synchronise all of the cultures in a 96-well plate. Third, only a single image was captured for each mutant. Specifically for the TS screen, the same restrictive temperature was used for all mutants despite different reported restrictive temperatures ranging from 26˚C to 38˚C. It should also be noted that many TS alleles are not fully functional at the permissive temperature and/or not fully mutant at the restrictive temperature.

Despite these limitations, the screen generated data for most mutants across the genome. The images were analysed both objectively using automated image analysis software (Ledesma-Fernandez and Thorpe, 2015) and subjectively by visual examination. Both approaches are time consuming taking months to analyse all the data. This meant that reanalysing the data using different parameters is currently beyond the scope of the project.

The mutants that affect the levels or localization of Dad4 are enriched for those encoding:

- Other kinetochore and mitotic spindle proteins.
- Chromatin remodelers and DNA associated proteins
- Mitotic exit proteins
- Nonsense-mediated RNA decay proteins.
- Threonine/serine biosynthesis enzymes.

Many of the mutants that lead to high Dad4-YFP fluorescence lead to multiple populations of kinetochore foci with different intensities. This heterogeneity may in some

cases be due to aneuploidy (Hughes et al 2000) although not all the “high Dad4-YFP intensity” mutants are reported to have CIN. Alternatively different mutants could lead to cell cycle changes that affect Dad4. For instance, if a mutant blocks cells from entering mitosis then kinetochores could have duplicated but not separated – effectively doubling the Dad4 concentration. However, examination of the images typically allows cell cycle stage to be judged by cell morphology, and most “high Dad4-YFP intensity” mutants have bright foci in both G1 and early S phase. Furthermore, the mutants identified in this screen are enriched for genes involved in maintaining chromosomal stability (Table 4.1). In summary therefore, I am confident that the majority of the mutants identified in this screen do affect Dad4 protein levels at the kinetochore and are not artefacts of the methodology or imaging process. It would be interesting to compare my screen data with microscopy screens of other kinetochore proteins, which we expect to be forthcoming in the near future (Brenda Andrews personal communication). These data will provide a foundation to study the regulation of kinetochore homeostasis.

5. Chapter V: Results 3: *PKC1* alleles cause a kinetochore phenotype

5.1. Introduction

5.1.1. *PKC1* is the homolog of the mammalian PKC

PKC1 is the budding yeast homolog of the mammalian Protein Kinase C (PKC), that encodes a serine/threonine protein kinase involved in multiple signalling pathways. Its multiple roles in mammalian cells are reflected in its multiple isoforms and localisations. The 12 human isoforms are subdivided into subfamilies: classical, novel, atypical and PKNs, according to their enzymatic properties and homology of domains involved in their localisation and activation (Figure 5.1) (Mellor and Parker, 1998; Rosse et al., 2010). The number of isoforms is reduced to 5 in *C. elegans*, 2 in fission yeast and a single one in budding yeast. Although some domains are present and/or absent in the different mammalian isoforms, all of these domains (except the PB1 domain which is only present in atypical PKC isoforms) are present in the only budding yeast copy, Pkc1 (Figure 5.1) (Mellor and Parker, 1998).

The budding yeast Pkc1 is thought to primarily be involved in maintaining cell wall integrity, since the growth defect in *pkc1* mutants can be rescued by the osmotic stabiliser sorbitol (Levin and Bartlett-Heubusch, 1992). Temperature sensitive alleles of *PKC1* were identified as having low levels of Dad4 in my genome-wide screen and I wished to further examine the mechanism underlying this phenotype.

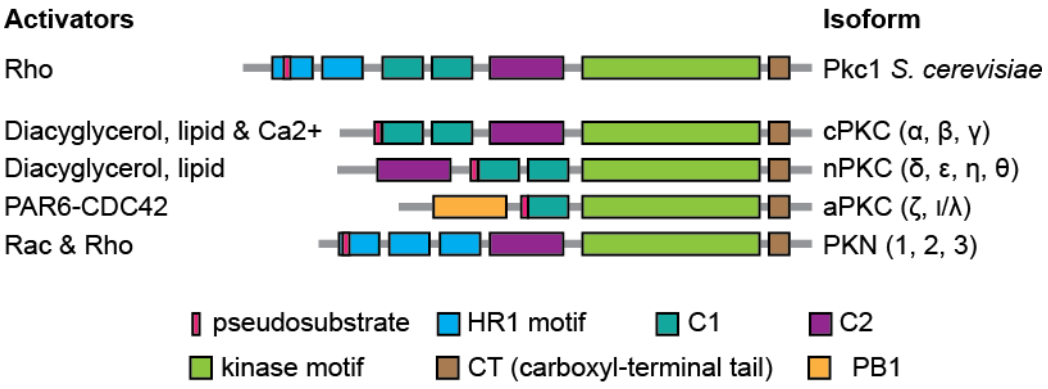

Figure 5.1. Protein Kinase C (PKC) isoforms and domains. Representation of the different mammalian isoforms of PKC and their domains compared to the one copy of the budding yeast Pkc1. Figure based in Rosse et al. (2010). (c is classical, n is novel, a is atypical).

5.1.2. Pkc1 and the CWI pathway

Pkc1 is the upstream activator kinase (MKKKK) of the cell wall integrity (CWI) pathway, which senses cell wall stress, both caused by environmental changes and during growth, to allow these signals to be transduced to the nucleus. Several sensors at the cell surface (Wsc1/2/3, Mid2 and Mtl1) together with the GEFs Rom1 and Rom2 activate this signalling cascade by stimulating the small G-protein Rho1. Rho1 is able to activate several effectors, one of them being the kinase Pkc1. Pkc1 starts the MAP cascade by activating the MAPK kinase kinase (MAPKKK) Bck1 that in turn activates the two MAPK kinases (MAPKKs) Mkk1 and Mkk2, and finally, those activate the MAPK Slt2/Mpk1. This cascade leads to the activation of transcription factors in the nucleus (Rlm1 and Swi4) that regulate expression of genes primarily encoding for cell wall biogenesis proteins (Figure 5.2) (Levin, 2005; Levin, 2011). The CWI pathway can be activated by conditions that require cell wall remodelling. These are hypotonic shock, heat shock and polarised growth, either cell cycle-dependent or as a response to nitrogen starvation or mating pheromone (Mellor and Parker, 1998). In addition to Rho1, Pkh1/2 must also phosphorylate Pkc1 for full activation when under heat shock (Levin, 2011).

Cell wall synthesis and remodelling must be coordinated with the cell cycle. The regulator of the cell cycle Cdc28 (Cdk1) controls the activity of Rho1 by activating its GEF Tus1 and in addition, it can inhibit Bem2, a Rho1 inhibitor. Rho1 can activate other effectors involved in cell wall remodelling and bud growth in addition to Pkc1 and thus the CWI pathway, such as the formin Bni1, which promotes actin cable assembly necessary for polarised growth. Other effectors include the exocyst member Sec3, the cell wall components of β1,3-glucan synthase (GS) (Fks1/2) and the transcription factor Skn7 involved in osmoregulation and G1/S transition (reviewed in Enserink and Kolodner et al., 2010) During cytokinesis, Cdc5 (Polo-like kinase) is known to phosphorylate Tus1 and possibly Rom2, thus controlling Rho1 activity at a different time than Cdc28 (Yoshida et al., 2006) (Figure 5.2).

Under cell wall stress Pkc1 can also induce transient depolarisation of actin in a pathway that involves the sensor Wsc1, the GEF Rom2 and the G-protein Rho1 but not the downstream members of the CWI pathway, although they are involved in repolarisation (Delley and Hall, 1999), and oxidative stress promotes actin cable formation via Mtl1, Rom2 and Pkc1 (Vilella et al., 2005).

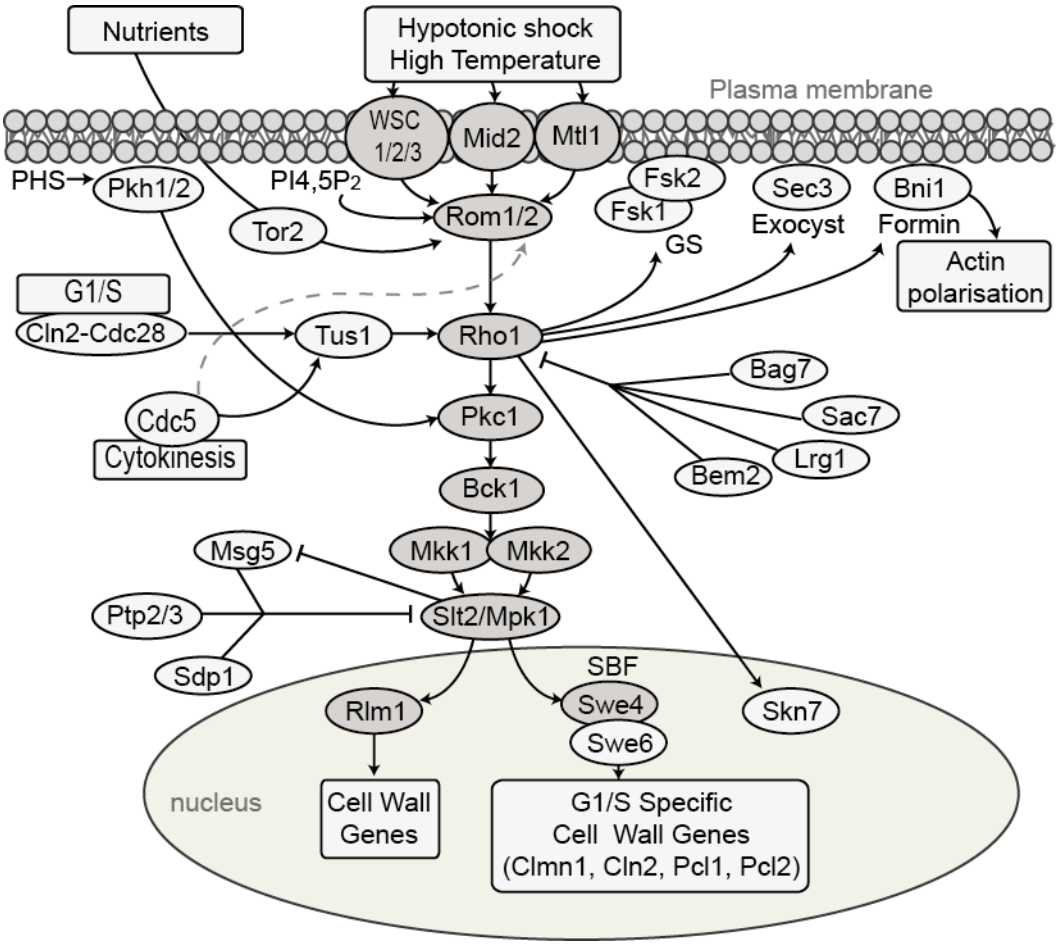

Figure 5.2. Budding yeast Cell Wall Integrity (CWI) pathway. Illustrative representation of the signalling cascade involving Pkc1 that signals cell wall stress to the nucleus. Figure based on Levin, 2005 and Levin, 2011. The CWI pathway is shown in light brown. Other activators and inhibitors, as well as some connections with the cell cycle are also shown (light grey). (PHS is phytosphingosine, GS is β1,3-glucan synthase).

5.1.3. Pkc1 localisation

Pkc1 in budding yeast localises to sites of polarised growth, which is dependent upon Rho1. Pkc1 appears diffusely localised most of the time but it accumulates at the tips of small-medium buds and at the bud neck of cells with large buds. In addition, it relocates to sites of damaged cell wall (Andrews and Stark, 2000). However Denis and Cyert, 2005, found that the C2 domain of Pkc1 is important for nuclear localisation and that Pkc1 lacking the HR1 domain localised to the mitotic spindle. Since the different roles of PKC isoforms are likely determined by their cellular localisations, these data suggest that yeast Pkc1 could be modified to change localisation and thus have additional roles to CWI.

5.1.4. PKC nuclear roles in other organisms

Mammalian PKC isoforms have been shown in different cell types to have regulatory roles in cell proliferation. For example, different stress conditions and protein modifications can switch the roles of PKCδ between stimulating cell proliferation or apoptosis (reviewed in Jackson and Foster, 2004).

More specifically, several PKC isoforms have been reported to have nuclear roles and localisation in several organisms. In organisms with open mitosis, PKC is implicated in nuclear envelope disassembly from zebra fish (Collas, 1999) to HeLa cells (Mall et al., 2012). Moreover, atypical PKCs regulate mitotic spindle orientation in polarised mammalian epithelia (asymmetric cell division) (Durgan et al., 2011) and Drosophila epithelia (symmetric cell division) (Guilgur et al., 2012).

Further, PKC-βII is tethered to centrosomes by pericentrin (Spc110 homolog in budding yeast) and has a role in cytokinesis (Chen et al., 2004). PKC isoforms have also been shown to bind microtubules in neurons to regulate their dynamics (Kabir et al., 2001) and microtubule related proteins have been shown to be substrates of PKC. For instance, PKC phosphorylates α-tubulin in human breast cells causing microtubule elongation (Abeyweera et al., 2009), and the microtubule associated protein (MAP) Tau (a microtubule stabiliser in neurons) *in vitro* reducing its binding to microtubules (Correas et al., 1992). In addition, atypical PKCζ in shark rectal gland cells can discriminate between astral and spindle microtubules and localises to β-tubulin in the mitotic spindle during mitosis (Lehrich and Forrest, 1994). Additionally, a signalling pathway involving PKC has been suggested to link microtubules, via the plus end protein EB1, with actin and cell polarity (Schober et al, 2012).

Recently, the Parker lab described a pathway controlled by PKCε that maintains chromosome integrity in cells with unresolved catenation in mitosis by delaying exit from the SAC into anaphase in those conditions (Brownlow et al., 2014).

In summary, PKC isoforms perform a multitude of roles involving the mitotic spindle and cell division regulation that differ according to cell type, cell cycle stage and environmental conditions.

5.1.5. Pkc1 nuclear roles in budding yeast

In budding yeast no nuclear functions for Pkc1 have been fully described, although several additional roles to the cell wall integrity pathway and actin depolarisation have been suggested, a number of which point to functions in the nucleus, both through transcriptional regulation and thought links to the spindle or spindle pole bodies.

For example, multiple genetic interactions have been reported between the Pkc1 pathway members and genes involved in SPB duplication, which are thought to be independent of the role in cell wall integrity, and the phenotype of a phospho-mimetic form of the SPB protein Spc110 was rescued by a temperature sensitive allele of *PKC1* (Khalfan, Ivanovska and Rose, 2000). A role of Pkc1 in microtubule function was proposed when the TBZ sensitivity and the delay in G2 progression phenotypes of a temperature sensitive allele were rescued by overexpressing the EB1 homolog, *BIM1* (Hosotani et al., 2001).

Furthermore, high-copy suppressor screens for temperature sensitive alleles of the RSC complex member Nps1/Sth1 (*sth1-105*), identified Pkc1 and Bim1/EB1 as suppressors of the temperature and TBZ sensitivity (Hosotani et al., 2001) and the sensors Wsc1 and Mid2 as suppressors of the G2/M arrest of *sth1-3* (Chai et al., 2002). Similarities between Pkc1 pathway mutants and *sth1-3*, such as defects in actin, TBZ sensitivity and TS sensitivity rescued by sorbitol, together with the fact that only Pkc1 and upstream members of the CWI pathway are suppressors, led to the suggestion of an alternative Pkc1 pathway linking chromatin remodelers with the organisation of microtubule and actin cytoskeletons (Chai et al., 2002).

Recently, Pkc1 was shown to be required for the activation of the DNA integrity checkpoint independently of the CWI pathway and this is conserved in human cells (Soriano-Carot et al., 2014). Finally, Pkc1 has been shown to associate with CLB2 cluster genes and repress their expression by phosphorylating Ndd1 at the Mcm1-Fkh2-Ndd1 complex to prevent this complex from activating the cluster (Darieva et al., 2012). In summary, novel roles have been suggested for the Pkc1 pathway and especially for alternative branches involving only the upstream members and for which other players could still remain undiscovered. These links reflect unknown roles of the multiple isoforms of mammalian PKC and will need to be investigated further.

5.2. Results

5.2.1. Pkc1 temperature sensitive allele mutations causes a phenotype on the outer kinetochore component Dad4

I identified two alleles of *PKC1*, *pkc1-1 and pkc1-ts*, that decreased Dad4-YFP intensity in the genome-wide screen and confirmed this phenotype. Qualitative assessment of these images revealed a visual phenotype in which at the permissive temperature (23˚C) 100% of the cells have visible foci for both Dad4-YFP and Spc42-RFP, whereas at the restrictive temperature (37˚C), 75% of the cells appear to have lost the Dad4-YFP discrete foci showing a more dispersed YFP signal, while retaining the Spc42-RFP foci (Figure 5.3 A-B). At 37˚C, many of the cells that have still visible Dad4-YFP foci look enlarged, and the cells with dispersed signal have often an abnormal appearance and are smaller. In addition, even at 23˚C some cells have smaller extra YFP foci that do not localise adjacent to the RFP foci (Figure 5.3 B, arrows). To determine whether the cells without Dad4-YFP foci are dead and can't thus recover, I switched cultures from 37˚C back at 23˚C and performed time-lapse imaging. I found that cells lacking Dad4-YFP foci underwent no further cell divisions (data not shown). Furthermore, I tested the proportion of cells that could recover at 23˚C after growth at 37˚C for 3 hours. Individual cells from cultures grown at 23˚C and 37˚C were separated and grown in rich media plates at 23˚C. From the 23˚C cultures 91% (+/- 7%) of 110 cells were viable versus 43% (+/- 10%) of 112 cells grown at 37˚C (Figure 5.3 C). Imaging of the 37˚C cultured showed that 60% (+/- 4%) had retained Dad4-YFP foci. Dead cells (identified by bright fluorescence throughout) were excluded from the analysis. These data support the notion that once cells have lost their kinetochore focus they are no longer viable.

I then quantified the YFP signal by a manual quantification method (Volocity), only in cells that had both RFP and YFP foci at 23˚C and 37˚C. Although the values obtained with Volocity are not comparable with the ImageJ values, the Dad4-YFP signal does not decrease significantly in this subset of cells (Figure 5.3 D). The RFP signal in cells that retain the YFP signal versus the ones that don't (both at 37˚C) didn't decrease significantly either (Figure 5.3 E). These data show that a proportion of *pkc1-1* cells retain Dad4-YFP foci even at the restrictive temperature.

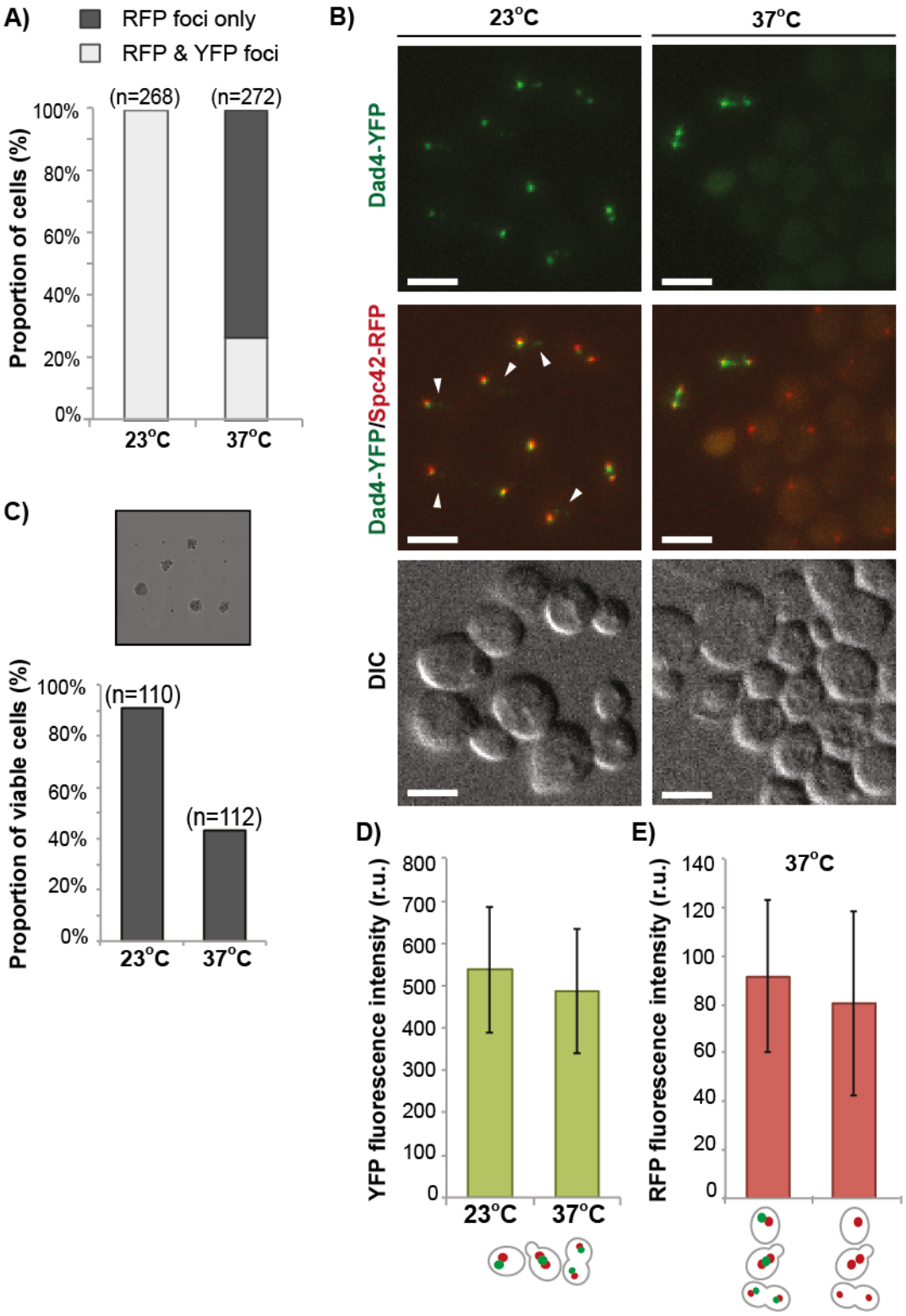
A)
RFP foci only
RFP & YFP foci
(n=268)
(n=272)
Proportion of cells (%)
100%
80%
60%
40%
20%
0%
23°C
37°C
B)
23°C
37°C
Dad4-YFP
Dad4-YFP/Spc42-RFP
DIC
C)
Proportion of viable cells (%)
(n=110)
(n=112)
D)
YFP fluorescence intensity (r.u.)
800
700
600
500
400
300
200
100
0
E)
RFP fluorescence intensity (r.u.)
140
120
100
80
60
40
20
0

Figure 5.3. Effect of *pkc1-1* on the kinetochore protein Dad4.
A) Manual cell count of the proportion of cells with either visible green (YFP) and red foci (RFP) or only red foci in a *pkc1-1* background. **B)** Images of cells with Dad4 (outer kinetochore protein) tagged with YFP (green foci) and Spc42 (SPB protein) tagged with RFP (red foci) in a *pkc1-1* background. Arrows point to YFP foci that do not colocalise to RFP foci. Scale bars are 5 μm. **C)** Proportion of cells that grew into a colony in rich solid media from single cells dissected from cultures grown at either 23˚C or 37˚C for ~3hours in synthetic complete media with adenine. Insert shows and example with 5 colonies growing out of 16 plated. **D)** Dad4-YFP intensity quantified manually by Volocity software. At 37˚C only cells with visible foci were quantified. **E)** Spc42-RFP intensity quantified manually by Volocity software. All cells were grown at 37˚C. SPB intensity was measured in cells with YFP foci versus cells with loss of YFP foci. For **D** and **E** error bars are standard deviation of the mean. All the strains in Figure 5.3 were imaged after ~4-5 hours growth (except **C**) at the indicated temperatures in synthetic complete media with adenine.

5.2.2. A wild-type copy of *PKC1* in the *URA3* locus complements the phenotype

Since, the *pkc1-1* strain is part of a large collection of TS strains, I wanted to confirm that the strain was a genuine *PKC1* allele. I used PCR to confirm that the *KANMX* cassette is indeed inserted at the genomic *PKC1* locus.

To further confirm that the phenotype described was caused by the *pkc1-1* allele and not by a possible additional mutation in the TS collection strain undetected by previous methods, I complemented the allele with a wild-type copy of *PKC1* by genomic integration at the *URA3* locus. *PKC1* with its endogenous promoter was cloned into an integrating *URA3*+ plasmid. This was transformed into a wild-type strain doubly tagged for Dad4-YFP and SPc42-RFP (T34) and then crossed with the *pkc1-1* strain from the TS collection. The complemented strain (PT213-11B, *pkc1-1 ura3-1::PKC1::URA3*) has 100% of cells with discrete Dad4-YFP foci when grown at 37˚C, compared with 15% for the *pkc1-1* strain (Figure 5.4 A-B).
The complementation is not complete since the Dad4-YFP foci, are visually abnormal, in some cases even at 23˚C (Figure 5.4 A). The *pkc1-1 PKC1* strain has extra Dad4-YFP foci and stronger signal extending along what appears to be the spindle. There is a further increase of YFP fluorescence on the complemented strain when switched to 37˚C, while the RFP fluorescence doesn't change (Figure 5.4 C). This Dad4-YFP phenotype may be due to either the presence of the defective Pkc1 protein or the excess of Pkc1.

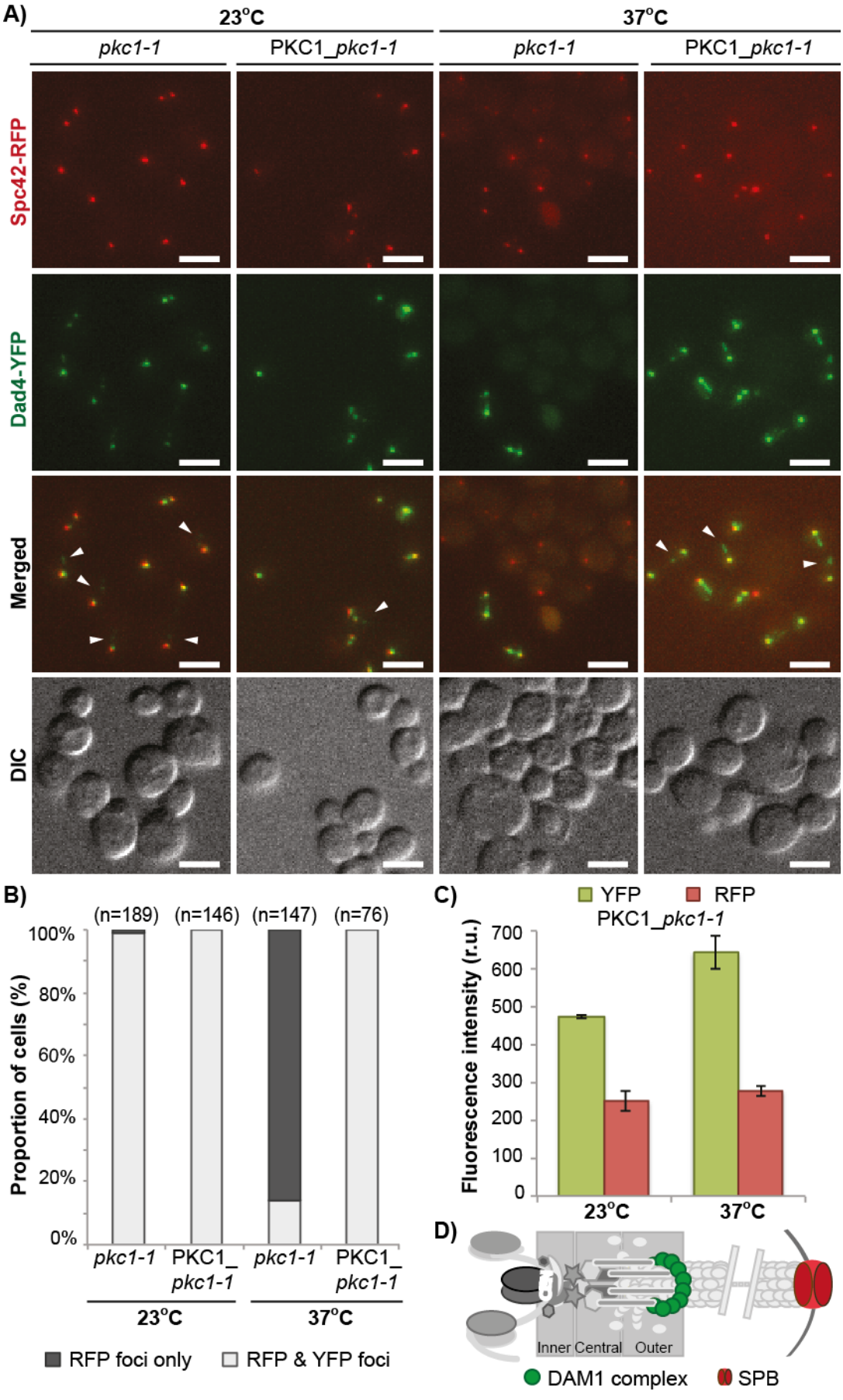
A)
23°C
37°C
pkc1-1
PKC1_pkc1-1
pkc1-1
PKC1_pkc1-1
Spc42-RFP
Dad4-YFP
Merged
DIC
B)
(n=189)
(n=146)
(n=147)
(n=76)
100%
80%
60%
40%
20%
0%
Proportion of cells (%)
pkc1-1
PKC1_ pkc1-1
pkc1-1
PKC1_ pkc1-1
23°C
37°C
RFP foci only
RFP & YFP foci
C)
YFP
RFP
PKC1_pkc1-1
Fluorescence intensity (r.u.)
700
600
500
400
300
200
100
0
23°C
37°C
D)
Inner Central Outer
DAM1 complex
SPB

Figure 5.4 *PKC1* at *URA3* locus complements the *pkc1-1* phenotype.
A) Images of cells with Dad4 (outer kinetochore protein) tagged with YFP (green) and Spc42 (SPB protein) tagged with RFP (red) in a *pkc1-1* mutant strain and the same strain complemented with a wild-type copy of *PKC1* inserted at the *URA3* locus (*PKC1_pkc1*). Imaged after growth at 23˚C and 37˚C. The white arrowheads indicate YFP foci that do not colocalise to RFP foci. Scale bars are 5 µm. **B)** Manual cell count of proportion of cells with either visible green and red foci or only red foci in the *pkc1-1* mutant and the complemented strain (PKC1*_pkc1*). **C)** YFP and RFP background-subtracted intensities of foci quantified by automated FociQuant for the complemented strain (PKC1*_pkc1*). Error bars show standard deviation of the mean **D)** A cartoon representing the kinetochore illustrates the position of the Dad4-containing DAM1 complex within the kinetochore.

5.2.3. The *pkc1-1* allele has an effect on the entire kinetochore

I wanted to test whether the *pkc1-1* phenotype was specific for Dad4-YFP or whether the same effect could be seen in other kinetochore-tagged proteins. First, I crossed the *MAT***a** *pkc1-1* strain (from the TS collection) with two different *MATα* strains, both of which contain *SPC42-RFP::HYGMX* and either *DAD3-YFP::NATMX* or *MTW1-YFP::NATMX*. Like Dad4, Dad3 is a member of the outer kinetochore DAM1 complex whereas Mtw1 is a component of the central MIND complex (Figure 5.5 E). I selected spores containing both the RFP and YFP alleles plus the *pkc1-1* mutation. These two strains were then imaged as before after growth at 23˚C and 37˚C. In both cases a large proportion of cells, 78% for Dad3 and 70% for Mtw1, had dispersed YFP foci specifically after growth at 37˚C (Figure 5.5 A-B). In both kinetochore proteins the YFP signal decreased by approximately half (Figure 5.5 C-D).

Additionally, I transformed a PCR product consisting of the *pkc1-ts* allele into a strain with the inner kinetochore protein Ndc10 (Figure 5.5 E) tagged with GFP (from the GFP collection). The restrictive temperature for *pkc1-ts* is 35C versus 37˚C for *pkc1-1*. At 23˚C cells have a GFP focus but when switched to 35˚C, the GFP becomes dispersed in over 70% of the cells. In addition, in 7% of cells, an intermediate phenotype is visible in which many smaller foci are present instead of having a single or double focus (Figure 5.5 F-G).

Together, these results indicate that the effect of the *pkc1* mutants is general to the kinetochore and not specific to the outer DAM1 complex or specifically the Dad4 protein.

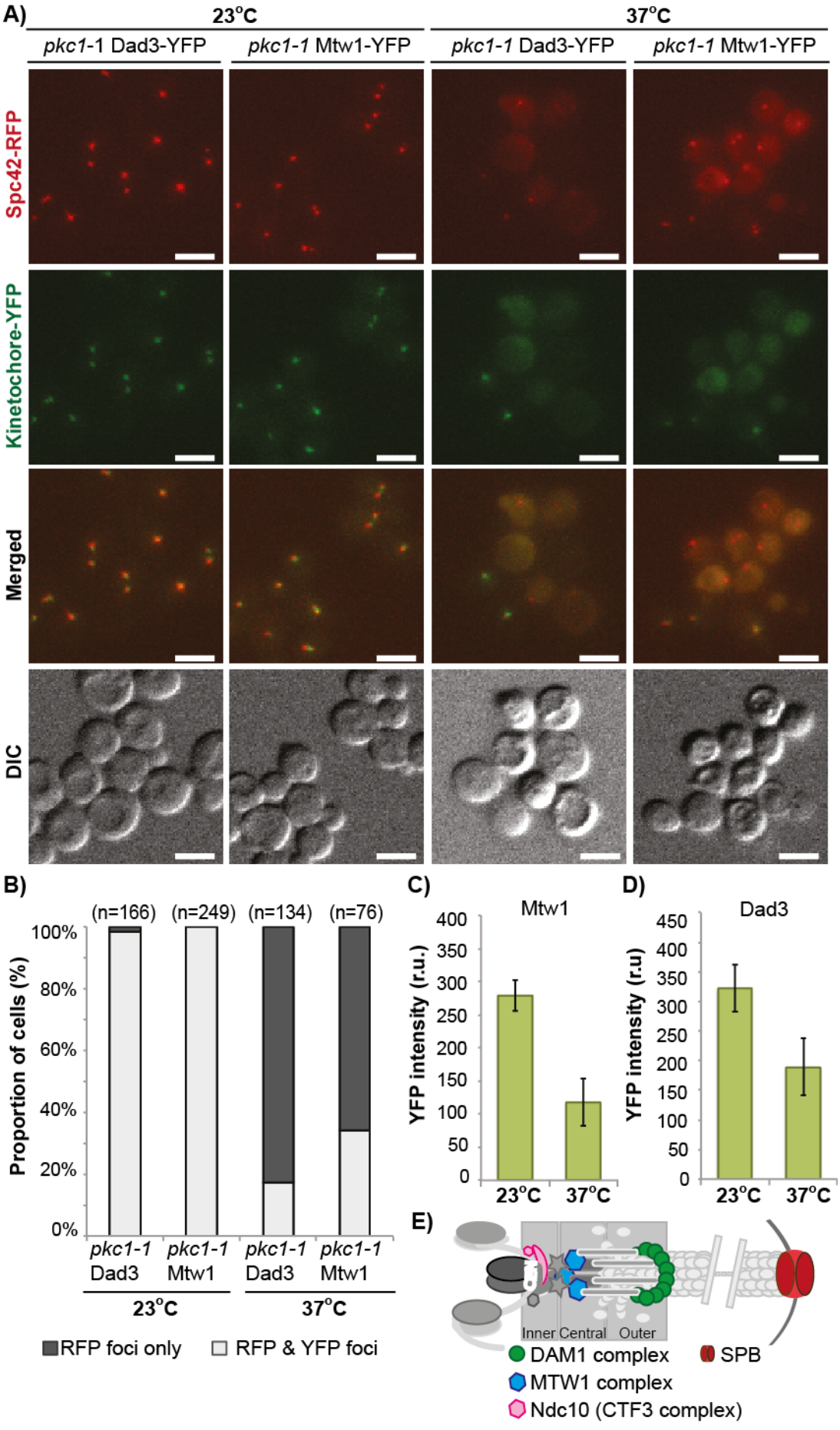
A)
23°C
37°C
pkc1-1 Dad3-YFP
pkc1-1 Mtw1-YFP
pkc1-1 Dad3-YFP
pkc1-1 Mtw1-YFP
Spc42-RFP
Kinetochore-YFP
Merged
DIC
B)
(n=166)
(n=249)
(n=134)
(n=76)
Proportion of cells (%)
100%
80%
60%
40%
20%
0%
pkc1-1 Dad3
pkc1-1 Mtw1
pkc1-1 Dad3
pkc1-1 Mtw1
23°C
37°C
RFP foci only
RFP & YFP foci
C)
Mtw1
YFP intensity (r.u.)
400
350
300
250
200
150
100
50
0
23°C
37°C
D)
Dad3
YFP intensity (r.u.)
450
400
350
300
250
200
150
100
50
0
23°C
37°C
E)
Inner
Central
Outer
DAM1 complex
SPB
MTW1 complex
Ndc10 (CTF3 complex)

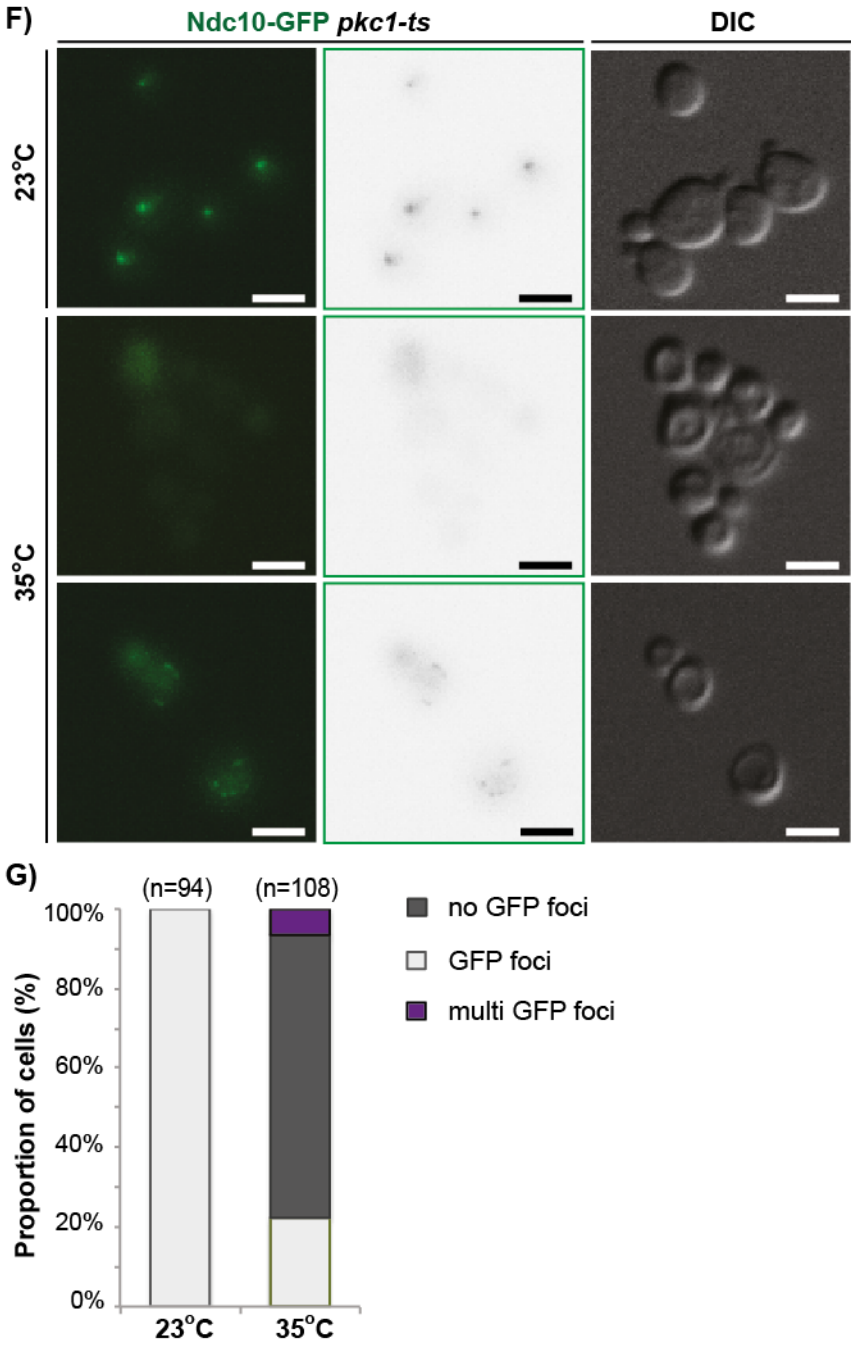

Figure 5.5. Effect of *pkc1-1* on the kinetochore proteins Dad3, Mtw1 and Ndc10. A) Images of cells with Dad3 (outer kinetochore protein) or Mtw1 (central kinetochore) tagged with YFP (green) and Spc42 (SPB protein) tagged with RFP (red) in a *pkc1-1* mutant strain. Cells were imaged after 5 hours growth at 23˚C or 37˚C as indicated. Scale bars are 5 µm. **B)** Manual cell count of the proportion of cells with either visible green and/or red foci. **C-D)** Dad4-YFP background-subtracted intensity of foci quantified by automated FociQuant. **E)** A cartoon representing the kinetochore and position of the 3 proteins tested **F)** Images of cells with Ndc10 (inner kinetochore protein) tagged with GFP (green) in a *pkc1-ts* mutant strain. Imaged after growing at 23˚C and 35˚C. Scale bars are 5 µm. **G)** Manual cell count of proportion of cells containing either visible Dad4-YFP single or double metaphase foci, multifoci, or no foci in a *pkc1-ts* Ndc10-GFP strain.

5.2.4. Kinetochore declustering may occur prior to the *pkc1-1* phenotype

As described previously, the kinetochore fluorescence for the inner (Ndc10), central (Mtw1) outer (Dad3, Dad4) proteins appears dispersed after ~5 hours at 35-37˚C in a *pkc1-1* or *pkc1-ts* background. Ndc10-YFP has a more intermediate phenotype in *pkc1-ts* cells with multiple foci in some cells and dispersed in others. Multiple Dad4 foci are seen in some *pkc1* mutant cells even at 23˚C. It is possible therefore that kinetochores become unclustered prior to the signal becoming diffuse. To test this notion, I performed a timecourse to see if declustering preceded the diffuse kinetochore pattern.

The difference in Dad4-YFP intensity of *pkc1* mutant cells between the permissive and restrictive temperatures increases with time, only starting to be significant after 120 minutes. After 255 minutes the Dad4-YFP signal has halved (consistent with results from the original screen) (Figure 5.6 A). This decrease in Dad4-YFP signal appears to correspond to an increase in number of cells with no discrete YFP foci at 37˚C, which increases from 2% after 20 minutes to over 80% after 255 minutes (Figure 5.6 B). Additionally, also increasingly with time, cells have extra foci and aberrant kinetochores. Some cells have a YFP focus localised to the RFP focus (in some cases very enlarged) plus multiple smaller YFP foci within a small radius (Figure 5.6 C, arrows). A small percentage of cells have a large bud undistinguishable by eye from the mother, in which one has foci for both fluorescent signals while in the other (bud or mother) has only RFP foci (Figure 5.6 D). Also in a small number of cells a strong YFP signal forms a line between Spc42-RFP foci (4 in this image) (Figure 5.6 E). In this last example the Dad4-YFP signal may be colocalised with a misaligned spindle, additionally the cell has 2 pairs of SPBs. These data indicates that the kinetochore defects accumulate after the function of Pkc1 is perturbed finally resulting in the diffuse Dad4-YFP signal. These observations also suggest there may be a problem with kinetochore segregation in these cells.

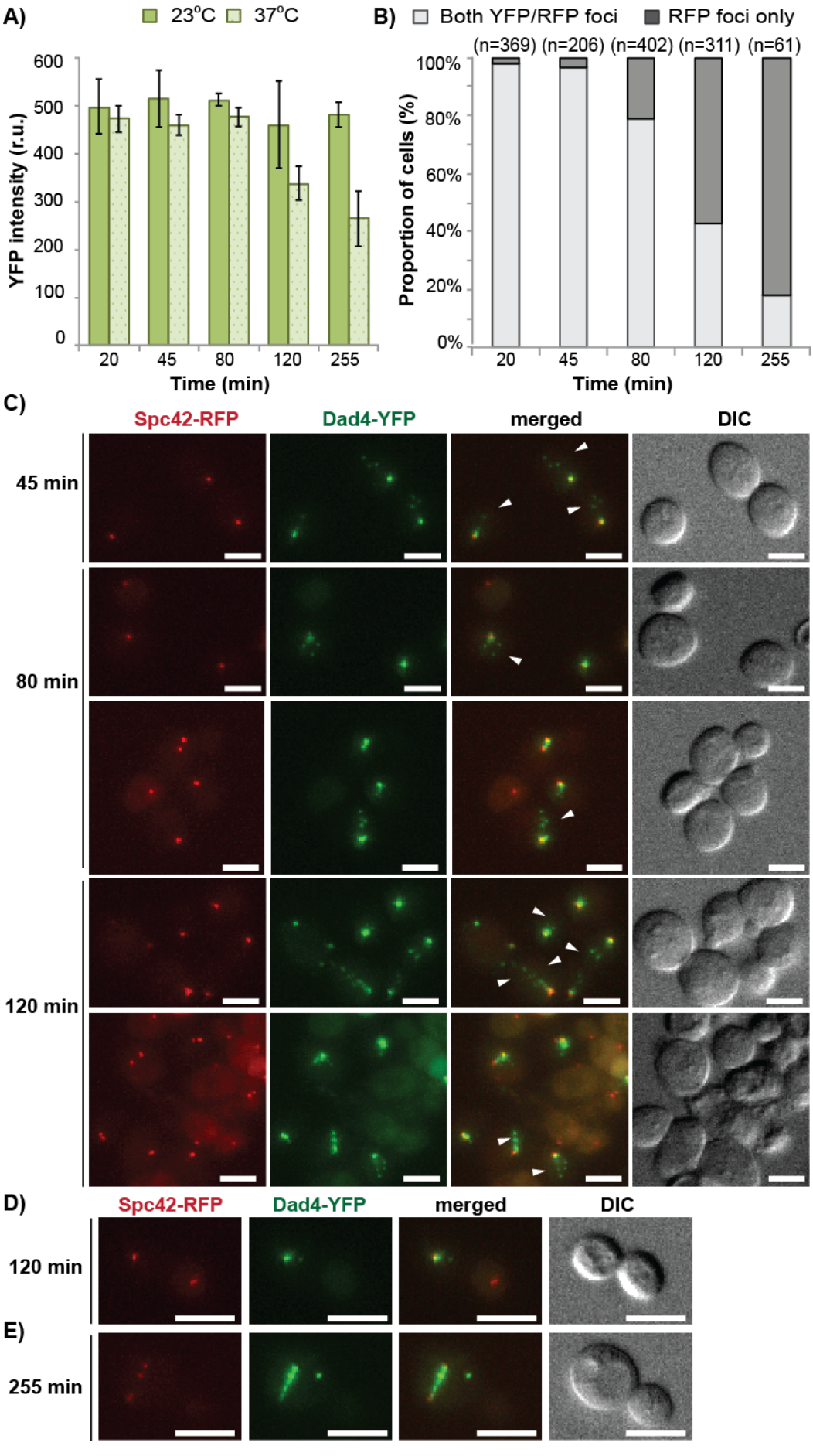
A)
23°C
37°C
YFP intensity (r.u.)
600
500
400
300
200
100
0
20
45
80
120
255
Time (min)
B)
Both YFP/RFP foci
RFP foci only
(n=369) (n=206) (n=402) (n=311) (n=61)
Proportion of cells (%)
100%
80%
60%
40%
20%
0%
20
45
80
120
255
Time (min)
C)
Spc42-RFP
Dad4-YFP
merged
DIC
45 min
80 min
120 min
D)
Spc42-RFP
Dad4-YFP
merged
DIC
120 min
E)
255 min

Figure 5.6. *Pkc1-1* timecourse at 37˚C. A) YFP intensity background subtracted of foci quantified by automated FociQuant. Error bars show standard deviation of the mean **B**) Manual cell count of proportion of cells with either visible green and red foci or only red foci after growth at 37C for the indicated times. **C-E**) Images of cells with Dad4 (outer kinetochore protein) tagged with YFP (green) and Spc42 (SPB protein) tagged with RFP (red) in a *pkc1-1* background. Imaged after growth at 37˚C for the indicated time. Scale bars are 5 µm.

5.2.5. Localisation of Pkc1

I examined at the localisation of Pkc1 by imaging a strain tagged with GFP (from the GFP library (Huh et al., 2003). In some cases the localisation was as reported in the literature: in unbudded G1 cells Pkc1-GFP showed diffuse localisation, in budding cells the GFP becomes very bright in the bud of small budded cells and at the periphery of larger buds, finally in cells with a large bud, GFP can be seen at the bud neck (Figure 5.7 A). However, the majority of cells had diffuse signal at any stage of the cell cycle (as in the left panel of Figure 5.7 A), consistent with images from high-throughput studies (e.g. see Tkach et al 2012). In addition, some Pkc1 foci were observed in both G1 and budded cells (Figure 5.7 B).

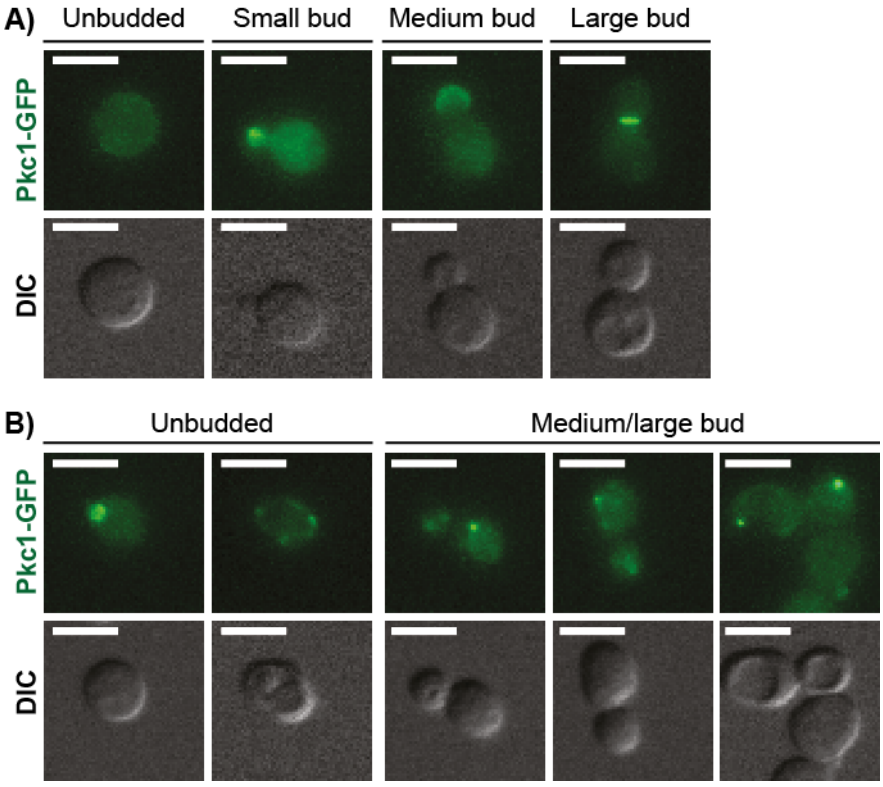

Figure 5.7. Localisation of Pkc1-GFP. Cells with Pkc1-GFP (green) present expected localisations reported from the literature (**A**) as well as other localisations observed (**B**) Scale bars are 5 µm.

5.2.6. Do increased or decreased levels of Pkc1 cause an opposed phenotype on Dad4?

In the *pkc1-1* cells at high temperature the Dad4-YFP intensity decreases and in the complemented strain, which has both, a wild type and a mutant copy, the intensity increases and foci appear enlarged. Hence, I wanted to test the hypothesis that an increase of Pkc1 protein may increase or mislocalise Dad4 while a decrease on Pkc1 protein may decrease Dad4 or de-cluster kinetochores.

5.2.6.1. The Pkc1 overexpression phenotype is background dependent

To address the first possibility I overexpressed *PKC1* by inserting a galactose-induced wild-type copy of *PKC1* in the *URA3* locus (*ura3-1::GALpr-PKC1::URA3*), in various strains fluorescently tagged for kinetochore and SPB proteins. This allows me to overexpress *PKC1* by growth on galactose media. Although some minor effects of *PKC1* overexpression could be seen, these were not reproducible between strains. Furthermore, there were differential effects of *PKC1* overexpression on cell viability, but again these were not consistent across different genetic backgrounds (Figure B appendix 2). These data do not support the notion of a kinetochore defect in cells overexpressing *PKC1*, however, more work needs to be done as I can't confirm that Pkc1 is overexpressed at the time of imaging.

5.2.6.2. Auxin degradation of Pkc1

The second possibility I wanted to address was whether a decrease in Pkc1 levels in the cell would produce a reduction/diffusion of YFP signal at the kinetochore or an increase in kinetochore declustering, comparable to the phenotype seen in the TS allele. I decided to use a method in which Pkc1 is selectively degraded and thus, cells don't need to be grown at high temperature, which could be contributing to a CWI phenotype. A degron (AID) system has been described in yeast that is inducible by auxin, a plant hormone, to target the protein of interest to the proteasome for degradation (Nishimura et al., 2009). In summary, a short degron (AID) was added to the C terminus of Pkc1 followed by FLAG epitopes for Western Blot detection (*PKC1-AID*). An integrative plasmid coding for the ABF2/TIR1 F-box protein was introduced into the strain encoding the Pkc1-AID. ABF2 is a F-box protein and part of the Skp, Cullin, F-box (SCF) E3 ubiquitin ligase. Addition of auxin to the media promotes the interaction between the AID and the E3 (ABF2) and thus targets AID-tagged protein for degradation (see methods).

Addition of 0.5 mM auxin for 2 hours leads to 40% of cells displaying normal SPB foci with dispersed Dad4-YFP foci and this did not change when the auxin concentration was doubled (Figure 5.8 A). However, manual quantification of only the Dad4-YFP foci close to RFP foci shows a reduction in YFP intensity that halves each time auxin concentration is doubled (Figure 5.8 B). This quantitative analysis can clearly be seen in the fluorescence images (Figure 5.8 C) and in the distribution of foci intensities (Figure 5.8 D). In addition to these weak Dad4-YFP foci in the auxin treated cells, a few cases can be seen when the foci has disappeared only in one of the mother/bud pair (Figure 5.8 E). This phenotype in a very small number of cells had been already seen in *pkc1-1* (Figure 5.6 D).

Introducing both the AID and the ABF2/TIR1 at the same time in the strain was problematic, which may suggest that even in the absence of auxin, Pkc1 becomes unstable when the degron is added. This work is incomplete as the controls constructed need to be tested and Western Blot needs to be performed to test that the degradation of Pkc1 is occurring as well as the timing. However, my preliminary examination reported here suggests that the Dad4-YFP phenotype of *PKC1* TS alleles can be recapitulated with degradation of Pkc1.

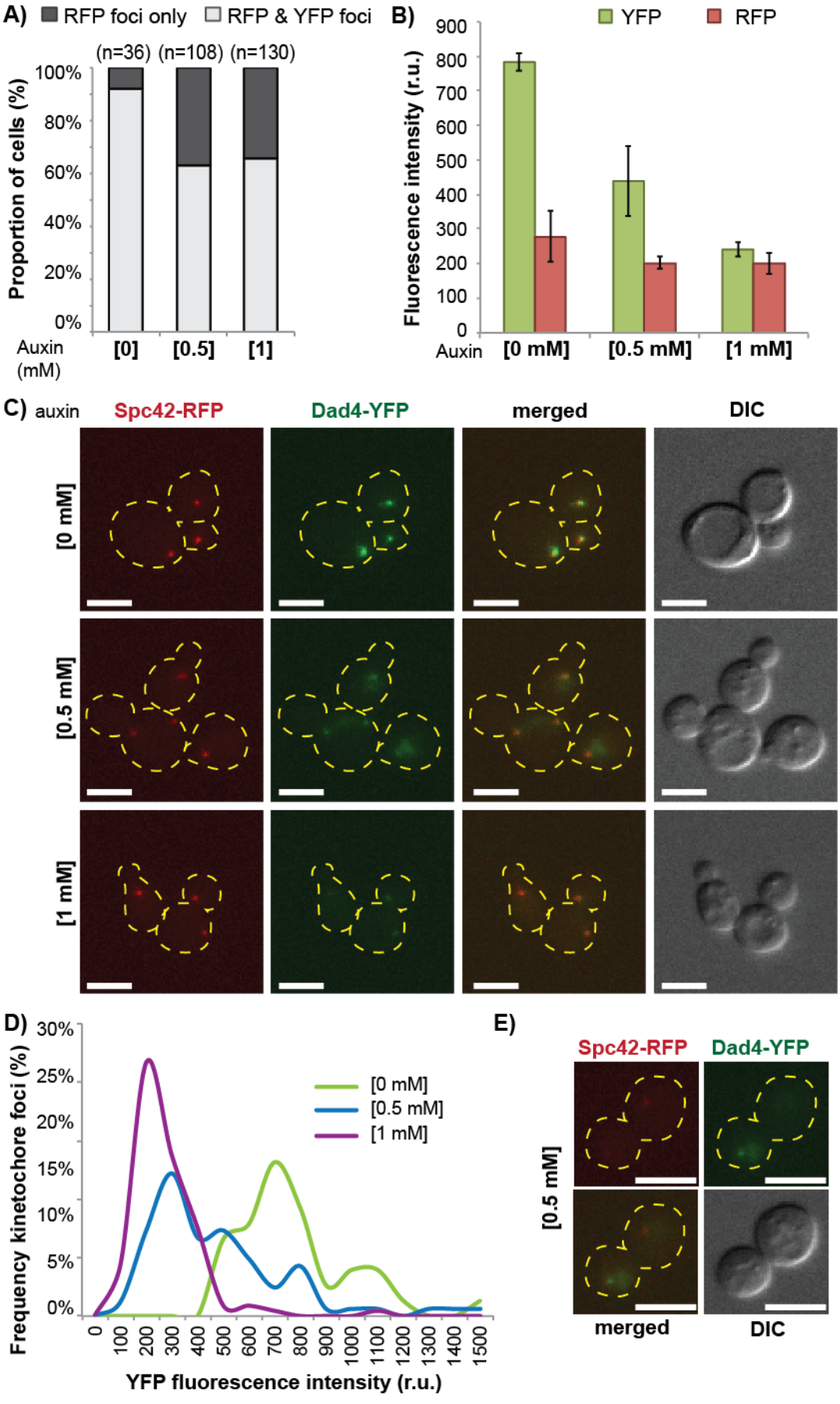
A)
RFP foci only
RFP & YFP foci
(n=36) (n=108) (n=130)
Proportion of cells (%)
100%
80%
60%
40%
20%
0%
Auxin (mM)
[0]
[0.5]
[1]
B)
YFP
RFP
Fluorescence intensity (r.u.)
900
800
700
600
500
400
300
200
100
0
Auxin
[0 mM]
[0.5 mM]
[1 mM]
C)
auxin
Spc42-RFP
Dad4-YFP
merged
DIC
[0 mM]
[0.5 mM]
[1 mM]
D)
Frequency kinetochore foci (%)
30%
25%
20%
15%
10%
5%
0%
[0 mM]
[0.5 mM]
[1 mM]
0
100
200
300
400
500
600
700
800
900
1000
1100
1200
1300
1400
1500
YFP fluorescence intensity (r.u.)
E)
Spc42-RFP
Dad4-YFP
[0.5 mM]
merged
DIC

Figure 5.8. Pkc1 degradation by an auxin system. A) Manual cell count of the proportion of cells with either visible green and red foci or only red foci on cells grown for 2 hours at 23˚C on synthetic media with adenine and auxin at the indicated concentrations. The strain contains Pkc1-AID and the ABF2/TIR1 F-box receptor **B**) YFP and RFP background-subtracted intensities of foci quantified by the manual FociQuant for the same cells in (**A**). Error bars show standard deviation of the mean. **C** and **E**) Cells as in (**A-B**) with Dad4 tagged with YFP (green) and Spc42 tagged with RFP (red). Scale bars are 5 µm. **D**) Foci distribution curves for the same cells.

5.2.7. Pkc1 phenotype relationship to the CWI pathway

5.2.7.1. The Pkc1 phenotype can be rescued by sorbitol

Pkc1 is a member of the CWI pathway. Sorbitol has been shown to stabilize yeast cells against osmotic stress and to rescue phenotypes caused by mutations in components of the CWI pathway. It is possible to add sorbitol (1 M) to the medium as an osmo-protectant (Levin and Bartlett-Heubusch, 1992).

I grew cultures of a *pkc1-1* strain with Spc42-RFP and Dad4-YFP in sc+ade media with or without 1 M sorbitol for 5 hours at 37˚C before imaging. The number of cells with RFP foci and no YFP foci was reduced from over 85% to less than 5% with the addition of sorbitol (Figure 5.9 A-B). This indicates that sorbitol rescues the *pkc1-1* kinetochore phenotype and thus suggests a possible relationship with the CWI pathway. However, some *pkc1-1* cells have extra Dad4-YFP foci at 37˚C (8%) and this was not reduced with addition of sorbitol, in fact, it increased to nearly 50% (Figure 5.9 A-B). The YFP signal was also higher in the images with sorbitol than without for *pkc1-1* after growth at 37˚C, while the RFP signal remained unchanged (Figure 5.9 C). Consequently, although sorbitol did rescue the absence of Dad4-YFP foci seen in *pkc1-1* cells at high temperature, it also gave an additional phenotype of increased Dad4-YFP signal at kinetochore and increased the number of Dad4 foci, which was not in in the wild type.

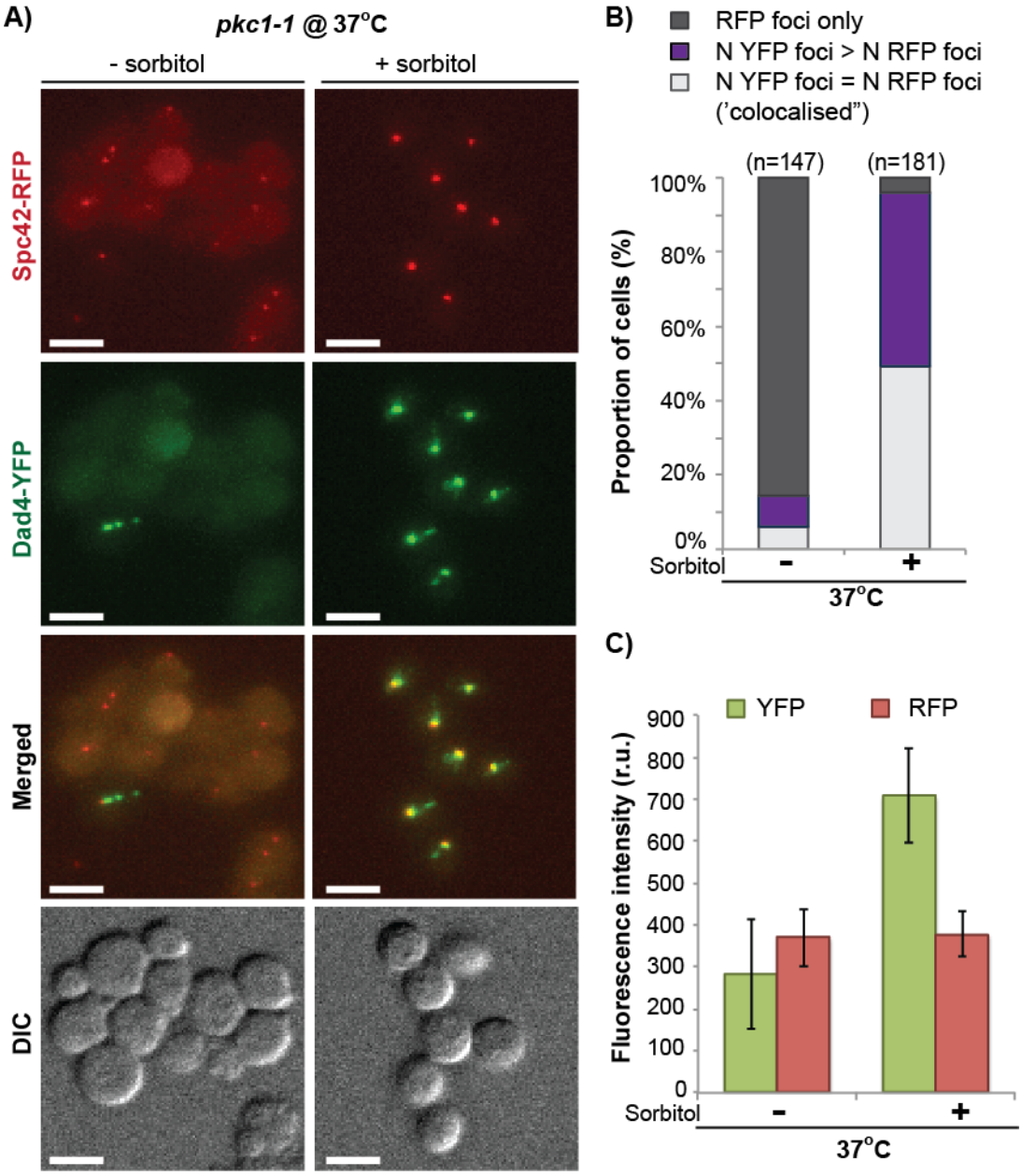

Figure 5.9. Sorbitol rescue of *pkc1-1* Dad4-YFP phenotype. A) Images of cells with Dad4-YFP (green) and Spc42 (SPB protein) tagged with RFP (red) in a *pkc1-1* mutant strain grown at 37˚C with or without addition of 1 M sorbitol. Scale bars are 5 µm. **B**) Manual cell count of proportion of cells with either equal number of visible green and red foci, more YFP foci than RFP foci or only red foci after growth at 37˚C. **C**) YFP and RFP foci intensities (background subtracted) quantified by automated FociQuant for the strain shown in panel (**A**) after growth at 37˚C bars are standard deviation of the mean.

5.2.7.2. The effect of other members of the CWI pathway on Dad4

As described earlier, Pkc1 is a kinase in the CWI pathway (Figure 5.10 A). The downstream members of this pathway (Bck1, Mkk1/2 and Slt2) were not identified in my screens. However, they are non-essential so they were not exposed to high temperature, a factor that could activate or sensitise the CWI pathway. I thus tested whether these non-essential deletions would cause the same phenotype as *pkc1-1* if they were grown at 37˚C. I counted the number of cells with RFP foci and YFP diffused after growing cells at 23˚C and at 37˚C with or without sorbitol for at least 4 hours. Most cells in the *pkc1-1* mutant had lost the YFP focus after 5 hours at 37˚C and this was largely rescued by sorbitol as shown previously. In contrast, less than 2% of *mkk1*Δ cells had this phenotype after 4 hours and none in the *mkk2*Δ mutant after 6 hours. *Bck1*Δ and *slt2*Δ mutants present an intermediate phenotype with 20% after over 5 hours and 45% after 4hours respectively. In both cases there is a partial rescue with sorbitol, as for the *pkc1-1* cells (Figure 5.10 B).

Additionally, 10% of *bck1*Δ cells grown at 37˚C have a medium to large bud and either only one SPB or one large and one very small SPB present at or near the bud neck. An apparently single and very bright focus of YFP can be seen, unlike in typical metaphase and early anaphase cells where two foci can clearly be distinguished close to each other. The number of these cells is reduced to 2% when sorbitol is added to the growth media (Figure 5.10 C-D).

I then looked at the members of the CWI pathway upstream of Pkc1. Pkc1's activator Rho1 is essential. Only one allele is included in the TS collection and it produced no Dad4-YFP phenotype in my screen. Rom1 and Rom2 are redundant, Rom2 being the main GEF in the Pkc1 pathway (Krause et al., 2012). Less than 7% of *rom2*Δ cells had lost the YFP foci at any temperature/condition (Figure 5.10 E). However, foci in these cells were very variable in size and intensity. The distribution of foci (Figure 5.10 F) shows two populations at 23˚C, one with fewer cells at low intensity. At 37˚C the number of low intensity foci increases becoming the largest population, and other foci are more variable and reach higher values. Addition of sorbitol reduces the number of low intensity foci and increases the higher intensity populations. Since this analysis was done with the automated analysis method and this selects all foci in the image even if they are not kinetochores, I repeated the analysis with the manual method only selecting YFP foci that localised to RFP foci. Using this analysis the smaller population of low intensity is not present (Figure 5.10 G). This suggests that at 37˚C *rom2*Δ mutants have an increase on the number of extra foci uncolocalised to the kinetochore. In addition, the

foci localised to the SPBs have a tighter range of intensities at 23˚C, but this dramatically changes at 37˚C where a wider and higher range of intensities appear that are expanded by sorbitol addition (Figure 5.10 G). The different intensities of Dad4-YFP foci in *rom2*Δ cells are clearly visible when comparing average foci at 23˚C (Figure 5.10 H) to two examples from the same image at 37˚C (Figure 5.10 I).

In summary, with perhaps the exception of Slt2 and Bck1 to a lesser extent, most of the members of the CWI pathway don't recapitulate the *pkc1-1* phenotype in which YFP signal becomes diffused. However, other phenotypes are observed in a proportion of cells for members both upstream and downstream of Pkc1.

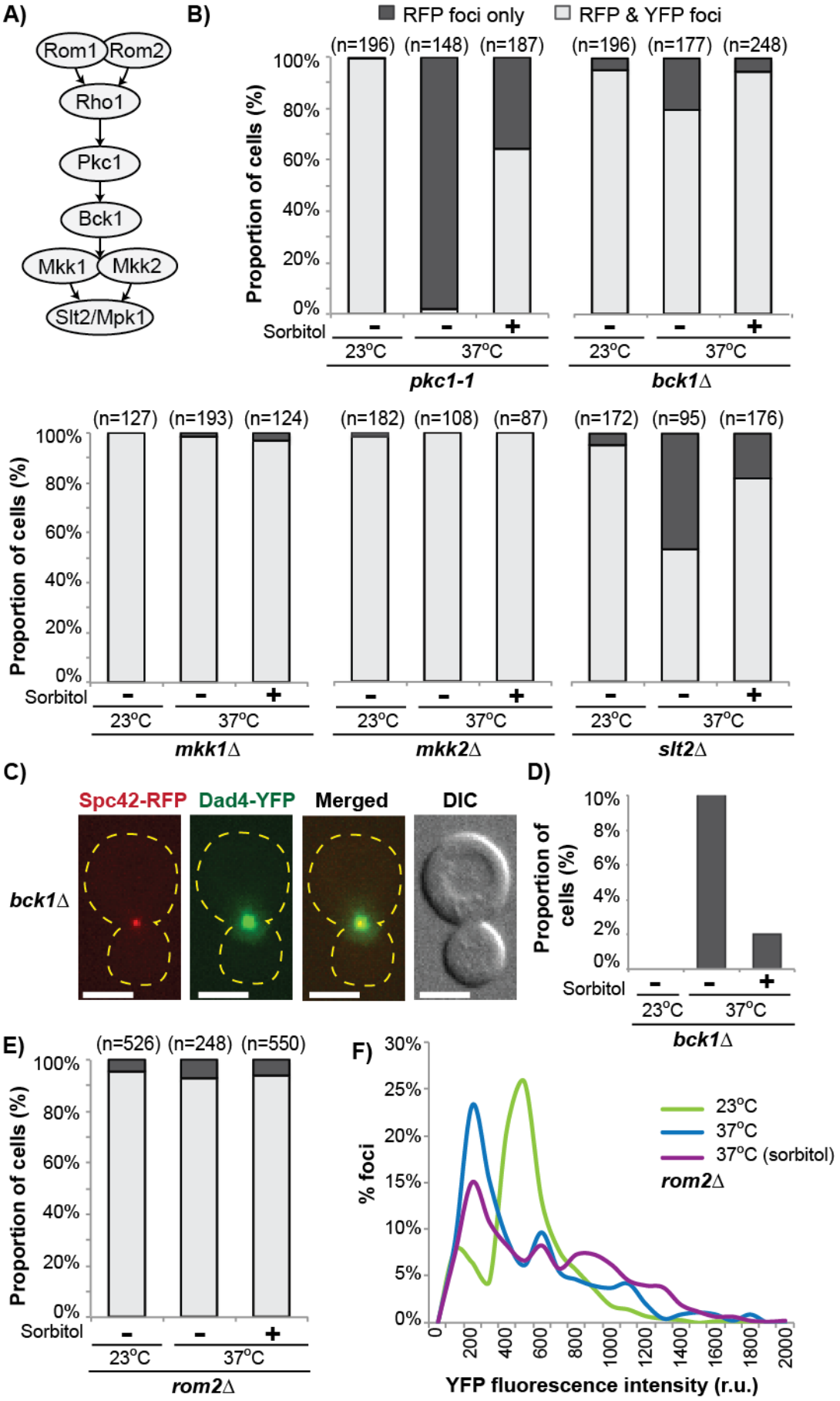
A)
Rom1
Rom2
Rho1
Pkc1
Bck1
Mkk1
Mkk2
Slt2/Mpk1
B)
RFP foci only
RFP & YFP foci
Proportion of cells (%)
Sorbitol
23°C
37°C
pkc1-1
bck1Δ
mkk1Δ
mkk2Δ
slt2Δ
C)
Spc42-RFP
Dad4-YFP
Merged
DIC
bck1Δ
D)
Proportion of cells (%)
E)
rom2Δ
F)
% foci
YFP fluorescence intensity (r.u.)
23°C
37°C
37°C (sorbitol)
rom2Δ

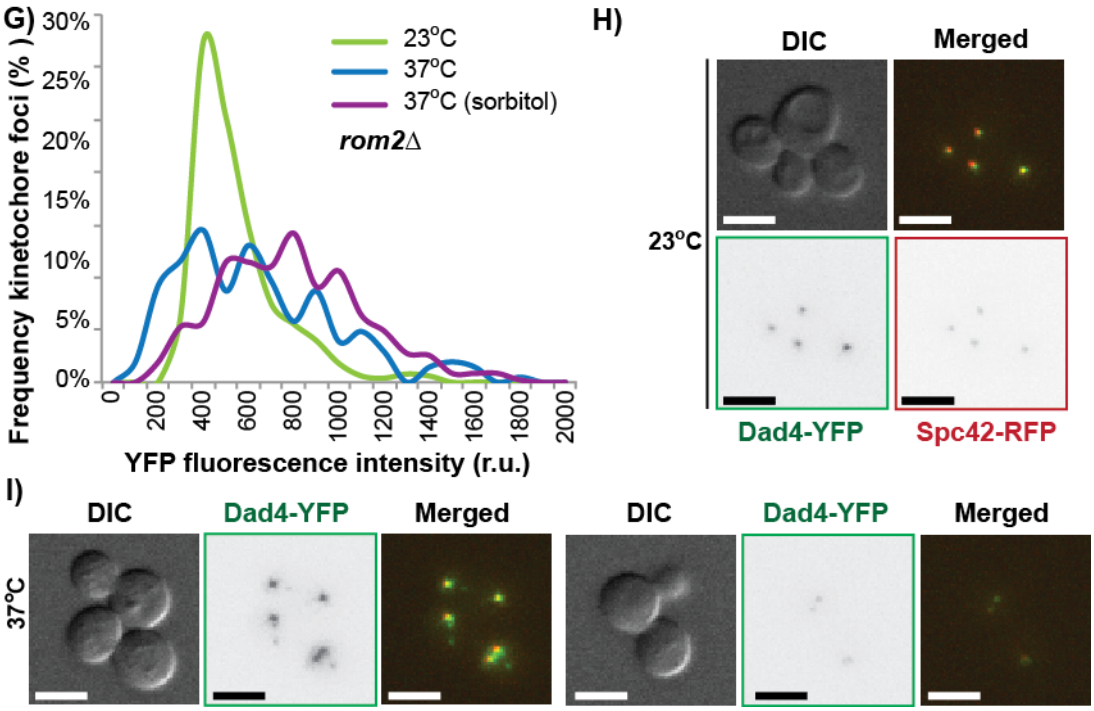

Figure 5.10 Disrupting the CWI pathway cause a Dad4-YFP phenotype. **A**) Illustrative representation of the core of the CWI signalling pathway. **B** and **E**) Manual cell count of proportion of cells with either visible green and red foci or only red foci on cells with the indicated gene deletions. **C**) An example of a budded *bck1*Δ cell . Green foci represent Dad4-YFP and red foci Spc42-RFP. The proportion of cells having the phenotype is quantified in (**D**). **F-G**) Foci distribution curves of *rom2*Δ foci intensities quantified by the automated (**F**) and the manual (**G**) FociQuant. (**H-I**) *rom2*Δ cells with Dad4 tagged with YFP (green) and Spc42 tagged with RFP (red). Scale bars in all images are 5 µm.

5.2.8. Is the phenotype of *pkc1-1* connected to the stress response pathway?

In fission yeast the major stress pathway is controlled by the Sty1/Wis1 pathway (SRP), this is orthologous to the HOG1 pathway in budding yeast. A second pathway is involved in response to osmotic stress, the Pmk1 pathway (CIP) equivalent to the cell integrity pathway in *cerevisae*. Robertson and Hagan, 2008, showed that osmotic stress lead to depolymerisation of F-actin patches as well as to transient arrest of the dynamic behaviour of microtubules, which was independent of the SRP pathway, although the arrest duration was determined by this pathway.

5.2.8.1. Many actin and microtubule mutants produce a quantitative or qualitative phenotype in the screens with Dad4

A number of mutants related to actin and microtubules were identified in the screen for increasing, decreasing or altering the localisation of Dad4 (Table L appendix 1), and multiple genetic and physical interactions between these two groups of mutants, and between those with some kinetochore members and the CWI pathway have been reported. The greatest number of interactions is between kinetochore members and microtubule related genes or between actin related genes and the CWI pathway. However there are some interactions between the kinetochore and actin related-genes, as well as the kinetochore and the CWI pathway (Figure 5.11 A).

Specifically, Pkc1 has physical and genetic interactions with members of the kinetochore (inner, central and outer complexes), the SAC, and microtubule associated and motor proteins (Figure 5.11 B).

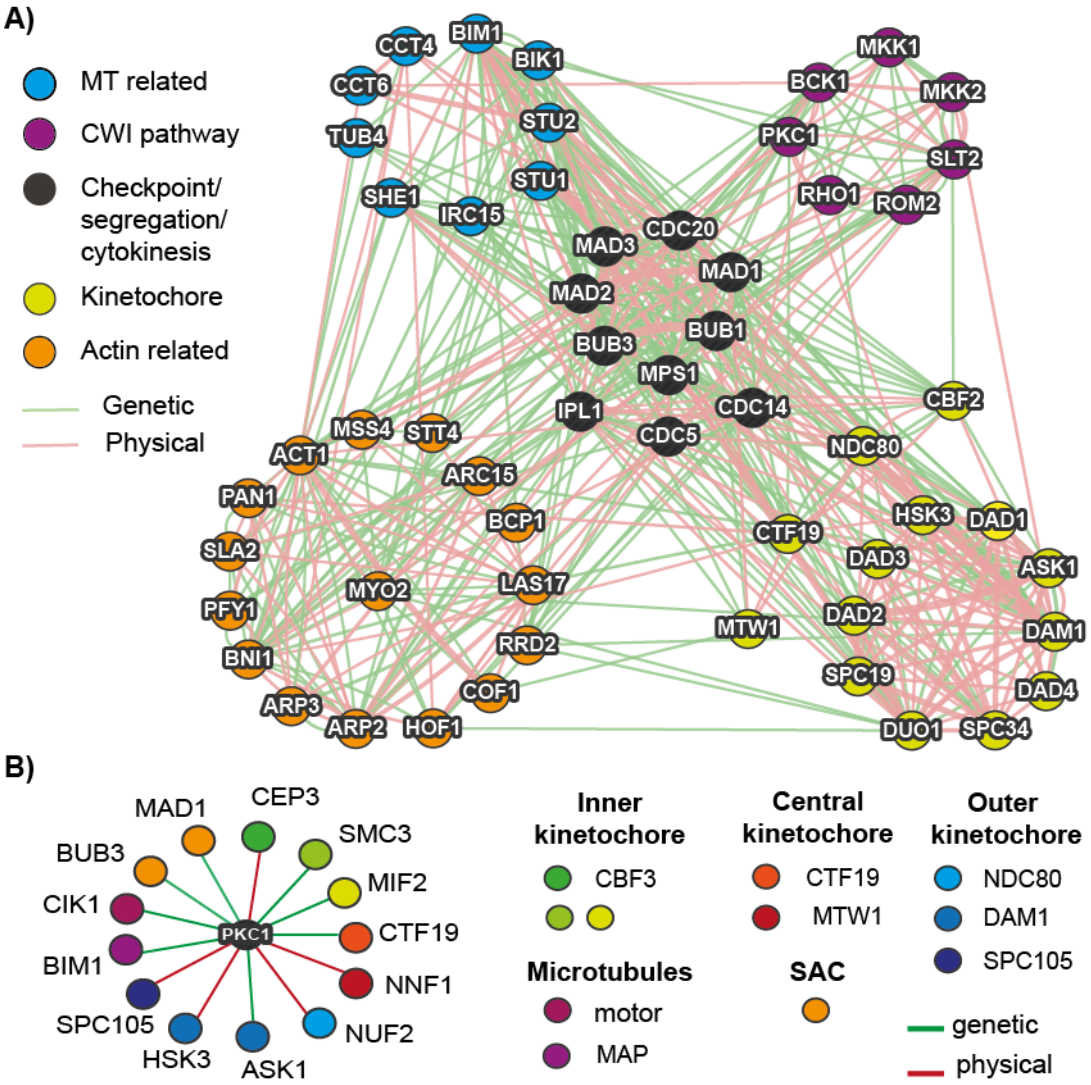

Figure 5.11. Genetic and physical interactions linking actin and microtubule related mutants with the kinetochore and CWI pathway. A) Genetic (green) and physical (red) interactions between mutants identified in the screen to cause a phenotype in Dad4-YFP, which are actin-related (orange) or microtubule-related (blue) with members of the CWI pathway (purple) and the DAM1 complex (yellow circle). Other members of the kinetochore (yellow outside the circle) have been added to represent inner, central and outer in addition to the DAM1 complex. Also some genes from the SAC and involved in chromosome segregation and cytokinesis have been added in black. **B**) Kinetochore, SAC and spindle members know to have physical (red) or genetic interactions (green) with Pkc1. The legend indicates the complex each gene belongs to when applicable.

5.2.8.2. Actin and acting-related genes cause a phenotype in Dad4

Several actin alleles are present in the TS collection and not all gave the same Dad4-YFP phenotype. However, *act-111* has a similar phenotype to that observed for *pkc1-1*, with large proportion of cells having lost the YFP signal while retaining the RFP foci (Figure 5.12). *ARP3* mutants, *arp3-D11A* and *arp3-G306G,* also have a large number of cells with the same phenotype. In the DIC images these cells look even sicker than *pkc1-1* or *act1-111* cells. Within the remaining cells that still retain the YFP foci, *arp3-D11A* contains much brighter and enlarged foci (Figure 5.12). The *arp3-D11A* mutation confers a lower nucleotide binding affinity and these mutants have a growth defect at high temperature or high osmolality with actin patches being depolarised (Martin et al., 2005). This would suggest that disruption of actin patches can produce a similar phenotype than that of *pkc1-1*. In contrast, mutants of *LAS17*, an actin assembly factor*,* produced a phenotype with low intensity Dad4-YFP foci (Figure 5.12).

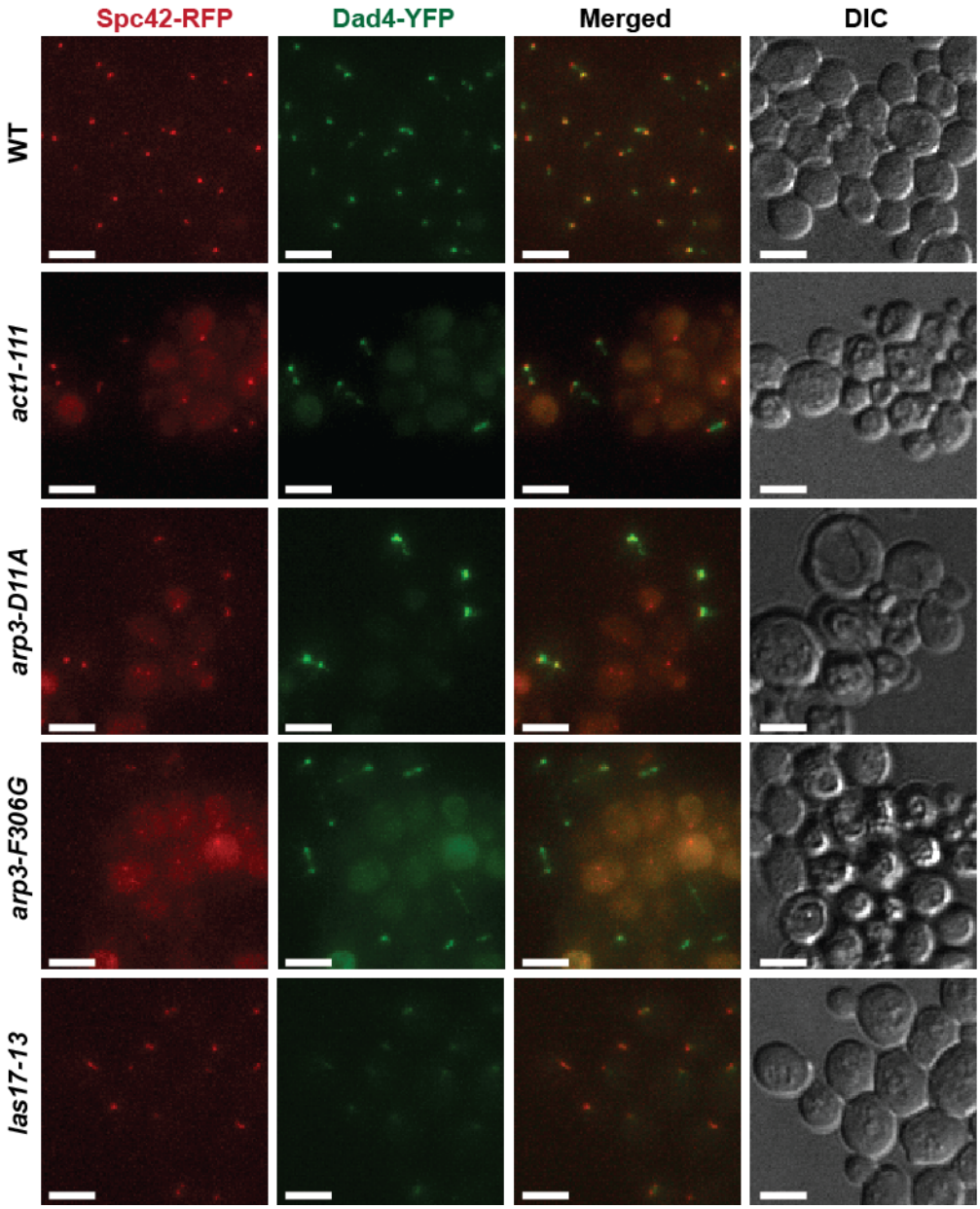

Figure 5.12. Actin and actin-related mutants produce a phenotype on Dad4. Cells with Dad4 tagged with YFP (green) and Spc42 tagged with RFP (red) in various actin-related mutants. Images are from the Dad4 screen in which strains were imaged in pads after growth at 37˚C for ~5 hours. Scale bars are 5 μm.

5.2.8.3. Microtubules are defective in the *pkc1-1* mutant

To investigate if there is a microtubule defect in the *pkc1-1* cells, I tagged Tub1 with CFP (*ura3-1::TUB1-CFP::URA3*) in wild type and *pkc1-1* cells, also doubly tagged with Dad4-YFP and Spc42-CFP.

Tubulin linked fluorophores localise as a single focus in G1 cells but as either short or long lines in metaphase and anaphase cells respectively, although not all cells have this defined Tub1 staining (Figure 5.13 A, and previous results from high-throughput studies). In *pkc1-1* cells grown at 23˚C the tubulin signal is similar to the wild type although the background seems slightly higher and thus harder to see the foci/lines in most cells, while others have a very strong foci (top right or middle left in panel b), and for example, a cell has disrupted tubulin (bottom right in panel b). When switched to 37˚C some cells have very strong tubulin signal thought-out the entire cell. Most of these cells have lost the Dad4-YFP foci but retained the RFP foci (panel d) except a large budded cell, which has aberrant Dad4-YFP foci with some extra foci (top right in panel d, arrow). There are also some aberrant CFP foci, for example, in panel (f), one cell has lost the YFP foci while retaining a RFP focus and the CFP signal is punctate, with a few small foci and high background. The bigger cell in panel (e) cell has one SPB (RFP) in the mother and one in the bud and multiple kinetochore (YFP) foci in the mother with none in the bud, as well as multiple tubulin (CFP) foci, none of which co-localize.

These data suggest that there is disruption of tubulin in the *pkc1-1* mutant and that this disruption may be linked to changes in Dad4-YFP fluorescence.

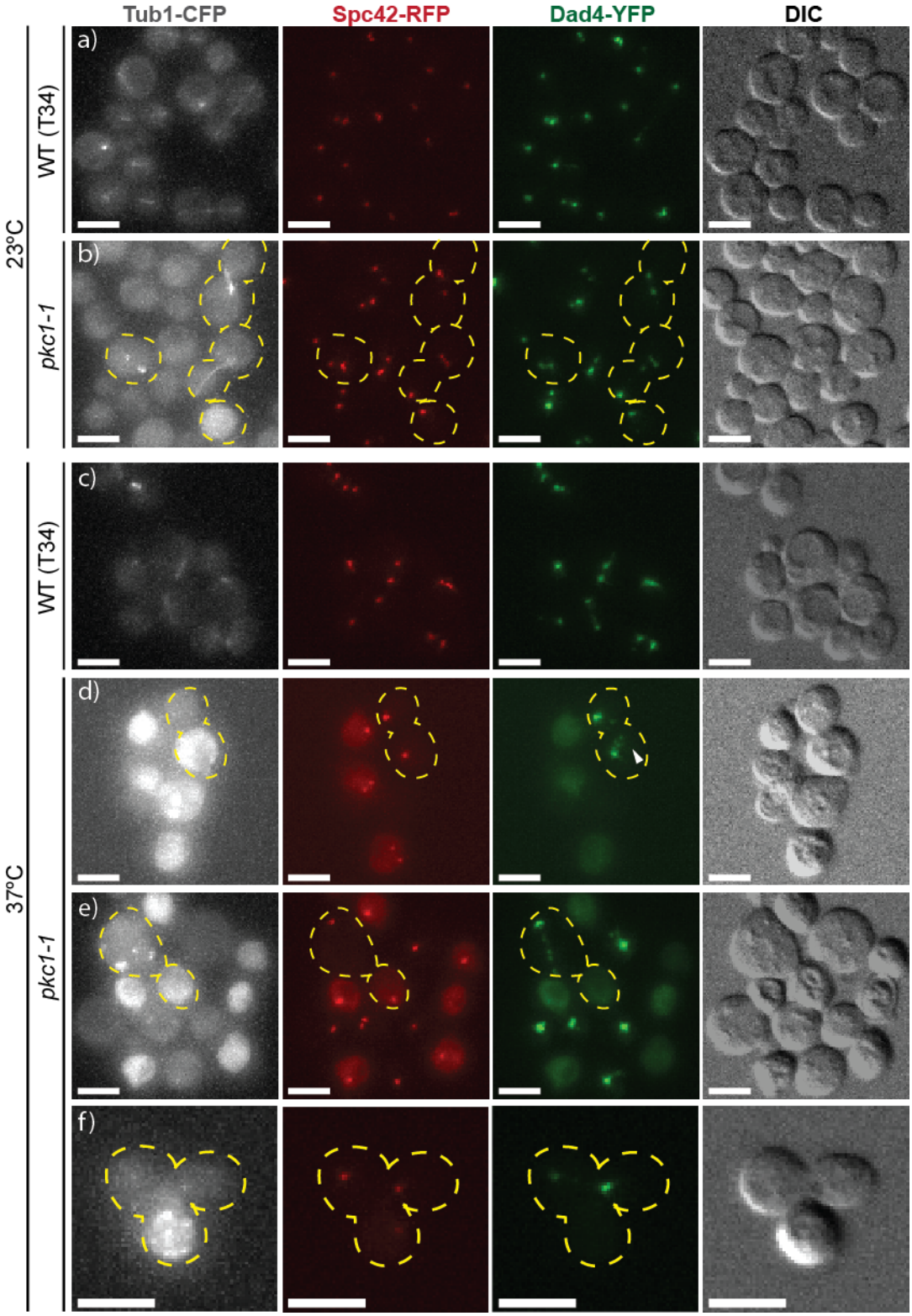

Figure 5.13. Tubulin may be defective in *pkc1-1* mutants. Wild type (**A, C**) and *pkc1-1* (**B, E, F**) cells showing foci for Dad4-YFP (green), Spc42-RFP (red) and Tub1-CFP (white) after growth 23˚C and 37˚C. Scale bars are 5 µm.

5.2.8.4. Recapitulating the *pkc1-1* phenotype with microtubule drugs

One hypothesis to explain the Dad4 phenotype in the *pkc1-1* mutant is that microtubules are disrupted and this leads to the kinetochore phenotype. I wanted to see if I could recreate the *pkc1-1* Dad4-YFP phenotype in a wild type strain by disrupting microtubules using drugs.

Nocodazole is commonly used to arrest cells and de-cluster kinetochores, it inhibits tubulin polymerisation (Bray, 2001). Nocodazole was gradually added to wild-type yeast cells for ~4 hours from 20 µg/ml to ~50 µg/ml until a phenotype similar to that produced by *pkc1-1* mutants in Dad4 was observed (Figure 5.14 A). Mitotic death induced by nocodazole has been shown to have apoptotic features (Endo et al., 2010).

On the other hand, thiabendazole (TBZ) works by destabilising existing microtubules (Bray, 2001). After addition of 50 ug/ml TBZ for 10 minutes resulted in 30% of the cells with diffuse Dad4-YFP with RFP foci, and this increased to 70% on 100 ug/ml of TBZ. Addition of 1 M sorbitol only reduced the percentage of these cells slightly at the lower TBZ concentration but rescued 75% of the affected cells at the higher TBZ concentration.

These data supports my hypothesis that disrupting the microtubules leads to the same Dad4-YFP phenotype observed in the *PKC1* mutant.

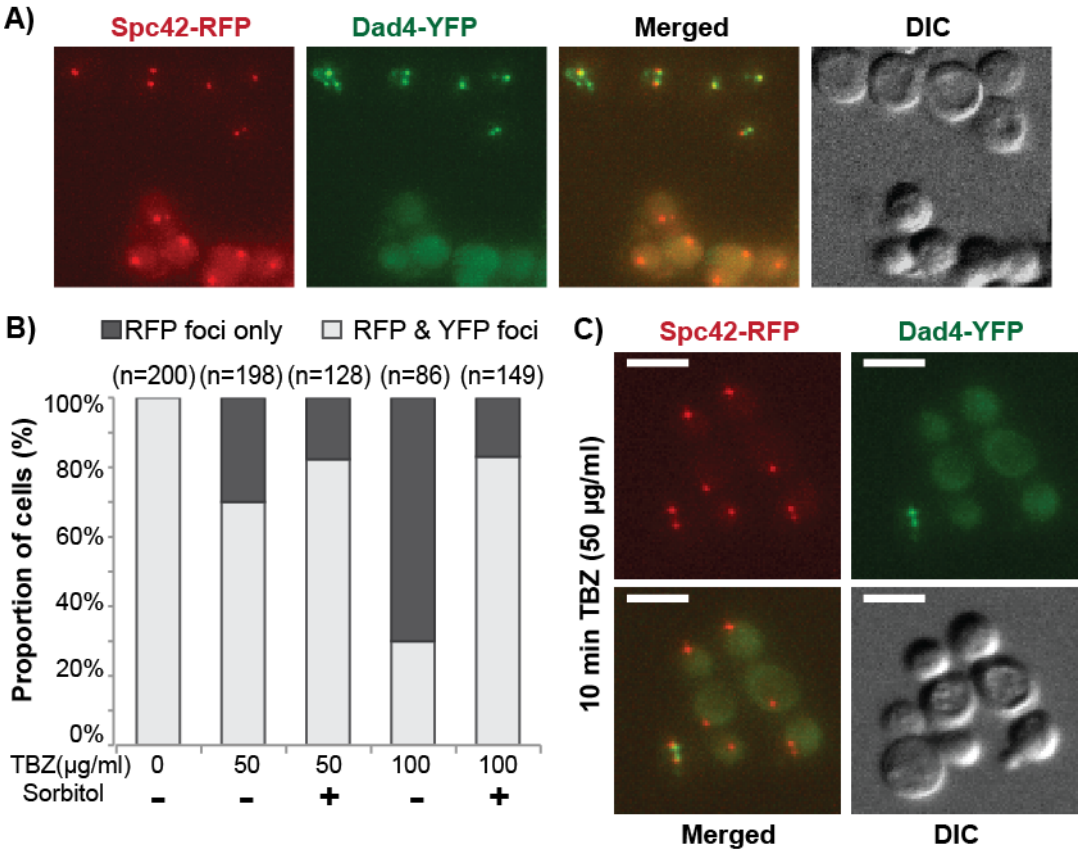

Figure 5.14. Effect of microtubule poisons on Dad4. A) Manual cell count of proportion of cells with either visible green and red foci or only red foci on cells incubated for 10 minutes at room temperature with or without the indicated concentrations of TBZ and 1 M sorbitol. **B-C**) Cells with Dad4 tagged with YFP (green) and Spc42 tagged with RFP (red) incubated on media containing TBZ for 10 minutes (B) or nocodazole for 4 hours (C). Scale bars are 5 µm.

5.2.8.5. The Hog1 pathway is activated on *pkc1-1* mutants

As mentioned before (Section 5.2.8), in fission yeast, two pathways are involved in osmotic stress and related to microtubule and actin destabilisation, and those are orthologous of the CWI and HOG1 pathways, I wanted to investigate the possibility of the HOG1 pathway being active in *pkc1-1* cells. I performed a Western Blot with p38-MAPK antibody on cells grown at 23˚C and 37˚C with and without the MAPK inhibitor SP600125. The p38 MAP Kinase (MAPK) is the homolog of the yeast Hog1 kinase. The p38-MAPK antibody recognises the phosphorylated form of the downstream MAP kinase Hog1 and consequently indicates whether or not the HOG1 pathway is active. The inhibitor SP600125 has been shown to work in fission yeast to inhibit Sty1

(equivalent to Hog1 pathway) but not Pmk1 (equivalent to CWI pathway) (Hartmuth and Petersen, 2009).

The Hog1 phosphorylation is present in *pkc1-1* cells both at 23˚C and at 37˚C (Figure 5.15). The addition of the inhibitor SP600125 reduces the phosphorylated Hog1 signal at both temperatures although it doesn't completely eliminate it. It should be noted however, that this inhibitor may not be specific to Hog1 activation in budding yeast, for example it has been shown to affect SAC function (Schmidt et al.,2005). These data suggests that the Hog1 pathway is activated in the *pkc1-1* mutant.

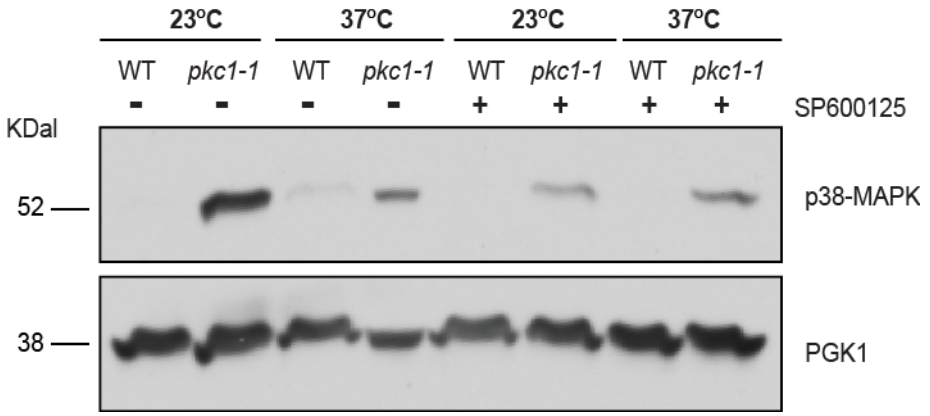

Figure 5.15. **Hog1 is active in the *pkc1-1* mutant.** Western Blot analysis of *pkc1-1* mutant. The antibody p38 was used to detect activated Hog1 MAPK. PGK1 was used as control for protein amounts. MAPK inhibitor SP600125 was used at a concentration of 100 μM.

5.3. Summary and discussion results 3

PKC1 alleles produced a decrease in fluorescence of kinetochore proteins that corresponds to an increase in the number of cells with diffuse Dad4-YFP. Although the RFP signal decreased slightly and more RFP background was seen, foci were still visible and were visually comparable to wild-type SPBs. In addition, extra Dad4-YFP foci were also seen in the *pkc1* mutant strain when cells were grown for a shorter time at 37˚C, suggesting kinetochore declustering or unattachment. However, since the nucleus is not tagged in these strains, is not possible to be sure that the extra foci are all nuclear. Nevertheless, the data indicates that the effect of *PKC1* mutants on Dad4 is not specific to the DAM1 complex and ultimately affects the entire kinetochore.

The phenotype was rescued by complementation of the mutant allele with a wild-type copy of *PKC1* at a different locus. However, foci in this strain looked enlarged and aberrant and YFP intensity increased at 37˚C compared to 23˚C. This strain contains both a wild-type copy of *PKC1* at the *URA3* locus and the mutant copy at the endogenous locus. The data shows that having some wild-type Pkc1 is enough to rescue the diffuse Dad4-YFP signal phenotype, suggesting that retaining the Dad4 foci requires normal function of Pkc1. However, either the extra Pkc1 protein present or the defective protein is enough to cause a different phenotype at the kinetochore. When I overexpressed *PKC1* in a wild-type strain, I did not see a significant increase in fluorescence or any obvious aberrant foci. This could be because the GAL system needs more time to induce the overexpression of *PKC1*. However, the GAL system is functional since a spot test showed a growth defect of the overexpressing *PKC1* at all temperatures and more at 37˚C (Figure B appendix 2). Nonetheless, because this strain did not have a tag that could be detected by Western Blot, the timing of Pkc1 accumulation is unclear and I can't be sure that at the time of microscopy Pkc1 levels were significantly elevated. Another possibility is that it is not the overexpression alone but the combination of wild-type and mutant copies in the cell that causes these larger foci. Cells are unsynchronised and it is possible that the *pkc1-1* mutant is affecting more than one function of Pkc1. The presence of the wild-type copy could be enough for the cell to perform one of those functions while the aberrant protein could be competing and interfering with a different function or timing of the cell cycle. This notion is supported by the fact that at 23˚C, when the mutant Pkc1 should behave wild type-like it actually has a defect.

The fact that the Pkc1 phenotype was rescued by sorbitol suggests that this is a cell wall defect-related phenotype. However other members of the CWI pathway didn't share the

same phenotype or at least not to the same extent. In addition, growth in sorbitol seems to cause the opposite phenotype with enlarged and brighter foci. It has been suggested that sorbitol stabilises microtubules since it supresses benomyl sensitivity of kinesin motors mutants (Korolyev, Steinberg-Neifach and Eshel, 2005) and its been shown to correct midzone defects and spindle rigidity in double mutants of the motors dynein and Cin8 (Gerson-Gurwiz et al., 2009).

In the *pkc1-1* mutant microtubules were defective (Figure 5.13). To test the possibility that sorbitol is stabilising microtubules, the strain with Tub1-CFP in the *pkc1-1* mutant background should be grown in sorbitol to see if tubulin is wild-type-like in cells that retain the Dad4-YFP foci after sorbitol addition. However, tubulin was not visible in all cells even in a wild-type strain, which makes difficult the visual analysis. A better way to visualise tubulin may be by immunofluorescence. An alternative method would be to test if the diffused Dad4-YFP phenotype in *pkc1-1* that is rescued by sorbitol is also rescued by taxol (a microtubule stabiliser). Nevertheless, my data supports the idea that sorbitol is stabilising microtubules as the *pkc1-1* phenotype with diffused or low levels of Dad4-YFP was recapitulated by addition of high concentration of TBZ and this was largely rescued by sorbitol (Figure 5.14 B).

This opens the possibility of Pkc1 having a function related to microtubule stability. This has already been suggested. Overexpression of the microtubule associated protein Bim1 (EB1) was shown to rescue the phenotypes of a *PKC1* mutant allele, which included TBZ sensitivity, G2 delay and defective nuclear position. However, it did not rescue the cell wall lysis in this mutant and Pkc1 overexpression did not rescue the sensitivity of *BIM1* mutants to TBZ (Hosotani et al., 2001). The authors suggested that Bim1 works downstream of Pkc1 in a novel pathway. Following this and my data, the next step would be to test whether Bim1 overexpression could rescue my observed *pkc1-1* phenotype.

There are only two reports of Pkc1 localisation in the nucleus and only one showed localisation to the spindle (Denis and Cyert, 2005). One possibility for this could be that only a small amount of Pkc1 is ever associated with the spindle or alternatively that spindle localization of Pkc1 is only transient at a specific time in the cell cycle. In either case this possibility may make the detection of Pkc1 at the spindle and identification of substrates problematic. Mascaraque et al, (2013) performed SILAC to identify new Pkc1 substrates. No kinetochore or mitotic spindle proteins were identified, although 4 actin related proteins were within the possible substrates. One of them, Abp1, is important for activation or the Arp2/3 complex. Since *ARP3* TS mutants produced a very similar

phenotype on my screen to that seen in *pkc1-1* (Figure 5.12), it is tempting to speculate that the *pkc1-1* phenotype may be linked to the Arp2/3 complex function, or more generally to actin, as *act1-111* mutant had also a similar phenotype (Figure 5.12). Two other possible substrates of Pkc1 (Lsb3, Bbc1) bind Las17, which decreased Dad4-YFP signal at the kinetochore (Figure 5.12).

SILAC may not be sensitive enough to detect Pkc1 kinetochore/spindle substrates if Pkc1 interaction with spindle members is transient and only a small pool of Pkc1 is present. The Pkc1 sequence has NLS and NES signals. Denis and Cyert, (2005) were able to retain Pkc1 in the nucleus by disrupting the NES and using the mutant *Xpo1-1.* Perhaps taking advantage of this mutant, cells with high levels of nuclear Pkc1 could be isolated and analysed by SILAC for substrates.

5.3.1. Proposed model

In the proposed model (Figure 5.16), *pkc1-1* would act as an osmotic stressor that would destabilise actin, perhaps by hyperactivating the Hog1 pathway. This would result in microtubule destabilisation, which would be transferred to the kinetochore by possibly destabilising the outer kinetochore-microtubule attachment. However, it is also possible that *pkc1-1* can have a more direct function on the microtubules.

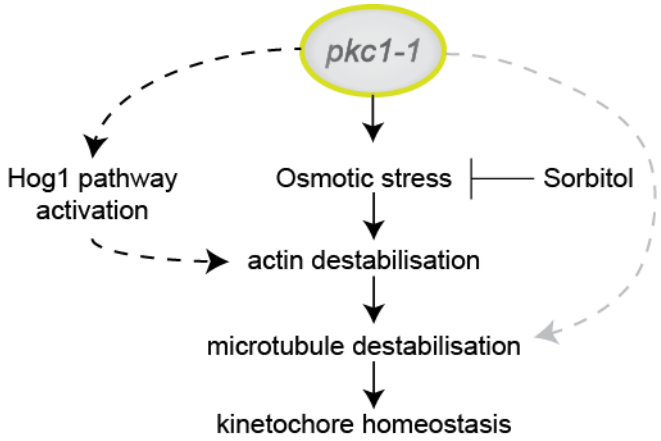

Figure 5.16. Proposed Model for the mechanism behind the *pkc1-1* phenotype on Dad4.

6. Chapter VI: General conclusions and future directions

In this work I have shown the results of a genome-wide fluorescent microscopy screen with the outer kinetochore Dad4 (from the DAM1 complex) tagged with YFP and the SPB protein Spc42 tagged with RFP. The hypothesis was that genes affecting kinetochore function would produce phenotypic changes detectable by fluorescence microscopy. This screen has identified mutants corresponding to ~6% of the yeast ORFs that increase, decrease and alter the localisation of Dad4.

First, I created an array of plasmids with the SPB protein Spc42 tagged with RFP and different kinetochore proteins tagged with YFP (together with a sandwich student Erika Aquino). This array can be used for future work as it allows, for example, a deletion mutant of interest to be rapidly combined with this array to examine its effect across the kinetochore. Since these plasmids have a *CUP1* promoter, the tagged proteins can also be overexpressed. However, as I showed in Chapter III, the use of plasmids has disadvantages for quantitative analysis. A plasmid-base fluorescent screen had set precedent for this work in qualitative analysis (Alvaro, Lisby and Rothstein, 2007), however, recent quantitative fluorescent screens have been performed using endogenous tagging (Koh et al., 2015; Chong et al., 2015).

Next, I compared quantitation methods available and we developed a freely available ImageJ script that can be used to quantify foci in high throughput studies (Ledesma-Fernández and Thorpe, 2015). Although the fully-automated version of the script used here has some limitations, the method is flexible and future adaptations will likely eliminate some of these problems.

The genome-wide screen that I performed generated images that in this work were analysed quantitatively and qualitatively looking for changes in YFP intensity and aberrant foci. Nevertheless, these images could be reanalysed in the future to identify, for example, mutants that affect spindle orientation, SPB separation and duplication, or even cell size. The collection of images has been sent to Sue Jaspersen's lab for analysis of SPB phenotypes, and in addition, images are going to be available in the near future in the Image Data Repository. It would be interesting to compare my results with other kinetochore fluorescent screens (Brenda Andrews personal communication), as well as with different studies, such as a cell cycle profile of the deletion collection or data about fitness/slow growth mutants.

It needs to be noted that some phenotypes observed in the screen were not reproduced when deleting the gene in a different background (not shown), and in addition, some mutants were found to have both the deletion and the wild-type copy of the gene. It was recently shown that yeast compensates for the knockout of most genes by reproducibly acquiring a secondary mutation in another gene (Teng et al., 2013). Furthermore, the compact nature of the budding yeast genome means that in some deletions also remove part of an overlapping gene. Thus, these caveats need to be taken into account when working with the deletion collection.

An interesting observation was that, for the mutants analysed, the decrease in Dad4-YFP intensity had a tight population of cells with genuine weaker foci than the wild-type whereas mutants that increase Dad4-YFP intensity were heterogeneous with several populations, some wild-type like. High intensity mutants were enriched for mitochondria, translation, RNA and metabolic processes while low intensity mutants were enriched for cell cycle and mitotic processes. This was supported by the fact that most of the benomyl sensitive mutants were low intensity mutants. In addition, the fact that the wild-type population was not as tight as the low mutants population suggests differences in fluorescence at different stages of the cell cycle, as cultures were unsynchronised.

Mutants identified in this screen include some that have well characterised roles in kinetochore homeostasis and consequently serve as proof of principle. However, other mutants had no known role in kinetochore or mitotic spindle homeostasis. A two-hybrid screen by Wong et al (2007) identified novel interactions between the kinetochore, and specifically members of the DAM1 complex (including Dad4), and chromatin remodelers as well as members of the mediator complex, both identified in my screen. Some possible regulators of RNA levels such as the NMD pathway and the spliceosome, were identified in my Dad4-YFP screen. Recently, a novel mechanism, the spliceosome-mediated decay (SMD), has been described in budding yeast, as a regulator of mRNA expression levels in the nucleus for non-intronic genes by coupling splicing and RNA decay (Volanakis et al., 2013). In addition, the SCF^{Cdc4} and SCF^{Dia2} ubiquitin ligase complexes also affected Dad4 levels. However, the effect of all these mutants could be indirect, affecting other transcripts in the cell that then impact upon kinetochore levels. Finally, the link between chromatin and replication and a defect in the outer kinetochore has also been suggested in my screen.

The effect of some mutants upon Dad4 (outer kinetochore) was not seen on the central kinetochore protein Mtw1, for instance, for the MAPs Bim1 and Bik1 suggesting a possible role of these proteins specifically in the outer kinetochore complex DAM1 or an indirect effect due to changes in microtubule dynamics. However, other phenotypes

were observed across the entire kinetochore. One example is the budding yeast PKC (Pkc1). PKC has been shown to have roles in mitosis in other organisms but it has not been described in yeast besides the suggestion of a novel pathway involving the MAP Bim1 (Hosotani et al., 2001). My work suggests a common mechanism between the *pkc1-1* mutant phenotype and the effect of disrupted microtubule function, for instance by inhibition of dynamic instability with microtubule poisons. A caveat to this work with the *PKC1* temperature sensitive mutant is that high temperature can activate the Pkc1 pathway (Cell Wall Integrity Pathway (CWI)). I have now used an auxin-inducible degradation system to deplete Pkc1 gradually at low temperature and preliminary work indicates that the phenotype in which Dad4 is lost from the kinetochore is reproducible with this method. I plan to investigate whether the effect of Pkc1 in the microtubules is direct, for instance by acting on Bim1, or indirect. An actin TS mutant showed a similar phenotype and several actin-related mutants also produced phenotypes on Dad4 suggesting a link between the kinetochore and the state of the cytoskeleton via Pkc1.

In summary the work presented here provides a set of candidate genes that regulate kinetochore homeostasis and the image dataset may be mined in the future to provide further information on other genes that regulate spindle function.

References

Abeyweera, T., Chen, X. and Rotenberg, S. (2009). Phosphorylation of α6-Tubulin by Protein Kinase Cα Activates Motility of Human Breast Cells. *Journal of Biological Chemistry*, 284(26), pp.17648-17656.

Adams, A. Gottschling D. and Kaiser, C. 1997. *Methods in Yeast Genetics: a Cold Spring Harbor Manual*, N. Y., Cold Spring Harbor Laboratory Press.

Adams, R. and Kilmartin, J. (1999). Localization of core Spindle Pole Body (SPB) components during SPB duplication in *Saccharomyces cerevisiae. The Journal of Cell Biology*, 145(4), pp.809-823.

Akiyoshi, B., Nelson, C., Ranish, J. and Biggins, S. (2009). Quantitative proteomic analysis of purified yeast kinetochores identifies a PP1 regulatory subunit. *Genes & Development*, 23(24), pp.2887-2899.

Akiyoshi, B. and Biggins, S. (2010). Cdc14-Dependent Dephosphorylation of a Kinetochore Protein Prior to Anaphase *in Saccharomyces cerevisiae*. *Genetics*, 186(4), pp.1487-1491.

Akiyoshi, B., Sarangapani, K., Powers, A., Nelson, C., Reichow, S., Arellano-Santoyo, H., Gonen, T., Ranish, J., Asbury, C. and Biggins, S. (2010). Tension directly stabilizes reconstituted kinetochore-microtubule attachments. *Nature*, 468, pp.576-581.

Akiyoshi, B., Nelson, C., Duggan, N., Ceto, S., Ranish, J. and Biggins, S. (2013). The Mub1/Ubr2 Ubiquitin Ligase Complex Regulates the Conserved Dsn1 Kinetochore Protein. *PLoS Genetics*, 9(2), p.e1003216.

Altenfeld, A., Wohlgemuth, S., Wehenkel, A., Vetter, I. and Musacchio, A. (2015). Complex assembly, crystallization and preliminary X-ray crystallographic analysis of the human Rod-Zwilch-ZW10 (RZZ) complex. *Acta Cryst Sect F*, 71(4), pp.438-442.

Alvaro, D., Lisby, M. and Rothstein, R. (2007). Genome-wide analysis of Rad52 foci reveals diverse mechanisms impacting recombination. *PLoS Genetics*, 3(12), p.e228.

Andress, E., Holic, R., Edelmann, M., Kessler, B. and Yu, V. (2011). Dia2 Controls Transcription by Mediating Assembly of the RSC Complex. *PLoS ONE*, 6(6), p.e21172.

Andrews, P. and Stark, M. (2000). Dynamic, Rho1p-dependent localization of Pkc1p to sites of polarized growth. *Journal of Cell Science*, 113, pp.2685-2693.

Aravamudhan, P., Goldfarb, A. and Joglekar, A. (2015). The kinetochore encodes a mechanical switch to disrupt spindle assembly checkpoint signalling. *Nature Cell Biology*, 17(7), pp.868-879.

Armond, J., Vladimirou, E., Erent, M., McAinsh, A. and Burroughs, N. (2015). Probing microtubule polymerisation state at single kinetochores during metaphase chromosome motion. *Journal of Cell Science*, 128(10), pp.1991-2001.

Asbury, C., Gestaut, D., Powers, A., Franck, A. and Davis, T. (2006). The Dam1 kinetochore complex harnesses microtubule dynamics to produce force and movement. *Proceedings of the National Academy of Sciences*, 103(26), pp.9873-9878.

Asbury, C., Tien, J. and Davis, T. (2011). Kinetochores' gripping feat: conformational wave or biased diffusion?. *Trends in Cell Biology*, 21(1), pp.38-46.

Baryshnikova, A., Costanzo, M., Kim, Y., Ding, H., Koh, J., Toufighi, K., Youn, J., Ou, J., San Luis, B., Bandyopadhyay, S., Hibbs, M., Hess, D., Gingras, A., Bader, G., Troyanskaya, O., Brown, G., Andrews, B., Boone, C. and Myers, C. (2010). Quantitative analysis of fitness and genetic interactions in yeast on a genome scale. *Nature Methods*, 7(12), pp.1017-1024.

Baum, P., Furlong, C. and Byers, B. (1986). Yeast gene required for spindle pole body duplication: homology of its product with Ca2+-binding proteins. *Proceedings of the National Academy of Sciences*, 83(15), pp.5512-5516.

Ben-Aroya, S., Coombes, C., Kwok, T., O'Donnell, K., Boeke, J. and Hieter, P. (2008). Toward a Comprehensive Temperature-Sensitive Mutant Repository of the Essential Genes of Saccharomyces cerevisiae. *Molecular Cell*, 30(2), pp.248-258.

Bloom, J. and Cross, F. (2007). Multiple levels of cyclin specificity in cell-cycle control. *Nature Reviews Molecular Cell Biology*, 8(2), pp.149-160.

Bock, L., Pagliuca, C., Kobayashi, N., Grove, R., Oku, Y., Shrestha, K., Alfieri, C., Golfieri, C., Oldani, A., Maschio, M., Bermejo, R., Hazbun, T., Tanaka, T. and De Wulf, P. (2012). Cnn1 inhibits the interactions between the KMN complexes of the yeast kinetochore. *Nature Cell Biology*, 14(6), pp.614-624.

Boeckmann, L., Takahashi, Y., Au, W., Mishra, P., Choy, J., Dawson, A., Szeto, M., Waybright, T., Heger, C., McAndrew, C., Goldsmith, P., Veenstra, T., Baker, R. and Basrai, M. (2013). Phosphorylation of centromeric histone H3 variant regulates chromosome segregation in *Saccharomyces cerevisiae. Molecular Biology of the Cell*, 24(12), pp.2034-2044.

Bouck, D. and Bloom, K. (2005). The kinetochore protein Ndc10p is required for spindle stability and cytokinesis in yeast. *Proceedings of the National Academy of Sciences*, 102(15), pp.5408-5413.

Bray, D. (2001). *Cell movements*. New York: Garland Pub.

Brownlow, N., Pike, T., Zicha, D., Collinson, L. and Parker, P. (2014). Mitotic catenation is monitored and resolved by a PKCÎµ-regulated pathway. *Nature Communications*, 5, pp.5685.

Butt, T., Sternberg, E., Gorman, J., Clark, P., Hamer, D., Rosenberg, M. and Crooke, S. (1984). Copper metallothionein of yeast, structure of the gene, and regulation of expression. *Proceedings of the National Academy of Sciences*, 81(11), pp.3332-3336.

Buttrick, G., Lancaster, T., Meadows, J. and Millar, J. (2012). Plo1 phosphorylates Dam1 to promote chromosome bi-orientation in fission yeast. *Journal of Cell Science*, 125(7), pp.1645-1651.

Cabernard, C. and Doe, C. (2009). Apical/Basal Spindle Orientation Is Required for Neuroblast Homeostasis and Neuronal Differentiation in Drosophila. *Developmental Cell*, 17(1), pp.134-141.

Camahort, R., Li, B., Florens, L., Swanson, S., Washburn, M. and Gerton, J. (2007). Scm3 Is Essential to Recruit the Histone H3 Variant Cse4 to Centromeres and to Maintain a Functional Kinetochore. *Molecular Cell*, 26(6), pp.853-865.

Campbell, C. and Desai, A. (2013). Tension sensing by Aurora B kinase is independent of surviving-based centromere localization. *Nature*, 497, pp.118-121.

Carmena, M., Wheelock, M., Funabiki, H. and Earnshaw, W. (2012). The chromosomal passenger complex (CPC): from easy rider to the godfather of mitosis. *Nature Reviews Molecular Cell Biology*, 13(12), pp.789-803.

Chai, B., Hsu, J., Du, J. and Laurent, B. (2002). Yeast RSC Function Is Required for Organization of the Cellular Cytoskeleton via an Alternative PKC1 Pathway. *Genetics*, 161, pp.575-584.

Chee, M. and Haase, S. (2010). B-Cyclin/CDKs Regulate Mitotic Spindle Assembly by Phosphorylating Kinesins-5 in Budding Yeast. *PLoS Genetics*, 6(5), p.e1000935.

Cheeseman, I., Brew, C., Wolyniak, M., Desai, A., Anderson, S., Muster, N., Yates, J., Huffaker, T., Drubin, D. and Barnes, G. (2001). Implication of a novel multiprotein Dam1p complex in outer kinetochore function. *The Journal of Cell Biology*, 155(7), pp.1137-1146.

Cheeseman, I., Drubin, D. and Barnes, G. (2002). Simple centromere, complex kinetochore: linking spindle microtubules and centromeric DNA in budding yeast. *The Journal of Cell Biology*, 157(2), pp.199-203.

Cheeseman, I., Anderson, S., Jwa, M., Green, E., Kang, J., Yates, J., Chan, C., Drubin, D. and Barnes, G. (2002). Phospho-Regulation of Kinetochore-Microtubule Attachments

by the Aurora Kinase Ipl1p. *Cell*, 111(2), pp.163-172.

Cheeseman, I. (2014). The Kinetochore. *Cold Spring Harbor Laboratory Press*, 6(7), p.a015826.

Chen, D., Purohit, A., Halilovic, E., Doxsey, S. and Newton, A. (2004). Centrosomal Anchoring of Protein Kinase C betaII by Pericentrin Controls Microtubule Organization, Spindle Function, and Cytokinesis. *The Journal of Biological Chemistry*, 279(6), pp.4829-4839.

Chen, G., Rubinstein, B. and Li, R. (2012). Whole chromosome aneuploidy: Big mutations drive adaptation by phenotypic leap. *Bioessays*, 34(10), pp.893-900.

Cho, U. and Harrison, S. (2011). Ndc10 is a platform for inner kinetochore assembly in budding yeast. *Nat Struct Mol Biol*, 19(1), pp.48-55.

Chong, Y., Koh, J., Friesen, H., Duffy, S., Cox, M., Moses, A., Moffat, J., Boone, C. and Andrews, B. (2015). Yeast Proteome Dynamics from Single Cell Imaging and Automated Analysis. *Cell*, 162(1), p.221.

Clayton, R., White, O., Ketchum, K. and Venter, J. (1997). The first genome from the third domain of life. *Nature*, 387(6632), pp.459-462.

Coffman, V., Wu, P., Parthun, M. and Wu, J. (2011). CENP-A exceeds microtubule attachment sites in centromere clusters of both budding and fission yeast. *The Journal of Cell Biology*, 195(4), pp.563-572.

Collas, P. (1999). Sequential PKC- and Cdc2-mediated phosphorylation events elicit zebrafish nuclear envelope disassembly. *Journal of Cell Science*, 112, pp.977-987.

Collins, K., Castillo, A., Tatsutani, S. and Biggins, S. (2005). De Novo Kinetochore Assembly Requires the Centromeric Histone H3 Variant. *Molecular Biology of the Cell*, 16(12), pp.5649-5660.

Correas, I., Diaz-Nido, J. and Avila, J. (1992). Microtubule-associated protein Tau is phosphorylated by Protein Kinase C on its tubulin binding domain. *The Journal of Biological Chemistry*, 267(22), pp.15721-15728.

Costanzo, M., Baryshnikova, A., Bellay, J., Kim, Y., Spear, E. D., Sevier, C. S., Ding, H., Koh, J. L. Y., Toufighi, K., Mostafavi, S., Prinz, J., ST Onge, R. P., Vandersluis, B., Makhnevych, T., Vizeacoumar, F. J., Alizadeh, S., Bahr, S., Brost, R. L., Chen, Y., Cokol, M., Deshpande, R., Li, Z., Lin, Z. Y., Liang, W., Marback, M., Paw, J., San Luis, B. J., Shuteriqi, E., Tong, A. H. Y., Van Dyk, N., Wallace, I. M., Whitney, J. A., Weirauch, M. T., Zhong, G., Zhu, H., Houry, W. A., Brudno, M., Ragibizadeh, S., Papp, B., Pal, C., Roth, F. P., Giaever, G., Nislow, C., Troyanskaya, O. G., Bussey, H., Bader, G. D., Gingras, A. C., Morris, Q. D., Kim, P. M., Kaiser, C. A., Myers, C. L., Andrews, B. J. & Boone, C. (2010). The Genetic Landscape of a Cell. *Science,* 327**,** 425-431.

Crasta, K., Ganem, N., Dagher, R., Lantermann, A., Ivanova, E., Pan, Y., Nezi, L., Protopopov, A., Chowdhury, D. and Pellman, D. (2012). DNA breaks and chromosome pulverization from errors in mitosis. *Nature*, 482(7383), pp.53-58.

Dahlseid, J., Puziss, J., Shirley, R., Atkin, A., Hieter, P. and Culbertson, M. (1998). Accumulation of mRNA Coding for the Ctf13p Kinetochore Subunit of Saccharomyces cerevisiae Depends on the Same Factors That Promote Rapid Decay of Nonsense mRNAs. *Genetics*, 150, pp.1019-1035.

Darieva, Z., Han, N., Warwood, S., Doris, K., Morgan, B. and Sharrocks, A. (2012). Protein Kinase C Regulates Late Cell Cycle-Dependent Gene Expression. *Molecular and Cellular Biology*, 32(22), pp.4651-4661.

Davies, A. and Kaplan, K. (2010). Hsp90-Sgt1 and Skp1 target human Mis12 complexes to ensure efficient formation of kinetochore-microtubule binding sites. *The Journal of Cell Biology*, 189(2), pp.261-274.

De Wulf, P., McAinsh, A. and Sorger, P. (2003). Hierarchical assembly of the budding yeast kinetochore from multiple subcomplexes. *Genes & Development*, 17(23), pp.2902-

2921.

Delley, P. and Hall, M. (1999). Cell Wall Stress Depolarizes Cell Growth Via Hyperactivation of RHO1. *The Journal of Cell Biology*, 147(1), pp.163-174.

Denis, V. and Cyert, M. (2005). Molecular Analysis Reveals Localization of *Saccharomyces cerevisiae* Protein Kinase C to Sites of Polarized Growth and Pkc1p Targeting to the Nucleus and Mitotic Spindle. *Eukaryotic Cell*, 4(1), pp.36-45.

Dephoure, N., Hwang, S., O'Sullivan, C., Dodgson, S., Gygi, S., Amon, A. and Torres, E. (2014). Quantitative proteomic analysis reveals posttranslational responses to aneuploidy in yeast. *eLife*, 3.

Desai, A. and Mitchison, T. (1997). Microtubule polymerization dynamics. *Annual Review of Cell and Developmental Biology*, 13(1), pp.83-117.

Dittmar, J., Reid, R. and Rothstein, R. (2010). ScreenMill: A freely available software suite for growth measurement, analysis and visualization of high-throughput screen data. *BMC Bioinformatics*, 11(1), p.353.

Dorn, J., Jaqaman, K., Rines, D., Jelson, G., Sorger, P. and Danuser, G. (2005). Yeast kinetochore microtubule dynamics analyzed by high-resolution three-dimensional microscopy. *Biophysical Journal*, 89, pp.2835-2854.

Driver, J., Powers, A., Sarangapani, K., Biggins, S. and Asbury, C. (2014). Measuring kinetochore-microtubule interaction in vitro. *Methods in Enzymology*, 540, pp.321-337.

Duesberg, P., Li, R., Sachs, R., Fabarius, A., Upender, M. and Hehlmann, R. (2007). Cancer drug resistance: The central role of the karyotype. *Drug Resistance Updates*, 10(1-2), pp.51-58.

Durgan, J., Kaji, N., Jin, D. and Hall, A. (2011). Par6B and Atypical PKC Regulate Mitotic Spindle Orientation during Epithelial Morphogenesis. *Journal of Biological Chemistry*, 286(14), pp.12461-12474.

Eden, E., Lipson, D., Yogev, S. and Yakhini, Z. (2007). Discovering Motifs in Ranked Lists of DNA Sequences. *PLoS Comput Biol*, 3(3), p.e39.

Eden, E., Navon, R., Steinfeld, I., Lipson, D. and Yakhini, Z. (2009). GOrilla: a tool for discovery and visualization of enriched GO terms in ranked gene lists. *BMC Bioinformatics*, 10(1), p.48.

Endo, K., Mizuguchi, M., Harata, A., Itoh, G. and Tanaka, K. (2010). Nocodazole induces mitotic cell death with apoptotic-like features in Saccharomyces cerevisiae. *FEBS Letters*, 584(11), pp.2387-2392.

Engel, S., Dietrich, F., Fisk, D., Binkley, G., Balakrishnan, R., Costanzo, M., Dwight, S., Hitz, B., Karra, K., Nash, R., Weng, S., Wong, E., Lloyd, P., Skrzypek, M., Miyasato, S., Simison, M. and Cherry, J. (2014). The Reference Genome Sequence of *Saccharomyces cerevisiae*: Then and Now. *G3-Genes/Genomes/Genetics*, 4(3), pp.389-398.

Enserink, J. and Kolodner, R. (2010). An overview of Cdk1-controlled targets and processes. *Cell Div*, 5(1), p.11.

Espelin, C., Simons, K., Harrison, S. and Sorger, P. (2003). Binding of the Essential *Saccharomyces cerevisiae* Kinetochore Protein Ndc10p to CDEII. *Molecular Biology of the Cell*, 14(11), pp.4557-4568.

Fachinetti, D., Diego Folco, H., Nechemia-Arbely, Y., Valente, L., Nguyen, K., Wong, A., Zhu, Q., Holland, A., Desai, A., Jansen, L. and Cleveland, D. (2013). A two-step mechanism for epigenetic specification of centromere identity and function. *Nature Cell Biology*, 15(9), pp.1056-1066.

Faust, A., Wong, C., Yates III, J., Drubin, D. and Barnes, G. (2013). The FEAR Protein Slk19 Restricts Cdc14 Phosphatase to the Nucleus until the End of Anaphase, Regulating Its Participation in Mitotic Exit in *Saccharomyces cerevisiae*. *PLoS ONE*, 8(9), p.e73194.

Freed, E., Lacey, K., Huie, P., Lyapina, S., Deshaies, R., Stearns, T. and Jackson, P.

(1999). Components of an SCF ubiquitin ligase localize to the centrosome and regulate the centrosome duplication cycle. *Genes & Development*, 13(17), pp.2242-2257.

Fukagawa, T. and Earnshaw, W. (2014). The Centromere: Chromatin Foundation for the Kinetochore Machinery. *Developmental Cell*, 30(5), pp.496-508.

Funabiki, H. and Wynne, D. (2013). Making an effective switch at the kinetochore by phosphorylation and dephosphorylation. *Chromosoma*, 122(3), pp.135-158.

Furuyama, S. and Biggins, S. (2007). Centromere identity is specified by a single centromeric nucleosome in budding yeast. *Proceedings of the National Academy of Sciences*, 104(37), pp.14706-14711.

Gao, Q., Courtheoux, T., Gachet, Y., Tournier, S. and He, X. (2010). A non-ring-like form of the Dam1 complex modulates microtubule dynamics in fission yeast. *Proceedings of the National Academy of Sciences*, 107(30), pp.13330-13335.

Gardner, M., Haase, J., Mythreye, K., Molk, J., Anderson, M., Joglekar, A., O'Toole, E., Winey, M., Salmon, E., Odde, D. and Bloom, K. (2008). The microtubule-based motor Kar3 and plus end binding protein Bim1 provide structural support for the anaphase spindle. *The Journal of Cell Biology*, 180(1), pp.91-100.

Gerson-Gurwitz, A., Movshovich, N., Avunie, R., Fridman, V., Moyal, K., Katz, B., Hoyt, M. and Gheber, L. (2009). Mid-anaphase arrest in *S. cerevisiae* cells eliminated for the function of Cin8 and dynein. *Cell. Mol. Life Sci.*, 66(2), pp.301-313.

Gestaut, D., Graczyk, B., Cooper, J., Widlund, P., Zelter, A., Wordeman, L., Asbury, C. and Davis, T. (2008). Phosphoregulation and depolymerization-driven movement of the Dam1 complex do not require ring formation. *Nature Cell Biology*, 10(4), pp.407-414.

Gestaut, D., Cooper, J., Asbury, C., Davis, T. and Wordeman, L. (2010). Reconstitution and functional analysis of kinetochore subcomplexes. *Methods in Cell Biology*, 95(641-656).

Giaever, G., Chu, A., Ni, L., Connelly, C., Riles, L., Veronneau, S., Dow, S., Lucau-Danila, A., Anderson, K., Andre, B., Arkin, A., Astromoff, A., El Bakkoury, M., Bangham, R., Benito, R., Brachat, S., Campanaro, S., Curtiss, M., Davis, K., Deutschbauer, A., Entian, K., Flaherty, P., Foury, F., Garfinkel, D., Gerstein, M., Gotte, D., Guldener, U., Hegemann, J., Hempel, S., Herman, Z., Jaramillo, D., E. Kelly, D., Kelly, S., Kotter, P., LaBonte, D., Lamb, D., Lan, N., Liang, H., Liao, H., Liu, L., Luo, C., Lussier, M., Mao, R., Menard, P., Ooi, S., Revuelta, J., Roberts, C., Rose, M., Ross-Macdonald, P., Scherens, B., Schimmack, G., Shafer, B., Shoemaker, D., Sookhai-Mahadeo, S., Storms, R., Strathern, J., Valle, G., Voet, M., Volckaert, G., Wang, C., Ward, T., Wilhelmy, J., Winzeler, E., Yang, Y., Yen, G., Youngman, E., Yu, K., Bussey, H., Boeke, J., Snyder, M., Philippsen, P., Davis, D. and Johnston, M. (2002). Functional profiling of the *Saccharomyces cerevisiae* genome. *Nature*, 418, pp.387-391.

Giaever, G. and Nislow, C. (2014). The Yeast Deletion Collection: A Decade of Functional Genomics. *Genetics*, 197(2), pp.451-465.

Giam, M. and Rancati, G. (2015). Aneuploidy and chromosomal instability in cancer: a jackpot to chaos. *Cell Div*, 10(3).

Gietz, R. and Woods, R. (2002). Transformation of yeast by lithium acetate/single-stranded carrier DNA/polyethylene glycol method. *Methods in Enzymology*, 350, pp.87-96.

Godek, K., Kabeche, L. and Compton, D. (2015). Regulation of kinetochore-microtubule attachments through homeostatic control during mitosis. *Nature Reviews Molecular Cell Biology*, 16(1), pp.57-64.

Goffeau, A., Barrell, B., Bussey, H., Davis, R., Dujon, B., Feldmann, H., Galibert, F., Hoheisel, J., Jacq, C., Johnston, M., Louis, E., Mewes, H., Murakami, Y., Philippsen, P., Tettelin, H. and Oliver, S. (1996). Life with 6000 Genes. *Science*, 274(5287), pp.546-567.

Gonen, S., Akiyoshi, B., Iadanza, M., Shi, D., Duggan, N., Biggins, S. and Gonen, T. (2012). The structure of purified kinetochores reveals multiple microtubule-attachment sites. *Nat Struct Mol Biol*, 19(9), pp.925-929.

Grishchuk, E., Spiridonov, I., Volkov, V., Efremov, A., Westermann, S., Drubin, D., Barnes, G., Ataullakhanov, F. and McIntosh, J. (2008). Different assemblies of the DAM1 complex follow shortening microtubules by distinct mechanisms. *Proceedings of the National Academy of Sciences*, 105(19), pp.6918-6923.

Guacci, V., Hogan, E. and Koshland, D. (1997). Centromere position in budding yeast: evidence for anaphase A. *Molecular Biology of the Cell*, 8(6), pp.957-972.

Guilgur, L., Prudencio, P., Ferreira, T., Pimenta-Marques, A. and Martinho, R. (2012). Drosophila aPKC is required for mitotic spindle orientation during symmetric division of epithelial cells. *Development*, 139(3), pp.503-513.

Hartmuth, S. and Petersen, J. (2009). Fission yeast Tor1 functions as part of TORC1 to control mitotic entry through the stress MAPK pathway following nutrient stress. *Journal of Cell Science*, 122(11), pp.1737-1746.

Hartwell, L. (1974). *Saccharomyces cerevisiae* Cell Cycle. *Bacteriological Reviews*, 38(2), pp.164-198.

Hasle, H., Clemmensen, I. and Mikkelsen, M. (2000). Risks of leukaemia and solid tumours in individuals with Down's syndrome. *The Lancet*, 355(9199), pp.165-169.

He, F., Brown, A. and Jacobson, A. (1997). Upf1p, Nmd2p, and Upf3p Are Interacting Components of the Yeast Nonsense-Mediated mRNA Decay Pathway. *Molecular and Cellular Biology*, 17(3), pp.1580-1594.

He, X., Rines, D., Espelin, C. and Sorger, P. (2001). Molecular Analysis of Kinetochore-Microtubule Attachment in Budding Yeast. *Cell*, 106(2), pp.195-206.

Herbert, A., Carr, A. and Hoffmann, E. (2014). FindFoci: A Focus Detection Algorithm with Automated Parameter Training That Closely Matches Human Assignments, Reduces Human Inconsistencies and Increases Speed of Analysis. *PLoS ONE*, 9(12), p.e114749.

Herskowitz, I. (1988). Life Cycle of the Budding Yeast *Saccharomyces cerevisiae*. *Microbiological reviews*, 52(4), pp.536-553.

Hewawasam, G., Shivaraju, M., Mattingly, M., Venkatesh, S., Martin-Brown, S., Florens, L., Workman, J. and Gerton, J. (2010). Psh1 is an E3 Ubiquitin Ligase that Targets the Centromeric Histone Variant Cse4. *Molecular Cell*, 40(3), pp.444-454.

Hill, T. (1985). Theoretical problems related to the attachment of microtubules to kinetochores. *Proceedings of the National Academy of Sciences*, 82(13), pp.4404-4408.

Hillenmeyer, M., Fung, E., Wildenhain, J., Pierce, S., Hoon, S., Lee, W., Proctor, M., St.Onge, R., Tyers, M., Koller, D., Altman, R., Davis, R., Nislow, C. and Giaever, G. (2008). The Chemical Genomic Portrait of Yeast: Uncovering a Phenotype for All Genes. *Science*, 320(5874), pp.362-365.

Hinshaw, S. and Harrison, S. (2013). An Iml3-Chl4 Heterodimer Links the Core Centromere to Factors Required for Accurate Chromosome Segregation. *Cell Reports*, 5(1), pp.29-36.

Ho, K., Tsuchiya, D., Oliger, A. and Lacefield, S. (2014). Localization and Function of Budding Yeast CENP-A Depends upon Kinetochore Protein Interactions and Is Independent of Canonical Centromere Sequence. *Cell Reports*, 9(6), pp.2027-2033.

Hoffman, C. and Winston, F. (1987). A ten-minute DNA preparation from yeast efficiently releases autonomous plasmids for transformaion of Escherichia coli. *Gene*, 57(2-3), pp.267-272.

Holland, A. and Cleveland, D. (2009). Boveri revisited: chromosomal instability, aneuploidy and tumorigenesis. *Nature Reviews Molecular Cell Biology*, 10(7), pp.478-487.

Hornung, P., Maier, M., Alushin, G., Lander, G., Nogales, E. and Westermann, S. (2011). Molecular Architecture and Connectivity of the Budding Yeast Mtw1 Kinetochore Complex. *Journal of Molecular Biology*, 405(2), pp.548-559.

Hosotani, T., Koyama, H., Uchino, M., Miyakawa, T. and Tsuchiya, E. (2001). PKC1, a protein kinase C homologue of *Saccharomyces cerevisiae*, participates in microtubule function through the yeast EB1 homologue, BIM1. *Genes to Cells*, 6(9), pp.775-788.

Hsia, K., Wilson-Kubalek, E., Dottore, A., Hao, Q., Tsai, K., Forth, S., Shimamoto, Y., Milligan, R. and Kapoor, T. (2014). Reconstitution of the augmin complex provides insights into its architecture and function. *Nature Cell Biology*, 16(9), pp.852-863.

Hsu, K. and Toda, T. (2011). Ndc80 Internal Loop Interacts with Dis1/TOG to Ensure Proper Kinetochore-Spindle Attachment in Fission Yeast. *Current Biology*, 21(3), pp.214-220.

Huh, W., Falvo, J., Gerke, L., Carroll, A., Howson, R., Weissman, J. and O'Shea, E. (2003). Global analysis of protein localization in budding yeast. *Nature*, 425(6959), pp.686-691.

Hughes, T., Roberts, C., Jones, A., Meyer, M., Slade, D., Burchard, J., Dow, S., Ward, T., Kidd, M., Friend, S. and Marton, M. (2000). Widespread aneuploidy revealed by DNA microarray expression profiling. *Nature Genetics*, 25(3), pp.333-337.

Jackson, D. and Foster, D. (2004). The enigmatic protein kinase Cdelta: complex roles in cell proliferation and survival. *The FASEB Journal*, 18(6), pp.627-636.

Janke, C., Ortiz, J., Lechner, J., Shevchenko, A., Shevchenko, A., Magiera, M., Schramm, C. and Schiebel, E. (2001). The budding yeast proteins Spc24p and Spc25p interact with Ndc80p and Nuf2p at the kinetochore and are important for kinetochore clustering and checkpoint control. *The EMBO Journal*, 20(4), pp.777-791.

Janke, C., Ortiz, J., Tanaka, T., Lechner, J. and Schiebel, E. (2002). Four new subunits of the Dam1-Duo1 complex reveal novel functions in sister kinetochore biorientation. *The EMBO Journal*, 21(1), pp.181-193.

Janssen, A., van der Burg, M., Szuhai, K., Kops, G. and Medema, R. (2011). Chromosome Segregation Errors as a Cause of DNA Damage and Structural Chromosome Aberrations. *Science*, 333(6051), pp.1895-1898.

Jaspersen, S. and Winey, M. (2004). The Budding Yeast Spindle Pole Body: Structure, Duplication, and Function. *Annual Review of Cell and Developmental Biology*, 20(1), pp.1-28.

Joglekar, A., Bouck, D., Molk, J., Bloom, K. and Salmon, E. (2006). Molecular architecture of a kinetochore-microtubule attachment site. *Nature Cell Biology*, 8(6), pp.581-585.

Joglekar, A., Bouck, D., Finley, K., Liu, X., Wan, Y., Berman, J., He, X., Salmon, E. and Bloom, K. (2008). Molecular architecture of the kinetochore-microtubule attachment site is conserved between point and regional centromeres. *The Journal of Cell Biology*, 181(4), pp.587-594.

Kabir, N., Schaefer, A., Nakhost, A., Sossin, W. and Forscher, P. (2001). Protein Kinase C Activation Promotes Microtubule Advance in Neuronal Growth Cones by Increasing Average Microtubule Growth Lifetimes. *The Journal of Cell Biology*, 152(5), pp.1033-1044.

Kebaara, B. and Atkin, A. (2009). Long 3'-UTRs target wild-type mRNAs for nonsense-mediated mRNA decay in Saccharomyces cerevisiae. *Nucleic Acids Research*, 37(9), pp.2771-2778.

Keith, K. and Fitzgerald-Hayes, M. (2000). CSE4 Genetically Interacts With the Saccharomyces cerevisiae Centromere DNA Elements CDE I and CDE II but Not CDE III: Implications for the Path of the Centromere DNA Around a Cse4p Variant Nucleosome. *Genetics*, 156, pp.973-981.

Khalfan, W., Ivanovska, I. and Rose, M. (2000). Functional Interaction Between the PKC1 Pathway and CDC31 Network of SPB Duplication Genes. *Genetics*, 155, pp.1543-1559.

Kitagawa, K., Skowyra, D., Elledge, S., Harper, J. and Hieter, P. (1999). SGT1 Encodes an Essential Component of the Yeast Kinetochore Assembly Pathway and a Novel Subunit of the SCF Ubiquitin Ligase Complex. *Molecular Cell*, 4(1), pp.21-33.

Kitamura, E., Tanaka, K., Kitamura, Y. and Tanaka, T. (2007). Kinetochore microtubule interaction during S phase in *Saccharomyces cerevisiae*. *Genes & Development*, 21(24), pp.3319-3330.

Knockleby, J. and Vogel, J. (2009). The COMA complex is required for Sli15/INCENP-mediated correction of defective kinetochore attachments. *Cell Cycle*, 8(16), pp.2570-2577.

Koh, J., Chong, Y., Friesen, H., Moses, A., Boone, C., Andrews, B. and Moffat, J. (2015). CYCLoPs: A Comprehensive Database Constructed from Automated Analysis of Protein Abundance and Subcellular Localization Patterns in Saccharomyces cerevisiae. *G3: Genes|Genomes|Genetics*, 5(6), pp.1223-1232.

Korolyev, E., Steinberg-Neifach, O. and Eshel, D. (2005). Mutations in the yeast kinesin-like Cin8p are alleviated by osmotic support. *FEMS Microbiology Letters*, 244(2), pp.379-383.

Krause, S., Cundell, M., Poon, P., McGhie, J., Johnston, G., Price, C. and Gray, J. (2012). Functional specialisation of yeast Rho1 GTP exchange factors. *Journal of Cell Science*, 125(11), pp.2721-2731.

Lacefield, S., Lau, D. and Murray, A. (2009). Recruiting a microtubule-binding complex to DNA directs chromosome segregation in budding yeast. *Nature Cell Biology*, 11(9), pp.1116-1120.

Lampert, F., Hornung, P. and Westermann, S. (2010). The Dam1 complex confers microtubule plus end-tracking activity to the Ndc80 kinetochore complex. *The Journal of Cell Biology*, 189(4), pp.641-649.

Lau, D. and Murray, A. (2012). Mad2 and Mad3 Cooperate to Arrest Budding Yeast in Mitosis. *Current Biology*, 22(3), pp.180-190.

Lawrimore, J., Bloom, K. and Salmon, E. (2011). Point centromeres contain more than a single centromere-specific Cse4 (CENP-A) nucleosome. *The Journal of Cell Biology*, 195(4), pp.573-582.

Lechner, J. and Carbon, J. (1991). A 240 kd multisubunit protein complex, CBF3, is a major component of the budding yeast centromere. *Cell*, 64(4), pp.717-725.

Ledesma-Fernández, E. and Thorpe, P. (2015). Fluorescent foci quantitation for high-throughput analysis. *J Biol Methods*, 2(2), p.22.

Lehrich, R. and Forrest, J. (1994). Protein KinaseC ζ Is Associated with the Mitotic Apparatus in Primary Cell Culturesof the Shark Rectal Gland. *The Journal of Biological Chemistrry*, 269(51), pp.32446-32450.

Levin, D. and Bartlett-Heubusch, E. (1992). Mutants in the *S. cerevisiae* PKC1 gene display a cell cycle-specific osmotic stability defect. *The Journal of Cell Biology*, 116(5), pp.1221-1229.

Levin, D. (2005). Cell Wall Integrity Signaling in *Saccharomyces cerevisiae*. *Microbiology and Molecular Biology Reviews*, 69(2), pp.262-291.

Levin, D. (2011). Regulation of Cell Wall Biogenesis in *Saccharomyces cerevisiae*: The Cell Wall Integrity Signaling Pathway. *Genetics*, 189(4), pp.1145-1175.

Lew, D. (2003). The morphogenesis checkpoint: how yeast cells watch their figures. *Current Opinion in Cell Biology*, 15(6), pp.648-653

Li, Z., Vizeacoumar, F., Bahr, S., Li, J., Warringer, J., Vizeacoumar, F., Min, R., VanderSluis, B., Bellay, J., DeVit, M., Fleming, J., Stephens, A., Haase, J., Lin, Z., Baryshnikova, A., Lu, H., Yan, Z., Jin, K., Barker, S., Datti, A., Giaever, G., Nislow, C., Bulawa, C., Myers, C., Costanzo, M., Gingras, A., Zhang, Z., Blomberg, A., Bloom, K., Andrews, B. and Boone, C. (2011). Systematic exploration of essential yeast gene function with temperature-sensitive mutants. *Nat Biotechnol*, 29(4), pp.361-367.

Lin, H., Carvalho,, P., Kho, D., Tai, C., Pierre, P., Fink, G. and Pellman, D. (2001). Polyploids require Bik1 for kinetochore-microtubule attachment. *The Journal of Cell Biology*, 155(7), pp.1173-1184.

Li, J., Li, Y. and Elledge, S. (2005). Genetic Analysis of the Kinetochore DASH Complex Reveals an Antagonistic Relationship with the Ras/Protein Kinase A Pathway and a Novel Subunit Required for Ask1 Association. *Molecular and Cellular Biology,* 25(2), pp.767-778.

London, N., Ceto, S., Ranish, J. and Biggins, S. (2012). Phosphoregulation of Spc105 by Mps1 and PP1 Regulates Bub1 Localization to Kinetochores. *Current Biology*, 22(10), pp.900-906.

London, N. and Biggins, S. (2014). Mad1 kinetochore recruitment by Mps1-mediated phosphorylation of Bub1 signals the spindle checkpoint. *Genes & Development*, 28(2), pp.140-152.

Looke, M., Kristjuhan, K. and Kristjuhan, A. (2011). Extraction of Genomic DNA from Yeasts for PCR-based Applications. *Biotechniques*, 50(5), pp.325-328.

Makhnevych, T., Sydorskyy, Y., Xin, X., Srikumar, T., Vizeacoumar, F., Jeram, S., Li, Z., Bahr, S., Andrews, B., Boone, C. and Raught, B. (2009). Global Map of SUMO Function Revealed by Protein-Protein Interaction and Genetic Networks. *Molecular Cell*, 33(1), pp.124-135.

Makrantoni, V., Corbishley, S., Rachidi, N., Morrice, N., Robinson, D. and Stark, M. (2014). Phosphorylation of Sli15 by Ipl1 Is Important for Proper CPC Localization and Chromosome Stability in *Saccharomyces cerevisiae*. *PLoS ONE*, 9(2), p.e89399.

Mall, M., Walter, T., Gorjanacz, M., Davidson, I., Nga Ly-Hartig, T., Ellenberg, J. and Mattaj, I. (2012). Mitotic lamin disassembly is triggered by lipid-mediated signaling. *The Journal of Cell Biology*, 198(6), pp.981-990.

Martin, A., Xu, X., Rouiller, I., Kaksonen, M., Sun, Y., Belmont, L., Volkmann, N., Hanein, D., Welch, M. and Drubin, D. (2005). Effects of Arp2 and Arp3 nucleotide-binding pocket mutations on Arp2/3 complex function. *The Journal of Cell Biology*, 168(2), pp.315-328.

Mascaraque, V., Hernaez, M., Jimenez-Sanchez, M., Hansen, R., Gil, C., Martin, H., Cid, V. and Molina, M. (2013). Phosphoproteomic Analysis of Protein Kinase C Signaling in *Saccharomyces cerevisiae* Reveals Slt2 Mitogen-activated Protein Kinase (MAPK)-dependent Phosphorylation of Eisosome Core Components. *Molecular & Cellular Proteomics*, 12(3), pp.557-574.

Mascorro-Gallardo, J., Covarrubias, A. and Gaxiola, R. (1996). Construction of a CUP1 promoter-based vector to modulate gene expression in Saccharomyces cerevisiae. *Gene*, 172(1), pp.169-170.

Maskell, D., Hu, X. and Singleton, M. (2010). Molecular architecture and assembly of the yeast kinetochore MIND complex. *The Journal of Cell Biology*, 190(5), pp.823-834.

Matson, D. and Stukenberg, P. (2012). Cdt1 throws kinetochore-microtubule attachments for a loop. *Nature Cell Biology*, 14(6), pp.561-563.

Matson, D., Demirel, P., Stukenberg, P. and Burke, D. (2012). A conserved role for COMA/CENP-H/I/N kinetochore proteins in the spindle checkpoint. *Genes & Development*, 26(6), pp.542-547.

Maure, J., Komoto, S., Oku, Y., Mino, A., Pasqualato, S., Natsume, K., Clayton, L., Musacchio, A. and Tanaka, T. (2011). The Ndc80 Loop Region Facilitates Formation of Kinetochore Attachment to the Dynamic Microtubule Plus End. *Current Biology*, 21(3), pp.207-213.

McAinsh, A., Tytell, J. and Sorger, P. (2003). Structure, function, and regulation of budding yeast kinetochores. *The Annual Review of Cell and Developmental Biology*, 19, pp.519-39.

Measday, V., Hailey, D., Pot, I., Givan, S., Hyland, K., Cagney, G., Davis, T. and Hieter, P. (2002). Ctf3p, the Mis6 budding yeast homolog, interacts with Mcm22p and Mcm16p at the yeast outer kinetochore. *Genes & Development*, 16(1), pp.101-113

Mellor, H. and Parker, P. (1998). The extended protein kinase C superfamily. *Biochem. J.*,

332(2), pp.281-292.

Miranda, J., Wulf, P., Sorger, P. and Harrison, S. (2005). The yeast DASH complex forms closed rings on microtubules. *Nat Struct Mol Biol*, 12(2), pp.138-143.

Miranda, J., King, D. and Harrison, S. (2007). Protein Arms in the Kinetochore-Microtubule Interface of the Yeast DASH Complex. *Molecular Biology of the Cell*, 18(7), pp.2503-2510.

Mitchison, T. and Kirschner, M. (1984). Dynamic instability of microtubule growth. *Nature*, 312(5991), pp.237-242.

Montpetit, B., Hazbun, T., Fields, S. and Hieter, P. (2006). Sumoylation of the budding yeast kinetochore protein Ndc10 is required for Ndc10 spindle localization and regulation of anaphase spindle elongation. *The Journal of Cell Biology*, 174(5), pp.653-663.

Morgan, D. O. 2007. *The Cell Cycle. Principles of Control*, London, New Science Press.

Moseley, J. and Goode, B. (2006). The Yeast Actin Cytoskeleton: from Cellular Function to Biochemical Mechanism. *Microbiology and Molecular Biology Reviews*, 70(3), pp.605-645.

Nannas, N., O'Toole, E., Winey, M. and Murray, A. (2014). Chromosomal attachments set length and microtubule number in the *Saccharomyces cerevisiae* mitotic spindle. *Molecular Biology of the Cell*, 25(25), pp.4034-4048.

Nishimura, K., Fukagawa, T., Takisawa, H., Kakimoto, T. and Kanemaki, M. (2009). An auxin-based degron system for the rapid depletion of proteins in nonplant cells. *Nature Methods*, 6(12), pp.917-922.

Novak, B., Sible, J. and Tyson, J. (2002). Checkpoints in the Cell Cycle. *Encyclopedia of Life Sciences*.

Ohkuni, K., Abdulle, R., Tong, A., Boone, C. and Kitagawa, K. (2008). Ybp2 Associates with the Central Kinetochore of *Saccharomyces cerevisiae* and Mediates Proper Mitotic Progression. *PLoS ONE*, 3(2), p.e1617.

Olafsson, G. and Thorpe, P. (2015). Synthetic physical interactions map kinetochore regulators and regions sensitive to constitutive Cdc14 localization. *Proceedings of the National Academy of Sciences*, 112(33), pp.10413-10418.

Ortiz, J., Funk, C., Schafer, A. and Lechner, J. (2009). Stu1 inversely regulates kinetochore capture and spindle stability. *Genes & Development*, 23(23), pp.2778-2791.

Pagliuca, C., Draviam, V., Marco, E., Sorger, P. and De Wulf, P. (2009). Roles for the Conserved Spc105p/Kre28p Complex in Kinetochore-Microtubule Binding and the Spindle Assembly Checkpoint. *PLoS ONE*, 4(10), p.e7640.

Pease, J. and Tirnauer, J. (2011). Mitotic spindle misorientation in cancer - out of alignment and into the fire. *Journal of Cell Science*, 124(7), pp.1007-1016.

Pellman, D. (2007). Aneuploidy and cancer. *Nature*, 446.

Perriches, T. and Singleton, M. (2012). Structure of yeast kinetochore Ndc10 DNA-binding domain reveals unexpected evolutionary relationship to tyrosine recombinases. *The Journal of Biological Chemistry*, 287(7), pp.5173-5179.

Peters, J. (2006). The anaphase promoting complex/cyclosome: a machine designed to destroy. *Nature Reviews Molecular Cell Biology*, 7(9), pp.644-656.

Pinsky, B., Tatsutani, S., Collins, K. and Biggins, S. (2003). An Mtw1 Complex Promotes Kinetochore Biorientation that Is Monitored by the Ipl1/Aurora Protein Kinase. *Developmental Cell*, 5(5), pp.735-745.

Pinsky, B., Nelson, C. and Biggins, S. (2009). Protein Phosphatase 1 Regulates Exit from the Spindle Checkpoint in Budding Yeast. *Current Biology*, 19(14), pp.1182-1187.

Pot, I., Measday, V., Snydsman, B., Cagney, G., Fields, S., Davis, T., Muller, E. and Hieter, P. (2003). Chl4p and Iml3p Are Two New Members of the Budding Yeast Outer Kinetochore. *Molecular Biology of the Cell*, 14(2), pp.460-476.

Pot, I., Knockleby, J., Aneliunas, V., Nguyen, T., Ah-Kye, S., Liszt, G., Snyder, M., Hieter, P. and Vogel, J. (2005). Spindle Checkpoint Maintenance Requires Ame1 and Okp1. *Cell Cycle*, 4(10), pp.1448-1456

Queralt, E. and Uhlmann, F. (2008). Separase cooperates with Zds1 and Zds2 to activate Cdc14 phosphatase in early anaphase. *The Journal of Cell Biology*, 182(5), pp.873-883.

Ramey, V., Wong, A., Fang, J., Howes, S., Barnes, G. and Nogales, E. (2011). Subunit organization in the Dam1 kinetochore complex and its ring around microtubules. *Molecular Biology of the Cell*, 22(22), pp.4335-4342.

Rancati, G., Pavelka, N., Fleharty, B., Noll, A., Trimble, R., Walton, K., Perera, A., Staehling-Hampton, K., Seidel, C. and Li, R. (2008). Aneuploidy Underlies Rapid Adaptive Evolution of Yeast Cells Deprived of a Conserved Cytokinesis Motor. *Cell*, 135(5), pp.879-893.

Ranjitkar, P., Press, M., Yi, X., Baker, R., MacCoss, M. and Biggins, S. (2010). An E3 Ubiquitin Ligase Prevents Ectopic Localization of the Centromeric Histone H3 Variant via the Centromere Targeting Domain. *Molecular Cell*, 40(3), pp.455-464.

Reid, R., Gonzalez-Barrera, S., Sunjevaric, I., Alvaro, D., Ciccone, S., Wagner, M. and Rothstein, R. (2011). Selective ploidy ablation, a high-throughput plasmid transfer protocol, identifies new genes affecting topoisomerase I-induced DNA damage. *Genome Research*, 21(3), pp.477-486.

Richmond, D., Rizkallah, R., Liang, F., Hurt, M. and Wang, Y. (2013). Slk19 clusters kinetochores and facilitates chromosome bipolar attachment. *Molecular Biology of the Cell*, 24(5), pp.566-577.

Ricke, R. and Deursen, J. (2013). Aneuploidy in health, disease, and aging. *The Journal of Biological Chemistry*, 201(1), pp.11-21.

Rieder, C. and Salmon, E. (1998). The vertebrate cell kinetochore and its roles during mitosis. *Trends in Cell Biology*, 8(8), pp.310-318.

Robertson, A. and Hagan, I. (2008). Stress-regulated kinase pathways in the recovery of tip growth and microtubule dynamics following osmotic stress in S. pombe. *Journal of Cell Science*, 121(24), pp.4055-4068.

Rodrigo-Brenni, M., Thomas, S., Bouck, D. and Kaplan, K. (2004). Sgt1p and Skp1p Modulate the Assembly and Turnover of CBF3 Complexes Required for Proper Kinetochore Function. *Molecular Biology of the Cell*, 15(7), pp.3366-3378.

Rosse, C., Linch, M., Kermorgant, S., Cameron, A., Boeckeler, K. and Parker, P. (2010). PKC and the control of localized signal dynamics. *Nature Reviews Molecular Cell Biology*, 11(2), pp.103-112.

Rothstein, R. (1983). One-step gene disruption in yeast. *Methods in Enzymology*, 101, pp.202-11.

Sambrook, J. & Russell, D. W. 2001. *Molecular Cloning: A Laboratory Manual*. Cold Spring Harbor Laboratory Press.

Samel, A., Cuomo, A., Bonaldi, T. and Ehrenhofer-Murray, A. (2012). Methylation of CenH3 arginine 37 regulates kinetochore integrity and chromosome segregation. *Proceedings of the National Academy of Sciences*, 109(23), pp.9029-9034.

Santaguida, S. and Musacchio, A. (2009). The life and miracles of kinetochores. *The EMBO Journal*, 28(17), pp.2511-2531.

Schober, J., Kwon, G., Jayne, D. and Cain, J. (2012). The microtubule-associated protein EB1 maintains cell polarity through activation of protein kinase C. *Biochemical and Biophysical Research Communications*, 417(1), pp.67-72.

Schmidt, M., Budirahardja, Y., Klompmaker, R. and Medema, R. (2005). Ablation of the spindle assembly checkpoint by a compound targeting Mps1. *EMBO Rep*, 6(9), pp.866-872.

Shang, C., Hazbun, T., Cheeseman, I., Aranda, J., Fields, S., Drubin, D. and Barnes, G. (2003). Kinetochore Protein Interactions and their Regulation by the Aurora Kinase Ipl1p. *Molecular Biology of the Cell*, 14(8), pp.3342-3355.

Shivaraju, M., Camahort, R., Mattingly, M. and Gerton, J. (2011). Scm3 Is a Centromeric Nucleosome Assembly Factor. *Journal of Biological Chemistry*, 286(14), pp.12016-12023.

Shivaraju, M., Unruh, J., Slaughter, B., Mattingly, M., Berman, J. and Gerton, J. (2012). Cell-Cycle-Coupled Structural Oscillation of Centromeric Nucleosomes in Yeast. *Cell*, 150(2), pp.304-316.

Sidorova, J. and Breeden, L. (1997). Rad53-dependent phosphorylation of Swi6 and down-regulation of CLN1 and CLN2 transcription occur in response to DNA damage in *Saccharomyces cerevisiae*. *Genes & Development*, 11(22), pp.3032-3045.

Siegel, J. and Amon, A. (2012). New Insights into the Troubles of Aneuploidy. *Annual Review of Cell and Developmental Biology*, 28(1), pp.189-214.

Singh, P., Rathinasamy, K., Mohan, R. and Panda, D. (2008). Microtubule assembly dynamics: An attractive target for anticancer drugs. *IUBMB Life*, 60(6), pp.368-375.

Soriano-Carot, M., Quilis, I., Bano, M. and Igual, J. (2014). Protein kinase C controls activation of the DNA integrity checkpoint. *Nucleic Acids Research*, 42(11), pp.7084-7095.

Sotillo, R., Hernando, E., Díaz-Rodríguez, E., Teruya-Feldstein, J., Cordón-Cardo, C., Lowe, S. and Benezra, R. (2007). Mad2 Overexpression Promotes Aneuploidy and Tumorigenesis in Mice. *Cancer Cell*, 11(1), pp.9-23.

Stephens, P., Greenman, C., Fu, B., Yang, F., Bignell, G., Mudie, L., Pleasance, E., Lau, K., Beare, D., Stebbings, L., McLaren, S., Lin, M., McBride, D., Varela, I., Nik-Zainal, S., Leroy, C., Jia, M., Menzies, A., Butler, A., Teague, J., Quail, M., Burton, J., Swerdlow, H., Carter, N., Morsberger, L., Iacobuzio-Donahue, C., Follows, G., Green, A., Flanagan, A., Stratton, M., Futreal, P. and Campbell, P. (2011). Massive Genomic Rearrangement Acquired in a Single Catastrophic Event during Cancer Development. *Cell*, 144(1), pp.27-40.

Stirling, P., Bloom, M., Solanki-Patil, T., Smith, S., Sipahimalani, P., Li, Z., Kofoed, M., Ben-Aroya, S., Myung, K. and Hieter, P. (2011). The Complete Spectrum of Yeast Chromosome Instability Genes Identifies Candidate CIN Cancer Genes and Functional Roles for ASTRA Complex Components. *PLoS Genetics*, 7(4), p.e1002057.

Tanaka, T., Stark, M. and Tanaka, K. (2005). Kinetochore capture and bi-orientation on the mitotic spindle. *Nature Reviews Molecular Cell Biology*, 6(12), pp.929-942.

Tanaka, K., Mukae, N., Dewar, H., van Breugel, M., James, E., Prescott, A., Antony, C. and Tanaka, T. (2005). Molecular mechanisms of kinetochore capture by spindle microtubules. *Nature*, 434(7036), pp.987-994.

Tanaka, T. and Desai, A. (2008). Kinetochore-microtubule interactions: the means to the end. *Current Opinion in Cell Biology*, 20(1), pp.53-63.

Teng, X., Dayhoff-Brannigan, M., Cheng, W., Gilbert, C., Sing, C., Diny, N., Wheelan, S., Dunham, M., Boeke, J., Pineda, F. and Hardwick, J. (2013). Genome-wide Consequences of Deleting Any Single Gene. *Molecular Cell*, 52(4), pp.485-494.

Thorpe, P., Bruno, J. and Rothstein, R. (2008). Kinetochore asymmetry defines a single yeast lineage. *Proceedings of the National Academy of Sciences*, 106(16), pp.6673-6678.

Thorpe, P., Dittmar, J. and Rothstein, R. (2012). ScreenTroll: a searchable database to compare genome-wide yeast screens. *Database*, 2012(0), pp.bas022-bas022.

Tien, J., Umbreit, N., Gestaut, D., Franck, A., Cooper, J., Wordeman, L., Gonen, T., Asbury, C. and Davis, T. (2010). Cooperation of the Dam1 and Ndc80 kinetochore complexes enhances microtubule coupling and is regulated by aurora B. *The Journal of Cell Biology*, 189(4), pp.713-723.

Tkach, J., Yimit, A., Lee, A., Riffle, M., Costanzo, M., Jaschob, D., Hendry, J., Ou, J., Moffat, J., Boone, C., Davis, T., Nislow, C. and Brown, G. (2012). Dissecting DNA damage response pathways by analysing protein localization and abundance changes during DNA replication stress. *Nature Cell Biology*, 14(9), pp.966-976.

Tong, A., Evangelista, M., Parsons, A., Xu, H., Bader, G., Page, N., Robinson, M., Raghibizadeh, S., Hogue, C., Bussey, H., Andrews, B., Tyers, M. and Boone, C. (2001). Systematic Genetic Analysis with Ordered Arrays of Yeast Deletion Mutants. *Science*, 294(5550), pp.2364-2368.

Treco, D. and Winston, F. (2008). *Growth and Manipulation of Yeast*. Current Protocols in Molecular Biology.

Tytell, J. and Sorger, P. (2006). Analysis of kinesin motor function at budding yeast kinetochores. *The Journal of Cell Biology*, 172(6), pp.861-874.

Umbreit, N., Miller, M., Tien, J., Ortolá, J., Gui, L., Lee, K., Biggins, S., Asbury, C. and Davis, T. (2014). *Nature Communications*, 5, pp.4951.

Vanoosthuyse, V. and Hardwick, K. (2009). Overcoming inhibition in the spindle checkpoint. *Genes & Development*, 23(24), pp.2799-2805.

Verdaasdonk, J. and Bloom, K. (2011). Centromeres: unique chromatin structures that drive chromosome segregation. *Nature Reviews Molecular Cell Biology*, 12(5), pp.320-332.

Vilella, F., Herrero, E., Torres, J. and de la Torre-Ruiz, M. (2005). Pkc1 and the Upstream Elements of the Cell Integrity Pathway in *Saccharomyces cerevisiae*, Rom2 and Mtl1, Are Required for Cellular Responses to Oxidative Stress. *Journal of Biological Chemistry*, 280(10), pp.9149-9159.

Visintin, R., Craig, K., Hwang, E., Prinz, S., Tyers, M. and Amon, A. (1998). The Phosphatase Cdc14 Triggers Mitotic Exit by Reversal of Cdk-Dependent Phosphorylation. *Molecular Cell*, 2(6), pp.709-718.

Vizeacoumar, F., van Dyk, N., S.Vizeacoumar, F., Cheung, V., Li, J., Sydorskyy, Y., Case, N., Li, Z., Datti, A., Nislow, C., Raught, B., Zhang, Z., Frey, B., Bloom, K., Boone, C. and Andrews, B. (2010). Integrating high-throughput genetic interaction mapping and high-content screening to explore yeast spindle morphogenesis. *The Journal of Cell Biology*, 188(1), pp.69-81.

Volanakis, A., Passoni, M., Hector, R., Shah, S., Kilchert, C., Granneman, S. and Vasiljeva, L. (2013). Spliceosome-mediated decay (SMD) regulates expression of nonintronic genes in budding yeast. *Genes & Development*, 27(18), pp.2025-2038.

Von der Haar, T. (2007). Optimized Protein Extraction for Quantitative Proteomics of Yeasts. *PLoS ONE*, 2(10), p.e1078.

Weaver, B. and Cleveland, D. (2006). Does aneuploidy cause cancer?. *Current Opinion in Cell Biology*, 18(6), pp.658-667.

Weaver, B. A., Silk, A. D., Putkey, F. R., & Cleveland, D. W. 2007. Aneuploidy and chromosomal instability caused by CENP-E heterozygosity contribute to tumorigenicity. *Cancer Cell*, 11, 25-36

Werner, J., Chen, E., Guberman, J., Zippilli, A., Irgon, J. and Gitai, Z. (2009). Quantitative genome-scale analysis of protein localization in an asymmetric bacterium. *Proceedings of the National Academy of Sciences*, 106(19), pp.7858-7863.

Westermann, S., Cheeseman, a., Anderson, S., Yates III, J., Drubin, D. and Barnes, G. (2003). Architecture of the budding yeast kinetochore reveals a conserved molecular core. *The Journal of Cell Biology*, 163(2), pp.215-222

Westermann, S., Avila-Sakar, A., Wang, H., Niederstrasser, H., Wong, J., Drubin, D., Nogales, E. and Barnes, G. (2005). Formation of a Dynamic Kinetochore- Microtubule Interface through Assembly of the Dam1 Ring Complex. *Molecular Cell*, 17(2), pp.277-290.

Westermann, S., Drubin, D. and Barnes, G. (2007). Structures and Functions of Yeast Kinetochore Complexes. *Annu. Rev. Biochem.*, 76(1), pp.563-591.

Westhorpe, F., Fuller, C. and Straight, A. (2015). A cell-free CENP-A assembly system defines the chromatin requirements for centromere maintenance. *The Journal of Cell Biology*, 209(6), pp.789-801.

Winey, M. (1995). Three-dimensional ultrastructural analysis of the *Saccharomyces cerevisiae* mitotic spindle. *The Journal of Cell Biology*, 129(6), pp.1601-1615.

Winey, M. and O'Toole, E. (2001). The spindle cycle in budding yeast. *Nature Cell Biology*, 3, pp.e23-27.

Winey, M. and Bloom, K. (2012). Mitotic Spindle Form and Function. *Genetics*, 190(4), pp.1197-1224.

Winzeler, E., Shoemaker, D., Astromoff, A., Liang, H., Anderson, K., Andre, B., Bangham, R., Benito, R., Boeke, J., Bussey, H., Chu, A., Connelly, C., Davis, K., Dietrich, F., Whelen Dow, S., El Bakkoury,, M., Foury, F., Friend, S., Gentalen, E., Giaever, G., Hegemann, J., Jones, T., Laub, M., Liao, H., Liebundguth, N., Lockhart, D., Lucau-Danila, A., Lussier, M., M'Rabet, N., Menard, P., Mittmann, M., Pai, C., Rebischung, C., Revuelta, J., Riles, L., Roberts, C., Ross-MacDonald, P., Scherens, B., Snyder, M., Sookhai-Mahadeo, S., Storms, R., Veronneau, S., Voet, M., Volckaert, G., Ward, T., Wysocki, R., Yen, G., Yu, K., Zimmermann, K., Philippsen, P., Johnston, M. and Davis, R. (1999). Functional Characterization of the *S. cerevisiae* Genome by Gene Deletion and Parallel Analysis. *Science*, 285(5429), pp.901-906.

Wisniewski, J., Hajj, B., Chen, J., Mizuguchi, G., Xiao, H., Wei, D., Dahan, M. and Wu, C. (2014). Imaging the fate of histone Cse4 reveals de novo replacement in S phase and subsequent stable residence at centromeres. *eLife*, 3.

Wong, J., Nakajima, Y., Westermann, S., Shang, C., Kang, J., Goodner, C., Houshmand, P., Fields, S., Chan, C., Drubin, D., Barnes, G. and Hazbun, T. (2007). A Protein Interaction Map of the Mitotic Spindle. *Molecular Biology of the Cell*, 18(10), pp.3800-3809.

Wu, J., McCormick, C. and Pollard, T. (2008). Counting Proteins in Living Cells by Quantitative Fluorescence Microscopy with Internal Standards. In: *Methods In Cell Biology*, 1st ed. pp.253-273.

Yanagida, M. (2005). Basic mechanism of eukaryotic chromosome segregation. *Philosophical Transactions of the Royal Society B: Biological Sciences*, 360(1455), pp.609-621.

Yoshida, S., Kono, K., Lowery, D., Bartolini, S., Yaffe, M., Ohya, Y. and Pellman, D. (2006). Polo-Like Kinase Cdc5 Controls the Local Activation of Rho1 to Promote Cytokinesis. *Science*, 313(5783), pp.108-111.

Yuen, K., Warren, C., Chen, O., Kwok, T., Hieter, P. and Spencer, F. (2007). Systematic genome instability screens in yeast and their potential relevance to cancer. *Proceedings of the National Academy of Sciences*, 104(10), pp.3925-3930.

Zeng, X., Kahana, J., Silver, P., Morphew, M., McIntosh, J., Fitch, I., Carbon, J. and Saunders, W. (1999). Slk19p Is a Centromere Protein That Functions to Stabilize Mitotic Spindles. *The Journal of Cell Biology*, 146(2), pp.415-425.

Zimniak, T., Stengl, K., Mechtler, K. and Westermann, S. (2009). Phosphoregulation of the budding yeast EB1 homologue Bim1p by Aurora/Ipl1p. *The Journal of Cell Biology*, 186(3), pp.379-391.

Table A. Non-essential deletions that decrease Dad4-YFP intensity.

Gene Name	ORF	YFP-Intensity	Gene Name	ORF	YFP-Intensity	Gene Name	ORF	YFP-Intensity	Gene Name	ORF	YFP-Intensity
RPL1B	YGL135W	77.74	*YDR417C*	YDR417C	130.53	*CNM67*	YNL225C	142.97	*IOC2*	YLR095C	154.29
CLC1	YGR167W	85.76	*XYL2*	YLR070C	132.16	*MAD1*	YGL086W	143.68	*ATP15*	YPL271W	154.40
DRS2	YAL026C	98.70	*SHM2*	YLR058C	134.46	*YHL044W*	YHL044W	144.69	*NUP84*	YDL116W	154.78
FYV4	YHR059W	107.61	*YGL072C*	YGL072C	136.36	*DHH1*	YDL160C	145.76	*VMA6*	YLR447C	154.99
CTK3	YML112W	109.70	*YGL024W*	YGL024W	136.45	*SGF29*	YCL010C	146.66	*CYT1*	YOR065W	155.73
ATG10	YLL042C	114.33	*MET7*	YOR241W	136.48	*RPB9*	YGL070C	147.89	*YOR302W*	YOR302W	156.64
VPS52	YDR484W	118.55	*MSK1*	YNL073W	136.67	*LYS9*	YNR050C	147.97	*QRI5*	YLR204W	156.84
YMR074C	YMR074C	119.69	*ISA1*	YLL027W	137.27	*TAF14*	YPL129W	148.32	*RSA1*	YPL193W	158.04
YDR433W	YDR433W	120.93	*PBI2*	YNL015W	137.63	*MRPL25*	YGR076C	149.12	*SCP160*	YJL080C	158.51
VPS69	YPR087W	122.20	*VPS41*	YDR080W	137.79	*SNF12*	YNR023W	149.15	*POP2*	YNR052C	158.97
SPC72	YAL047C	123.02	*KRE6*	YPR159W	139.12	*LYP1*	YNL268W	149.70	*MUB1*	YMR100W	163.05
DPH5	YLR172C	124.44	*PHO80*	YOL001W	139.12	*YBL083C*	YBL083C	151.07	*IMP2'*	YIL154C	164.13
REI1	YBR267W	124.66	*PEP3*	YLR148W	139.47	*CUP5*	YEL027W	153.10	*HNT3*	YOR258W	165.32
GON7	YJL184W	125.29	*HOM3*	YER052C	140.84	*APN1*	YKL114C	153.76	*LSM1*	YJL124C	165.41
RAD18	YCR066W	127.62	*HPR1*	YDR138W	141.20	*GGC1*	YDL198C	153.86	*TRM9*	YML014W	165.73
LEA1	YPL213W	128.74	*ARC1*	YGL105W	141.71	*SHE1*	YBL031W	153.87	*PRO2*	YOR323C	166.08
MRPL44	YMR225C	129.58	*RSC2*	YLR357W	142.11	*LDB7*	YBL006C	153.97	*GON7*	YJL184W	166.58
NUP120	YKL057C	130.47	*SLA2*	YNL243W	142.87	*PET191*	YJR034W	154.00	*KTR2*	YKR061W	166.94

Cut off used up to second wild type (72 mutants). Blue indicates mutants up to first wild type (47 mutants). Grey indicates extra mutant included with 3 STD cut off.

Table B. Non-essential deletions that increase Dad4-YFP intensity.

Gene Name	ORF	YFP-Intensity	Gene Name	ORF	YFP-Intensity	Gene Name	ORF	YFP-Intensity	Gene Name	ORF	YFP-Intensity
RIB4	YOL143C	528.84	*RPA34*	YJL148W	410.73	*ADE2*	YOR128C	387.23	*FCY22*	YER060W-A	371.22
BUD23	YCR047C	506.84	*TGS1*	YPL157W	410.34	*LYS14*	YDR034C	386.96	*YGR160W*	YGR160W	368.77
HOM2	YDR158W	475.19	*YNL213C*	YNL213C	408.52	*TUF1*	YOR187W	385.93	*YKL134C*	YKL134C	366.75
ATP17	YDR377W	463.91	*NAM7*	YMR080C	403.36	*MRPL31*	YKL138C	382.24	*YDJ1*	YNL064C	363.07
CGR1	YGL029W	451.58	*MRPL38*	YKL170W	401.99	*COR1*	YBL045C	381.60	*KIN82*	YCR091W	361.88
YNR036C	YNR036C	450.80	*COQ6*	YGR255C	397.85	*MRPL15*	YLR312W-	379.79	*BDH2*	YAL061W	361.39
MIP1	YOR330C	441.27	*MRPL49*	YJL096W	397.50	*RRF1*	YHR038W	379.00	*MEF2*	YJL102W	359.32
RIM1	YCR028C-A	439.37	*SLM6*	YBR266C	395.73	*LIP2*	YLR239C	378.99	*YPR116W*	YPR116W	357.03
UPF3	YGR072W	437.97	*YOR309C*	YOR309C	394.97	*RRP6*	YOR001W	377.22	*YOR205C*	YOR205C	356.33
COX16	YJL003W	435.13	*RSM23*	YGL129C	393.23	*COA1*	YIL157C	376.58	*IRA2*	YOL081W	355.90
CYC3	YAL039C	433.68	*PET494*	YNR045W	391.27	*YMR293C*	YMR293C	376.15	*MRPS8*	YMR158W	355.83
MRF1	YGL143C	430.07	*DIA4*	YHR011W	391.19	*MRPL20*	YKR085C	374.59	*RPS10A*	YOR293W	355.08
MRPS9	YBR146W	428.03	*RSM7*	YJR113C	391.01	*RNH1*	YMR234W	373.73	*SIC1*	YLR079W	354.53
MST1	YKL194C	420.99	*CTF18*	YMR078C	390.85	*YJL120W*	YJL120W	373.36	*EAF1*	YDR359C	352.70
PET123	YOR158W	418.16	*BNI1*	YNL271C	390.63	*TIF2*	YJL138C	372.55	*RPP1B*	YDL130W	352.49
TFP1	YDL185W	416.51	*ATP4*	YPL078C	389.29	*YDR340W*	YDR340W	371.71			

Cut off used up to second wild type (56 mutants). Blue indicates mutants up to first wild type (40 mutants). In grey are shown extra mutants included by selecting the 3 STDs cut off.

Table C. Non-essential deletions that produce a visual phenotype on Dad4-YFP.

Gene Name	ORF	Gene Name	ORF	Gene Name	ORF	Gene Name	ORF	Gene Name	ORF
AAT2	YLR027C	*DIA2*	YOR080W	*MAD2*	YJL030W	*RPS6A*	YPL090C	*TIF3*	YPR163C
ADK1	YDR226W	*FAB1*	YFR019W	*MCM22*	YJR135C	*RPS9B*	YBR189W	*UGO1*	YDR470C
ARG5,6	YER069W	*HMO1*	YDR174W	*MED2*	YDL005C	*RRD2*	YPL152W	*UPF3*	YGR072W
BIK1	YCL029C	*HNT3*	YOR258W	*MMS1*	YPR164W	*RSC1*	YGR056W	*VAN1*	YML115C
BIM1	YER016W	*HOM2*	YDR158W	*MRC1*	YCL061C	*SGS1*	YMR190C	*VMA10*	YHR039C-A
BRO1	YPL084W	*HOM3*	YER052C	*NAT3*	YPR131C	*SKI2*	YLR398C	*VMA7*	YGR020C
CCS1	YMR038C	*HSP31*	YDR533C	*NGG1*	YDR176W	*SLA2*	YNL243W	*VPS52*	YDR484W
CDC73	YLR418C	*IML3*	YBR107C	*PAA1*	YDR071C	*SLK19*	YOR195W	*VPS65*	YLR322W
CTF18	YMR078C	*IRC15*	YPL017C	*PFD1*	YJL179W	*SNF4*	YGL115W	*VPS66*	YPR139C
CTF19	YPL018W	*ISA1*	YLL027W	*PGD1*	YGL025C	*SOH1*	YGL127C	*YDR149C*	YDR149C
CTF4	YPR135W	*KAP123*	YER110C	*REF2*	YDR195W	*SPT7*	YBR081C	*YDR417C*	YDR417C
CTK3	YML112W	*KRE28*	YDR532C	*RPD3*	YNL330C	*SRB2*	YHR041C	*YEL045C*	YEL045C
CUP5	YEL027W	*KRE6*	YPR159W	*RPL13B*	YMR142C	*SST2*	YLR452C	*YER068C-A*	YER068C-A
CYS4	YGR155W	*LGE1*	YPL055C	*RPL1B*	YGL135W	*SWI4*	YER111C	*YLR358C*	YLR358C
DBF2	YGR092W	*LSM6*	YDR378C	*RPL31A*	YDL075W	*THO2*	YNL139C	*YLR407W*	YLR407W
DCC1	YCL016C	*LYS4*	YDR234W	*RPL34B*	YIL052C	*THP1*	YOL072W	*YMR074C*	YMR074C
DHH1	YDL160C	*MAD1*	YGL086W	*RPS12*	YOR369C	*THR1*	YHR025W	*YOR302W*	YOR302W

Visual phenotypes include abnormally weak, bright of enlarged foci as well as mislocalised YFP signal (e.g. lines) (85 mutants).

Table D. Essential mutant alleles that decrease Dad4-YFP intensity.

Allele	ORF	YFP-Intensity	Allele	ORF	YFP-Intensity	Allele	ORF	YFP-Intensity	Allele	ORF	YFP-Intensity
taf8-7	YML114C	74.91	*abf1-103*	YKL112W	146.73	*spt16-ts*	YGL207W	175.78	*yif1-td*	YNL263C	193.60
brl1-C371R	YHR036W	85.05	*dam1-9*	YGR113W	150.91	*sub2-1*	YDL084W	176.34	*abf1-103*	YKL112W	194.78
rat1-1	YOR048C	94.69	*cdc20-1*	YGL116W	151.82	*qri1-ts6*	YDL103C	176.43	*rpn5-1*	YDL147W	196.44
pkc1-ts	YBL105C	95.46	*rse1-1*	YML049C	152.76	*spt6-14*	YGR116W	179.40	*pri1-M4*	YIR008C	197.35
bcp1-ts	YDR361C	102.06	*smc1-259*	YFL008W	153.52	*rio2-1*	YNL207W	181.05	*pol1-17*	YNL102W	197.51
sec6-4	YIL068C	119.29	*nop2-10*	YNL061W	155.71	*sly1-ts*	YDR189W	182.17	*hrp1-7*	YOL123W	197.87
cog2-1	YGR120C	119.64	*spt5-194*	YML010W	157.88	*srp102-510*	YKL154W	182.63	*act1-136*	YFL039C	198.76
rat1-1	YOR048C	124.55	*cdc5-1*	YMR001C	160.19	*tem1-3*	YML064C	183.85	*sec22-1*	YLR268W	200.88
rat1-1	YOR048C	136.43	*dad2-9*	YKR083C	162.31	*cdc5-1*	YMR001C	185.12	*pri1-M4*	YIR008C	201.15
nup192-15	YJL039C	137.84	*dbp5-2*	YOR046C	163.84	*cdc1-1*	YDR182W	185.61	*duo1-2*	YGL061C	201.79
ceg1-C354	YGL130W	138.67	*imp4-2*	YNL075W	164.09	*ils1-1*	YBL076C	186.47	*cdc40-ts*	YDR364C	202.39
dam1-5	YGR113W	138.84	*tfb1-1*	YDR311W	164.09	*mps1-6*	YDL028C	186.86	*sec12-1*	YNR026C	203.16
lst8-6	YNL006W	139.33	*nop2-10*	YNL061W	165.10	*ceg1-C354*	YGL130W	191.42	*emg1-1*	YLR186W	203.31
cks1-35	YBR135W	140.44	*sgv1-23*	YPR161C	165.42	*cdc53-1*	YDL132W	191.59	*rat1-1*	YOR048C	203.32
taf4-18	YMR005W	140.45	*cdc14-3*	YFR028C	169.70	*nip7-1*	YPL211W	191.59	*duo1-2*	YGL061C	203.81
rox3-182	YBL093C	143.22	*sec7-1*	YDR170C	171.73	*act1-133*	YFL039C	192.18			
dim1-2	YPL266W	144.84	*clf1-1*	YLR117C	174.12	*use1-ts*	YGL098W	192.72			
sec22-3	YLR268W	145.00	*ydr196c-1*	YDR196C	175.56	*pol1-12*	YNL102W	193.31			

Cut off used up to ~200 (r.u.). Blue indicates mutants up to 3 STD and grey up to 2 STD (69 mutants corresponding to 60 unique alleles and 56 unique ORFs).

Table E. Essential mutant alleles that increase Dad4-YFP intensity.

Allele	ORF	YFP-Intensity	Allele	ORF	YFP-Intensity	Allele	ORF	YFP-Intensity	Allele	ORF	YFP-Intensity
arp2-14	YDL029W	585.11	*sfi1-7*	YLL003W	472.49	*prp39-1*	YML046W	430.72	*swc4-4*	YGR002C	409.43
dim1-2	YPL266W	567.83	*pre1-1*	YER012W	468.37	*ask1-3*	YKL052C	429.83	*stt3-1*	YGL022W	409.35
cdc20-1	YGL116W	556.68	*cdc31-2*	YOR257W	465.12	*mob2-19*	YFL034C-B	429.52	*cct6-18*	YDR188W	408.04
cdc16-1	YKL022C	555.84	*prp31-1*	YGR091W	462.41	*cdc11-4*	YJR076C	429.51	*cdc37-1*	YDR168W	407.37
prp6-1	YBR055C	548.88	*cdc4-1*	YFL009W	461.53	*prp2-1*	YNR011C	427.15	*swd2-1*	YKL018W	406.32
cdc4-1	YFL009W	541.63	*prp3-1*	YDR473C	460.98	*rpt6-1*	YGL048C	426.93	*prp18-1202*	YGR006W	405.96
yhc1-1	YLR298C	534.60	*rpn7-3*	YPR108W	460.32	*alg1-1*	YBR110W	426.38	*cdc24-5*	YAL041W	405.39
gpi19-2	YDR437W	529.82	*hym1-15*	YKL189W	459.20	*stu2-11*	YLR045C	423.17	*act1-159*	YFL039C	405.01
sgv1-23	YPR161C	529.12	*orc2-1*	YBR060C	455.69	*stu1-7*	YBL034C	422.42	*tfb3-ts*	YDR460W	404.80
prp5-1	YBR237W	525.73	*prp2-1*	YNR011C	449.57	*sec14-3*	YMR079W	421.73	*cdc21-1*	YOR074C	404.58
hrp1-1	YOL123W	516.81	*cse4-1*	YKL049C	448.52	*myo2-16*	YOR326W	420.68	*cdc31-1*	YOR257W	404.52
slu7-ts2	YDR088C	511.96	*act1-101*	YFL039C	445.93	*yif1-td*	YNL263C	418.78	*cdc9-1*	YDL164C	403.96
sup45-ts	YBR143C	510.64	*stu2-13*	YLR045C	445.72	*cus1-3*	YMR240C	416.89	*smp3-1*	YOR149C	403.63
arp3-F306G	YJR065C	503.52	*abd1-5*	YBR236C	445.40	*ura6-4*	YKL024C	416.43	*pap1-1*	YKR002W	402.89
stu2-10	YLR045C	499.32	*cse4-1*	YKL049C	443.67	*cdc3-3*	YLR314C	415.78	*cct4-1*	YDL143W	402.85
bbp1-2	YPL255W	496.67	*prp22-1*	YER013W	441.20	*ura6-4*	YKL024C	415.71	*brl1-2221*	YHR036W	402.61
tfb3-ts	YDR460W	495.17	*gna1-ts*	YFL017C	440.68	*rrp4-1*	YHR069C	413.84	*ipl1-1*	YPL209C	402.25
tfc1-E447K	YBR123C	494.23	*yhc1-8*	YLR298C	440.36	*rpn6-1*	YDL097C	413.70	*esp1-1*	YGR098C	402.18
ebp2-1	YKL172W	493.74	*dbf4-3*	YDR052C	439.08	*rpn1-821*	YHR027C	412.27	*rpt6-1*	YGL048C	401.35
cef1-13	YMR213W	492.72	*arp3-F306G*	YJR065C	437.15	*ulp1-333*	YPL020C	411.21	*cdc3-1*	YLR314C	401.16
cdc20-1	YGL116W	488.87	*rpt6-20*	YGL048C	436.44	*prp24-ts*	YMR268C	410.98	*pre2-2*	YPR103W	400.82
ndc1-4	YML031W	484.77	*cdc28-td*	YBR160W	436.39	*cdc10-2*	YCR002C	410.92	*bms1-1*	YPL217C	400.10
pre2-V214A	YPR103W	479.84	*orc2-1*	YBR060C	435.78	*rrn3-S213P*	YKL125W	410.52			
spt15-P65S	YER148W	478.28	*mob2-19*	YFL034C-	433.86	*hyp2-3*	YEL034W	410.20			
pre2-127	YPR103W	474.86	*cdc4-1*	YFL009W	433.18	*mvd1-1296*	YNR043W	409.44			

Cut off used over ~400 (r.u.). Blue indicates mutants up to 3 STD and grey up to 2 STD (97 mutants corresponding to 86 unique alleles and 77 unique ORFs).

Table F. Non-essential deletions that alter Spc42-RFP intensity.

Gene Name	ORF	YFP-Intensity	Gene Name	ORF	YFP-Intensity	Gene Name	ORF	YFP-Intensity	Gene Name	ORF	YFP-Intensity
Non-essential deletions that decrease Spc42-RFP Intensity											
RTG2	YGL252C	53.06	*APN1*	YKL114C	80.48	*YDR230W*	YDR230W	86.78	*EAF1*	YDR359C	88.91
ISA1	YLL027W	68.36	*SEC22*	YLR268W	81.68	*DNM1*	YLL001W	88.18	*CNM67*	YNL225C	90.34
Non-essential deletions that increase Spc42-RFP Intensity											
YGL024W	YGL024W	499.47	*YDR203W*	YDR203W	297.46	*YIL024C*	YIL024C	259.30	*CIN1*	YOR349W	238.04
HFM1	YGL251C	443.02	*VMA10*	YHR039C-A	292.47	*YMR295C*	YMR295C	256.69	*RPA34*	YJL148W	237.46
PHD1	YKL043W	439.28	*BUD20*	YLR074C	291.88	*MCM21*	YDR318W	251.04	*BDH2*	YAL061W	237.03
YJR087W	YJR087W	367.06	*APQ13*	YJL075C	290.55	*ARG82*	YDR173C	250.96	*YBR141C*	YBR141C	236.23
ALD6	YPL061W	343.01	*PPA1*	YHR026W	284.56	*RPD3*	YNL330C	249.71	*YLR358C*	YLR358C	235.52
YBR134W	YBR134W	337.64	*RCY1*	YJL204C	266.45	*YFR016C*	YFR016C	247.23	*ADK1*	YDR226W	234.41
AAC1	YMR056C	333.52	*NKP2*	YLR315W	264.54	*YPR004C*	YPR004C	246.92	*SGF73*	YGL066W	233.89
GDA1	YEL042W	329.91	*AIR1*	YIL079C	263.27	*ATG14*	YBR128C	245.75	*YIL032C*	YIL032C	231.16
SLA2	YNL243W	312.66	*DCC1*	YCL016C	263.20	*REX3*	YLR107W	241.92	*YER039C-A*	YER039C-A	230.87
HTB2	YBL002W	303.88	*MAD1*	YGL086W	262.27	*NUP42*	YDR192C	241.50			
HAM1	YJR069C	302.93	*RIM20*	YOR275C	261.66	*OPI3*	YJR073C	239.67			

Cut off used up to 3 STDs (8 mutants decrease and 42 mutants increase Spc42-RFP intensity).

Table G. Essential mutant alleles that alter Spc42-RFP intensity.

Allele	ORF	YFP-Intensity	Allele	ORF	YFP-Intensity	Allele	ORF	YFP-Intensity	Allele	ORF	YFP-Intensity
Essential mutant alleles that decrease Spc42-RFP Intensity											
						arp2-14	YDL029W	25.00			
Essential mutant alleles that increase Spc42-RFP Intensity											
cdc31-1	YOR257W	206.51	*arc15-10*	YIL062C	228.29	*cdc34-1*	YDR054C	293.42	*cdc4-2*	YFL009W	398.47
prp18-	YGR006W	208.59	*fcp1-1*	YMR277W	233.39	*gna1-ts*	YFL017C	301.36	*cog2-1*	YGR120C	410.28
cdc31-1	YOR257W	208.94	*hrp1-7*	YOL123W	242.62	*arp3-*	YJR065C	304.63	*yip1-4*	YGR172C	432.35
cdc4-3	YFL009W	213.34	*prp43-ts2*	YGL120C	248.15	*cdc4-1*	YFL009W	335.87	*cdc10-5*	YCR002C	437.35
taf12-	YDR145W	214.86	*cdc4-1*	YFL009W	266.54	*sgv1-23*	YPR161C	339.46	*yif1-td*	YNL263C	611.75
cdc10-4	YCR002C	226.41	*cdc4-3*	YFL009W	279.93	*cdc4-1*	YFL009W	344.47	*phs1-1*	YJL097W	646.26
cdc4-1	YFL009W	226.63	*cdc28-td*	YBR160W	284.89	*cdc16-1*	YKL022C	352.85			

Cut off used is 2 STD (1 mutant decreases Spc42-RFP intensity) or 3 STDs (27 mutants increase Spc42-RFP intensity).

Table H. Non-essential deletions that decrease Dad4-YFP intensity in the retest plate.

Gene Name	ORF	YFP-Intensity	Gene Name	ORF	YFP-Intensity	Gene Name	ORF	YFP-Intensity	Gene Name	ORF	YFP-Intensity
UAF30	YOR295W	96.08	*HPR1*	YDR138W	112.07	*HOF1*	YMR032W	119.26	*CCS1*	YMR038C	125.76
CTK3	YML112W	98.48	*MAD1*	YGL086W	112.32	*THI12*	YNL332W	120.46	*RAD18*	YCR066W	126.00
HOM3	YER052C	99.40	*KRE6*	YPR159W	112.33	*CLC1*	YGR167W	120.57	*NUP84*	YDL116W	126.39
VMA7	YGR020C	99.69	*SHE1*	YBL031W	113.16	*YGL024W*	YGL024W	120.86	*YNL320W*	YNL320W	128.73
YLR358C	YLR358C	102.10	*SNF12*	YNR023W	113.37	*LYP1*	YNL268W	121.44	*KAR9*	YPL269W	129.39
LEA1	YPL213W	102.13	*VIK1*	YPL253C	113.44	*SLA2*	YNL243W	121.52	*NUP133*	YKR082W	129.45
VPS52	YDR484W	103.98	*HNT3*	YOR258W	114.41	*PRS3*	YHL011C	121.71	*YJL175W*	YJL175W	129.57
THP1	YOL072W	104.46	*TRM9*	YML014W	114.52	*PFD1*	YJL179W	122.03	*CKB2*	YOR039W	130.37
ARC1	YGL105W	105.13	*KTR2*	YKR061W	115.07	*PEP3*	YLR148W	122.20	*RSC1*	YGR056W	130.41
YGL072C	YGL072C	105.33	*RPL1B*	YGL135W	115.22	*RSA1*	YPL193W	122.84	*YEL045C*	YEL045C	130.51
BRO1	YPL084W	106.26	*VPS65*	YLR322W	115.48	*APN1*	YKL114C	122.84	*VMA10*	YHR039C-A	130.65
NUP120	YKL057C	107.22	*CUP5*	YEL027W	115.95	*YBL083C*	YBL083C	123.22	*MED2*	YDL005C	130.89
LYS9	YNR050C	107.87	*VPS41*	YDR080W	116.94	*RPB9*	YGL070C	123.67	*PRO2*	YOR323C	131.86
GLY1	YEL046C	108.82	*PET191*	YJR034W	117.51	*CYS4*	YGR155W	123.78	*SCP160*	YJL080C	132.19
SPC72	YAL047C	109.33	*RPS9B*	YBR189W	118.60	*RSB1*	YOR049C	124.06	*YNL254C*	YNL254C	132.22
QRI5	YLR204W	110.46	*DHH1*	YDL160C	118.83	*DRS2*	YAL026C	124.39	*REI1*	YBR267W	132.26

Cut off used up to first wild type (64 mutants).

Table I. Non-essential deletions that increase Dad4-YFP intensity in the retest plate.

Gene Name	ORF	YFP-Intensity	Gene Name	ORF	YFP-Intensity	Gene Name	ORF	YFP-Intensity	Gene Name	ORF	YFP-Intensity
NAT3	YPR131C	488.33	*SFP1*	YLR403W	305.38	*MRPL20*	YKR085C	284.02	*MCM16*	YPR046W	266.57
PGD1	YGL025C	418.50	*TSR2*	YLR435W	302.31	*RRF1*	YHR038W	282.11	*XYL2*	YLR070C	266.43
NMD2	YHR077C	398.50	*SOH1*	YGL127C	302.12	*DPH5*	YLR172C	282.04	*COQ5*	YML110C	265.78
SPT3	YDR392W	379.19	*TUF1*	YOR187W	301.80	*CBP3*	YPL215W	280.78	*MRPL49*	YJL096W	265.61
NAM7	YMR080C	365.05	*ACO1*	YLR304C	301.44	*MMS1*	YPR164W	280.63	*HOM2*	YDR158W	264.85
CTF18	YMR078C	362.44	*TFP1*	YDL185W	301.32	*RPS29B*	YDL061C	280.48	*MRPL38*	YKL170W	264.64
YOR309C	YOR309C	361.89	*ITC1*	YGL133W	300.10	*CTF4*	YPR135W	279.33	*COX16*	YJL003W	264.31
UPF3	YGR072W	357.00	*MSD1*	YPL104W	299.73	*YDL068W*	YDL068W	279.13	*MRPS9*	YBR146W	264.11
LYS14	YDR034C	355.06	*RSM23*	YGL129C	299.50	*ELM1*	YKL048C	278.99	*YDR149C*	YDR149C	264.00
TIF3	YPR163C	342.04	*YGR102C*	YGR102C	298.88	*MTG2*	YHR168W	278.33	*YDL032W*	YDL032W	263.13
ROX3	YBL093C	337.52	*ISM1*	YPL040C	297.58	*COR1*	YBL045C	275.16	*COA1*	YIL157C	261.32
GAL11	YOL051W	337.50	*KIP3*	YGL216W	297.06	*RIM1*	YCR028C-	274.97	*NUP188*	YML103C	261.29
LSM1	YJL124C	336.81	*MRPL28*	YDR462W	296.57	*YNL213C*	YNL213C	274.12	*RPL34B*	YIL052C	260.55
RRP6	YOR001W	328.85	*SNF4*	YGL115W	296.00	*HAP3*	YBL021C	273.78	*BEM4*	YPL161C	259.30
CYC3	YAL039C	324.23	*REF2*	YDR195W	293.29	*LIP2*	YLR239C	273.39	*SLK19*	YOR195W	259.13
PET123	YOR158W	322.66	*RRD2*	YPL152W	292.86	*IML3*	YBR107C	272.46	*RRP8*	YDR083W	258.90
YVH1	YIR026C	320.57	*MRF1*	YGL143C	291.84	*RSM7*	YJR113C	272.25	*RPP1B*	YDL130W	258.79
BUD23	YCR047C	319.03	*CYT1*	YOR065W	290.86	*MRP51*	YPL118W	271.46	*SRB2*	YHR041C	257.26
COQ6	YGR255C	313.53	*MIP1*	YOR330C	290.82	*CDC73*	YLR418C	271.30	*FAR10*	YLR238W	256.20
YKL134C	YKL134C	312.95	*SWI4*	YER111C	290.35	*BUB1*	YGR188C	271.26	*TIF2*	YJL138C	255.76
SST2	YLR452C	312.55	*SGF29*	YCL010C	289.04	*MRPL4*	YLR439W	270.75	*RCR1*	YBR005W	255.34
GSH1	YJL101C	308.51	*MRPL31*	YKL138C	289.02	*YOR205C*	YOR205C	270.62	*MRS1*	YIR021W	254.56
DIA2	YOR080W	307.61	*LGE1*	YPL055C	288.27	*MRPS8*	YMR158W	269.98	*MST1*	YKL194C	253.45
YMR293C	YMR293C	307.54	*MEF2*	YJL102W	288.13	*MAD3*	YJL013C	269.94	*ISA2*	YPR067W	251.65
MAD2	YJL030W	306.83	*CHL4*	YDR254W	286.70	*YNR036C*	YNR036C	269.28	*NOT3*	YIL038C	251.45
VAN1	YML115C	305.67	*PET494*	YNR045W	285.29	*RPL13B*	YMR142C	268.77	*COX14*	YML129C	251.25
DIA4	YHR011W	305.60	*THR1*	YHR025W	284.46	*CTF19*	YPL018W	266.85	*MRM2*	YGL136C	250.40

Cut off used up to first wild type (108 mutants).

Table J. Non-essential deletions that produce a visual phenotype on Dad4-YFP in the retest plate.

Gene Name	ORF	Gene Name	ORF	Gene Name	ORF	Gene Name	ORF	Gene Name	ORF
ADE2	YOR128C	*HSP31*	YDR533C	*LYS4*	YDR234W	*RPL31A*	YDL075W	*VMA6*	YLR447C
ADK1	YDR226W	*IOC2*	YLR095C	*MCM22*	YJR135C	*RPS6A*	YPL090C	*VPS69*	YPR087W
DBF2	YGR092W	*IRC15*	YPL017C	*NGG1*	YDR176W	*TAF14*	YPL129W	*YDR417C*	YDR417C
DCC1	YCL016C	*LDB7*	YBL006C	*PHO80*	YOL001W	*THO2*	YNL139C	*YDR433*	YDR433W
GON7	YJL184W	*LSM6*	YDR378C	*RPD3*	YNL330C	*UGO1*	YDR470C	*YHL044W*	YHL044W
HMO1	YDR174W								

Visual phenotypes include abnormally weak, bright of enlarged foci as well as mislocalised YFP signal (e.g. lines) (26 mutants).

Table K. Non-essential deletions that are benomyl sensitive.

Gene Name	ORF	Z-Score	Gene Name	ORF	Z-Score	Gene Name	ORF	Z-Score	Gene Name	ORF	Z-Score
PAC2	YER007	4.44	*PHO80*	YOL001W	2.24	*YGL072C*	YGL072C	1.70	*YDR433W*	YDR433W	1.28
BUB3	YOR026	4.02	*RSC2*	YLR357W	2.19	*HOM3*	YER052C	1.63	*SWR1*	YDR334W	1.25
DHH1	YDL160	2.95	*VMA6*	YLR447C	2.04	*RSA1*	YPL193W	1.58	*BRO1*	YPL084W	1.24
VPS41	YDR080	2.72	*CUP5*	YEL027W	2.02	*GLY1*	YEL046C	1.57	*QRI5*	YLR204W	1.20
GON7	YJL184	2.71	*YHL044W*	YHL044W	1.94	*PRS3*	YHL011C	1.56	*YOR302W*	YOR302W	1.20
KTR2	YKR061	2.58	*HNT3*	YOR258W	1.92	*SPC72*	YAL047C	1.55	*RPL1B*	YGL135W	1.19
PET191	YJR034	2.54	*YEL045C*	YEL045C	1.91	*POP2*	YNR052C	1.50	*YJL175W*	YJL175W	1.14
ELM1	YKL048C	2.51	*NPL3*	YDR432W	1.87	*LDB7*	YBL006C	1.44	*VPS65*	YLR322W	1.08
SGO1	YOR073	2.50	*REI1*	YBR267W	1.85	*NUP120*	YKL057C	1.42	*GAL11*	YOL051W	1.07
PFD1	YJL179	2.46	*HOM2*	YDR158W	1.85	*YLR358C*	YLR358C	1.40	*CYS4*	YGR155W	1.07
RSC1	YGR056	2.42	*CCS1*	YMR038C	1.81	*SLA2*	YNL243W	1.33	*RTS1*	YOR014W	1.06
TAF14	YPL129	2.39	*EAF1*	YDR359C	1.78	*RPS6A*	YPL090C	1.30	*GGC1*	YDL198C	1.05
VIK1	YPL253C	2.35	*RPB9*	YGL070C	1.78	*HTZ1*	YOL012C	1.30	*HOF1*	YMR032W	1.04
BUB3	YOR026	2.30	*CDC73*	YLR418C	1.75	*HTL1*	YCR020W-B	1.29	*CTK3*	YML112W	1.03

Cut off used over 1 Z-score (54 mutants plus 2 controls in blue).

Table L. Actin and microtubule mutants that affect Dad4-YFP intensity or localisation.

Mutant/allele	Description/Function	Phenotype produced on Dad4
act1	actin	Increased, decreased and visual
arp2	Arp2/3 complex; actin nucleation	Increased
arp3	Arp2/3 complex; actin nucleation	Increased
las17	activates Arp2/3 complex-mediated nucleation of branched actin filaments	Decreased
arc15	ARP2/3 complex; motility and integrity of cortical actin patches	Increased
pan1	Binds/activates Arp2/3 complex in vitro; regulated by MAPK Hog1p in response to osmotic stress	Increased
mss4	actin cytoskeleton organization and cell morphogenesis	Decreased
bcp1	nuclear export of Mss4; actin cytoskeleton organization	Decreased
*hof1*Δ	cytokinesis, and control of actin cable levels/organization	Decreased
*sla2*Δ	actin cortical patch of the emerging bud tip	Decreased and visual
cct4	Cct ring complex; assembly of actin and tubulins	Increased
cct6	Cct ring complex; assembly of actin and tubulins	Increased
cof1	Cofilin, pH-dependent actin filament depolarization	Increased
stt4	Pkc1p protein kinase pathway; required for cell wall integrity, and actin cytoskeleton organization	Increased
*bni1*Δ	Formin; nucleates formation of linear actin filaments	Increased
pfy1	Profilin; binds actin; cytoskeleton organization	Increased
myo2	myosin motor; actin-based transport of cargos	Increased
*bim1*Δ	MAP (EB1)	Visual
*bik1*Δ	MAP (CLIP-170)	Visual
*stu2*Δ	MAP (XMAP215/Dis1)	Increased
she1	Mitotic spindle protein; interacts with (DASH) complex, Sli15p, and Bim1	Decreased
*Irc15*Δ	MAP; regulates microtubule dynamics	Visual
*Rrd2*Δ	microtubule dynamics	Visual
tub4	Gamma-tubulin; microtubule nucleation	Increased

Phenotype indicates change in YFP fluorescence.

Table M. List of oligos used.

Name	Sequence 5' 3'
A-BIR1-F	AATTCCAGCTGACCACCATGGATGGTCAAATAGATAAAATG
YFP-BIR1-R	GTGAAAAGTTCTTCTCCTTTACTCATAGCTGCAGCTGCTAAAATGCCCATTTTCTTAGC
midBIR1-F	GCGAAAATGGGAAAAGAGAAGTG
BIR1-4982-F	CAGTATCACGAAAAATTGCG
BIR1-6461-R	GGTTCCAGTCTCAAAAAGTAAC
A-NDC80-F	AATTCCAGCTGACCACCATGCAAAGCTCAACAAGTAC
YFP-NDC80-R	GTGAAAAGTTCTTCTCCTTTACTCATAGCTGCAGCTGCATTTGTTACGTTATGTTCAG
NDC80-5034-F	GAGCTAATGGTGGAGAAACTG
A-NNF1-F	AATTCCAGCTGACCACCATGGTTAACTCACATGGAATACG
YFP-NNF1-R	GTGAAAAGTTCTTCTCCTTTACTCATAGCTGCAGCTGCATAGTTTTCCTTCAATTCCAAG
A-NSL1-F	AATTCCAGCTGACCACCATGTCACAAGGTCAGTCCAAAAAAC
YFP-NSL1-R	GTGAAAAGTTCTTCTCCTTTACTCATAGCTGCAGCTGCATCCTCCTCCAGGAAGTCCATTAAG
A-SPC19-F	AATTCCAGCTGACCACCATGACAGATGCTTTGGAACAG
YFP-SPC19-R	GTGAAAAGTTCTTCTCCTTTACTCATAGCTGCAGCTGCTTTCTGTTTGAGTATTTCCAAC
A-SPC25-F	AATTCCAGCTGACCACCATGGCCAGCATAGACGCATTTTCG
YFP-SPC25-R	GTGAAAAGTTCTTCTCCTTTACTCATAGCTGCAGCTGCTAAAGATGCCAGAAGCATATCGC
A-CIN8-F	AATTCCAGCTGACCACCATGCCAGCGGAAAACCAAAATACG
YFP-CIN8-R	GTGAAAAGTTCTTCTCCTTTACTCATAGCTGCAGCTGCTTCAATCTTTAACATTTTTCTCG
midCIN8-F_814	CAACAACAGGCAGTGAATTCC
midCIN8-F_1627	GAAATTGAAAGTTTGACATCG
CIN8-782-F	CACTGCCGAATACCATCAAGC
CIN8-1691-R	GGCAATTTTGAGATTGAATAG
A-MAD3-F	AATTCCAGCTGACCACCATGAAAGCGTACGCAAAGAAACG
YFP-MAD3-R	GTGAAAAGTTCTTCTCCTTTACTCATAGCTGCAGCTGCACGCTGTGGTGGGTACGATATG
A-SPC34-F	AATTCCAGCTGACCACCATGGGGGAAAGCTTGGATAG
YFP-SPC34-R	GTGAAAAGTTCTTCTCCTTTACTCATAGCTGCAGCTGCCTCTTGCAAGTTGGCTATCTCC
A-PAC1-F	AATTCCAGCTGACCACCATGACTAACTGGCAGCAACAGC
YFP-PAC1-R	GTGAAAAGTTCTTCTCCTTTACTCATAGCTGCAGCTGCTCTCATGAAAACGTTAGACTTGC
A-CTF13-F	AATTCCAGCTGACCACCATGCCTTCTTTCAATCCTG
YFP-CTF13-R	GTGAAAAGTTCTTCTCCTTTACTCATAGCTGCAGCTGCTATTACCAAAACCTGAGAG
A-CTF19-F	AATTCCAGCTGACCACCATGGATTTTACGTCTGATACG
YFP-CTF19-R	GTGAAAAGTTCTTCTCCTTTACTCATAGCTGCAGCTGCCCTGGCGTACATGTCCGGGAATAG
A-DAM1-F	AATTCCAGCTGACCACCATGAGCGAAGATAAAGCTAAATTAG
YFP-DAM1-R	GTGAAAAGTTCTTCTCCTTTACTCATAGCTGCAGCTGCTCTGAAGGGGGGCCTTGTATTTAT
A-DAD2-F	AATTCCAGCTGACCACCATGGATTCAATAGATGAAC
YFP-DAD2-R	GTGAAAAGTTCTTCTCCTTTACTCATAGCTGCAGCTGCTTCGTTACCATCTACCCTAATTC
DAD2-UP-F	CCGAAATAACTCAGTAGAAGG
MX-DAD2-Start-R	AGGGTATTCTGGGCCTCCATGTCTGTCTGAATTATGAGTTTTTC
MX-DAD2-End-F	GTGAATGCTGGTCGCTATACTGGAAAAGGATCTTATATAAATCG
DAD2-Down-R	GAAATATCTCAAGTGGAAACG
A-DAD3-F	AATTCCAGCTGACCACCATGGAACACAATCTTTCACC
YFP-DAD3-R	GTGAAAAGTTCTTCTCCTTTACTCATAGCTGCAGCTGCTTTAGAATTGCTACCCAAAG
DAD3-UP-F	GGCAAAAAAAAATAAAAGAAAAGG
MX-DAD3-Start-R	AGGGTATTCTGGGCCTCCATGTCTGTGACTACAACGCCGTGTATG

MX-DAD3-End-F	GTGAATGCTGGTCGCTATACTGGGTTTGGTGCAAGAAATTG
DAD3-Down-R	CGGCCAAATCACACAAGTCTC
mid-DAD3-F	CACAGGCAACAGCATTCACAGC
Mxend-DAD3dss-F	GTGAATGCTGGTCGCTATACTGTGGTTTGGTGCAAGAAATTGATTC
DAD4-UP-F	CATCTGGGCAGATGGTAGTG
MX-DAD4-Start-R	AGGGTATTCTGGGCCTCCATGTGCTTTCTTTCCTAAACTCAC
MX-DAD4-End-F	GTGAATGCTGGTCGCTATACTGCACCAATTTTCTATATACGC
DAD4-Down-R	CTTGGATGCAGATGCAGAGTCC
mid-DAD4-F	GCGTGGCAATTCTTAACCAGG
Mxend-DAD4dss-F	GTGAATGCTGGTCGCTATACTGTTCACCAATTTTCTATATACGC
MxR-F-dssDad4-F	GTGAATGCTGGTCGCTATACTGTTCACCAATTTTCTATATACGC
Linker-endDad4-R	AGCTGCAGCTGCAAGAGGTGGCTTCTTGTTATTGG
MxR-F-dssDad4-F	GTGAATGCTGGTCGCTATACTGTTCACCAATTTTCTATATACGC
Linker-endDad4-R	AGCTGCAGCTGCAAGAGGTGGCTTCTTGTTATTGG
A-DAD4-F	AATTCCAGCTGACCACCATGGAGAACCCTCATGAACAAGTGC
YFP-DAD4-R	GTGAAAAGTTCTTCTCCTTTACTCATAGCTGCAGCTGCAAGAGGTGGCTTCTTGTTATTGG
A-CBF2-F	AATTCCAGCTGACCACCATGAGATCATCGATTTTGTTTC
YFP-CBF2-R	GTGAAAAGTTCTTCTCCTTTACTCATAGCTGCAGCTGCGTTAGATAGATATACTAACAG
CBF2-mid-F	GCCGGGCCACCATCAAC
midCBF2-R	GTTGATGGTGGCCCGGC
CBF2-UP-F	GCTAAACAACAGTGTAATTGC
MX-CBF2-Start-R	AGGGTATTCTGGGCCTCCATGTGTTTTCTACTTTTTCTTGTTTG
MX-CBF2-End-F	GTGAATGCTGGTCGCTATACTGGGGAGCTTCGAAGTTTAAACTG
CBF2-Down-R	GGTAATAAAGAAGCCTTCTTCC
end-CBF2-F	GGTTCATTTTCGCGCTTGGC
far-down-CBF2-R	GTGGTTCTCCTTTATAGAATCG
mid-CBF2-F	CGTGGAGAGCTAATTGTGAAGC
Mxend-CBF2dss-F	GTGAATGCTGGTCGCTATACTGGGGAGCTTCGAAGTTTAAACTG
A-CBF2-F	AATTCCAGCTGACCACCATGAGATCATCGATTTTGTTTC
CBF2-1528mid-F	CCCATTTTATCATTCGATATAC
A-STU1-F	AATTCCAGCTGACCACCATGTCGTCCTTCAACAATGAG
YFP-STU1-R	GTGAAAAGTTCTTCTCCTTTACTCATAGCTGCAGCTGCTTCGTTTGAGGCGATGAACATG
midSTU1-F_797	AGGACCAGCATGGTTCACAAG
midSTU1-F_1731	CTCTACTGCCTCCGCCTCC
midSTU1-F_2564	TGAATCCTGAAAAGCCCTACGAG
midSTU1-R_797	CTTGTGAACCATGCTGGTCCT
midSTU1-R_1731	GGAGGCGGAGGCAGTAGAG
midSTU1-R_2564	CTCGTAGGGCTTTTCAGGATTCA
YFP-KRE28-R	GTGAAAAGTTCTTCTCCTTTACTCATAGCTGCAGCTGCTTCGTTTGTTAGCTCGCTTATAATG
A-KRE28-F	AATTCCAGCTGACCACCATGGATACAGGGAGTGCGAGC
A-KAR9-F	AATTCCAGCTGACCACCATGGATAATGATGGACCCAG
YFP-KAR9-R	GTGAAAAGTTCTTCTCCTTTACTCATAGCTGCAGCTGCATAAGTTGGGGTTTTATCTAAACG
A-STU2-F	AATTCCAGCTGACCACCATGTCAGGAGAAGAAGAAGTAG
YFP-STU2-R	GTGAAAAGTTCTTCTCCTTTACTCATAGCTGCAGCTGCCGTCCTGGTTGTCCCTTCCCGCC
midSTU2-F	CCATATTATCGAATGATGAGGG
midSTU2-R	CCCTCATCATTCGATAATATGG

STU2-F	ATGTCAGGAGAAGAAGAAGTAG
STU2-R	CGTCCTGGTTGTCCCTTCCCGCC
STU2-5162-F	CACCTTCAGTATGCTACCGG
STU2-6400-R	AGCTTATTGACATCAATCTCC
UP-HOM2-F	CCTGTAGCAGCAGCCTTGCCC
MID-HOM2-R	CCAGCACCTGAGATTGCTTGC
UP-HOM3-F	CGGCAATACTCGATGCATGCC
MID-HOM3-R	GCAACTGCTATCAAAGCGGC
HOM2-Check-UP-F	CCATGAATACCATCAGCGGC
Down-HOM2-R	TACCTTCCAAGAGTATTACC
HOM3-Check-UP-F	CTTTGACAAGTTTCCAATGGC
Down-HOM3-R	AATTTCTTCTTGTCCGCCACG
HOM3_1560-R	TTCTAAACGTTCATCAATGGC
Down-HOM3_216-R	TTGTATCTTTTATTTCATCC
HOM2-Check-2-UP-F	AGCCTCAACATCGACACCAACC
endMX-HOM3-1408-F	GTGAATGCTGGTCGCTATACTGTGATTTCTCAAGGGGCAAATG
ds50HOM3-KANMX-R	ATAAAGGGAAAATTAATATTCTATCATTAAAGTGAAGAAGAAAGGTGGATCAGTATAGCGACCAGCATTCAC
mid293-TUB1-F	AGGACGCGGCTAATAATTATGC
mid1090-TUB1-F	ACACCAAACTCACAATTGG
UP-PKC1-F	CCCACTCCAGGTTGCACCTGCC
MID-PKC1-R	GCACCATGACGATGTAGTCC
C_SacI_UP-PKC1-F	CCGGCCGCTCTAGAACTAGAGCTCCCCACTCCAGGTTGCACCTGCC
E_SalI_DOWN-PKC1-R	CCGCCGCCGCAAGGAATGGTCGACTTATAAAATTTTTGTATCTG
mid322-PKC1-F	GATTGCCCTTCTTTGGCGC
mid-1262-PKC1-F	CCTTCGGTATACTGGGTTCC
mid-2209-PKC1-F	CCACACACACAAATCCATTCC
mid3083-PKC1-F	CTTATACCCAATAGATATGGC
CRB-link-PKC1-R	CCACCAGCTGCACATCGGCCATTGATCCAGAACCTGATCCAGAACCTAAATCCAAATCATCTGGCATAAAGG
down358-PKC1-R	ATAAAATTTTTGTATCTGTTC
MID-PKC1-R	TAGCCGCTCTCTTTTTATGC
endPKC1-AAAA-AIDStart-R	GGTTTGGCTGGATCTTTAGGAGCTGCAGCTGCTAAATCCAAATCATCTGGCATAAAGG
endFLAGstop-dssPKC1-F	CGACGATGACAAGTCTAGATGAAGAAAAGGTCATGCCATG
end-noStop-PKC1-R	TAAATCCAAATCATCTGGC
dssFLAG15-dssPKC1-F	GGCGCGCCAGATCTGAGAAAAGGTCATGCCATG
MID-PKC-F	GGACTACATCGTCATGGTGC
EndNoStopPKC1-R	TAAATCCAAATCATCTGGCATAAAGGAAAATCCTCTAAACTCTTCTTGCTGGCTCG
EndNoStopPKC1-StartLINKER-F	CGAGCCAGCAAGAAGAGTTTAGAGGATTTTCCTTTATGCCAGATGATTTGGATTTAGGTCGACGG
endPKC1-AAAA-upFLAG-R	TAATGTATCCCGGGTGATACAGCTGCAGCTGCTAAATCCAAATCATCTGGCATAAAGG
endPKC1-MxF-R	AGGGTATTCTGGGCCTCCATGTTCATAAATCCAAATCATCTGG
endMx-dsspkc1-F	GTGAATGCTGGTCGCTATACTGAGAAAAGGTCATGCCATG
mid883-PKC1-F	GATATCGCTGAAGAAATTCG
mid1888-PKC1-F	GAGAAACTAAATAAATTTATCG
mid2656-PKC1-F	TTCTTAACCAATCTATACTGC
endPKC1no stop_link-CFP-R	AAAGTTCTTCTCCTTTACTCATAGCTGCAGCTGCTAAATCCAAATCATCTGGC
AIDStart-F	CCTAAAGATCCAGCCAAACC
endFLAGstop-R	TCATCTAGACTTGTCATCGTCG

endFLAGSTOP-5'Kc_URA3-F	CGACGATGACAAGTCTAGATGATGATTCTGGGTAGAAGATCGGTCTGC
3'Kc_URA3-AIDStart-R	GGTTTGGCTGGATCTTTAGGGATGATGTAGTTTCTGG
endFLAGdss15-R	CAGATCTGGCGCGCCTCATCTAGACTTGTCATCGTCG
dssFLAG15-5'Kc_URA3-F	GGCGCGCCAGATCTGTGATTCTGGGTAGAAGATCGGTCTGC
upFLAG_StartFLAG-F	GTATCACCCGGGATACATTATACGAAGTTATGCATGCTCACTAGTGACTACAAGG
3'KcURA3-upFLAG-R	TAATGTATCCCGGGTGATACGATGATGTAGTTTCTGG
mid777_amp-F	CTACACGACGGGCAGTCAGG
AFB2-R	TTACAAAGTCGAATACATGC
midSPC42-F	TGTCTTTAAATAACCAACTCCAA
MX-ADHterm-R	AGGGTATTCTGGGCCTCCATGTCGCCGCCGCAAGGAATG
Mxend-SPC42dss-F	GTGAATGCTGGTCGCTATACTGTGATTTAAAAAGCAGTTAAGGAG
SPC42dss-R	GTAGGATTGGAATGTATTTTCTAAGG
Mx-YFP-R	AGGGTATTCTGGGCCTCCATGTTTTGTATCGTTCATCCATGCC
CUP1p-F	ACTAGTGGATCCCATTACCG
mid502-CFP-F	AGACACAACATTGAAGATGG
Linker-start_CFP-F	GCAGCTGCAGCTATGAGTAAAGGAGAAGAAC
End_CFP-Stop-MxF-R	AGGGTATTCTGGGCCTCCATGTTCATTTGTATAGTTCATCCATGCC
Linker-start_CFP-F	GCAGCTGCAGCTATGAGTAAAGGAGAAGAAC
End_CFP-Stop-MxF-R	AGGGTATTCTGGGCCTCCATGTTCATTTGTATAGTTCATCCATGCC
UP-SPC42-F	CATGGCAATTCCCGGGGATCTTCTATTACGCGTCGTGGTTGG
RFP-SPC42-R	GATGACGTCCTCGGAGGAGGCCATAGCTGCAGCTGCTCGATTATTGGGAGTGGGAGTTGC
RFP-F	ATGGCCTCCTCCGAGGACGTCATC
DOWN-RFP-R	ACCAAACCTCTGGCGAAGAAGTCCATTAGGCGCCGGTGGAGTGGCGGC
midRFP-R	CCCTCCATGCGCACCTTGAAGCGC

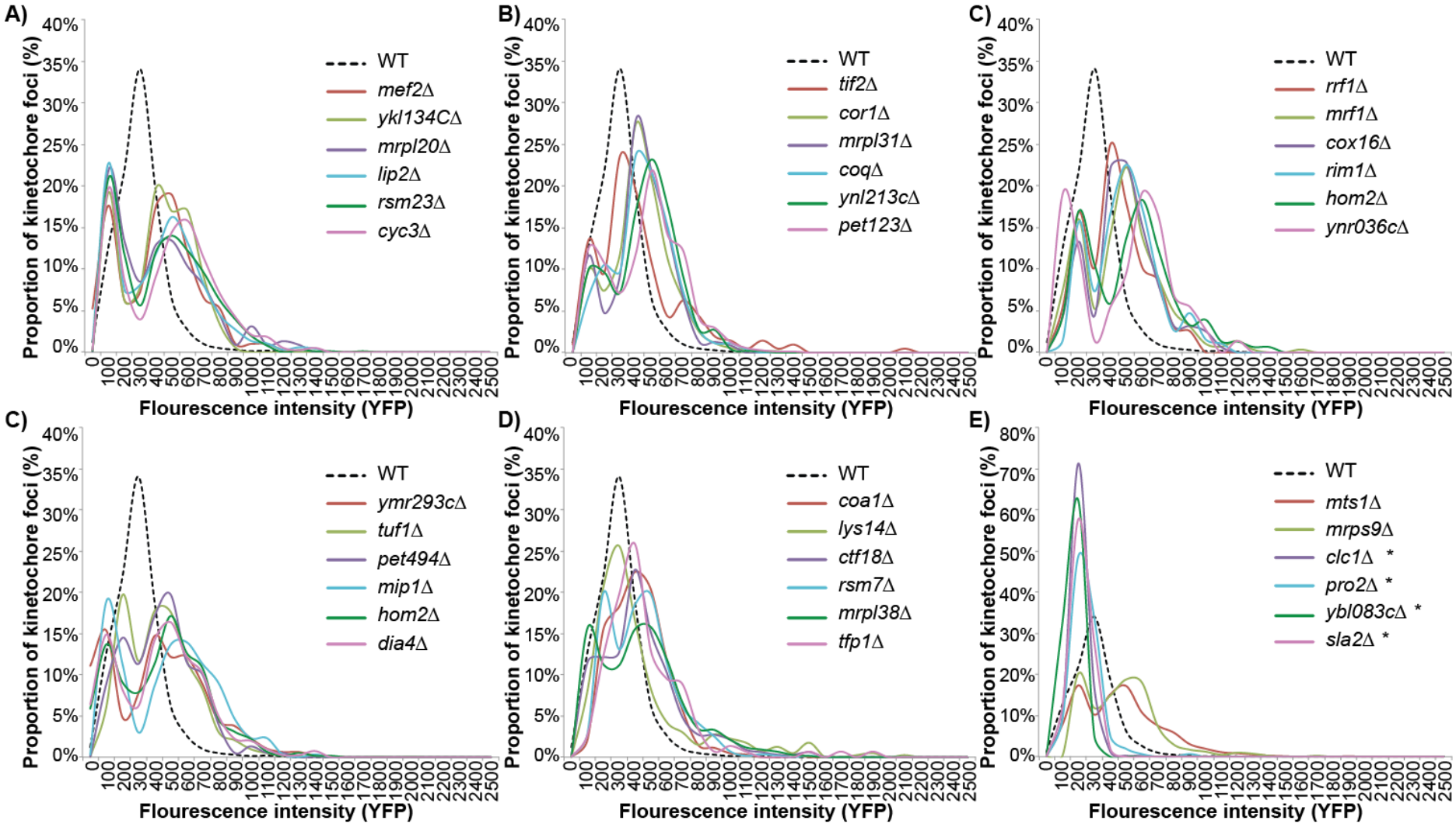
A)
Proportion of kinetochore foci (%)
Flourescence intensity (YFP)
WT
mef2Δ
ykl134CΔ
mrpl20Δ
lip2Δ
rsm23Δ
cyc3Δ
B)
Proportion of kinetochore foci (%)
Flourescence intensity (YFP)
WT
tif2Δ
cor1Δ
mrpl31Δ
coqΔ
ynl213cΔ
pet123Δ
C)
Proportion of kinetochore foci (%)
Flourescence intensity (YFP)
WT
rrf1Δ
mrf1Δ
cox16Δ
rim1Δ
hom2Δ
ynr036cΔ
C)
Proportion of kinetochore foci (%)
Flourescence intensity (YFP)
WT
ymr293cΔ
tuf1Δ
pet494Δ
mip1Δ
hom2Δ
dia4Δ
D)
Proportion of kinetochore foci (%)
Flourescence intensity (YFP)
WT
coa1Δ
lys14Δ
ctf18Δ
rsm7Δ
mrpl38Δ
tfp1Δ
E)
Proportion of kinetochore foci (%)
Flourescence intensity (YFP)
WT
mts1Δ
mrps9Δ
clc1Δ *
pro2Δ *
ybl083cΔ *
sla2Δ *

Figure A. Frequency curves. A-E) Foci distribution curves of wild type (WT) (black) and mutants (colours). Mutants with an asterisk next to the name in panel (**E**) were identified as decresing Dad4-YFP and have a single population tighter and with lower YFP median than the wild type. All other mutants were identify as increasing Dad4-YFP intensity and display two or more populations.

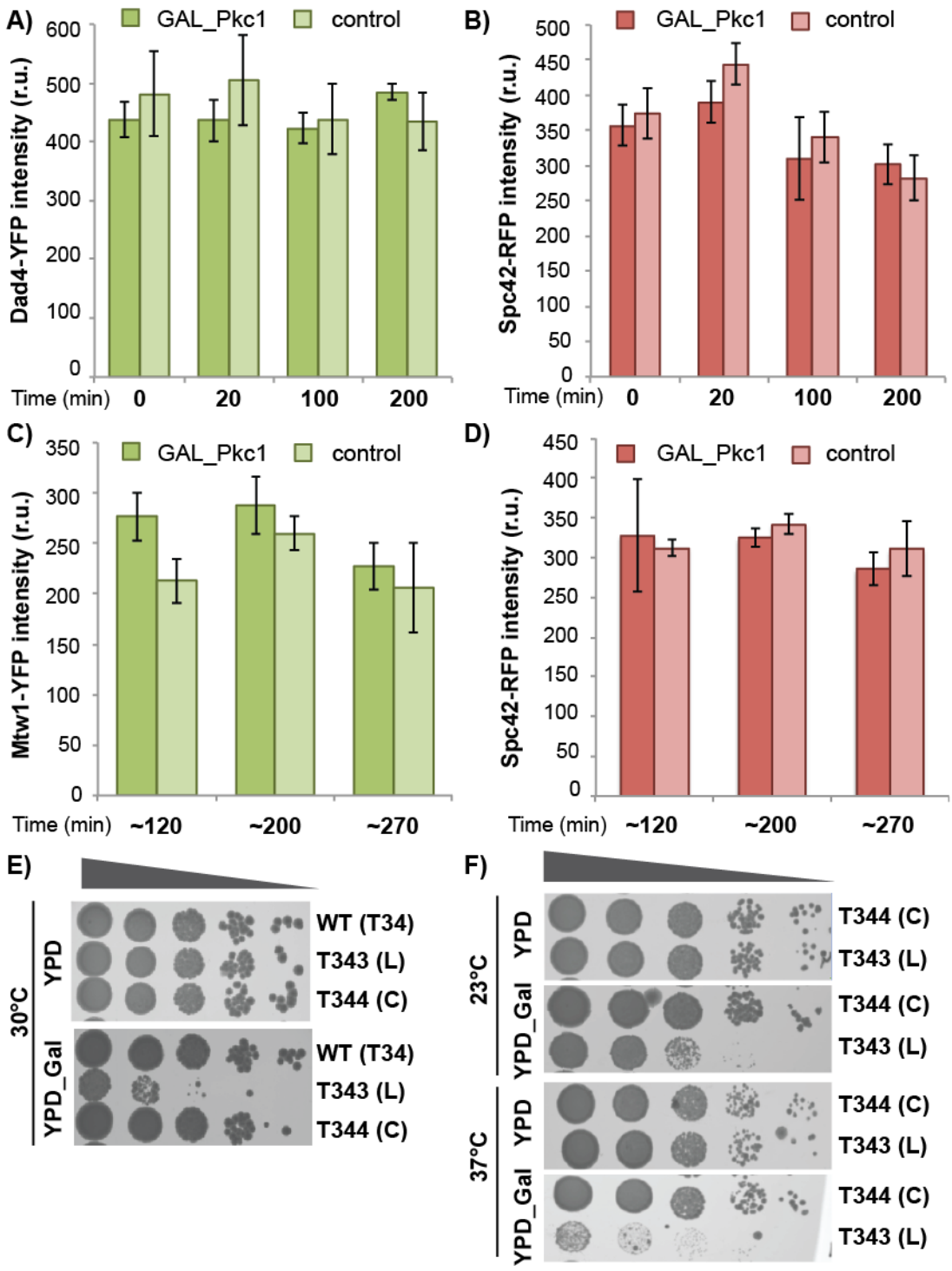

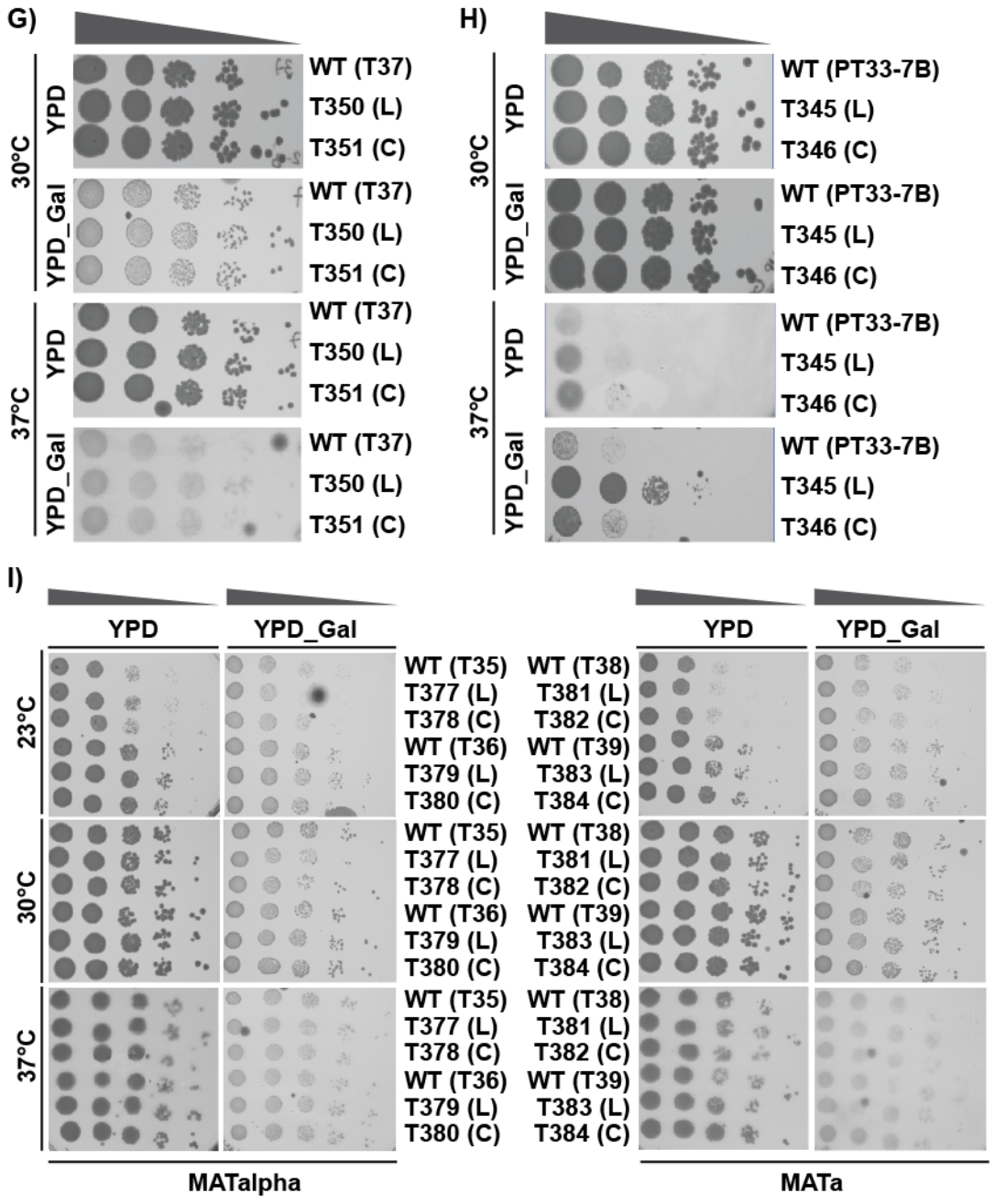

Figure B. Pkc1 overexpression. A-D) Dad4-YFP (**A**) or Mtw1-YFP (**C**) and Spc42-RFP in the corresponding strains (**B, D**). Fluorescence intensity values are background-subtracted and quantified by automated ImageJ FociQuant for the strain containing a galactose induced copy of *PKC1* at the URA3 locus (dark green/red) or a control (light green/red). Error bars show standard deviation of the mean. **E-I)** 10-fold series dilutions spoted onto YFP with or whitout 2% galactose at the indicated temperatures. An “L” next to the strain name means they contain the galactose-induced copy of *PKC1* at the *URA3* locus. A “C” next to the strain name means they are controls (same integration plasmids at the same locus without the *PKC1* gene). The background WT strain used for the integration is also shown. T34 contains *DAD4-YFP* (*MATα*), T37 *DAD4-YFP* (*MAT***a**), PT33-7B *MTW1-YFP* (*MATα*), T35 *DAD3-YFP* (*MATα*), T36 *NDC10-YFP* (*MATα*), T38 *DAD3-YFP* (*MAT***a**) and T39 *NDC10-YFP* (*MAT***a**). All contain *SPC42-RFP*. PT33-7B contains also *HTA1-CFP*. Strains genotypes are shown in Table 2.2.